5-14-2023

Synthetic Studies on Small Molecule Src Homology 2 Domain Containing Inositol 5'Phosphatase (SHIP) Modulators and Studies towards the Design and Synthesis of a SHIP PROTAC

Shawn Dormann
Syracuse University

Abstract

The PI3K pathway is a biological pathway of great importance to the biomedical community. PI3K and mutations associated with it have often associated as the cause for various disease states due to its role in signaling other enzymes such as AKT. Targeting PI3K is one way to help regulate the PI3K pathway but there are other enzymes such as SHIP that also contribute to the delicate balance of the cell. It has been proposed that the modulation of SHIP could also provide some therapeutic benefit as its behavior opposes that of PI3K. Detailed in this work is the design and synthesis of aminosteroid inhibitors as well as agonist studies involving the optimization of an AQX-1125 analog synthetic route. These inhibitors and agonists may be used further to help analyze the role SHIP plays in certain disease states such as Alzheimer's Disease.

Proteolysis Targeting Chimeras or PROTACs have become a topic of discussion in the biomedical community in recent years. They provide an alternate route of modulating proteins by lowering protein levels in cells as opposed to inhibitor-based strategies. The potential for this strategy to be of therapeutic relevance is immense as it allows for the targeting of proteins and receptors, even ones that do not have enzymatic roles. A proper PROTAC can also incorporate a weak binding inhibitor and still be a potent and selective therapeutic which expands the library of possibilities for protein targets. With these studies, two proposed SHIP based PROTACs were synthesized and made. If proven to degrade SHIP, these molecules could provide valuable knowledge towards the role SHIP plays in disease. These molecules would also be useful in probing the scaffolding role of SHIP which has not been investigated in human disease.

Synthetic Studies on Small Molecule Src Homology 2 Domain Containing Inositol 5'Phosphatase (SHIP) Modulators and Studies towards the Design and Synthesis of a SHIP PROTAC

By

Shawn M. Dormann

B.S, University at Buffalo, 2016

M. Phil., Syracuse University, 2019

Dissertation

Submitted in partial fulfillment of the requirements for the degree of Doctor of Philosophy in Chemistry

Syracuse University

May 2023

Acknowledgements

First of all, I would like to thank my mother for always being there and calming my anxiety when I had been overthinking or panicking for no reason. Countless phone calls were made during my time here at Syracuse and I could not have done it without you in my corner. To my grandfather, thank you for instilling in me at a young age the value of education and encouraging me to pursue further studies. All those Sunday morning trips to Tim Horton's where we talked about future goals led me to where I am today. I truly wish my grandmother had been here to see me complete my goals with you and I. To the rest of my family, Uncle Matt, Uncle Mark, Aunt Laurie, Brayden and Alex, thank you guys for supporting me throughout the years as well. I would also like to thank my future wife, Tess Marie, I met you halfway through my stay in Syracuse and I am glad we were able to survive a pandemic and find our love for each other. It was nice having you as a calming force while working on a PhD which is not the most calming.

To my research advisor, Dr. John Chisholm, thank you for guiding me through my research while being such a genuine and caring individual. I have learned so much working with you these past years and I truly appreciate all the advice given. To my labmates, Shea, Nilamber, Rowan, Christos, Angela, Rob, Katelyn and Otto, thank you all for tolerating as a friend and a colleague. When chemistry was not working and I didn't want to be in lab, it was nice having you guys there to lift my spirits and be able to laugh around with.

Lastly, to my committee members, Dr. Totah, Dr. Steinhardt, Dr. Sponsler, and Dr. Hougland thank you all for serving on my committee. It was a pleasure being able to work with and learn from you all. Dr. Hosein, thank you for agreeing to serve as the Chair for my defense and for how easy you made the scheduling process.

Table of Contents

Acknowledgements……...*iv*

List of Tables and Figures……..*vii*

List of Schemes……*ix*

List of Symbols/ Abbreviations……...*x*

Chapter 1 - Background on SHIP and the PI3K Pathway……1

1.1 Overview of Phosphoinositide Signaling and the PI3K Pathway……..1

1.2 PI3K Pathway in Disease and Therapeutic Potential of SHIP Modulators…….4

1.3 Investigating SHIP and its Role in Cancer……6

1.4 Investigating SHIP and its potential role in Alzheimer's Disease……..9

1.5 Targeting SHIP for Potential Therapeutics in Autoimmune Disease…….12

1.6 Targeting SHIP for Potential Therapeutics in Diabetes and Obesity…….....15

1.7 Summary……..……..16

1.8 References…….....16

Chapter 2 - Synthetic Studies on Small Molecule SHIP Modulators……..23

Abstract……23

2.1 SHIP Phosphatase, Proposed Mechanism and Structural Insights…….....24

2.2 Discovery of SHIP Antagonists……....26

2.3 Discovery of SHIP Agonists……..32

2.4 Synthesis of SHIP Inhibitors…….....37

2.5 Optimization of a new route to AQX-1125 analog.....…49

2.6 Summary/Conclusion……56

2.7 Experimental……57

2.8 References……....87

Chapter 3 – Studies towards the Design and Synthesis of a SHIP PROTAC.....93

Abstract.....93

3.1 The Ubiquitin-Proteasome System and Targeted Protein Degradation.....94

3.2 Proteolysis Targeting Chimeras (PROTACs).....95

3.3 Synthesis and Design of a Proteolysis Targeting Chimera for SHIP.....120

3.4 Testing Strategy and Preliminary Data.....130

3.5 Conclusion and Future Directions.....130

3.6 Experimental.....131

3.7 References.....154

Appendix: ^{1}H and ^{13}C NMR Spectra.....162

Curriculum Vitae.....217

List of Tables and Figures

Figure 1.1 PI3K Pathway Overview.....3

Figure 1.2 Phosphorylation Patterns of Signaling Active PIPs.....4

Figure 2.1 Mg2+ catalyzed cleavage of the 5'-phosphate by SHIP2……25

Figure 2.2 3AC(**2.1**) and Steroid Numbering System……..26

Figure 2.3 Quinoline and Tryptamine Based Pan-SHIP1/2 Inhibitors……..28

Figure 2.4 AS1949490 and AS1938909……...29

Figure 2.5 Pyridine motif-containing SHIP2 Inhibitors……30

Figure 2.6 Sulfonanilide SHIP2 Inhibitors.....31

Figure 2.7 Pelorol, Pelorol Derivatives and AQX-1125.....33

Figure 2.8 SHIP Agonists revealed through AtomWise Virtual Screen.....36

Figure 2.9 Epoxide Opening.....43

Figure 2.10 Side and bottom view of K116 benzamide (**2.43**).....44

Table 2.1 Malachite and FP Testing Data.....47

Figure 3.1 First Protac targeting MetAP-2.....96

Figure 3.2 VHL Ligands.....99

Figure 3.3 SGK3 based PROTAC Degraders.....101

Figure 3.4 ARV-771 Brd4 PROTAC.....102

Figure 3.5 TBK1 ligands and TBK1 PROTAC.....103

Figure 3.6 CRBN Ligands.....105

Figure 3.7 CRBN based Brd4 PROTAC.....106

Figure 3.8: CRBN PROTACs with their associated POI ligand.....108

Figure 3.9: IAP (**3.22**), MDM2 (**3.23**) and KEAP1 PROTAC's (**3.24**).....111

Figure 3.10: p38 isoform selective MAPK PROTACs.....113

Figure 3.11: MZ1 BET Protein Degrader.....115

Figure 3.12: SD-36, STAT3 PROTAC.....118

Figure 3.13: CCT367766 Pirin degradation probe.....119

List of Schemes

Scheme 2.1: K118 Synthesis.....39

Scheme 2.2: C3 Amine Substitution.....40

Scheme 2.3: Synthesis of Aminosteroid 5,6-Diols.....42

Scheme 2.4: Salt Formation of the Free Amine.....43

Scheme 2.5: Synthesis of Benzamide **2.43**.....44

Scheme 2.6: K351 (**2.44ab**) Formation.....46

Scheme 2.7: Aquinox Pharmaceuticals Synthesis of AQX-1125.....51

Scheme 2.8: Second generation approach to Aquinox AQX-1125 (**2.19**).....53

Scheme 2.9: Revised Synthesis of AQX-1125 Analog.....54

Scheme 2.10: New Allylic Oxidation Conditions.....55

Scheme 3.1: Retrosynthetic Analysis of First SHIP PROTAC.....122

Scheme 3.2: Synthesis of E3 Ligase ligand.....124

Scheme 3.3: Synthesis of the SHIP Ligand.....125

Scheme 3.4: Attempted Sonogashira Reactions.....126

Scheme 3.5: Second Retrosynthetic Analysis.....127

Scheme 3.6: Synthesis of Steroid Alkyne.....128

Scheme 3.7: Synthesis of SHIP Based PROTACs.....129

List of Abbreviations/Acronyms

AKT	Protein Kinase B
AML	Acute Myeloid Leukemia
Boc_2O	ditertbutyl dicarbonate
CD155	cluster of differentiation 155
CDK	Cyclin Dependent Kinase
CLL	chronic lymphocytic leukemia
CRBN	Cereblon
CSA	Camphorsulfonic acid
DC_{50}	concentration needed to degrade 50% of protein/target
EGFR	Epidermal Growth Factor Receptor
FP	Fluorescence Polarization
GLUT1/4	glucose transporter protein type ¼
GSK3β	Glycogen synthase kinase 3 beta
GWAS	Genome wide association studies
IC_{50}	concentration needed to inhibit 50% of protein/target
IL-6	interleukin-6
IFN-β	interferon-β
ITC	Isothermal Titration Calorimetry
kDa	kilodalton
K_d	Dissociation constant
K_i	Inhibitory constant
MM	Multiple Myeloma
MsCl	methanesulfonyl chloride
NF-κB	nuclear factor κB
NSCLC	Non-Small Cell Lung Cancer
PEG	Polyethylene Glycol
PtdIns	Phosphatidyl Inositol

PH	Pleckstrin Homology
PI3K	Phosphatidylinositol-3-Kinase
$PI(3,4)P_2$	phosphatidylinositol-3,4-bisphosphate
$PI(3,4,5)P_3$	phosphatidylinositol-3,4,5-trisphosphate
PI(4,5)P	phosphatidylinositol-4,5-bisphosphate
POI	Protein of Interest
PROTAC	Proteolysis Targeting Chimeras
PTEN	phosphate and tensin homolog protein
RTK	Receptor Tyrosine Kinase
SCLC	Squamous Cell Lung Cancer
SNIPERs	Specific and Non-genetic Protein Erasers
SPR	Surface Plasmon Resonance
TIGIT	T-cell immunoglobulin and ITIM domain
TLR4	toll like receptor 4
TNFα	Tumor necrosis factor alpha
TREM2	Triggering Receptor Expressed on Myeloid cells 2
TRIF	TIR-domain-containing adaptor-inducing interferon-β
UPS	Ubiquitin Proteasome System
VHL	von Hippel-Lindau
3AC	3α-amino cholestane
5xFAD	Five familial Alzheimers Disease Mutations

1.1 Overview of Phosphoinositide Signaling and the PI3K Pathway

There are many complexities to eukaryotic cell signaling, as cells have to transfer signals from outside the cell membrane to the nucleus to carry out processes necessary for survival such as protein synthesis, DNA replication, and cell differentiation. Phosphoinositides, which are otherwise known as phosphatidyl inositols (PtdIns) are important secondary messengers and play a key role in this cell signaling.[1-4] These phospholipids consist of long fatty acid chains joined by a glycerol linkage to an inositol ring. The long lipids are embedded on the interior of the cell membrane while the phosphorylated inositol is exposed to the cytoplasm. The positions along the inositol ring can be modified by different inositol kinases and phosphatases, leading to a variety of these lipids with differing phosphorylation. These phosphorylation patterns act as recognition elements for further signaling that occurs through recruitment of different effector proteins. The enzymes that catalyze these reactions are found in the cytosol of the cell and get recruited to the cell membrane by their PH (pleckstrin homology) domains, which bind phosphoinositides with high affinity and specificity.[5,6] One signaling pathway that utilizes these phosphoinositide secondary messengers is the Phosphatidylinositol-3-Kinase (PI3K) pathway (**Figure 1.1**). This pathway is one of the more heavily studied cellular signaling pathways due to its association with multiple disease states including some forms of cancer such as leukemia, non-small cell lung cancer, and breast cancer.[7-9] This signaling pathway is initiated by PI3K, which can be activated in a number of ways including binding of a nearby receptor tyrosine kinase (RTK) such as epidermal growth factor receptor (EGFR), through a Ras GTPase or heterotrimeric G proteins associated with GPCRs.[10,11] PI3K enzymes are classified in three different classes(I, II, and III) with class I being the most prominent in the cell. Class I PI3K's have four isoforms (p110α,

p110β, p110γ, p110δ) and all four of these isoforms catalyze the same reaction which is the conversion of phosphatidylinositol-4,5-bisphosphate ($PI(4,5)P_2$) to phosphatidylinositol-3,4,5-trisphosphate ($PI(3,4,5)P_3$). $PI(3,4,5)P_3$ can then bind to effector proteins such as the protein kinase AKT through their pleckstrin-homology (PH) domains.[12] Once AKT is bound it is then activated through phosphorylation by phosphoinositide-dependent kinase 1 (PDK1) at the T308 residue in the activation loop.[12] $PI(3,4,5)P_3$ can be converted back into $PI(4,5)P_2$ by phosphate and tensin homolog protein (PTEN). PTEN is often referred to as a tumor suppressor protein as it helps negatively regulate the pathway. Mutations to PTEN that lower phosphatase activity are often found to be detrimental to the overall balance of the pathway since this leads to an overall unchecked increase in $PI(3,4,5)P_3$ levels.[13,14] Loss of PTEN phosphatase activity has been linked to tumor growth and progression such as glioblastomas.[15] In both U87 MG and U373 MG which are glioblastoma cell lines, Akt is found to be hyperphosphorylated by the presence of upregulated $PI(3,4,5)P_3$ levels. Endometrial and Prostate cancers have also been shown to demonstrate lower levels of PTEN activity as well.[16,17]

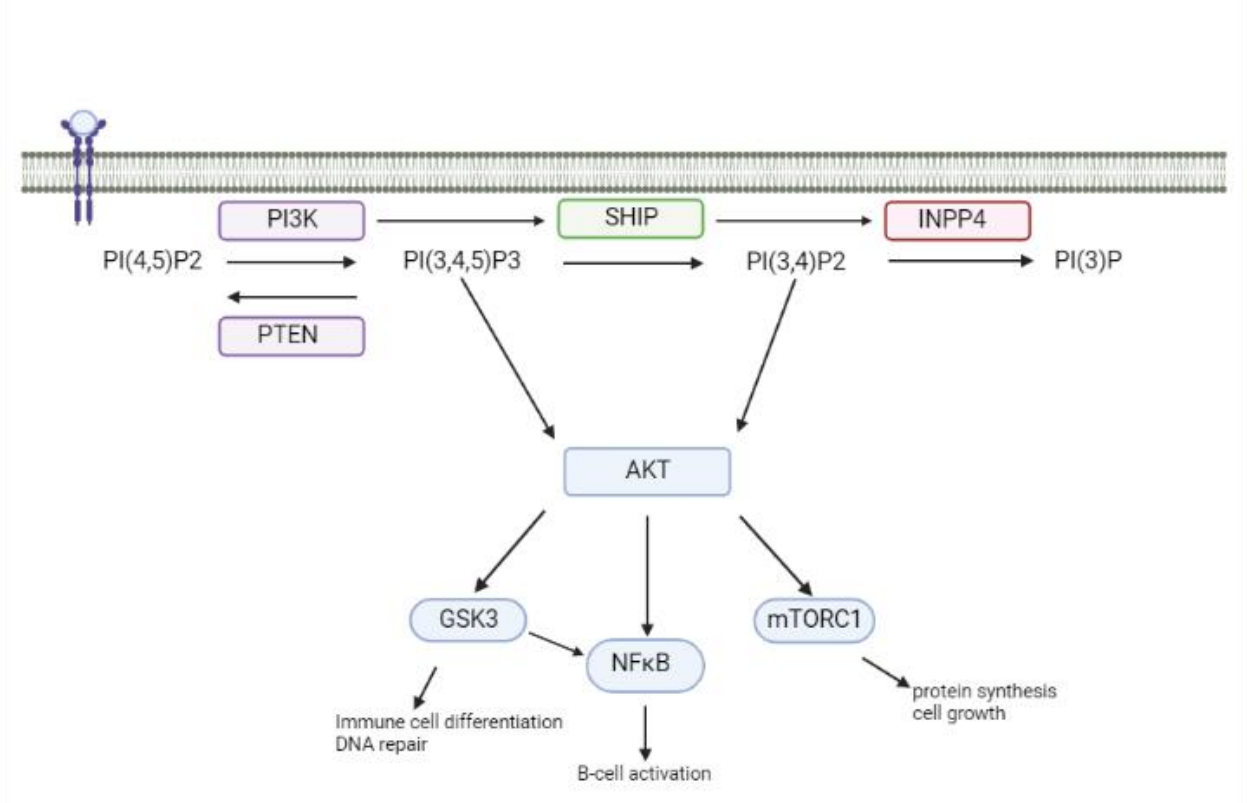

Figure 1.1: PI3K Pathway overview

$PI(3,4,5)P_3$ can be further modified by the SH2-domain containing inositol 5'phosphatase (SHIP) enzyme which hydrolyzes the 5'-phosphate making phosphatidylinositol-3,4-bisphosphate($PI(3,4)P_2$). This newly formed product also leads to the downstream activation of Akt.[18] Akt can bind the newly formed $PI(3,4)P_2$, which then leads to the subsequent phosphorylation of S473 by mTORC2. It is believed for full activation of Akt that both serine and threonine sites (T308 and S473) need to be phosphorylated. A recent study using surface plasmon resonance (SPR) demonstrated that Akt has the highest affinity for $PI(3,4,5)P_3$ and $PI(3,4)P_2$ out of all other phosphoinositide binding proteins indicating a high degree of selectivity for these secondary messengers.[19] $PI(3,4)P_2$ can then by metabolized by Inositol 4'-phosphatases (INPP4) to form the signaling inactive PI(3)P. INPP4 enzymes come in two main forms,

INPP4A and INPP4B.[18,20] Both catalyze similar reactions in that they hydrolyze $PI(3,4)P_2$ into PI(3)P which can be considered a way to regulate PI(3,4)P2 levels in cells. The key phosphorylation patterns are shown below in **Figure 1.2.**

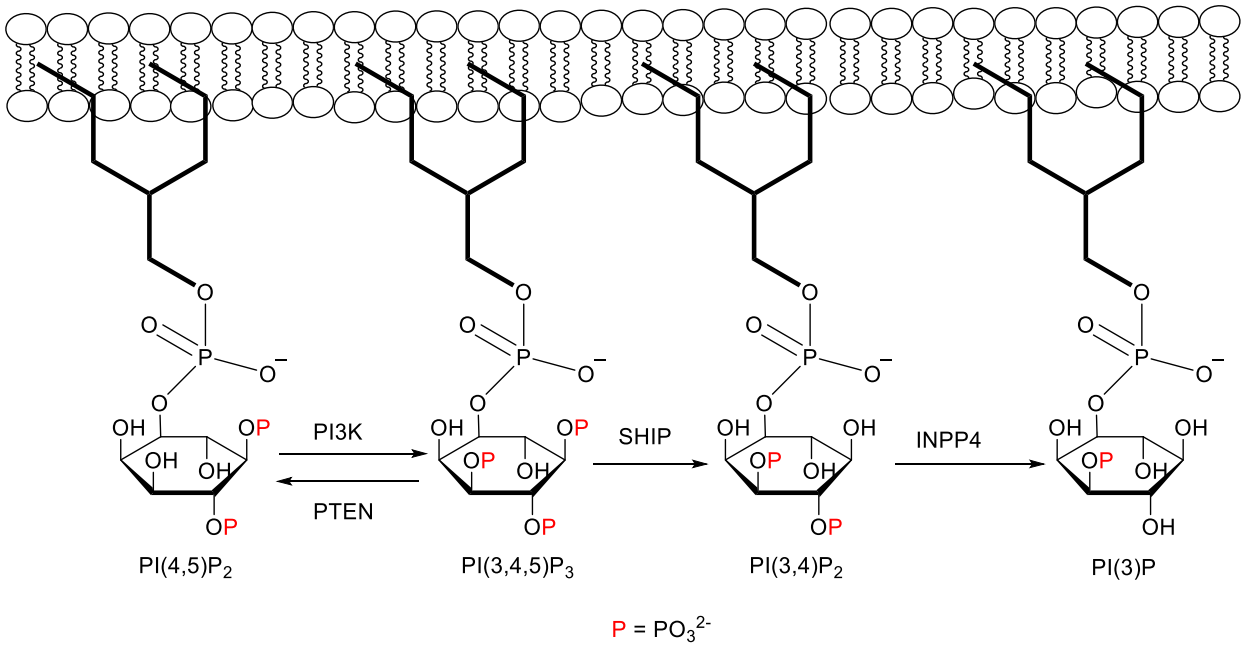

Figure 1.2: Phosphorylation Patterns of Signaling Active PIPs

1.2 PI3K Pathway in Disease and Therapeutic Potential of SHIP Modulators

The PI3K pathway has been an active area when it comes to potential drug targets. Phosphoinositide's are supposed to exist in a delicate balance to mediate signaling, however in many human diseases this signaling has been altered. This may be due to either mutations to an inositol kinase or phosphatase. These mutations can lead to aberrant signaling that can result in hyperactivity. This has led to a number of interesting developments and promising leads for the treatment of diseases that have impacted human society for decades. The usual suspects for over-activation usually involves the increased concentrations of secondary messengers, $PI(3,4)P_2$ and $PI(3,4,5)P_3$, which has pioneered research towards the surrounding enzymes that modify these messengers

such as PI3K, PTEN and SHIP.[21] For instance, PI3K class-1 inhibitors have been used to treat several forms of leukemia, typically as part of combination therapies.[22,23] There has also been developments in anti-inflammatories using PI3K inhibitors to treat asthma and other related respiratory diseases.[24] PI3K inhibitors have even shown therapeutic potential used in combination therapies to treat colorectal cancer (CRC) which is considered to be one of the more lethal forms of cancer.[25] PTEN which has widely been considered a tumor suppressor protein has also been considered for modulation. It was discovered that in tissue samples of humans with ovarian cancer, PTEN is downregulated when compared to normal human tissue samples. PTEN mutations and loss of function has also been implicated in advanced forms of lung cancer such as squamous cell lung cancer (SCLC) which is a form of non-small cell lung cancer (NSCLC).[26] PTEN has been shown to be upregulated through the use of Peroxisome Proliferator-Activated Receptor gamma (PPARγ) agonists, which may provide a new method of increasing PTEN acitivity. In certain forms of NSCLC, where traditional tyrosine kinase inhibitors are rendered ineffective by EGFR mutations, these agonists have shown promise.[27] PPARγ upregulates PTEN protein expression which results in reduced activity in the PI3K/Akt pathway. Western blot experiments confirmed that in the presence of PPARγ agonists efatutazone and gefitinib, PTEN expression was increased which led to the amount of phosphorylated Akt to decrease resulting in the inactivation of the pathway. This type of PTEN upregulation has also shown promise in different cancer cell lines such MCF-7 (Breast cancer) and K562 (chronic myeloid leukemia).[28,29] This strategy has also shown some efficacy in vivo against drug resistant cancer cell lines such as K562/DOX.[28] Certain miRNA's, such as miRNA-26b and miRNA-21, have been linked to the downregulation of

PTEN.[30-32] There have been several studies that have shown that downregulating these miRNA's in vivo has had some positive effects on restoring PTEN function based off the decrease in phosphorylated Akt. These treatments have yet to show any results in a clinical setting as there are no reported ongoing trials with these aims in mind. Another enzyme in the pathway, SHIP, has also been reported as a promising drug target for various human diseases. Both the substrate and product of SHIP seemingly contribute to various disease states and depending on the disease, inhibitors or agonists could be used for therapeutic effect.[33,34]

SHIP has two main isoforms, SHIP1 and SHIP2; both of them function similarly but vary in amino-acid composition and in what type of tissues they are expressed.[35,36] SHIP1 is a 145 kDa isoform that is expressed primarily in cells of hematopoietic origin. SHIP2 is a 142 kDa isoform expressed ubiquitously in most cell lineages including skeletal muscle tissues. The two isoforms share an overall 51% similarity in amino acid sequence.[37] This includes a 54% similarity in their SH2 domains and 64% similarity in their catalytic phosphatase domains. SHIP2 also has a slightly richer proline C-terminus domain when compared to SHIP1.[38] This is intriguing because these amino acid differences allow for possibilities in SHIP paralog specific modulators.

1.3 Investigating SHIP and its Role in Cancer

The role of SHIP has long been attributed as a negative regulator of the PI3K pathway since its enzymatic activity directly opposes that of PI3K. This relationship has been widely studied and has led to the pursuit of therapeutics that target either of these enzymes in the hopes of limiting some of the downstream effectors such as AKT. SHIP, and in particular its isoform SHIP1, have been studied for their role in some forms of

leukemia such as Acute Myeloid Leukemia (AML) due to the fact it is primarily expressed in hematopoietic cells.[39,40] Hematopoietic cells include but are not limited to hematopoietic stem cells (HSC), osteoclasts, mesenchymal stem cells, and NK (natural killer) cells.[41] In AML patients, certain SHIP1 mutations (such as N508D) are found to have an increased presence in the nucleus of leukemic cells.[40] These SHIP mutants tend to have decreased enzymatic activity and without enzymatic activity the tumor suppressor effect of SHIP is not observed as this leads to increased leukemic cell proliferation. In UKE-1 cells, which are a human acute leukemia cell line, tumor growth was suppressed with the introduction of exogenous SHIP1.[42] In addition, a study conducted on over 290 AML patients concluded that there is a positive correlation with SHIP expression and prolonged survival rate.[42] With these results in mind, a potential SHIP agonist could be therapeutic in certain cases of AML where the enzymatic activity of SHIP is lacking. SHIP1 inhibitors have also shown therapeutic promise against some other blood cancers as well at least in vitro. When KG-1 and C1498 leukemia cell lines were dosed with selective SHIP1 inhibitor 3AC there was an observed drop in cancer cell viability.[43] In order to test the hypothesis that the SHIP1 inhibition was the reason for the observed cytotoxic effects, K562 cells were dosed with 3AC and no effect was observed. K562 cells are a leukemia cell line that expresses SHIP2 and PTEN but do not express SHIP1. In a similar study, SHIP1 inhibition against multiple myeloma cell lines were observed.[34] In particular, OPM2 cells when dosed with the selective SHIP1 inhibitor 3AC, underwent apoptosis which was confirmed through western blot analysis by the presence of cleaved Poly ADP-Ribose Polymerase and cleaved caspase 3 proteins. Cervical cancer is responsible for roughly 4,000 deaths every year in the United States with approximately 13,000 new cases being

discovered every year, according to the Center for Disease Control.[44] Recently in a study conducted by Zhang et al,[45] they found that in cervical cancer cell lines that the T-cell immunoglobulin and ITIM domain (TIGIT) and cluster of differentiation 155 (CD155) proteins were upregulated and a possible link to the SHIP enzyme was observed. TIGIT recruits SHIP1 through the binding of its phosphorylated ITIM motif by the SH2 domain of SHIP. Consequently, in cervical cancer cells when TIGIT and CD155 proteins are upregulated so is the SHIP protein. The association of both TIGIT with SHIP inactivates the catalytic role SHIP1 which effects various immune response pathways. These effects may include the inactivation of cytokines by its inhibition of the NF-κB transcription factor and the NF-κB pathway.[45]

Priming the immune system by inhibition of SHIP1 could potentially serve as an immunotherapy-based treatment in response to cancer such as cervical cancer where SHIP is found to be upregulated.[45] While the previous study did not specifically target SHIP, two closely related receptor proteins (TIGIT and CD155) had been targeted in an effort to access SHIP activity indirectly which is some circumstances can also be a viable strategy. A SHIP inhibitor strategy could, in theory, also achieve the same desired effect. To reaffirm that cytokine production is affected through the use of SHIP inhibitors another study probed the benefit of trained immunity therapy in a mouse model in which mice were dosed with varying levels of a *C. albicans* ranging from non-lethal to lethal. Before exposure to the fungus, the mice were dosed with 3AC, a selective SHIP1 inhibitor. The SHIP deficient mice showed a primed immune response and were resistant to lethal doses of the fungus when compared to the wild-type mice.[46] In conclusion, pulsatile SHIP inhibition promotes cytokine production due to the fact that SHIP activation deactivates

MAPK and NF-κB pathways. These effects may help direct immune response towards cancer cells as well as through other mechanisms also trigger apoptosis of cancer cells.

1.4 Investigating SHIP and its potential role in Alzheimer's Disease

Alzheimer's disease is an aggressive neurological disorder that affects roughly 40 million people worldwide.[47] This disease typically presents itself in the form of dementia amongst the elderly but can also result in the decline of other cognitive functions in more severe cases. As average life expectancy increases, one can expect the number of potential Alzheimer's cases to increase as the risk associated with AD onset increases in elderly patients. Due to this the need for therapeutics that treat Alzheimer's disease has become a pressing societal need. To discover potential therapeutics, potential targets needed to be identified and the overall pathogenesis of the disease needed to be analyzed. Genome wide association studies (GWAS) have led to an identification of a number of AD risk genes which has served as a starting benchmark in the process of developing potential therapeutics.[48-50] INPP5D was one of the genes that was implicated and found to be upregulated in Alzheimer's disease. The INPP5D gene encodes for the inositol phosphatase SHIP1, and in particular has been associated with Late Onset Alzheimer's Disease (LOAD). One study used differential gene expression analysis and found that as the disease progressed the more the gene was expressed, which one can assume means that greater SHIP1 activity is also observed.[51] Furthermore, INPP5D is expressed by microglia which could also further implicate this gene in neurodegenerative diseases such as AD.[50] In order to study INPP5D expression and its relation to Alzheimer's pathogenesis, 5xFAD transgenic mice were used as a model system. 5xFAD mice possess an amyloid pathology showing increased deposition of amyloid beta protein

persistent with that observed in AD patients and in some studies shows cognitive decline consistent with AD.[52] In 5xFAD mice, INPP5D appeared to be upregulated with plaque-associated microglia when compared to WT mice. INPP5D and its association with microglia and in particular plaque-associated microglia seem to indicate that the upregulation could have some correlation to the aggregation of these plaques. Research conducted by the Kerr group at SUNY Upstate also seemed to suggest that the possible inhibition of the SHIP1 as well as its other isoform SHIP2 could possible help stimulate microglial phagocytosis and proliferation.[53] In addition to increased proliferation, microglia were shown to have an increased lysosomal compartment size when dosed with an SHIP inhibitor and it was hypothesized that this compartmental size increase helped to further stimulate dead neuron and Aβ protein phagocytosis. In addition to INPP5D being linked to key microglial functions, the gene is also closely related to the TREM2 gene which is widely considered an Alzheimer's risk gene in itself. SHIP1 directly opposes TREM2 activity through the binding of the TREM2-DAP12 intermembrane complex through its SH2-Domain which prevents recruitment of other downstream effectors such as PI3K which also binds to DAP12.[54] TREM2, which stands for Triggering Receptor Expressed on Myeloid cells 2 is found across the membrane on myeloid cells including microglia.[55] TREM2 signaling is carried out by an adaptor protein located inside the cytosol of the cell called DAP12. After the subsequent activation by TREM2, actin rearrangement followed by microglial phagocytosis occurs. In addition to phagocytotic activity, TREM2 also affects cytokine production by also inhibiting the NF-κB transcription factor which is a trait also shared by the SHIP1 enzyme.[56] In AD-mouse models where TREM2 has decreased or

loss of function, such as TREM2 variant R47H, myeloid microglial cells are found to have a decreased presence around amyloid-beta plaques.[57]

The other major isoform of SHIP, SHIP2 which is encoded by the INPPL1 gene which is also expressed in the brain including neuronal cells.[58,59] One study found a positive correlation between levels of the amyloid-beta protein and INPPL1 gene expression which could indicate a larger role of SHIP2 in the development of AD.[60] It has been hypothesized that a pan-SHIP inhibitor that targets both isoforms of SHIP could potentially be just as useful as an isoform selective inhibitor due to the interaction that SHIP2 has with the FcγRIIB receptor. Once FcγRIIB becomes phosphorylated in neurons, this signals for amyloid beta which helps recruit SHIP2 towards the receptor. SHIP2 associating with phosphorylated FcγRIIB then leads to the phosphorylation of the protein Tau.[58] Just like the accumulation of Aβ protein, tau phosphorylation is believed to be another marker of Alzheimer's disease progression. In summary, the role SHIP plays in the development of Alzheimer's appears to be significant. The phosphoinositide's leading to downstream signaling that leads to the negative regulation of a number of related pathways, like NF-κB. In addition to the role these secondary messengers play, they can also contribute to the disease pathogenesis through their SH2 domains as they can directly binding to various receptors such as TREM2 or FcγRIIB. The binding of TREM2 by SHIP1 further dampens microglial response to amyloid plaques and the binding of SHIP2 by FcγRIIB-Aβ complex by SHIP2 contributes to the increased phosphorylation of Tau in neurons. With both of these enzymes believed to progress Alzheimer's disease, the design and application of new small molecules that modulate SHIP activity, either one or both isoforms, could prove to be a novel therapeutic for the treatment of the disease.

1.5 Targeting SHIP for Potential Therapeutics in Autoimmune Disease

Autoimmune diseases occur when immune cells target healthy normal cells like they were foreign which usually results inflammation or other undesired side effects.[61] There are over 100 autoimmune diseases including Crohn's disease, Lupus, Rheumatoid Arthritis and Multiple Sclerosis, with roughly 5-9% of the total world population possessing some form of autoimmune disorder. These diseases typically possess no cure and can only be treated to mitigate some of the side effects. In order to combat drug resistance of existing autoimmune therapies new druggable targets are constantly being identified and studied for the treatment of these autoimmune disorders. One such target is the enzyme, SHIP, with both of its major isoforms having some role in immune cell function and mobilization including B cells, neutrophils, NK and T cells. SHIP1 has been shown to interact with the FcγRIIB receptor in B cells and mast cells which affects mast cell degranulation.[62] SHIP can also bind to FCεRI on the surface of mast cells which is believed to further regulates immune response through the activation of IgE antibodies.[63,64] There was a noticeable correlation between increased PI(,3,4,5)P_3 levels and increased mast cell degranulation which further reaffirmed the role of SHIP as a negative regulator.[65] Evidence would suggest that a SHIP agonist could potentially be applied in the event of mast cell hyperactivity. In one study, cultured human mast cells and blood basophils were incubated with a selective SHIP1 inhibitor. It was discovered that upon increased doses mast cell death and lower degranulation was observed meaning that immune response was attenable but also in higher doses demonstrated some cytotoxic effects.[66] In addition to the already stated effects on mast cell

degranulation, SHIP can also affect the levels of inflammatory cytokines, such as interleukin-6(IL-6) and tumor necrosis factor alpha (TNFα).[67]

The enzyme SHIP also plays a key role in toll like receptor signaling in the immune system, which is responsible for immune responses like neutrophil migration for tissue repair.[68,69] Ways to affect neutrophil responses have been discussed when it comes to autoimmune disorders such as Ulcerative Colitis and Crohn's disease where neutrophils are typically found in high concentrations at sites of inflammation.[70] As part of the immune response, neutrophils can generate reactive oxygen species to target foreign pathogens and tumor cells.[71] Neutrophils can directly interact with other immune cells such B cells and T cells.[70,72] Neutrophils are typically found in bone marrow and also possess relatively short life spans typically in the range of one to five days. SHIP1 being expressed primarily in hematopoietic cells including bone marrow could potentially be a useful target in regulating these key immune cells. Neutrophil chemotaxis is the process by which the immune cell migrates to the affected areas. This process is orchestrated through the release of chemoattractants which lead to the polarization of the cell. Upon polarization, this stimulates actin polymerization which pushes the cell towards to the area of polarization. PI3K is believed to play a role in this process as high concentrations of its key secondary messenger product, PIP_3, is found outside near the membrane during cell polarization events.[73] In zebrafish when PI3K is deleted from the cell, neutrophil migration was severely impaired suggesting that at least in zebrafish that PI3K is essential in establishing a chemotaxis gradient.[74] Subsequently, that would mean that SHIP should naturally play a role in chemotaxis as well since SHIP hydrolyzes the product of PI3K. Using the zebrafish as a model system again, it was demonstrated that SHIP knockouts

achieved greater neutrophil motility when compared to that of wild type.[75] When the SHIP knockouts were treated with a PI3K inhibitor cell motility speed reverted back to normal. This response is intriguing because in diseases like Crohn's and Colitis where inflammation is left unchecked, SHIP could be upregulated in response in order to quell inflammation.

SHIP also is expressed in cells of macrophage lineage including osteoclasts and bone marrow derived macrophages.[76] In SHIP knockouts, proinflammatory cytokines appear to be upregulated in macrophages.[67] Endotoxin or lipopolysaccharide(LPS) stimulates immune response by triggering multiple pathways through receptors/adaptor proteins such as toll like receptor 4(TLR4), TIR-domain-containing adaptor-inducing interferon-β (TRIF) and interferon-β (IFN-β).[77] Bone marrow derived macrophages upon dosing with LPS, resulted in the increase of levels of various proinflammatory cytokines (TNFα, IL-6, IL-1β, and NO). SHIP knockouts demonstrated a greater response when compared to that of wild type BMDM's. Wild type macrophages showed an increased resistance to further doses of LPS, which could mean that in the presence of SHIP is beneficial in instances of a hyperactive immune system.[78] This opens up a role for potential SHIP agonists in diseases where proinflammatory cytokines are left unchecked.

In summary, SHIP1 is expressed in a wide variety of immune cells and is involved in various processes associated with them. The role of SHIP in the PI3K pathway appears to be that of an immune suppressor and provides an interesting target for potential autoimmune therapies. SHIP deficiencies in mice have been shown in some capacity to result in autoimmune disorders in mice.[79,80] In the case of autoimmune disorders where the immune system is hyperactive and targeting healthy tissues, an agonist of SHIP could

be used to restore a healthy balance. SHIP's involvement in the motility and migration of immune cells also make it an interesting target since any upregulation of SHIP could help potential slow the movement of existing cells to the area in addition to the previous listed effects of lowering cytokines.

1.6 Targeting SHIP for Potential Therapeutics in Diabetes and Obesity

Diabetes is a disease that stems from insulin deficiencies in the body. Glucose is unable to transport from the blood into the cells without the help of insulin which can result in cases of both high and low blood sugar levels both of which can lead to complications.[81] Diabetes affects roughly one in four adults over the age of 65 with 90-95% of cases being type 2 diabetes.[81] SHIP2, the isoform of SHIP that is encoded by the INPPL1 gene, has been linked to the progression and onset of diabetes due to its role in insulin signaling.[82] After insulin activation of PI3K, PI(3,4,5)P3 is generated which activates Akt and then further activates GLUT4, which is a glucose transporter protein involved in glucose uptake for the cell.[83] SHIP2 regulates PI(3,4,5)P3 levels by dephosphorylating at the 5'-position and opposes PI3K activity and through doing so reduces glucose uptake. In podocytes of obese zucker rats, SHIP2 is found to be overexpressed which increases insulin resistance and prevents Akt activation.[84] Inhibition of SHIP2 could potentially be a useful treatment in combating insulin resistance and preventing the onset of type 2 diabetes. Pan SHIP1/2 inhibitors showed promise in certain studies. Mice that were dosed with a pan-SHIP inhibitor showed increased insulin sensitivity as well as lower blood glucose levels when compared to the control mice.[85] In the same study, despite being fed the same high calorie diet the mice that were dosed with the same pan inhibitors also demonstrated higher metabolism and lower body fat suggesting that a potential therapy for obesity.[85]

1.7 – Summary

Both isoforms of SHIP have been demonstrated to play key roles in many cellular processes including glucose uptake, immune cell differentiation and response, proliferation and survival. Loss of regulation in these pathways may lead to disease states including certain forms of cancer, Alzheimer's disease, autoimmune disorders, and diabetes. Depending on the specific application, upregulation or downregulation of SHIP could be a therapeutic benefit. Further studies involving the development of SHIP inhibitors and agonists could potentially lead to further insights on the role SHIP plays in the progression of these diseases as well as lead to the potential discovery of novel therapeutics.

1.8 - References

1) De Craene, J.-O.; Bertazzi, D. L.; Bär, S.; Friant, S. Phosphoinositides, Major Actors in Membrane Trafficking and Lipid Signaling Pathways. *International Journal of Molecular Sciences* **2017,** *18*, 634.
2) Wymann, M. P.; Schneiter, R. Lipid signalling in disease. *Nature Reviews Molecular Cell Biology* **2008,** *9*, 162+.
3) Krajnik, A.; Brazzo, J. A.; Vaidyanathan, K.; Das, T.; Redondo-Muñoz, J.; Bae, Y. Phosphoinositide Signaling and Mechanotransduction in Cardiovascular Biology and Disease. *Frontiers in Cell and Developmental Biology* **2020,** *8*,
4) Di Paolo, G.; De Camilli, P. Phosphoinositides in cell regulation and membrane dynamics. *Nature* **2006,** *443*, 651+.
5) Jadwin, J. A.; Oh, D.; Curran, T. G.; Ogiue-Ikeda, M.; Jia, L.; White, F. M.; Machida, K.; Yu, J.; Mayer, B. J. Time-resolved multimodal analysis of Src Homology 2 (SH2) domain binding in signaling by receptor tyrosine kinases. *eLife* **2016,** *5*, e11835.
6) Klippel, A. Membrane localization of phosphatidylinositol 3-kinase is sufficient to activate multiple signal-transducing kinase pathways. *Molecular and cellular biology 16*, 4117-4127.
7) Bunney, T. D.; Katan, M. Phosphoinositide signalling in cancer: beyond PI3K and PTEN. *Nat. Rev. Cancer* **2010,** *10*, 342-352.
8) Brown, K. K.; Toker, A. The phosphoinositide 3-kinase pathway and therapy resistance in cancer. *F1000Prime Rep.* **2015,** *7*, 1-8.

9) Wojtalla, A.; Arcaro, A. Targeting phosphoinositide 3-kinase signalling in lung cancer. *Critical Reviews in Oncology/Hematology* **2011,** *80*, 278-290.
10) Zaryouh, H. Recent insights in the PI3K/Akt pathway as a promising therapeutic target in combination with EGFR-targeting agents to treat head and neck squamous cell carcinoma. *Medicinal research reviews 42*, 112-155.
11) Fruman, D. A.; Chiu, H.; Hopkins, B. D.; Bagrodia, S.; Cantley, L. C.; Abraham, R. T. The PI3K pathway in Human Disease. *Cell (Cambridge, MA, U. S.)* **2017,** *170*, 605-635.
12) Truebestein, L.; Hornegger, H.; Anrather, D.; Hartl, M.; Fleming, K. D.; Stariha, J. T. B.; Pardon, E.; Steyaert, J.; Burke, J. E.; Leonard, T. A. Structure of autoinhibited Akt1 reveals mechanism of PIP_3-mediated activation. *Proceedings of the National Academy of Sciences* **2021,** *118*, e2101496118.
13) Peng, Y.; Wang, Y.; Zhou, C.; Mei, W.; Zeng, C. PI3K/Akt/mTOR Pathway and Its Role in Cancer Therapeutics: Are We Making Headway? *Frontiers in Oncology* **2022,** *12*,
14) Taylor, J.; Abdel-Wahab, O. PTEN isoforms with dual and opposing function. *Nature Cell Biology* **2019,** *21*, 1306+.
15) Alfieri, R.; Giovannetti, E.; Bonelli, M.; Cavazzoni, A. New Treatment Opportunities in Phosphatase and Tensin Homolog (PTEN)-Deficient Tumors: Focus on PTEN/Focal Adhesion Kinase Pathway. *Frontiers in Oncology* **2017,** *7*,
16) Mondal, S. K.; Sen, M. K. Loss of phosphatase activity in PTEN (phosphatase and tensin homolog deleted on chromosome ten) results in endometrial carcinoma in humans: An in-silico study. *Heliyon* **2020,** *6*, e03106.
17) Yin, Y.; Shen, W. H. PTEN: a new guardian of the genome. *Oncogene* **2008,** *27*, 5443+.
18) Gozzelino, L.; De Santis, M. C.; Gulluni, F.; Hirsch, E.; Martini, M. PI(3,4)P2 Signaling in Cancer and Metabolism. *Frontiers in Oncology* **2020,** *10*,
19) Nelson, N.; Razeto, A.; Gilardi, A.; Grättinger, M.; Kirchmair, J.; Jücker, M. AKT1 and PTEN show the highest affinities among phosphoinositide binding proteins for the second messengers PtdIns(3,4,5)P3 and PtdIns(3,4)P2. *Biochemical and Biophysical Research Communications* **2021,** *568*, 110-115.
20) Hawkins, P. T.; Stephens, L. R. Emerging evidence of signalling roles for PI(3,4)P2 in Class I and II PI3K-regulated pathways. *Biochemical Society Transactions* **2016,** *44*, 307-314.
21) Kerr, W. G. Inhibitor and activator: dual functions for SHIP in immunity and cancer. *Annals of the New York Academy of Sciences* **2011,** *1217*, 1-17.
22) Shiri Heris, R.; Pourbagheri-Sigaroodi, A.; Yousefi, A.-M.; Bashash, D. The Superior Cytotoxicity of Dual Targeting of BCR/ABL and PI3K in K562 Cells: Proposing a Novel Therapeutic Potential for the Treatment of CML. *Indian Journal of Hematology and Blood Transfusion* **2022,** *38*, 51-60.
23) Bohn, J.-P. New actionable targets and investigational drugs in chronic lymphocytic leukemia. *memo - Magazine of European Medical Oncology* **2022,** *15*, 53-57.
24) Sadiq, M. W.; Asimus, S.; Belvisi, M. G.; Brailsford, W.; Fransson, R.; Fuhr, R.; Hagberg, A.; Hashemi, M.; Jellesmark Jensen, T.; Jonsson, J.; Keen, C.; Körnicke, T.; Kristensson, C.; Mäenpää, J.; Necander, S.; Nemes, S.; Betts, J.

Characterisation of pharmacokinetics, safety and tolerability in a first-in-human study for AZD8154, a novel inhaled selective PI3Kγδ dual inhibitor targeting airway inflammatory disease. *British Journal of Clinical Pharmacology* **2022,** *88*, 260-270.
25) Laura Rosa, M.; Nicotra, A.; Turdo, A.; Gaggianesi, M.; Bianca, P.; Simone Di, F.; Sardina, D. S.; Veschi, V.; Signore, M.; Beyes, S.; Fagnocchi, L.; Fiori, M. E.; Bongiorno, M. R.; Melania Lo, I.; Pillitteri, I.; Ganduscio, G.; Gulotta, G.; Medema, J. P.; Zippo, A.; Todaro, M.; Ruggero De, M.; Stassi, G. PI3K-driven HER2 expression is a potential therapeutic target in colorectal cancer stem cells. *Gut* **2022,** *71*, 119-128.
26) Gkountakos, A.; Sartori, G.; Falcone, I.; Piro, G.; Ciuffreda, L.; Carbone, C.; Tortora, G.; Scarpa, A.; Bria, E.; Milella, M.; Rosell, R.; Corbo, V.; Pilotto, S. PTEN in Lung Cancer: Dealing with the Problem, Building on New Knowledge and Turning the Game Around. *Cancers* **2019,** *11*,
27) Ni, J.; Zhou, L.-l.; Ding, L.; Zhao, X.; Cao, H.; Fan, F.; Li, H.; Lou, R.; Du, Y.; Dong, S.; Liu, S.; Wang, Z.; Ma, R.; Wu, J.; Feng, J. PPARγ agonist efatutazone and gefitinib synergistically inhibit the proliferation of EGFR-TKI-resistant lung adenocarcinoma cells via the PPARγ/PTEN/Akt pathway. *Experimental Cell Research* **2017,** *361*, 246-256.
28) Yousefi, B.; Azimi, A.; Majidinia, M.; Shafiei-Irannejad, V.; Badalzadeh, R.; Baradaran, B.; Zarghami, N.; Samadi, N. Balaglitazone reverses P-glycoprotein-mediated multidrug resistance via upregulation of PTEN in a PPARγ-dependent manner in leukemia cells. *Tumor Biology* **2017,** *39*, 1010428317716501.
29) Teresi, R. E.; Shaiu, C.-W.; Chen, C.-S.; Chatterjee, V. K.; Waite, K. A.; Eng, C. Increased PTEN expression due to transcriptional activation of PPARγ by Lovastatin and Rosiglitazone. *International Journal of Cancer* **2006,** *118*, 2390-2398.
30) Li, C.; Xu, B.; Miu, X.; Deng, Z.; Liao, H.; Hao, L. Inhibition of miRNA-21 attenuates the proliferation and metastasis of human osteosarcoma by upregulating PTEN. *Experimental and Therapeutic Medicine* **2018,** *15*, 1036+.
31) Wang, S.; Guo, D.; Li, C. Downregulation of miRNA-26b inhibits cancer proliferation of laryngeal carcinoma through autophagy by targeting ULK2 and inactivation of the PTEN/AKT pathway. *Oncology Reports* **2017,** *38*, 1679+.
32) Simpson, L. J.; Patel, S.; Bhakta, N. R.; Choy, D. F.; Brightbill, H. D.; Ren, X.; Wang, Y.; Pua, H. H.; Baumjohann, D.; Montoya, M. M.; Panduro, M.; Remedios, K. A.; Huang, X.; Fahy, J. V.; Arron, J. R.; Woodruff, P. G.; Ansel, K. M. A microRNA upregulated in asthma airway T cells promotes TH2 cytokine production. *Nature Immunology* **2014,** *15*, 1162-70.
33) Blunt, M. D.; Ward, S. G. Targeting PI3K isoforms and SHIP in the immune system: new therapeutics for inflammation and leukemia. *Current Opinion in Pharmacology* **2012,** *12*, 444-451.
34) Fuhler, G. M.; Brooks, R.; Toms, B.; Iyer, S.; Gengo, E. A.; Park, M.-Y.; Gumbleton, M.; Viernes, D. R.; Chisholm, J. D.; Kerr, W. G. Therapeutic Potential of SH2 Domain-Containing Inositol-5′-Phosphatase 1 (SHIP1) and SHIP2 Inhibition in Cancer. *Molecular Medicine* **2012,** *18*, 65-75.
35) Sly, L. M.; Rauh, M. J.; Kalesnikoff, J.; Büchse, T.; Krystal, G. SHIP, SHIP2, and PTEN activities are regulated in vivo by modulation of their protein levels: SHIP is

up-regulated in macrophages and mast cells by lipopolysaccharide. *Experimental Hematology* **2003,** *31*, 1170-1181.
36) March, M. E.; Lucas, D. M.; Aman, M. J.; Ravichandran, K. S. p135 Src Homology 2 Domain-containing Inositol 5′-Phosphatase (SHIPβ) Isoform Can Substitute for p145 SHIP in FcγRIIB1-mediated Inhibitory Signaling in B Cells*. *Journal of Biological Chemistry* **2000,** *275*, 29960-29967.
37) Zhang, Y.; Wavreille, A.-S.; Kunys, A. R.; Pei, D. The SH2 Domains of Inositol Polyphosphate 5-Phosphatases SHIP1 and SHIP2 Have Similar Ligand Specificity but Different Binding Kinetics. *Biochemistry* **2009,** *48*, 11075-11083.
38) Pesesse, X.; Deleu, S.; De Smedt, F.; Drayer, L.; Erneux, C. Identification of a Second SH2-Domain-Containing Protein Closely Related to the Phosphatidylinositol Polyphosphate 5-Phosphatase SHIP. *Biochemical and Biophysical Research Communications* **1997,** *239*, 697-700.
39) Hao, F.; Wang, C.; Sholy, C.; Cao, M.; Kang, X. Strategy for Leukemia Treatment Targeting SHP-1,2 and SHIP. *Frontiers in Cell and Developmental Biology* **2021,** *9*,
40) Nalaskowski, M. M. Nuclear accumulation of SHIP1 mutants derived from AML patients leads to increased proliferation of leukemic cells. *Cellular signalling 49*, 87-94.
41) Iyer, S.; Margulies, B. S.; Kerr, W. G. Role of SHIP1 in bone biology. *Annals of the New York Academy of Sciences* **2013,** *1280*, 11-14.
42) Tager, M.; Horn, S.; Latuske, E.; Ehm, P.; Schaks, M.; Nalaskowski, M.; Fehse, B.; Fiedler, W.; Stocking, C.; Wellbrock, J.; Jucker, M. SHIP1, but not an AML-derived SHIP1 mutant, suppresses myeloid leukemia growth in a xenotransplantation mouse model. *Gene Therapy* **2017,** *24*, 749.
43) Brooks, R.; Fuhler, G. M.; Iyer, S.; Smith, M. J.; Park, M.-Y.; Paraiso, K. H. T.; Engelman, R. W.; Kerr, W. G. SHIP1 Inhibition Increases Immunoregulatory Capacity and Triggers Apoptosis of Hematopoietic Cancer Cells. *The Journal of Immunology* **2010,** *184*, 3582.
44) Cervical Cancer Statistics. https://www.cdc.gov/cancer/cervical/statistics/index.htm
45) Liu, L.; Wang, A.; Liu, X.; Han, S.; Sun, Y.; Zhang, J.; Guo, L.; Zhang, Y. Blocking TIGIT/CD155 signalling reverses CD8+ T cell exhaustion and enhances the antitumor activity in cervical cancer. *Journal of Translational Medicine* **2022,** *20*, 280.
46) Saz-Leal, P.; del Fresno, C.; Brandi, P.; Martínez-Cano, S.; Dungan, O. M.; Chisholm, J. D.; Kerr, W. G.; Sancho, D. Targeting SHIP-1 in Myeloid Cells Enhances Trained Immunity and Boosts Response to Infection. *Cell Reports* **2018,** *25*, 1118-1126.
47) Golde, T. E. Alzheimer's disease – the journey of a healthy brain into organ failure. *Molecular Neurodegeneration* **2022,** *17*, 18.
48) Frost, G. R.; Jonas, L. A.; Li, Y.-M. Friend, Foe or Both? Immune Activity in Alzheimer's Disease. *Frontiers in Aging Neuroscience* **2019,** *11*,
49) Sierksma, A.; Lu, A.; Mancuso, R.; Fattorelli, N.; Thrupp, N.; Salta, E.; Zoco, J.; Blum, D.; Buée, L.; De Strooper, B.; Fiers, M. Novel Alzheimer risk genes

determine the microglia response to amyloid-β but not to TAU pathology. *EMBO Molecular Medicine* **2020,** *12*, e10606.
50) Panitch, R.; Hu, J.; Xia, W.; Bennett, D. A.; Stein, T. D.; Farrer, L. A.; Jun, G. R. Blood and brain transcriptome analysis reveals APOE genotype-mediated and immune-related pathways involved in Alzheimer disease. *Alzheimer's Research & Therapy* **2022,** *14*, 30.
51) Tsai, A. P. INPP5D expression is associated with risk for Alzheimer's disease and induced by plaque-associated microglia. *Neurobiology of disease 153*,
52) Oblak, A. L.; Lin, P. B.; Kotredes, K. P.; Pandey, R. S.; Garceau, D.; Williams, H. M.; Uyar, A.; O'Rourke, R.; O'Rourke, S.; Ingraham, C.; Bednarczyk, D.; Belanger, M.; Cope, Z. A.; Little, G. J.; Williams, S.-P. G.; Ash, C.; Bleckert, A.; Ragan, T.; Logsdon, B. A.; Mangravite, L. M.; Sukoff Rizzo, S. J.; Territo, P. R.; Carter, G. W.; Howell, G. R.; Sasner, M.; Lamb, B. T. Comprehensive Evaluation of the 5XFAD Mouse Model for Preclinical Testing Applications: A MODEL-AD Study. *Frontiers in Aging Neuroscience* **2021,** *13*,
53) Pedicone, C.; Fernandes, S.; Dungan, O. M.; Dormann, S. M.; Viernes, D. R.; Adhikari, A. A.; Choi, L. B.; De Jong, E. P.; Chisholm, J. D.; Kerr, W. G. Pan-SHIP1/2 inhibitors promote microglia effector functions essential for CNS homeostasis. *J. Cell Sci.* **2020,** *133*, jcs238030.
54) Peng, Q.; Malhotra, S.; Torchia, J. A.; Kerr, W. G.; Coggeshall, K. M.; Humphrey, M. B. TREM2- and DAP12-Dependent Activation of PI3K Requires DAP10 and Is Inhibited by SHIP1. *Science Signaling* **2010,** *3*, ra38-ra38.
55) Malik, M.; Parikh, I.; Vasquez, J. B.; Smith, C.; Tai, L.; Bu, G.; LaDu, M. J.; Fardo, D. W.; Rebeck, G. W.; Estus, S. Genetics ignite focus on microglial inflammation in Alzheimer's disease. *Molecular Neurodegeneration* **2015,** *10*, 52.
56) Yao, H.; Coppola, K.; Schweig, J. E.; Crawford, F.; Mullan, M.; Paris, D. Distinct Signaling Pathways Regulate TREM2 Phagocytic and NFκB Antagonistic Activities. *Frontiers in Cellular Neuroscience* **2019,** *13*,
57) Cheng-Hathaway, P. J.; Reed-Geaghan, E. G.; Jay, T. R.; Casali, B. T.; Bemiller, S. M.; Puntambekar, S. S.; von Saucken, V. E.; Williams, R. Y.; Karlo, J. C.; Moutinho, M.; Xu, G.; Ransohoff, R. M.; Lamb, B. T.; Landreth, G. E. The Trem2 R47H variant confers loss-of-function-like phenotypes in Alzheimer's disease. *Molecular Neurodegeneration* **2018,** *13*, 29.
58) Kam, T.-I.; Park, H.; Gwon, Y.; Song, S.; Kim, S.-H.; Moon, S. W.; Jo, D.-G.; Jung, Y.-K. FcγRIIb-SHIP2 axis links Aβ to tau pathology by disrupting phosphoinositide metabolism in Alzheimer's disease model. *eLife* **2016,** *5*, e18691.
59) Ando, K.; Erneux, C.; Homa, M.; Houben, S.; de Fisenne, M.-A.; Brion, J.-P.; Leroy, K. Dysregulation of Phosphoinositide 5-Phosphatases and Phosphoinositides in Alzheimer's Disease. *Frontiers in Neuroscience* **2021,** *15*,
60) Mostafavi, S.; Gaiteri, C.; Sullivan, S. E.; White, C. C.; Tasaki, S.; Xu, J.; Taga, M. A molecular network of the aging human brain provides insights into the pathology and cognitive decline of Alzheimer's disease. *Nature Neuroscience* **2018,** *21*, 811+.
61) Autoimmune Diseases. https://www.niehs.nih.gov/health/topics/conditions/autoimmune/index.cfm (October 23),

62) Parry, R. V.; Harris, S. J.; Ward, S. G. Fine tuning T lymphocytes: A role for the lipid phosphatase SHIP-1. *Biochimica et Biophysica Acta (BBA) - Proteins and Proteomics* **2010,** *1804*, 592-597.
63) Huber, M. Activation/Inhibition of mast cells by supra-optimal antigen concentrations. *Cell communication and signaling* **2013,** *11*,
64) Ono, M.; Bolland, S.; Tempst, P.; Ravetch, J. V. Role of the inositol phosphatase SHIP in negative regulation of the immune system by the receptor Fc gamma RIIB. *Nature* **1996,** *383*, 263-6.
65) Huber, M.; Hughes, M. R.; Krystal, G. Thapsigargin-Induced Degranulation of Mast Cells Is Dependent on Transient Activation of Phosphatidylinositol-3 Kinase. *The Journal of Immunology* **2000,** *165*, 124-133.
66) Rasmussen, P.; Spillner, E.; Hoffmann, H. J. Inhibiting phosphatase SHIP-1 enhances suboptimal IgE-mediated activation of human blood basophils but inhibits IgE-mediated activation of cultured human mast cells. *Immunology Letters* **2019,** *210*, 40-46.
67) Dobranowski, P.; Sly, L. M. SHIP negatively regulates type II immune responses in mast cells and macrophages. *Journal of Leukocyte Biology* **2018,** *103*, 1053-1064.
68) Gabhann, J. N.; Higgs, R.; Brennan, K.; Thomas, W.; Damen, J. E.; Ben Larbi, N.; Krystal, G.; Jefferies, C. A. Absence of SHIP-1 Results in Constitutive Phosphorylation of Tank-Binding Kinase 1 and Enhanced TLR3-Dependent IFN-β Production. *The Journal of Immunology* **2010,** *184*, 2314-2320.
69) Strassheim, D.; Kim, J.-Y.; Park, J.-S.; Mitra, S.; Abraham, E. Involvement of SHIP in TLR2-Induced Neutrophil Activation and Acute Lung Injury. *The Journal of Immunology* **2005,** *174*, 8064-8071.
70) Ostanin, D. V.; Kurmaeva, E.; Furr, K.; Bao, R.; Hoffman, J.; Berney, S.; Grisham, M. B. Acquisition of Antigen-Presenting Functions by Neutrophils Isolated from Mice with Chronic Colitis. *The Journal of Immunology* **2012,** *188*, 1491-1502.
71) Shelef, M. A.; Tauzin, S.; Huttenlocher, A. Neutrophil migration: moving from zebrafish models to human autoimmunity. *Immunological Reviews* **2013,** *256*, 269-281.
72) Kruger, P. Neutrophils: Between Host Defence, Immune Modulation, and Tissue Injury. *PLoS pathogens* **2015,** *11*,
73) Gambardella, L.; Vermeren, S. Molecular players in neutrophil chemotaxis—focus on PI3K and small GTPases. *Journal of Leukocyte Biology* **2013,** *94*, 603-612.
74) Yoo, S. K.; Deng, Q.; Cavnar, P. J.; Wu, Y. I.; Hahn, K. M.; Huttenlocher, A. Differential Regulation of Protrusion and Polarity by PI(3)K during Neutrophil Motility in Live Zebrafish. *Developmental Cell* **2010,** *18*, 226-236.
75) Lam, P.-y.; Yoo, S. K.; Green, J. M.; Huttenlocher, A. The SH2-domain-containing inositol 5-phosphatase (SHIP) limits the motility of neutrophils and their recruitment to wounds in zebrafish. *Journal of Cell Science* **2012,** *125*, 4973-4978.
76) Moon, J. B.; Kim, J. H.; Kim, K.; Youn, B. U.; Ko, A.; Lee, S. Y.; Kim, N. Akt Induces Osteoclast Differentiation through Regulating the GSK3β/NFATc1 Signaling Cascade. *The Journal of Immunology* **2012,** *188*, 163-169.
77) Piao, W.; Song, C.; Chen, H.; Quevedo Diaz, M. A.; Wahl, L. M.; Fitzgerald, K. A.; Li, L.; Medvedev, A. E. Endotoxin tolerance dysregulates MyD88- and Toll/IL-1R

domain-containing adapter inducing IFN-β-dependent pathways and increases expression of negative regulators of TLR signaling. *Journal of Leukocyte Biology* **2009,** *86*, 863-875.

78) Sly, L. M.; Rauh, M. J.; Kalesnikoff, J.; Song, C. H.; Krystal, G. LPS-Induced Upregulation of SHIP Is Essential for Endotoxin Tolerance. *Immunity* **2004,** *21*, 227-239.

79) Kerr, W. G.; Park, M.-Y.; Maubert, M.; Engelman, R. W. SHIP deficiency causes Crohn's disease-like ileitis. *Gut* **2011,** *60*, 177.

80) Maxwell, M. J.; Srivastava, N.; Park, M. Y.; Tsantikos, E.; Engelman, R. W.; Kerr, W. G.; Hibbs, M. L. Ship-1 deficiency in the myeloid compartment is insufficient to induce myeloid expansion or chronic inflammation. *Genes and Immunity* **2014,** *15*, 233+.

81) What is Diabetes? https://www.niddk.nih.gov/health-information/diabetes/overview/what-is-diabetes (10/28),

82) Dyson, J. M.; Fedele, C. G.; Davies, E. M.; Becanovic, J.; Mitchell, C. A., Phosphoinositide Phosphatases: Just as Important as the Kinases. In *Phosphoinositides I: Enzymes of Synthesis and Degradation*, Balla, T.; Wymann, M.; York, J. D., Eds. Springer Netherlands: Dordrecht, 2012; pp 215-279.

83) Kagawa, S.; Sasaoka, T.; Yaguchi, S.; Ishihara, H.; Tsuneki, H.; Murakami, S.; Fukui, K.; Wada, T.; Kobayashi, S.; Kimura, I.; Kobayashi, M. Impact of SRC homology 2-containing inositol 5'-phosphatase 2 gene polymorphisms detected in a Japanese population on insulin signaling. *J Clin Endocrinol Metab* **2005,** *90*, 2911-9.

84) Hyvönen, M. E.; Saurus, P.; Wasik, A.; Heikkilä, E.; Havana, M.; Trokovic, R.; Saleem, M.; Holthöfer, H.; Lehtonen, S. Lipid phosphatase SHIP2 downregulates insulin signalling in podocytes. *Molecular and Cellular Endocrinology* **2010,** *328*, 70-79.

85) Srivastava, N. A small-molecule inhibitor of SHIP1 reverses age- and diet-associated obesity and metabolic syndrome. *JCI Insight 1*,

Chapter 2: Synthetic Studies on Small Molecule SHIP Modulators

Abstract

The SH2-domain containing inositol phosphatases (SHIP) plays a key role in the PI3K cell signaling pathway. Misregulation of the concentration of either or both the product and substrate of SHIP has been implicated in a number of disease states which has led to a focused research effort in the discovery of SHIP agonists and antagonists. Due to structural differences between SHIP paralogs, isoform selective small molecules may be developed, which may provide methods to further interrogate the biology of this pathway in different cell types. In some cases, pan-SHIP inhibitors may also prove to be useful, particularly in areas of where drug resistance can quickly develop. Several tactics have been used to find new small molecules with the aim of targeting SHIP, including library screening and virtual screening. The aim of this research was to develop new small molecule SHIP modulators and improve synthetic routes to these structures.

2.1 SHIP Phosphatase, Proposed Mechanism and Structural Insights

In order to attenuate SHIP phosphatase activity effectively through the use of small molecules, knowledge of the structure of the enzyme active site and position of key amino acid residues was vital. This information also could be used to provide an understanding the enzyme mechanism. Through bioinformatic analysis of amino acid sequences from the human proteome it was discovered that the eukaryotic 5'-phosphatases have a conserved phosphatase domain similar to that of Apurinic/Apyrimidinic base excision repair endonucleases (AP endonucleases).[1] The mechanisms of these DNA repair enzymes have been extensively studied and it is believed that 5'-phosphatases like SHIP follow a similar mechanism. This is considered an associative mechanism where the phosphate first coordinates to the metal ion in the active site (which acts as a Lewis acid) while a nearby aspartic acid sidechain directs a water molecule to the phosphate, promoting hydrolysis.[2,3] SHIP1 and SHIP2 both possess a metal binding site inside the active site, and it is believed that a Mg^{2+} ion primarily occupies this site. The active site is rich in polar residues such as aspartic acids, asparagines and arginines that help stabilize the polar phosphate group and also preorganize the participants for the hydrolysis.[4] The proposed mechanism using the SHIP2 active site is shown below in **Figure 2.1** where the magnesium ion first coordinates to the 5'-phosphate.[5] A nearby aspartic acid residue (Asp587 in SHIP1 and Asp586 in SHIP2) then directs a water molecule for nucleophilic attack on the phosphate.[6] This results in a magnesium bound $PI(3,4)P_2$ and a free phosphate counterion. The newly formed products are then released through proton transfer from any of the nearby residues, such as Asp586.

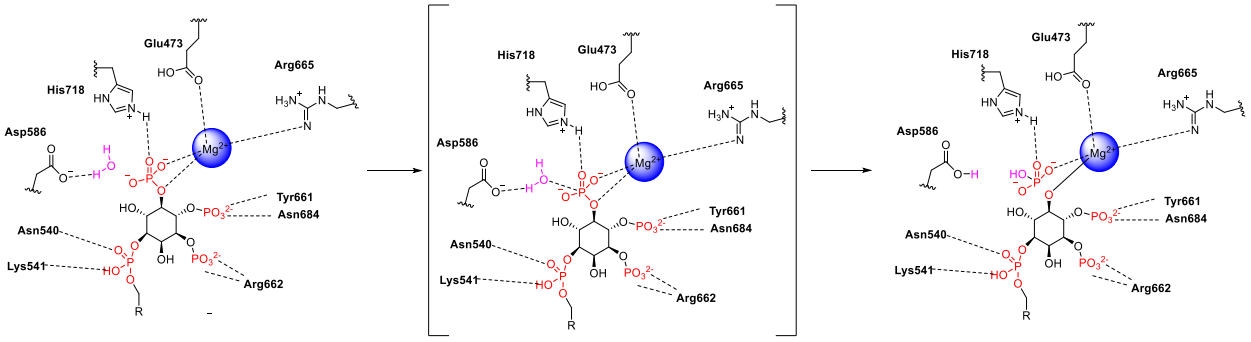

Figure 2.1: Mg^{2+} catalyzed cleavage of the 5'-phosphate by SHIP2

Inositol 5'-phosphatases demonstrate a high degree of specificity for the PI(3,4,5)P_3 substrate in large part due to the P4-interacting motif (P4IM) that is present in their C2 domains.[7,8] For the most part the P4IM loop is highly conserved across the phosphatases, however, SHIP1 and SHIP2 have an additional 7 amino acid residues in their P4IM loop. When comparing the P4-interacting motif in SHIP1 and SHIP2, the SHIP2 loop is slightly more rigid containing four prolines as opposed to three in SHIP1. The SHIP2 loop is also is slightly more polar with some subtle changes such as a tyrosine/lysine being present in SHIP1 vs a threonine/arginine in SHIP2.[7] Molecular dynamics simulations predict that when the substrate is bound inside the active site the P4IM loop folds over the 4'-phosphate of the inositol ring making several contacts between the amino acid sidechains and the 3'-phosphate.[9] Several crystal structures of sections of the SHIP enzymes have been reported with some including a catalytically active phosphatase domain, and these structures have proven to be useful when it comes to molecular modeling and docking studies with small molecules.[5,7,10] To this date no crystal structure of a fully intact SHIP protein has been reported, evidently the large size of the protein (~150 kDa) and the presence of the SH2 domain makes the formation of single crystals difficult.

2.2 Discovery of SHIP Antagonists

One of the first SHIP antagonists, 3α-aminocholestane (3AC, **2.1**), was discovered by the Kerr research group at SUNY Upstate. Screening of a small molecule library from the NIH using a fluorescence polarization assay that was adapted to test for recombinant SHIP1 activity ultimately led to the discovery of **2.1**.[11] This inhibitor possesses a dihydrocholesterol based steroid scaffold with an amine at the C3 position of the steroid **(Figure 2.2).**

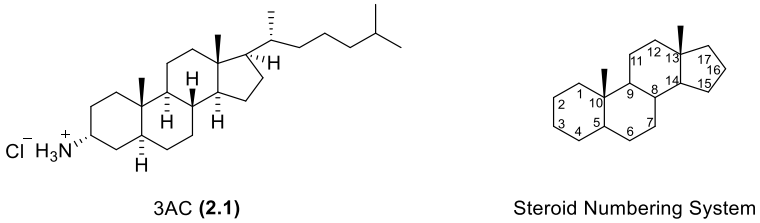

3AC **(2.1)** Steroid Numbering System

Figure 2.2: 3AC (**2.1**) and Steroid Numbering System

3AC (**2.1**) was shown to be a selective inhibitor of SHIP1, with other 5' inositol phosphatases including SHIP2 not being significantly effected by the molecule. 3AC has shown the capability to induce apoptosis of cancer cells, including multiple myeloma (MM) and acute myeloid leukemia cell lines.[11,12] Buchner and coworkers also discovered that SHIP1 was upregulated in chronic lymphocytic leukemia (CLL) B-cells and hypothesized SHIP1 inhibition should also induce apoptosis in CLL affected cells.[13] To test their hypothesis, MEC-1 and EHEB cells were treated with 3AC (**2.1**) and apoptosis was observed. MEC-1 and EHEB are cell lines derived from B cell chronic lymphocytic leukemia and are often used as model systems for CLL.[14] SHIP1 inhibition had no cytotoxic effects when applied to normal healthy B cells which shows promise towards the therapeutic potential of SHIP.

The same high through-put screen that discovered 3AC (**2.1**) also revealed a tryptamine (**2.4**) and two quinoline inhibitors NSC13480 (**2.2**) and NSC305787 (**2.3**)) of SHIP.[12] The quinoline inhibitors were derived from a program associated with the development of new antimalarial therapeutics at Walter Reed Medical Center. The program ultimately led to the discovery of mefloquine which in addition to its anti-malaria properties has also demonstrated anti-cancer properties. This led to the investigation of NSC13480 (**2.2**) and NSC305787 (**2.3**) (shown in **Figure 2.3**), which were found to be pan-SHIP1/2 inhbitors.[15] The tryptamine K103 (**2.4**), also a pan-SHIP1/2 inhibitor was identified from the same high throughput screen. Later work led to the synthesis of K149 (**2.5**), a second generation pan-SHIP1/2 inhibitor.[16] Compound **2.5** displayed fewer side effects when delivered in vivo when compared to K103 and showed promise in vitro against the colorectal cancer cell lines, HCT116 and CACO-2.[17] Upon treatment with K149, cancer cell viability was diminished. More recently, K149 has drawn interest in studies involving Alzheimer's disease since inhibition of both SHIP isoforms has been shown to increase microglial cell proliferation and increase amyloid beta fragment 1-42 (AB_{1-42}) phagocytosis.[18]

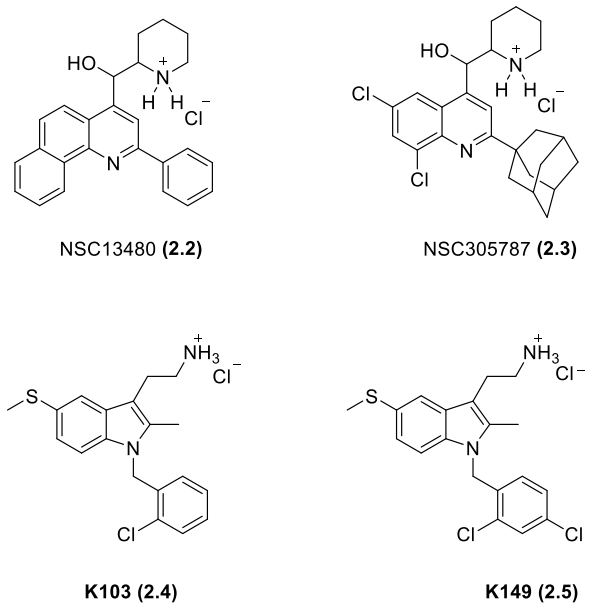

Figure 2.3: Quinoline and Tryptamine Based Pan-SHIP1/2 Inhibitors

Several SHIP2 selective inhibitors based on a thiophene core have also been reported. These molecules were first discovered by Suwa and co-workers at Astellas Pharmaceuticals.[19,20] These inhibitors were described as potential diabetes treatments with their observed effect of increased glucose uptake in cells. It was proposed that glucose consumption was increased due to the upregulation of glucose transporter protein type 1 (GLUT1) which allows for glucose to be metabolized by transporting the sugar across cell membranes.[20,21] In addition to increased glucose uptake, AS1949490 has also been tested in vitro on several breast cancer cell lines for its effect on cell migration.[22] Cell migration velocity was shown to be decreased in MDA-MB-231, MCF7, MDA-MB-468 and BT-549 cell lines which are all breast cancer cell lines that express SHIP2.[22] Decreased cell migration is believed to help prevent cancer metastasis. While these results are promising, thiophene based drugs have several drawbacks due to the fact they are readily oxidized by cytochrome P450.[23] Cytochrome P450 can either directly oxidize the sulfur or epoxidize the alkene of the thiophene and it is unclear which

metabolite predominates; often both are formed.[23] Both metabolites are considered toxic due to their electrophilic nature and the possibility for them to act as alkylating agents. More development is likely needed in these molecules to create clinically useful SHIP2 inhibitors.

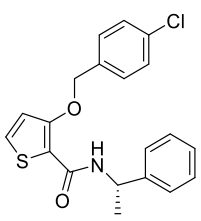

AS1949490 **(2.6)**

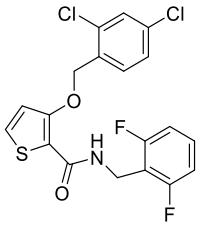

AS1938909 **(2.7)**

Figure 2.4: AS1949490 and AS1938909

Other groups have also been active in searching for SHIP inhibitors. For example, a high throughput screen conducted by Lim et al. identified crizotinib (**2.8)** as a SHIP2 selective inhibitor. Crizotinib (**2.8**) is already approved for clinical use as an anticancer drug, and displayed an IC_{50} value of 5.5 µM against SHIP2. Crizotinib was docked *in silico* inside the active site of SHIP2 using a previously reported crystal structure that resulted from co-crystallization with biphenyl 2,3',4,5',6- pentakisphosphate, a known SHIP2 inhibitor.[8] Upon docking it was revealed that **2.8** displayed poor docking scores due to many unfavorable interactions inside the binding pocket, especially regarding the piperidine ring and a serine sidechain (S435).[24] An analog program was then initiated to develop a more potent SHIP2 based on the pyridine core of **2.8**.

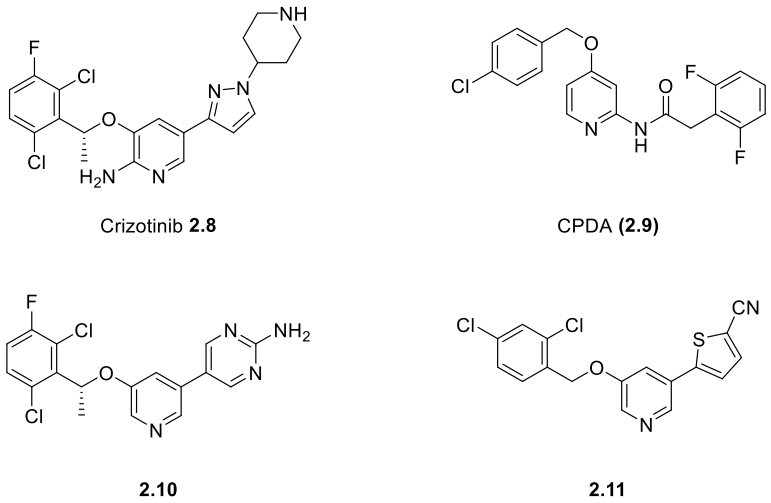

Figure 2.5: Pyridine motif-containing SHIP2 Inhibitors

Pyridine based SHIP inhibitors have been previously reported for use in ameliorating insulin resistance (see **2.9** in **Figure 2.5**).[25] The pyridine-based motif is one that was shared with crizotinib which led Lim and coworkers to investigate further SAR relationships around that core.[24,25] Upon doing so, they identified pyridines **2.10** and **2.11** as more active SHIP2 inhibitors with IC_{50} values of 2.0 μM and 3.2 μM respectively. Compound **2.10** swapped the pyrazole in crizotinib with a 2-aminopyrimidine and was by far the most potent inhibitor they discovered, however, this heterocycle displayed some problems with toxicity. Surprisingly, compound **2.11** showed better cell viability then **2.10** and crizotinib despite possessing a thiophene which is widely considered mutagenic and toxic. The newly discovered compounds were tested for their ability to block GSK3β activation through SHIP inhibition. GSK3β has been implicated as one of the major factors in tau hyperphosphorylation so modulating its activity through inhibition of SHIP2 can be seen as a potential Alzheimer's therapeutic.[24] Both compounds lowered levels of phosphorylated GSK3β and compound **2.10** displayed excellent pharmacokinetic

properties with its ability to cross the blood-brain barrier which is considered nearly essential for most Alzheimer's drug candidates.[24]

Recently, it was reported that sulfonanilides can bind to the active site of SHIP2, with compounds **2.12** and **2.13** being most potent inhibitors reported from that study.[26] In vitro assays revealed that **2.12** and **2.13** had IC_{50} values of 41.2 µM and 7.02 µM. Both analogs were tolerated well in vitro up to concentrations of 300 µM, with sulfonanilide **2.13** demonstrating no cytotoxic effects before 200 µM.[26] In addition to low toxicity, both analogs exhibited the ability to increase glucose uptake presumably through a mechanism associated with the GLUT4 transporter protein which was shown to have an increased presence around the cell membranes of L6-myotubes.[26]

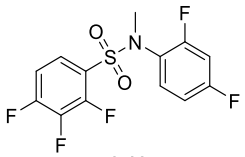

2.12

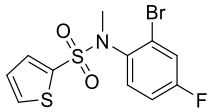

2.13

Figure 2.6: Sulfonanilide SHIP2 Inhibitors

In summary, several isoform selective SHIP2 inhibitors have been reported in the literature, utilizing sulfonanilides (**2.12, 2.13**), thiophene (**2.6, 2.7**) and pyridine (**2.8 – 2.11**) cores.[19,20,24,26] The SHIP1 selective inhibitor, 3AC (**2.1**), is one of the few SHIP1 selective inhibitors reported with research ongoing in this area to discover new SHIP1 selective inhibitors.[11] Several non-paralog specific dual inhibitors of SHIP, such as quinolines (like **2.2** and **2.3**) and tryptamine based structures (like **2.4**) have also been reported in literature.[15,17,18] SHIP inhibition appears to have a wide range of uses depending on which enzyme isoform is targeted. SHIP2 inhibition may be useful in ameliorating insulin resistance and helping to improve glucose uptake. Both pan inhibition and SHIP2 inhibition appear to also have some therapeutic potential for the treatment of

Alzheimer's disease. SHIP1 appears to have some benefit on triggering apoptotic response to hematologic cancer cells. Future work needs to be done in this area to help solidify SHIP inhibition as a target for a pharmaceutical. This includes finding more paralog specific inhibitors, especially for SHIP1, increasing their potency, and also finding more potent pan-SHIP1/2 inhibitors.

2.3 Discovery of SHIP Agonists

SHIP agonists are also of interest to the biomedical community, as these molecules could lower the concentration of $PI(3,4,5)P_3$ and modify PI3K signaling by a novel mechanism. The first SHIP1 agonist leads were discovered by screening natural product extracts by the Andersen group.[27] One SHIP1 agonist found from this screening was pelorol (**2.14** in **Figure 2.7**) which was identified from a methanol extract of the sponge *Dactylospongia elegans*. Purified pelorol (**2.14**) when tested in a colorimetric enzyme assay showed a 2-fold activity increase at 5 μg/mL. However, due to the ethical concerns of harvesting these sponges (they are not very abundant) and the scarcity of the natural product in the extracts there was a need for a synthetic route to make these compounds. Pelorol was then synthesized in 10 steps from commercially available (+)-sclareolide, which has a similar decalin core.[28] These synthetic studies led to the discovery of other SHIP1 agonists such as AQX-016A **(2.15)** and AQX-MN100 **(2.16)**. These small molecule agonists were shown to induce apoptosis in a drug resistant multiple myeloma cell line that expressed SHIP1.[29]

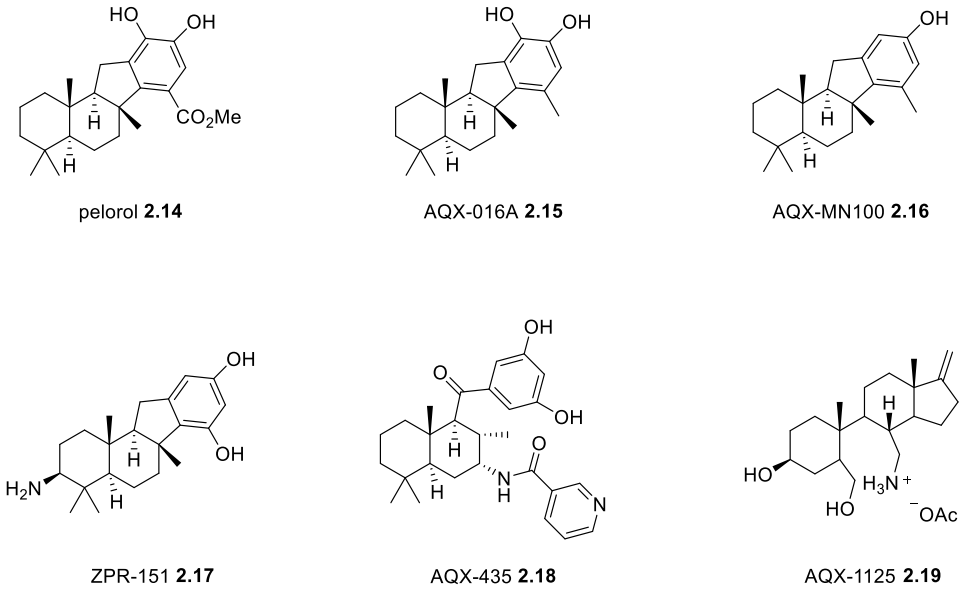

Figure 2.7: Pelorol, Pelorol Derivatives and AQX-1125

AQX-016A (**2.15**) was reported to be 3-fold more potent than pelorol as a SHIP1 agonist, but some concerns arose that the catechol moiety could cause off-target effects. Catechols are known for binding metals and can undergo oxidation to quinones which can act as alkylating agents, leading to mutagenic side effects. This led to the development of AQX-MN100 (**2.16**) in which the catechol was switched for a substituted phenol.[30] Enzyme kinetics using these compounds by Andersen and co-workers showed that these small molecule agonists are binding to SHIP1 at an allosteric site. This is evidenced by the Michaelis-Menten kinetics exhibited by this agonist, that showed a sigmoidal response with the increase in agonist concentration. This allosteric site was recently further characterized by the Mui and Potter groups.[31,32] Both agonists, when tested alongside mammalian 293T cells, demonstrated significant SHIP1 activation. With the endogenous ligand identified and potential binding sites located, optimization of the small molecule agonist was undertaken. Unfortunately, AQX-MN100 (**2.16**) had poor pharmacodynamic properties with the main issue being its poor water solubility. Attempts

were made to address poor water solubility through the incorpation of an amine as seen with ZPR-151 (**2.17**).[31,33] Eventually Aquinox pharmaceuticals decided to pursue an alternative seco-steroidal based scaffold.[27,34-36]

These studies led to the development of the indene based derivative, AQX-1125 (**2.19**), which had better oral bioavailability and moderate SHIP activation at concentrations of 300 μM. Aquinox Pharmaceuticals then filed a variety of patents and initiated clinical trials. AQX-1125 (**2.19**) was evaluated in the clinic as a potential therapeutic for interstitial cystitis/ bladder pain syndrome before eventually failing in Phase 3.[37,38] In general, the drug was well tolerated but ultimately there was no significant difference in patients receiving the placebo versus AQX-1125 (**2.19**). Since it was believed that a SHIP1 agonist could be useful for treating other inflammatory illnesses, **2.19** was also tested for effects on chronic obstructive pulmonary disease (COPD) and asthma patients.[39,40] While initial results seemed promising ultimately these studies were also discontinued for lack of efficacy. It was previously reported that allosteric activators (AQX-MN100 and -O16A) could induce apoptosis of several multiple myeloma cell lines such as OPM1, OPM2 and MM.1S.[41] Due to that observation, AQX-435 (**2.18**) has begun to be evaluated in a preclinical setting targeting SHIP's role in B cell signaling.[42] AQX-435 (**2.18)** was developed with the aim of having improved pharmacological properties with the goal of improving water solubility. In addition the replacement of the catechol with resorcinol was thought to address any side effects from metal chelation, so this molecule was chosen for this study.[42] Lemm et al. discovered that AQX-435 did in fact induce apoptosis through caspase activation in vivo. They also discovered that there was evidence **2.18** could be used in combination with Bruton's Tyrosine Kinase inhibitor (BTK)

ibrutinib to achieve a synergistic effect.[42] They detected that the levels of phosporylated Akt were greatly decreased as opposed to when the drugs were dosed in a standalone fashion. When tested in vivo with diffuse large B cell lymphoma (DLBCL) mice models, they noticed that, in combination with ibrutinib, AQX-435 was effective in tumor regression and volume.[42] Standalone dosing was not nearly as effective as the combination therapies but still resulted in reduced tumor growth when compared to the vehicle. This was promising as the need for anticancer therapies with novel mechanisms is always in demand in order to help fight drug resistance.

In order to identify new SHIP inhibitor scaffolds, the Kerr lab at SUNY Upstate Medical University conducted a virtual screen using a model of the SHIP1 phosphatase active site. The SHIP1 model was constructed using the SHIP2 crystal structures of the phosphatase domain.[7,8,43] Through the use of a computer algorithm and the SHIP1 phosphatase model, 76 different small molecule structures were identified and then tested seperately using the malachite green assay to assess their inhibitor capabilities.[44] Interestingly, four of the molecules actually ended up displaying agonist activity based off the malachite green assays.[44] There structures are revealed below in **Figure 2.8**.

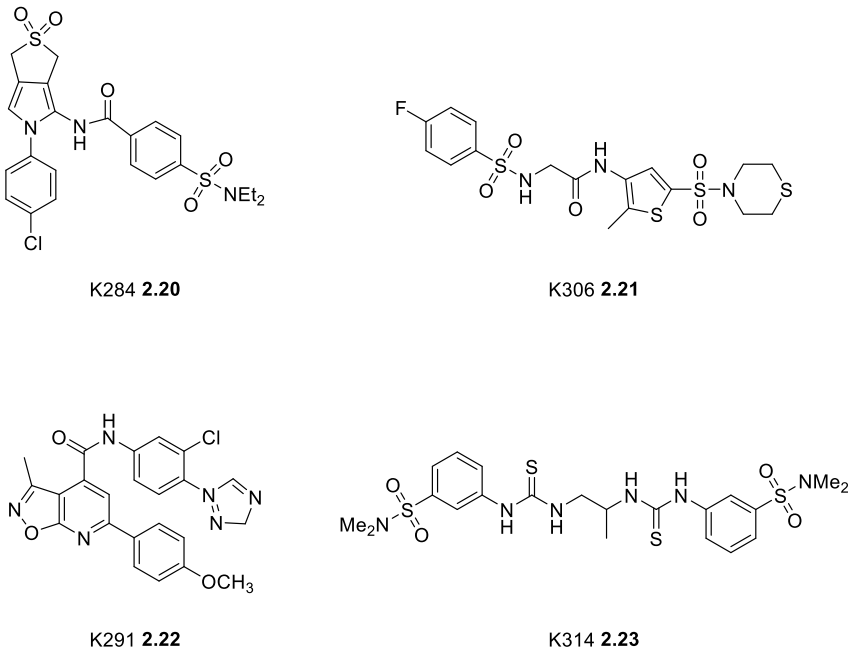

Figure 2.8: SHIP Agonists revealed through AtomWise Virtual Screen

All four compounds showed SHIP1 agonist activity, with some such as K306 (**2.21**) and K291 **(2.22**) being able to agonize SHIP2 as well.[44] Compound **2.21** only showed SHIP2 upregulation at concentrations of 500 µM and **2.22** only upregulated at the lowest concentration 62.5 µM. The newly discovered agonists were tested for their ability to regulate various inflammatory cytokines such as tumor necrosis factor alpha (TNF-α) and Interleukin-6 (IL-6) in vitro against lipopolysaccharide (LPS) stimulated BV2 microglial cells. All but one (**2.21**) failed to decrease TNF-α and IL-6 levels in vitro. K306 (**2.21**) possessed better pharmacological properties such as low lipophilicity and good water solubility when compard to AQX-MN100 **(2.16)** and pelorol **(2.14)**. Furthermore, **2.21** also seemed to increase phagocytosis of dead neurons and synaptosomes but did not affect $A\beta_{42}$. This activity of SHIP agonism could potentially suggest an alternative to the previously discussed SHIP inhbition strategy for Alzheimers's disease. In addition, SHIP agonism has widely been associated with other inflammatory diseases for SHIP's ability

to regulate production of cytokines, but so far no SHIP agonists have emerged as useful in the clinic.

2.4 Synthesis of Small Molecule SHIP Inhibitors

The aminosteroid 3AC (**2.1**) provided a starting point for the design and evaluation of new inhibitors of SHIP. Utilizing the steroid scaffold, modifications were studied with the primary aims including increasing potency, maintaining and/or improving water solubility, and studying the paralog selectivity of the steroid based SHIP inhibitors. K118 (**2.29**) was designed with the last two aims in mind since the dihydrocholesterol scaffold is quite hydrophobic and is poorly soluble in aqueous mediums.[45] K118 (**2.29**) utilizes a epiandrosterone (**2.24**) based steroid structure which possesses no C17 alkyl chain. This long alkyl chain significantly reduces water solubility and may also influence paralog selectivity. Aminosteroid **2.29** does demonstrate inhibition of both paralogs of SHIP with IC_{50} values of 16 µM against SHIP1 and 25 µM against SHIP2 respectively. Additionally, **2.29** has some solubility in water, whereas **2.1** is virtually insoluble in that medium. K118 is also soluble in DMSO, something that **2.1** lacks, which makes dosing cells and animals much easier. K118 (**2.29**) had been previously synthesized and was shown to stimulate mesenchymal stem cell and hematopoietic stem cell expansion.[45] **2.29** has been tested in vivo on diet induced obese mice and has demonstrated some efficacy at reducing body weight and fat percentage when compared to the control group.[46] More recently, pan-SHIP inhibitors including K118 were tested for their role in activating microglial response and microglial proliferation.[18] Both SHIP isoforms are expressed by microglia and our heavily involved in their function making pan-SHIP inhibitors a potential strategy for combating Alzheimer's.[47-49] Furthermore, K118 (**2.29**) showed the ability to enhance

microglial phagocytic functions such as the degradation of dead neuronal cells.[18] In order to provide our collaborators with material for further biological studies, a supply of K118 (**2.29**) was synthesized following the route in Scheme 1 below. This route starts with the Huang-Minlon modification of the Wolff-Kishner reduction, which converts epiandrosterone (**2.24**) to androstan-3-ol (**2.25**), which was accomplished in 41% yield.[50] Some issues regarding inconsistent yields in this reduction may be attributed to the ethylene glycol not reaching the appropriate temperature to eliminate the hydrazone intermediate. This difficulty may be due to boiling point depression by water present in solution after having formed as the by-product of the hydrazone formation. According to the reported procedure, the temperature of the solvent must reach >190°C for the extrusion of nitrogen to occur.[50] In order to address this problem, the solvent was slowly distilled off to remove water while monitoring the temperature. Once the temperature reached 196°C, the reflux condenser was reattached and allowed to reflux overnight. Following the reduction, the (3α,5α)-iodo-androstane (**2.26**) was synthesized in 63% yield using a Mitsunobu reaction using methyl iodide as the iodine source. In order to achieve the appropriate amine stereochemistry, the iodide was displaced by sodium azide in dimethylformamide (DMF) via an S_N2 substitution process to provide the 3β-azido-androstane (**2.27**) in 63% yield. The Staudinger reduction was then employed to reduce the azide.[51] The reduction gave the corresponding 3α-amino-androstane (**2.28**) in 52% yield. Addition of the amine to hydrogen chloride gas that was formed in situ and bubbling it into a solution of the amine in diethyl ether then gave **2.29** as the amine salt in 51% yield (**2.29**). Testing of this material verified that K118 (**2.29**) was indeed a pan-SHIP1/2

inhibitor, verifying that the C17 alkyl chain plays a role in the SHIP1 selectivity of 3AC (**2.1**).

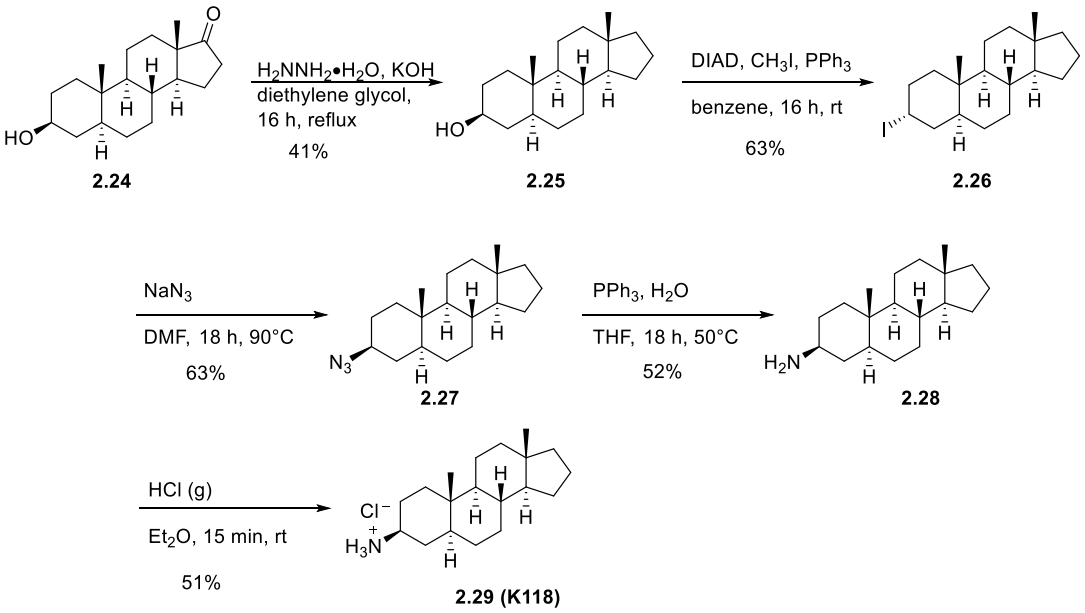

Scheme 2.1: K118 Synthesis

In order to assess the effects of substitution of the amine at the C3 position on SHIP inhibition, some alkyl groups were added to the amine. For this study a pregnenolone scaffold was used with the hope that the ethyl sidechain at C17 would lead to some selectivity for SHIP1 over SHIP2. Previous work had shown that a the C17 ethyl group and the C5-C6 alkene were tolerated and that similar compounds functioned as SHIP inhibitors.[52] The synthesis of these analogs begins with a Wolf-Kishner reduction of pregnenolone (**2.30**) which proceeded in a much improved yield of 84%. This is due to a change in the procedure where the water is distilled off prior to adding the potassium hydroxide which helped facilitate the formation of the hydrazone. Following the reduction of the ketone which provided **2.31**, the C3 α-azide (**2.32**) was installed using Mitsunobu conditions with diphenyl phosphoryl azide and diisopropyl azodicarboxylate.[53] The yield of this transformation was moderate due to difficulties in the removal of the by-products

formed in the transformation, specifically the hydrazine side product from the azodicarboxylate. A lithium aluminum hydride reduction of the azide then gave the amine (**2.33**). Reductive amination conditions employing excess aldehyde were used to form the disubstituted dimethylamine **2.34b**. Unfortunately, formaldehyde was the only aldehyde that gave product, with acetaldehyde resulting in just recovered starting material. The dimethyl substituted amine (**2.34b**) was then purified and sent for testing at SUNY Upstate. In the malachite green assay, the compound precipitated out of DMSO-water mixtures at all concentrations, so biological evaluation was impossible.

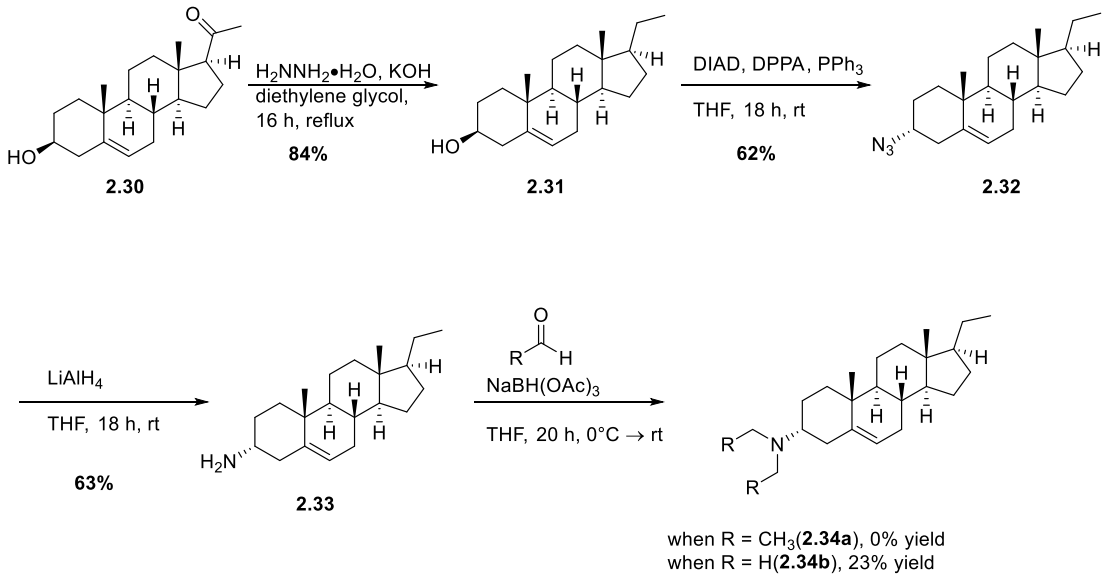

Scheme 2.2: C3 Amine Substitution

After the initial testing results, all future amine substitutions were halted and these reactions were not revisited. With the amine being vital for activity, and with substitution causing solubility difficulties, attention was shifted to different areas of the steroid where other modifications could be evaluated for biological activity. The next location chosen for modification were the C5 and C6 positions on the aminosteroid scaffold. This work was facilitated by the availability of steroids with alkenes at these positions. Additionally, some

docking studies indicated that the addition of more polar groups to these positions may make favorable contacts with polar amino acid residues in the active site, and perhaps increase potency. In addition to making more favorable contacts, it was also believed that a diol at those positions could further improve water solubility.

In order to functionalize the C5- and C6-positions on the steroid, pregnenolone (**2.30**), dehydroepiandrosterone (**2.35**) and cholesterol (**2.36c**) were used as starting materials since they possessed a C5-C6 alkene **(Scheme 2.3)**. For pregnenolone and dehydroepiandrosterone, the synthesis began with a Wolf Kishner reduction of their respective ketones, which proceeded with yields of 99% (**2.36a**) and 97% (**2.36b**) respectively. Cholesterol (**2.36c**) lacks the ketone at C17 so the synthesis picks up at the incorporation of the epoxide. In all three steroid structures, a mixture of epoxide diastereomers are obtained in a 5:1 ratio of α:β (**2.37a-c**); shown in **Figure 9** is a depiction of both epoxide diastereomers shown on a pregnenolone motif. The ratios of epoxides were obtained through the integration of the crude ^{1}H NMR. The proton located at the C6 position is noticeably more downfield in the β-epoxide (ex: **2.41a**) typically around 3.0-3.2 ppm and more upfield in the α-epoxide (ex: **2.38a**) around 2.7-2.9 ppm.[54] Unfortunately, the diastereomers (**2.37a-c**) are inseparable by chromatography and separation by recrystallization was unsuccessful. In each case, the mixture was taken onto the next step where the alcohol was converted to azide with Mitsunobu conditions. For most substrates, the products were difficult to separate from the hydrazine DIAD by-product. All of the Mitsunobu reactions performed on the epoxide diastereomers were subjected to an initial silica gel column to remove the starting alcohol to ensure only the epoxy azide reacted in the next step, but the excess DIAD and DIAD byproduct were not able to be completely

separated from the epoxy azides (**2.38a-c**). The mixture of epoxides in each case was then treated with perchloric acid in acetone to yield the respective diol (**2.39a-c**).

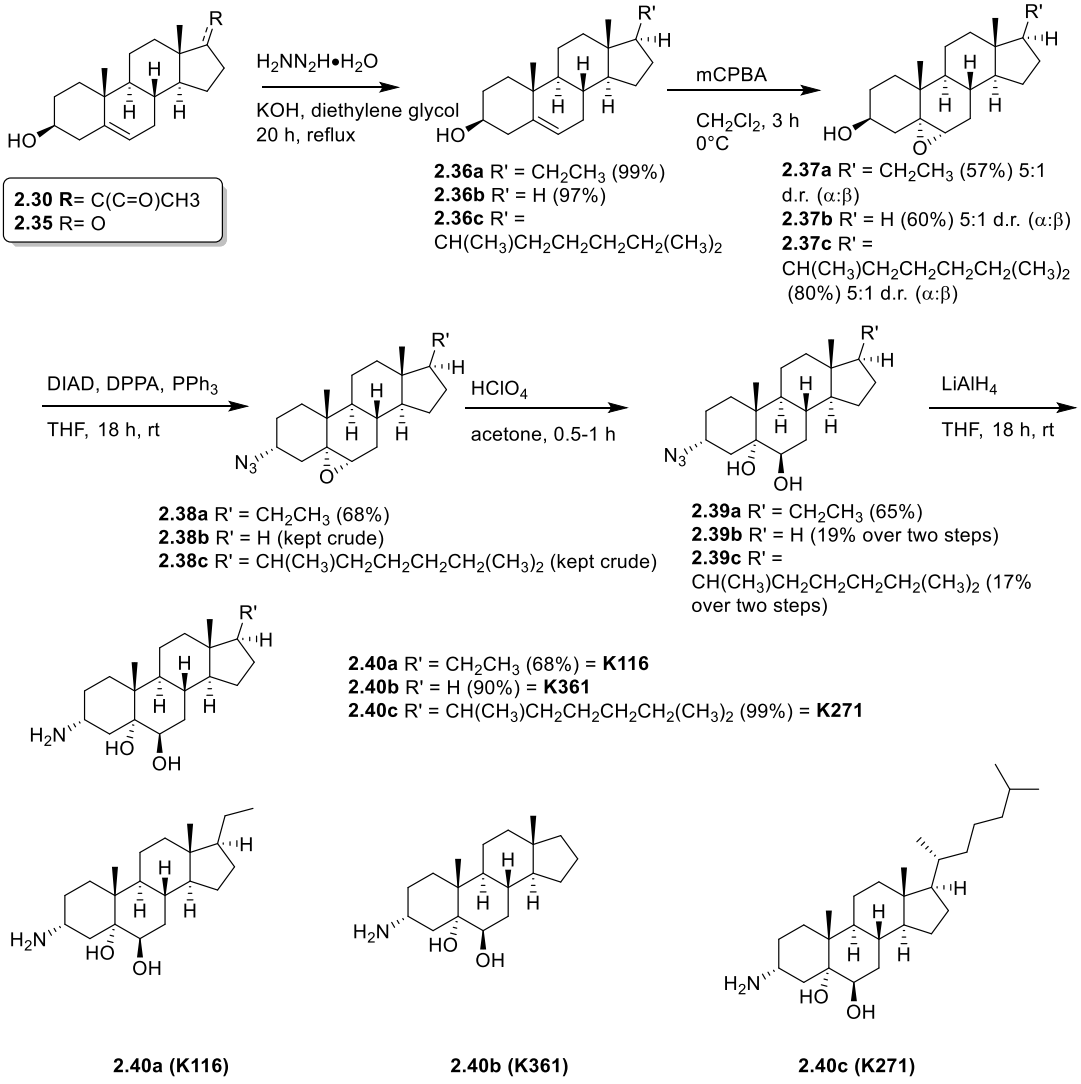

Scheme 2.3: Synthesis of Aminosteroid 5,6-Diols

Only one diol diastereomer is isolated upon final purification of the amine (**2.40a-c**) and this could be due to the reactivity of epoxides. Steroidal epoxides are known to be relatively unreactive without presence of an acid catalyst.[55,56] In particular, the 5,6β-epoxides, such as **2.41a**, are noticeably less reactive and, in most cases, inert under most reaction conditions. Under acid catalysis, the 5,6α-epoxides are known to undergo a trans

diaxial ring opening which results in the alcohol being alpha at the ring junction (**Figure 2.9**) leading to products like **2.39a** being favored.

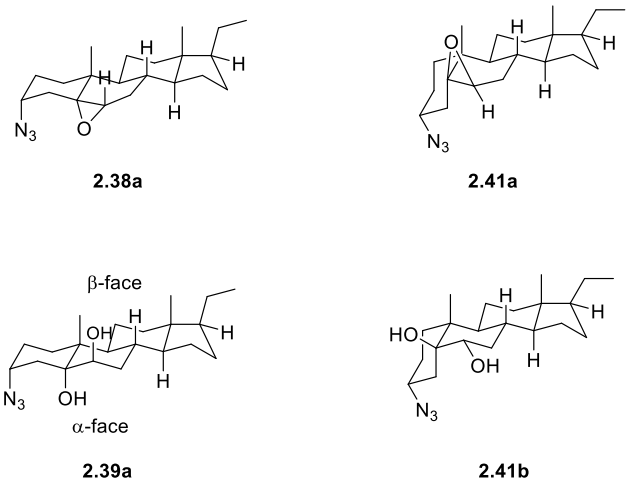

Figure 2.9: Epoxide Opening

Once the diol was in place, the azide was then reduced using lithium aluminum hydride which gave the free amine at C3 (**2.40a-c**). In some cases, the HCl salt (**2.42a-c**) was made to address solubility issues that arose during the biological evaluation of these compounds (**Scheme 2.4**).

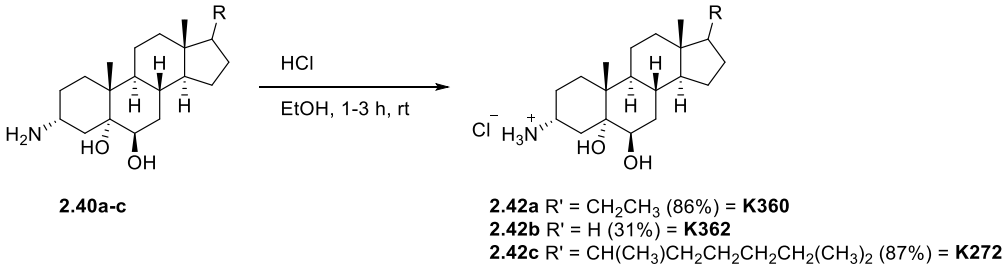

Scheme 2.4: Salt Formation of the Free Amine

In an effort to prove the structure the C5-C6 diols, especially the C5 tertiary alcohol stereochemistry, a crystal structure of **2.40a** was pursued, as this would help aid in the assignment and provide stereochemical confirmation. The diol stereochemistry has always been assumed to be 5α,6β but could also be 5β,6α. Attempts to grow x-ray quality

crystals of the amine **2.40a** and the hydrochloride salt **2.42a** were unsuccessful, so derivatives were explored. In order to generate a crystalline derivative, the amine **2.40a** was converted to the benzamide (**2.43**). After reacting amine **2.40a** with benzoyl chloride and triethylamine in the presence of dimethylaminopyridine, benzamide **2.43** was formed.

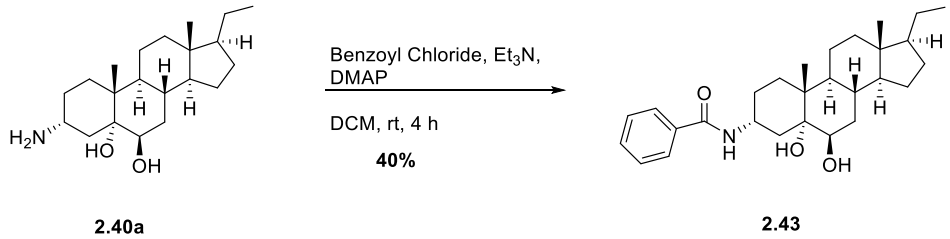

Scheme 2.5: Synthesis of Benzamide **2.43**

Benzamides are known for their ability to form organic crystalline solids and have been previously reported for the formation of crystals.[57,58] Slow crystallization over the course of a few days from chloroform formed tiny colorless crystals of **2.43** which were then analyzed with an x-ray diffractometer by Dr. Sara Dampf formerly of the Korter Lab at Syracuse University. The crystal structure, shown in **Figure 2.10,** proved the stereochemistry of C5-C6 diol.

Figure 2.10: Crystal structure of benzamide **2.43**.

In addition to the C5,C6-diols, it was decided that it would be interesting to determine the role that the C5,C6-epoxide would have on the inhibition of the SHIP

enzymes. Epoxides were once considered out of the realm of possibility for most pharmaceutical and drug compounds due to their reactivity as alkylating agents.[59] Epoxides have the capability of undergoing covalent interactions with nucleophilic amino acid sidechains like cysteine or nucleophilic DNA bases.[60] Those modifications were believed to lead to mutagenic effects, however, in some instances epoxides have been shown to have therapeutic benefits. For example, steroidal epoxides were discovered to have inhibitory activity against aromatase which has applications in the treatment of breast cancer.[61] With these facts in mind, there was little worry on the incorporation of an epoxide for the inhibition of SHIP especially given that 5,6-epoxides as stated earlier are relatively slow to react with nucleophiles.

A different synthetic route was developed to access the epoxide in a pure form so it could be tested without Mitsunobu side products being present. The synthesis of the first epoxide analog, **2.44ab**, is shown below in **Scheme 2.6**. The synthetic route starts with the Wolf-Kishner reduction of pregnenolone **2.30** followed by the epoxidation of C5,C6-alkene to provide epoxide **2.37a**. After these transformations, a mixture of epoxide diastereomers were formed but were inseparable so both were taken forward to the next step. The azide (**2.38a**) was formed with a Mitsunobu reaction and unfortunately at this point the two diastereomers were once again inseparable. The azide was reduced using Staudinger conditions generating a mixture of aminosteroid epoxide diastereomers (**2.44ab**). These amine diastereomers were inseparable, so the mixture was tested against SHIP1 and SHIP2.

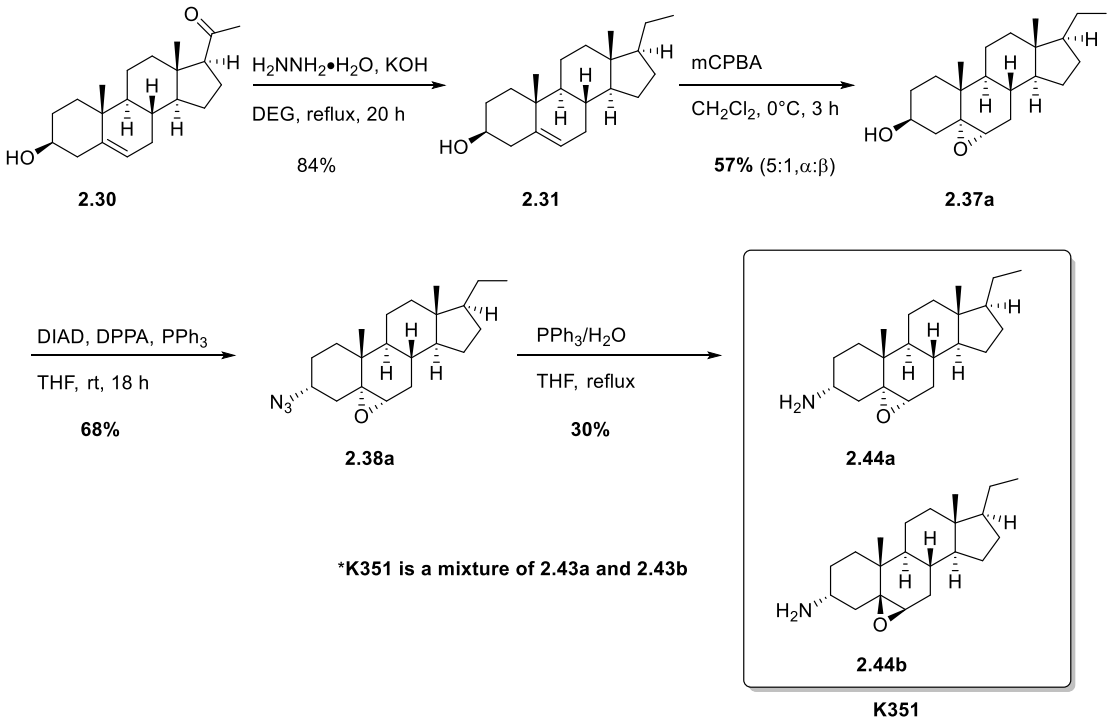

Scheme 2.6: K351 (**2.44ab**) Formation

In addition to the synthesis of these compounds, testing data on their activity was collected on our behalf by our collaborators at SUNY Upstate Medical University. Compiled below in **Table 2.1** are the combined Fluorescence Polarization (FP) and Malachite data against both SHIP paralogs, the structures are compiled above **Table 2.1** for reference.

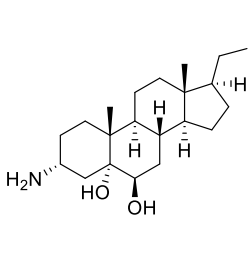

2.40a

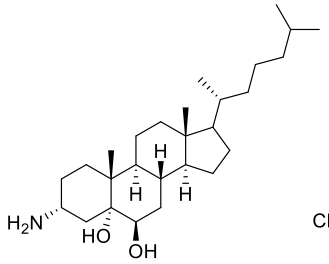

2.40c

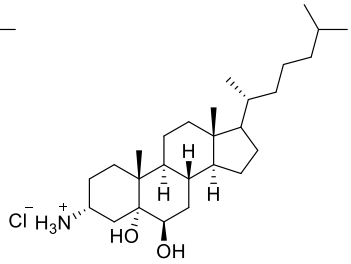

2.42c

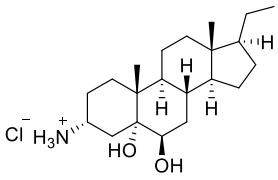

2.42a

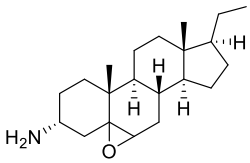

2.44ab

Compound	%Inhibition SHIP1 (0.5 mM) Malachite	%Inhibition SHIP2 (0.5 mM) Malachite	IC_{50} SHIP1 FP Assay	IC_{50} SHIP2 FP Assay
K116 (2.40a)	41	N/A	4 µM	10 µM
K271 (2.40c)	92	80	17.5 µM	17.5 µM
K272 (2.42c)	93	81	14.0 µM	31.1 µM
K351 (2.44ab)	92	92	48 µM	60 µM
K360 (2.42a)	62	40	N/A	N/A

Table 2.1: Malachite and FP Testing Data

The malachite green assay is a colorimetric assay used to detect the levels of free phosphate after the hydrolysis of the enzymatic substrate, the readings from these assays can be converted into a percentage of activity which in this case is percentage of inhibition. The fluorescence polarization assay monitors the concentrations of a fluorescent linked enzymatic product of SHIP which in turn can give an IC_{50}. The malachite green assay is less sensitive, although it has the advantage of being less expensive and is also insensitive to any fluorescent impurities that may give false readings. Steroid **2.40a** which was nearly three-fold selective for SHIP1 over SHIP2 with

an average IC_{50} value of 4 μM for SHIP1 and 10 μM for SHIP2 in the fluorescence polarization assay. In the malachite green assay, **2.40a** demonstrated 40% inhibition of SHIP activity at 0.5 mM concentration. The HCl salt of **2.40a** (**2.42a**), had slightly better results presumably due to increased solubility achieving an average percent inhibition of roughly 62% versus SHIP1 and 40% versus SHIP2. An FP assay was never run for **2.42a** but based off the percent inhibition data from the malachite assays it is a safe assumption that **2.42a** is SHIP1 selective. The cholesterol-based analogs also seemed to fare well in the malachite green assay with the hydrochloride salt (**2.42c**) performing slightly better. On average **2.40c** and **2.42c** achieved 92% and 93% inhibition in the malachite green assay versus SHIP1. Upon FP testing, the cholesterol derivatives (**2.40c/2.42c**) exhibited a 14.0 μM and 17.5 μM IC_{50} against SHIP1. Interestingly, for **2.40c** no difference was observed between IC_{50} values for both paralogs of SHIP which could be due to experimental error with testing. **2.42c** appeared to be nearly three-fold selective for SHIP1 since against SHIP2 only an IC_{50} value of 31.1 μM was observed. The epoxide analogs (**2.44ab**) were noticeably less active than the diol-based inhibitors possessing IC_{50} values of 48 and 60 μM versus SHIP1 and SHIP2 respectively. There seems to be a slight selectivity preference for SHIP1 over SHIP2 which could be due to the alkyl chain at C17. Some additional factors that could have influenced these IC_{50} values could be due to the fact that the mixture of diastereomers was roughly 5:1 which would have an impact on the relative dosing concentrations since one diastereomer could be SHIP active but the other SHIP inactive. Both **2.40b** and **2.42b** are missing from the above table since they both exhibited solubility problems, often crashing out in both the FP and malachite green assay which has caused inconsistent testing data. However, upon getting **2.40b** to

dissolve it appeared to be inactive at all concentrations versus SHIP1 and in low concentrations an agonist of SHIP2, but solid precipitate was observed in the testing wells. Compound **2.42b** was synthesized but has not been tested yet. Presumably, since **2.42b** is just the hydrochloride salt of **2.40b**; it is safe to assume they would have similar reactivity. In addition, both of these analogs seemed to lack the improved solubility properties they were predicted to have. Both **2.40b** and **2.42b** appeared to crash out of solution after some time which could have been the reason for the inconsistent testing results.

In summary, a number of new aminosteroid based SHIP inhibitors were synthesized and tested in vitro against both SHIP paralogs. The aminosteroid 5,6-diols showed varying levels of activity with the pregnenolone derivative performing the best against SHIP1. In the future, attempts to increase the potency of these diol-based compounds could be of therapeutic benefit. Using the crystal structure of the **2.43**, the structure of **2.40a** was verified. The lone epoxide derivative (**2.44ab**) that was synthesized was not able to be purified completely and was a mixture of diastereomers so in the future if these molecules were to be revisited it would be ideal to generate pure diastereomers and then test both separately for activity.

2.5 Optimization of a new synthetic route to AQX-1125 and related structures

Despite the lack of success of AQX-1125 (**2.19**) in the clinic, the molecule is still useful as a standard for groups who wish to find a more potent SHIP1 agonist. Unfortunately, the molecule only recently became commercially available and is quite expensive. To access the molecule the original patent detailed a 16 step synthetic sequence (**Scheme 2.7)**.[62-64] This sequence begins with the conversion of

dehydroepiandrosterone **2.35** to the ketal (**2.45**) using a catalytic amount of CSA and ethylene glycol. The alcohol at the C3 position of the steroid is then converted to the tertbutyldimethyl silyl ether (**2.46**). After purification, alkene **2.46** undergoes an allylic oxidation using *tert*-buyl peroxide and catalytic copper iodide. The yield in this step is relatively low but that can be attributed to the fact there is more then one allylic position and the reaction is not highly selective. Tandem reduction of the ketone and hydroboration-oxidation of enone **2.47** yielded diol **2.48** which was taken on without purification.[65] Treatment of diol **2.49** with 2,2-dimethyloxypropane and camphorsulfonic acid gave acetonide **2.50.** With the diol protected, the ketone was converted to alkene **2.51** with a Wittig reaction. The alcohol was converted into acetate **2.52** and then the acetonide was cleaved to provide diol **2.53**. Sodium periodate was then used to oxidatively cleave the diol generating dialdehyde **2.54**. The dialdehyde is then reduced to form diol **2.55** which was selectively acylated on the C6 alcohol (steroid numbering) to provide **2.56**. This acetate is isolated by chromatography, although no mention is made of the selectivity of this step. Based on the yield that the reaction is likely not very selective. Alcohol **2.56** is then converted into a mesylate which is then displaced with sodium azide to give azide **2.58**. Reduction of azide **2.58** with $LiAlH_4$ gives the free amine **2.59** which is then converted to the acetate salt (**2.19**).

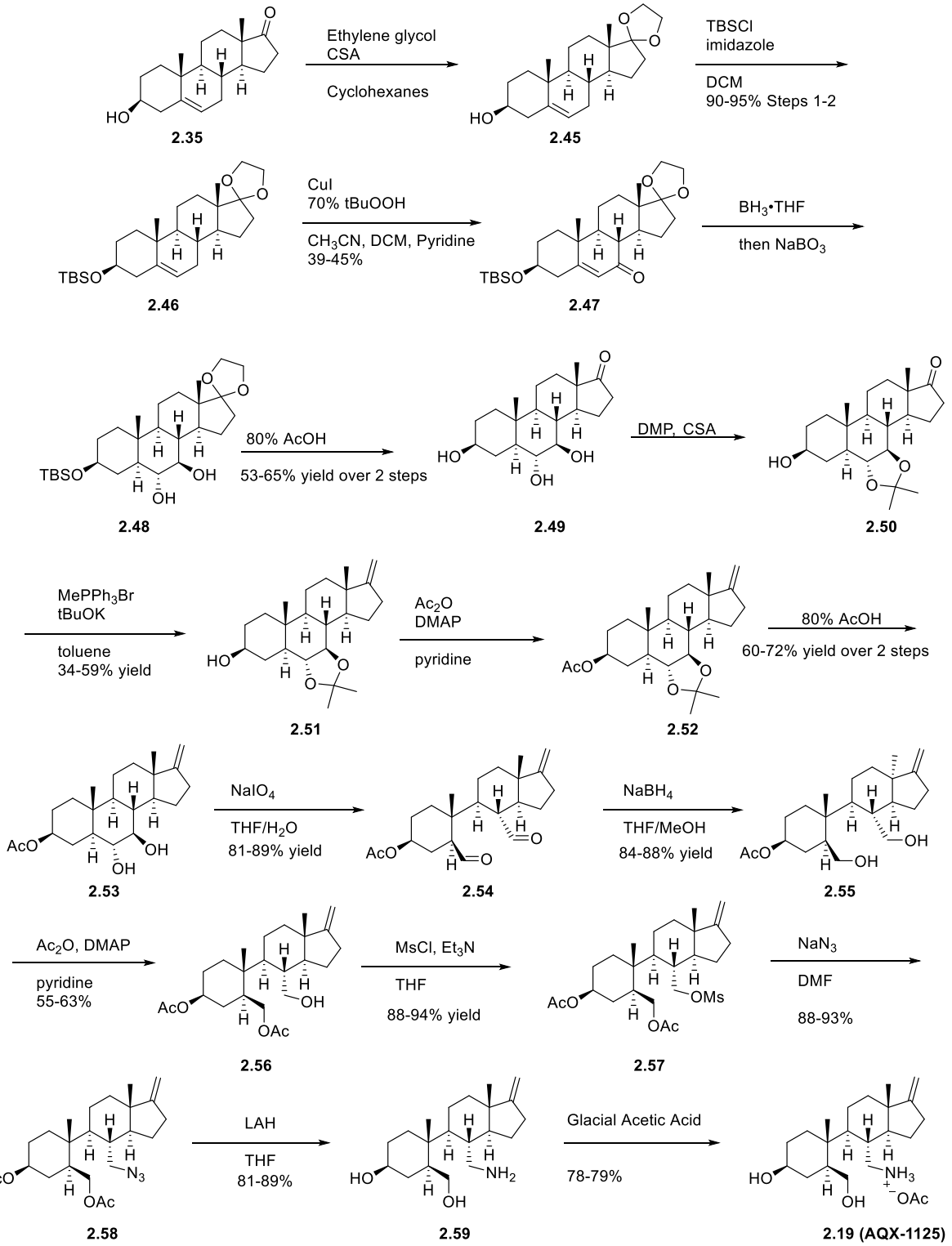

Scheme 2.7: Aquinox Pharmaceuticals Synthesis of AQX-1125[62]

A more recent patent details several other routes to AQX-1125(**2.19**) including a nine step sequence shown in **Scheme 2.8**. In this scheme the C17 acetal **2.60** is formed directly from dehydroepiandrosterone **2.35**. Acetal **2.60** is then subjected to a copper mediated allylic oxidation with *tert*-butyl hydroperoxide to generate **2.61** in 41% yield. The newly formed α,β-unsaturated ketone is converted into trans diol **2.62** by treatment with borane, a process that has been widely reported in literature.[65,66] The diol is taken onto the next step crude and cleaved with sodium periodate to generate aldehyde **2.63** in 85% yield over the two steps. A TEMPO oxidation of **2.63** converts the hemiacetal to the lactone **2.64**. The aldehyde was then treated with O-methylhydroxyamine which gave the O-methyl oxime **2.65**. Glacial acetic acid was then used to remove the ketal and to generate the ketone (**2.66**) needed to install the exocyclic alkene (**2.67**). The alkene (**2.67**) was then accessed through Wittig conditions using methyltriphenylphosphonium bromide and potassium t*ert*-butoxide. The azide in **2.67** was then treated with lithium aluminum hydride which simultaneously reduced the lactone and the oxime to generate the amino alcohol (**2.68**). Upon treatment with acetic acid, the acetate salt of the free amine was generated (**2.19/AQX-1125**). This synthesis is definitely an improvement over their first reported route with many moderate to excellent yielding steps. The allylic oxidation appears to still be an issue, presumably due to multiple oxidation products. Along with the allylic oxidation, the Wittig conditions could use some optimization since no yields higher then 49% were reported. Aside from those issues, their new synthesis provided a shorter way to access **2.19**.

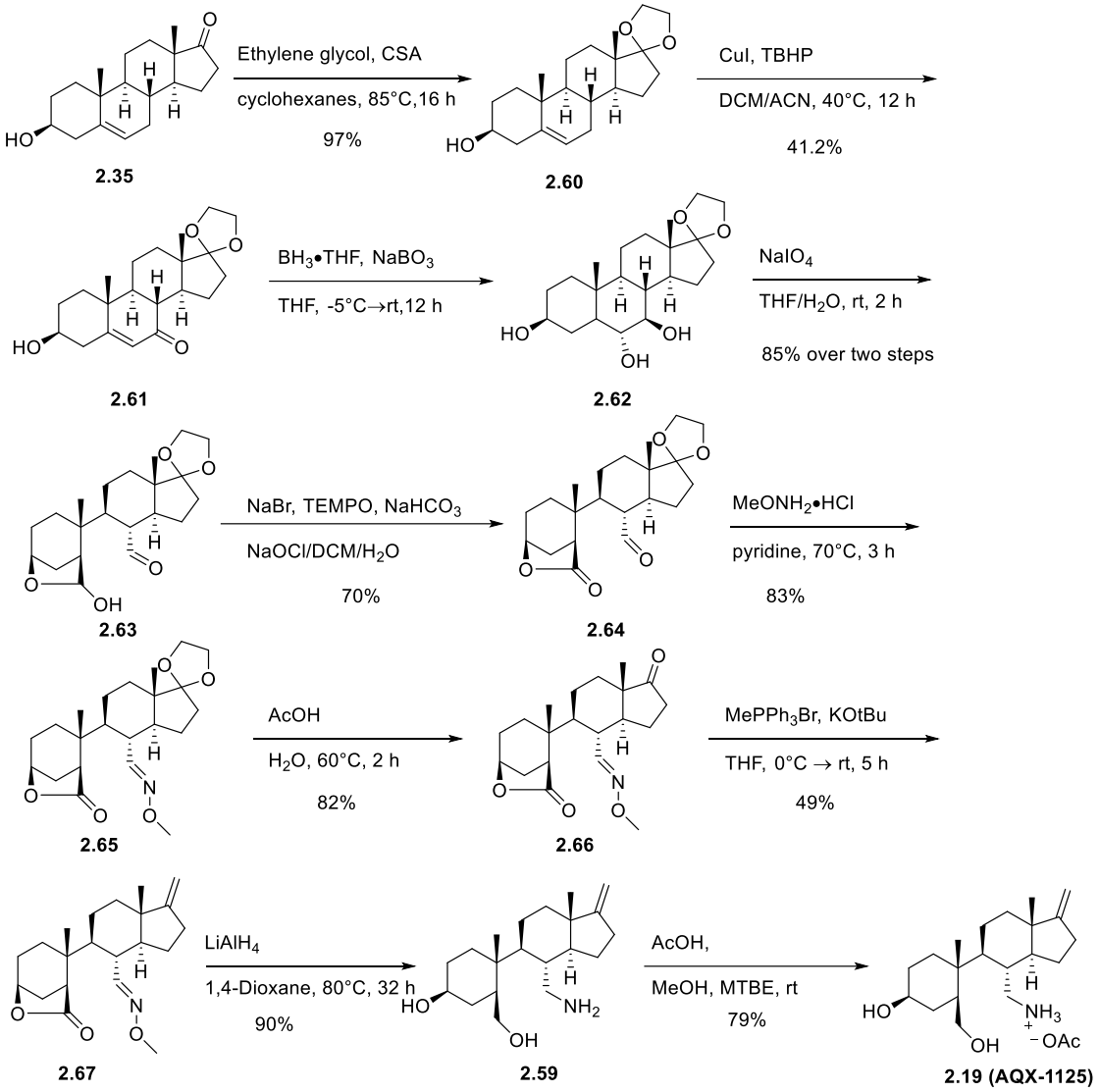

Scheme 2.8: Second generation approach to Aquinox AQX-1125 (**2.19**)

Synthetic efforts by the Chisholm lab, specifically by Brian Duffy and Otto Dungan in recent years has led to the development of a new synthetic route to AQX-1125. This also provided the opportunity to test new synthetic analogues of AQX-1125 for activity as well.[67] One of the newer AQX-1125 analogs (**2.78**) possessed no exocyclic alkene at C17 but otherwise the same structure, the full synthesis is shown in **Scheme 2.9.** The yields shown in bold in the scheme are those that were done by other labmates in the Chisholm lab. The synthesis starts from commercially available dehydroepiandrosterone (**2.35**). A

Wolf-Kishner reduction of dehydroepiandrosterone converted the ketone at C17 to alkane (**2.36a**).[50] Using TBSCl and imidazole, the alcohol was converted into the silyl ether (**2.69**) with a slight improvement in yield when compared to the previous synthesis. The first iteration of this synthesis used ruthenium trichloride and *tert*-butyl peroxide as oxidation reagents in employed in a biphasic solvent system of cyclohexanes and water. Unfortunately, this reaction resulted in the formation of multiple undesired products which made purification difficult and lowered yields.

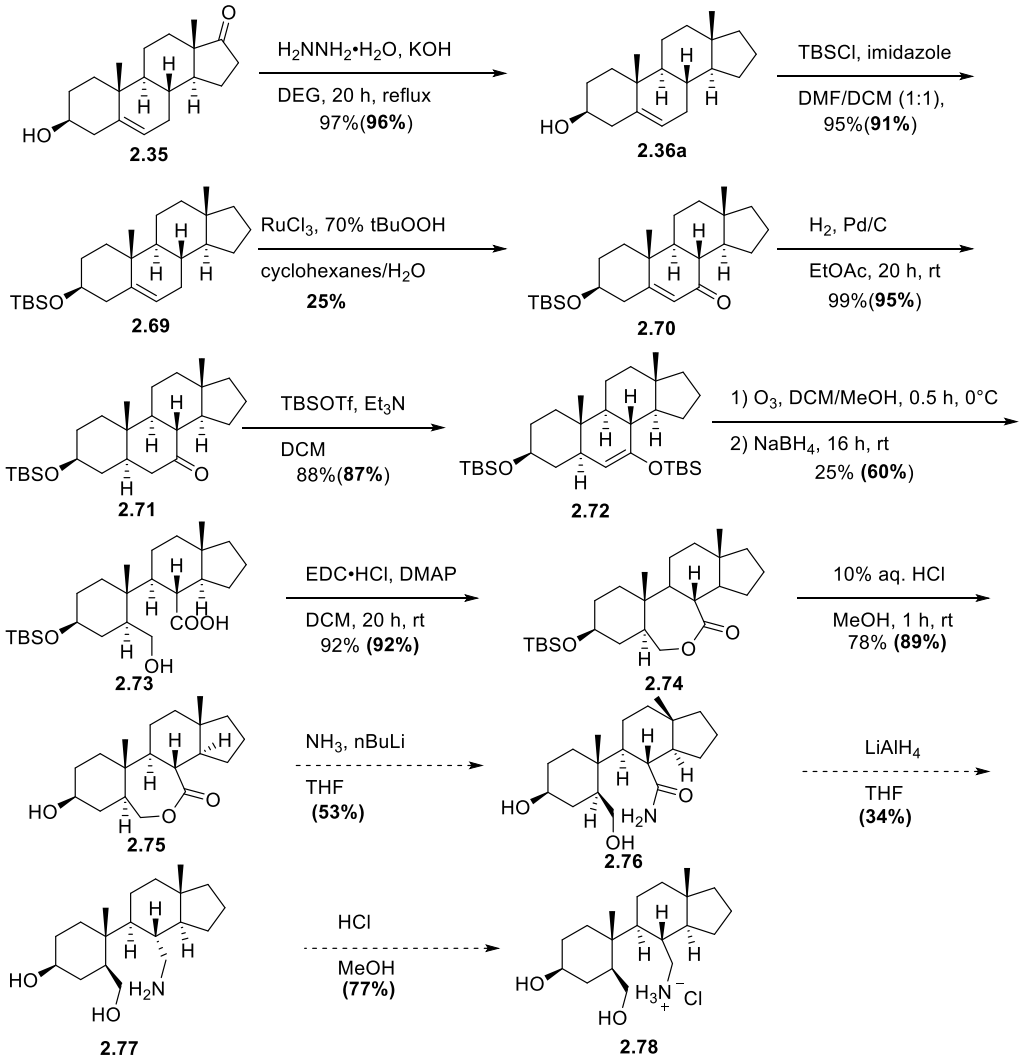

Scheme 2.9: Revised Synthesis of AQX-1125 Analog

A new procedure was proposed using a dirhodium catalyst reported in the literature and this is shown in **Scheme 2.10**.[68] While the previously reported $RuCl_3$ procedure required purification by recrystallization, this procedure formed relatively few side products and was able to be purified through silica gel column chromatography. The yield was much higher then the previously reported yield, increasing from 25% to 63%.

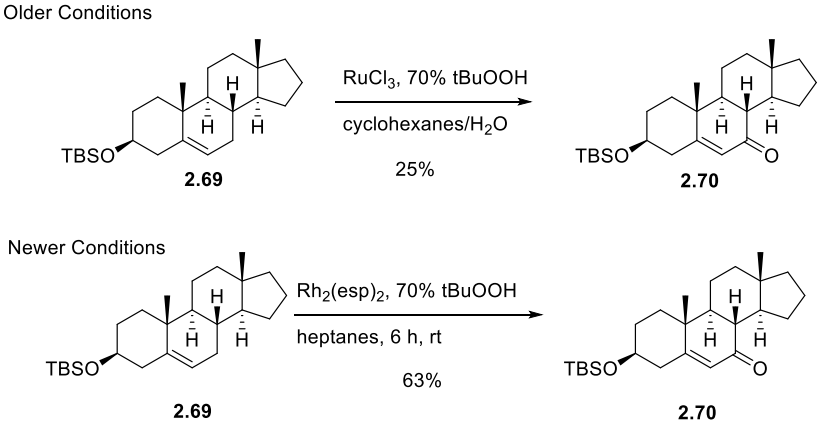

Scheme 2.10: New Allylic Oxidation Conditions

Compound **2.70** was then hydrogenated to form ketone **2.71** with a slight increase in yield from what was previously reported (**Scheme 2.9**). The formation of the silyl enol ether **2.72** proved to be a problem, having to be repeated numerous times due to the sensitivity of the silyl enol ether (**2.72**). The acidic nature of the silica gel was found to be the cause for the decomposition of **2.72**, which was addressed by switching to a basic solvent system (5% Et_3N in hexanes) which was a sufficient amount of base to prevent loss of product. This resulted in a 88% yield of the silyl enol ether **2.72**. Ozonolysis was used from there to open the B ring of the steroid and the resulting ozonide was reduced with sodium borohydride to provide alcohol **2.73**. Unfortunately, the yield that was previously reported was not able to be reproduced. The seco steroid was then closed by the formation of the lactone (**2.74**) using 1-ethyl-3-(3-dimethylaminopropyl)-carbodiimide

and dimethylaminopyridine in a 92% yield. The silyl ether was then deprotected and converted into the alcohol at C3 through reaction with aqueous HCl to give compound **2.75**. After that step, the synthesis was halted but the rest of the steps are shown with yields in bold from previous labmates. The intermediates that were made were sent for testing at SUNY Upstate Medical University. These compounds unfortunately were unable to accelerate any SHIP phosphatase activity.

2.6 Conclusion

Small molecules that target SHIP are of growing interest to the biomedical community with the number of disease states that are linked to the overexpression or absence of SHIP activity.[4] Both SHIP antagonists and agonists could be useful for disease states including autoimmune disorders, leukemia (AML and CLL), breast cancer and Alzheimer's. Through the use of high-throughput screening some early SHIP inhibitors and agonists have been discovered which served as the basis for many SAR studies. Based off existing aminosteroid scaffolds several new aminosteroid based compounds were proposed possessing various functionalities like epoxides and diols. Testing results revealed that the aminosteroid lacked potency but certain analogs such as **K116 (2.40a)** showed promising results and could be used as a basis for analogs going further. Through the modification of the amine at the three position of K**116** (**2.40a**)**,** a crystalline derivative was able to be synthesized which helped identify the exact configuration of the aminosteroid. Lastly, an analog of AQX-1125 (**2.78**) that had been previously synthesized by another lab mate was further optimized and the intermediates were synthesized, characterized and provided to collaborators at SUNY Upstate for further analysis.

2.7 Experimental

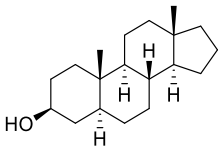

5α-Androstan-3β-ol (**2.25**)

Lit Ref: Jursic, B. S.; Upadhyay, S. K.; Creech, C. C.; Neumann, D. M., Novel and efficient synthesis and antifungal evaluation of 2,3-functionalized cholestane and androstane derivatives. *Bioorg. Med. Chem. Lett.* **2010,** *20* (24), 7372-7375.

In an oven dried 500 mL round-bottom flask equipped with stir bar, potassium hydroxide (3.08 g, 54.9 mmol) was dissolved in ethylene glycol (36 mL) by heating gently with a heat gun. Once dissolved, the solution was cooled to room temperature and epiandrosterone **1** (4.00 g, 13.8 mmol) was added. Hydrazine hydrate was then added (3.4 mL, 51.6 mmol) to the reaction mixture and a distillation head equipped with thermometer was attached to the flask. The reaction mixture was heated and in a separate collection flask distillate was collected. Once the reaction temperature reached 196 °C the distillation head was removed and replaced with a reflux condenser. The reaction was allowed to react overnight at reflux. After allowing the reaction to go overnight for 16 h, the reaction mixture was allowed to cool. Once at room temperature, dichloromethane (25 mL) and HCl (28 mL) were added and allowed to stir at room temperature for 10 minutes. The organic layer was separated, and the aqueous layer was extracted with CH_2Cl_2 (3 x 30 mL). The organic extracts were combined and washed with deionized water (2 x 30 mL) and brine (1 x 30 mL), dried over sodium sulfate, filtered and concentrated in vacuo. Purification by silica gel chromatography (15% ethyl acetate/ 85% hexanes) afforded compound **2** (1.56 g, 41%) as a white solid.

TLC R_f =0.48 (10% Ethyl Acetate/ 90% Hexanes); ^{1}H NMR (400 MHz, $CDCl_3$) δ 3.59 (m, 1H), 1.83- 1.76 (m, 1H), 1.73 – 1.55 (m, 7H), 1.51 – 1.24 (m, 8H), 1.19 – 1.06 (m, 4H), 1.01 – 0.84 (m, 3H), 0.81 (s, 3H), 0.68 (s, 3H), 0.67 – 0.61 (m, 1H).

*Alcohol proton is missing due to deuterium exchange from water in $CDCl_3$

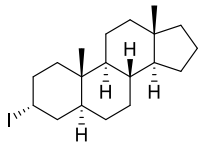

3α-Iodo-5α-androstane (**2.26**)

This compound has previously been made see: (Viernes, Dennis Racca, "Synthesis, Design, and Biological Evaluation of Inhibitors and Activators of Src Homology 2 Domain-Containing Inositol Phosphatase (SHIP) and Synthetic Studies of Apicularen A and Maoecrystal V" (2012). Chemistry - Dissertations, Syracuse University, 195. https://surface.syr.edu/che_etd/195)

In an oven dried round bottom flask equipped with stir bar, 5α-Androstan-3β-ol (1.50 g, 5.43 mmol) and triphenylphosphine (1.73 g, 6.60 mmol) were dissolved in dry benzene (45 mL) under a positive pressure of Argon. Diisopropyl azodicarboxylate (1.3 mL, 6.60 mmol) was added to the solution and stirred for ten minutes at room temperature. Methyl iodide (0.45 mL, 7.26 mmol) was added slowly and reaction was allowed to stir overnight for 18 h at room temperature. The reaction was concentrated in vacuo. Purification by silica gel chromatography (100% Hexanes) yielded compound **2.26** (1.30 g, 62%) as a pinkish-white solid. TLC R_f =0.82 (100% Hexanes); ^{1}H NMR (400 MHz, $CDCl_3$) δ 4.94 (t, J=4.0 Hz, 1H), 1.95 – 1.88 (m,1H), 1.73 – 1.55 (m, 10H), 1.49 – 1.38 (m, 3H), 1.32 – 1.09 (m, 8H), 1.04 – 0.87 (m, 2H), 0.80 (s, 3H), 0.69 (s, 3H).

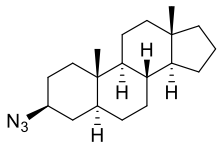

3β -Azido-5α-Androstane (**2.27**)

This compound has previously been made see: (Viernes, Dennis Racca, "Synthesis, Design, and Biological Evaluation of Inhibitors and Activators of Src Homology 2 Domain-Containing Inositol Phosphatase (SHIP) and Synthetic Studies of Apicularen A and Maoecrystal V" (2012). Chemistry - Dissertations, Syracuse University, 195. https://surface.syr.edu/che_etd/195)

In an oven dried round bottom flask equipped with stir bar, 3α-Iodo-5α-androstane **2.26** (1.30 g, 3.36 mmol) and sodium azide (2.19 g, 33.6 mmol) were suspended in dimethyl formamide (12 mL). The suspension was heated to 90°C and allowed to react for 18 h. The reaction mixture was allowed to cool to room temperature. The reaction mixture was diluted with 40 mL ethyl acetate and poured into a separatory funnel with 150 mL deionized water. The organic layer was collected and rinsed with deionized water (2 x 50 mL). Organic layer was dried over sodium sulfate and concentrated in vacuo. Purification by silica gel chromatography (100% hexanes) yielded compound (**2.27**) (0.640 g, 63%) as an off-white solid.

^{1}H NMR (400 MHz, $CDCl_3$) δ 3.25 (tt, J= 15.5, 4.4 Hz, 1H), 1.85 – 1.78 (m, 1H), 1.77 – 1.67 (m, 3H), 1.67 - 1.55 (m, 4H), 1.52 – 1.39 (m, 3H), 1.36 (d, *J =12.0* Hz, 1H), 1.31 – 1.23 (m, 4H), 1.18 – 1.09 (m, 4H), 0.99 – 0.86 (m, 3H), 0.78 (s, 3H), 0.68 (s, 3H), 0.61-0.66 (m, 1H).

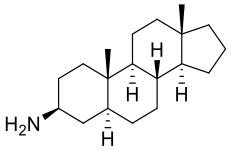

3β-Amino-5α-Androstane (**2.28)**

This compound has previously been made see: (Viernes, Dennis Racca, "Synthesis, Design, and Biological Evaluation of Inhibitors and Activators of Src Homology 2 Domain-Containing Inositol Phosphatase (SHIP) and Synthetic Studies of Apicularen A and Maoecrystal V" (2012). Chemistry - Dissertations, Syracuse University, 195. https://surface.syr.edu/che_etd/195)

In an oven dried round bottom flask, 3β -Azido-5α-Androstane (0.640 g, 2.12 mmol) and triphenyl phosphine (1.11 g, 4.24 mmol) were dissolved in dry tetrahydrofuran (15 mL) under positive pressure of Argon. After stirring at room temperature for thirty minutes, deionized water (3 mL) was added and the reaction was refluxed overnight. The solution was cooled to room temperature and the organic layer was extracted. The organic layer was dried over sodium sulfate and concentrated in vacuo. Purification by silica gel chromatography (1% triethylamine/ 9% Methanol/ 90% dichloromethane) yielded compound **2.28** (0.301 g, 52%) as a white solid.

TLC R_f=0.11 (1% triethylamine/ 9% Methanol/ 90% dichloromethane); ^{1}H NMR (400 MHz, $CDCl_3$) δ 2.65 (tt, J= 15.5, 4.4 Hz, 1H), 1.71 – 1.61 (m, 6H), 1.54 – 1.47 (m, 2H), 1.44 – 1.38 (m, 2H), 1.30 – 1.22 (m, 5H), 1.14 – 1.08 (m, 5H), 1.00 – 0.83 (m, 3H) 0.78 (s, 3H), 0.68 (s, 3H), 0.66-0.61 (m, 1H).

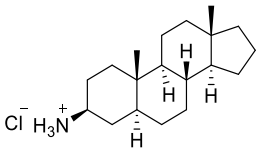

3β-Amino-5α-Androstane hydrochloride (1:1) **(2.29)**

This compound has previously been made see: (Viernes, Dennis Racca, "Synthesis, Design, and Biological Evaluation of Inhibitors and Activators of Src Homology 2 Domain-Containing Inositol Phosphatase (SHIP) and Synthetic Studies of Apicularen A and Maoecrystal V" (2012). Chemistry - Dissertations, Syracuse University, 195. https://surface.syr.edu/che_etd/195)

3β-Amino-5α-Androstane **2.28** (160 mg, 0.580 mmol) was suspended in 15 mL of Et_2O and allowed to stir while dry HCl gas was purged into the reaction mixture by the reaction of concentrated sulfuric acid and sodium chloride. During this time the solution turned a milky white. After approx. 15 min the reaction mixture was filtered and the white precipitate was collected and dried under vacuum producing the β-amine hydrochloride salt **2.29** (93 mg, 51%) as a white solid. TLC R_f =0.11 (1% triethylamine/ 9% Methanol/ 90% dichloromethane); ^{1}H NMR (400 MHz, $CDCl_3$) δ 8.30 (bs, 3H), 3.14 (m, 1H), 2.00 (d, J= 12 Hz, 1H), 1.80 – 1.62 (m, 6H), 1.57 – 1.37 (m, 4H), 1.37 – 1.19 (m, 5H), 1.19 – 1.05 (m, 4H), 1.00 – 0.86 (m, 3H), 0.83 (s, 3H), 0.68 (s, 3H), 0.67 – 0.63 (m, 1H).

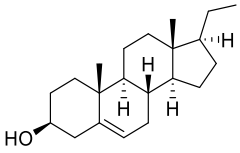

3β-Pregn-5-en-3-ol (**2.36a**)

This compound has been previously made before see: (Krausova, B.; Slavikova, B.; Nekardova, M.; Hubalkova, P.; Vyklicky, V.; Chodounska, H.; Vyklicky, L.; Kudova, E. Positive Modulators of the N-Methyl-d-aspartate Receptor: Structure–Activity Relationship Study of Steroidal 3-Hemiesters. *Journal of Medicinal Chemistry* **2018,** *61*, 4505-4516.)

In an oven dried 500 mL round-bottom flask equipped with stir bar, pregnenolone **2.30** (4.11 g, 12.9 mmol) was suspended in diethylene glycol (110 mL). Hydrazine hydrate (2.5 mL, 50.5 mmol) and n-butanol (5 mL) were added to the flask and a short path distillation head was attached. The suspension was heated to reflux until approximately 10 mL was collected in the collection flask. The reaction mixture was then cooled to 80°C and potassium hydroxide (2.83 g, 50.5 mmol) was added in one portion. The reaction was heated to reflux and allowed to react overnight for 20 h. The reaction mixture was allowed to cool to room temperature. Once at room temperature the flask was diluted with 250 mL of dichloromethane. The organics were washed with brine (2 x 150 mL) and dried over Na_2SO_4. Purification by silica gel chromatography (30% Ethyl Acetate/ 70% Hexanes) afforded compound **2.36a** (3.907 g, 99%) as a white solid. TLC R_f =0.47 (30% ethyl acetate/ 70 % hexanes); ^{1}H NMR (400 MHz, $CDCl_3$) δ 5.37 – 5.34 (m, 1H), 3.52 (m, 1H), 2.33 – 2.19 (m, 2H), 2.03 – 1.95 (m, 1H), 1.89 – 1.80 (m, 3H), 1.76 (dt, *J* = 12.4*,* 3.8 Hz, 1H), 1.66 – 1.57 (m, 2H), 1.56 – 1.38 (m, 6H), 1.28 – 1.04 (m, 6H), 1.01 (s, 3H), 1.00 – 0.91 (m, 2H), 0.88 (t, J=7.4 Hz, 3H), 0.58 (s, 3H).

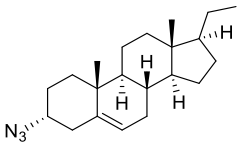

3α-azido-pregn-5-ene (**2.32**)

This compound has been previously made before see: (Cave; Jarreau; Khuong-Huu; Lebceuf; Serban, G. *Bulletin de la Société chimique de France* **1967,** *2*, 701-706.)

See also: Choi, L. M.S. Thesis, Syracuse University, Syracuse, NY, 2011.

Lit Ref: Choi, L. M.S. Thesis, Syracuse University, Syracuse, NY, 2011.

In an oven dried round bottom flask equipped with stir bar, 3β-pregn-5-en-3-ol (1.00 g, 3.31 mmol) and triphenylphosphine (1.04 g, 3.97 mmol) were dissolved in dry THF (30 mL) under a positive pressure of Argon. Diisopropyl azodicarboxylate (1.3 mL, 6.60 mmol) was added to the solution and stirred for ten minutes at room temperature. Diphenylphosphoryl azide (0.86 mL, 3.97 mmol) was added slowly and reaction was allowed to stir overnight at room temperature. The reaction was concentrated in vacuo. Purification by silica gel chromatography (100% Hexanes to 10% DCM/90%Hexanes) yielded compound **2.32** (1.30 g, 62%) as a white solid. TLC R_f =0.45 (100% Hexanes); ^{1}H NMR (400 MHz, $CDCl_3$) δ 5.40 (m, 1H), 3.87 (m, 1H), 2.55 – 2.50 (m, 1H), 2.19 (dt, J= 15.0,2.5 Hz, 1H), 2.08 (m, 1H), 1.91 – 1.81 (m, 1H), 1.80 -1.72 (m, 2H), 1.69 -1.59 (m, 3H), 1.50 -1.36 (m, 5H), 1.27 – 1.02 (m, 8H), 1.01 (s, 3H), 0.88 (t, J=7.4 Hz, 3H), 0.58 (s, 3H).

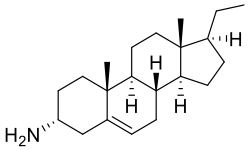

(3α)-3-amino-pregn-5-ene (**2.33**)

This compound has been previously made before see: (Cave; Jarreau; Khuong-Huu; Lebceuf; Serban, G. *Bulletin de la Société chimique de France* **1967,** *2*, 701-706.)

See also: Choi, L. M.S. Thesis, Syracuse University, Syracuse, NY, 2011.

In an oven dried round bottom flask with stir bar, 3α-azido-pregn-5-ene (1.33 g, 4.00 mmol) was dissolved in dry THF (20 mL) and cooled to 0°C under positive pressure of Argon. A 1.0 M solution of LAH in THF was then added (22.0 mL, 22.0 mmol) to the flask and the reaction was allowed to warm up to room temperature. The reaction was allowed to react over 18 hours. After 18 h, the reaction was diluted with THF (15 mL) and cooled

to 0°C. 0.84 mL of DI H_2O and 0.84 mL of 15% NaOH in H_2O were added to the flask and stirred for fifteen minutes. After fifteen minutes, 2.60 mL of DI H_2O and $MgSO_4$ were added to the flask. After ten minutes, the heterogenous mixture was filtered over Celite. After filtering, the crude compound was concentrated in vacuo. Purification by silica gel chromatography (1% triethylamine/ 19% Methanol/ 80% dichloromethane) yielded compound **2.33** (780 mg, 65% yield) as an off white solid.

TLC R_f =0.10 (1% triethylamine/ 9% Methanol/ 90% dichloromethane); ^1H NMR (400 MHz, $CDCl_3$) δ 5.37 – 5.34 (m, 1H), 3.18 – 3.13 (m, 1H), 2.60 - 2.55(m, 1H), 2.03 – 1.95 (m, 1H), 1.90 – 1.73 (m, 4H), 1.67 – 1.50 (m, 4H), 1.50 – 1.31 (m, 7H), 1.23 – 1.04 (m, 6H), 0.99 – 0.92 (m, 1H), 1.01 (s, 3H), 0.88 (t, J=7.4 Hz, 3H), 0.57 (s, 3H).

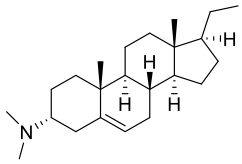

N,*N*-Dimethyl- Pregn-5-en-3β-amine (**2.34b**)

In an oven dried round bottom flask, (3α)-3-amino-pregn-5-ene (0.625 g, 2.07 mmol) was dissolved in dry THF (12 mL) under positive pressure of Argon. Formaldehyde (0.346 mL, 12.4 mmol) was added and the reaction was stirred for one hour. The reaction was cooled to 0°C and sodium tris(acetoxy)borohydride (2.62 g, 12.4 mmol) was added in one portion. The reaction was allowed to react for 20 h and then quenched with saturated sodium bicarbonate (10 mL). Reaction mixture was extracted with ethyl acetate (2x 20). The combined organic layers were washed with sodium bicarbonate (2 x 20 mL) and brine (1 x 20 mL). The organic layers were dried over $MgSO_4$ and concentrated in vacuo. Purification by silica gel chromatography (20% Methanol/ 80% Dichloromethane) yielded compound **2.34b** (160 mg, 23%) as a white powder. M.P. = 122.3 – 124.5°C TLC R_f =0.22

(20% Methanol/ 80% dichloromethane); IR (ATR, cm^{-1}) 2953, 2943, 2931, 2912, 2882, 2860, 2805 2762, 1456, 1427, 1374, 1361; ^{1}H NMR (400 MHz, $CDCl_3$) δ 5.30 (m, 1H), 2.28 – 2.25 (m, 3H), 2.30 (s, 6H), 1.98 – 1.78 (m, 3H), 1.74 – 1.31 (m, 11H),1.26- 1.04 (m, 5H), 1.01 (s, 3H), 0.99 – 0.92 (m, 1H), 0.88 (t, J=7.4 Hz, 3H), 0.54 (s, 3H). ^{13}C NMR (100 MHz, $CDCl_3$) δ 139.6, 121.9, 62.9, 56.1, 52.9, 49.6, 43.4, 41.9, 37.8, 37.2, 35.2, 33.5, 31.8, 31.7, 28.1, 24.8, 24.4, 23.0, 20.5, 19.8, 13.3, 12.4. Anal calcd for $C_{23}H_{39}N$: C, 83.82; H, 11.93; N, 4.25. Found: C, 83.89; H, 12.06; N, 4.17.

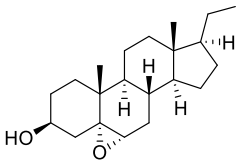

(3β)-Hydroxy-5,6-epoxy-pregnan-3-ol (**2.37a**)

This compound has been previously made before see, Lichtfouse, E.; Albrecht, P. Synthesis of triaromatic steroid hydrocarbons methylated at position 2, 3 or 6: molecular fossils of yet unknown biological origin. *Tetrahedron* **1994,** *50*, 1731-1744.

In an oven dried round bottom flask equipped with stir bar, 3β-pregn-5-en-3-ol (300 mg, 0.992 mmol) was dissolved in dry CH_2Cl_2 (10 mL). The solution was then cooled to 0°C. meta-Chloroperoxybenzoic acid (632 mg, 2.98 mmol) was then added. The solution was reacted for 3 h at 0°C. After 3 h the reaction was quenched by adding 10 mL of saturated sodium sulfite solution. The organic layer was separated and the aqueous layer was extracted with CH_2Cl_2 (3 x 15 mL). The organic extracts were combined and washed with deionized water (2 x 15 mL) and brine (1 x 30 mL), dried over sodium sulfate, filtered and concentrated in vacuo. Purification by silica gel chromatography (20% Ethyl Acetate/ 80% Hexanes) afforded compound **2.37a** (180 mg, 57%) as a white solid.

TLC R_f = 0.53 (50% Ethyl Acetate/50% Hexanes); ^{1}H NMR (400 MHz, $CDCl_3$) δ 3.90 (m, 1H), 2.90 (d, J = 4.4 Hz, 1H), 2.10 – 2.04 (m, 1H),1.97 – 1.89 (m, 2H), 1.87 – 1.77 (m, 1H), 1.72 – 1.57 (m, 4H), 1.55 – 1.46 (m, 2H), 1.44 – 1.35 (m, 5H), 1.32 – 1.23 (m, 4H), 1.22 – 1.09 (m, 3H), 1.06 (s, 3H), 1.05 – 1.01 (m, 1H), 0.99 – 0.89 (m, 1H), 0.85 (t, *J* = 7.4 Hz, 3H), 0.68 (s, 1H), 0.51 (s, 3H).

*mixture of epoxides so integrations may not equal exact number of hydrogens

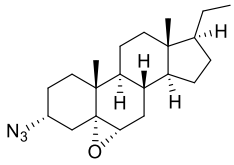

3α-Azido-5,6-epoxy-pregnane (**2.38a**)

In an oven dried round bottom flask equipped with stir bar, (3β)-hydroxy-5,6-epoxy-pregnan-3-ol (0.528 g, 1.65 mmol) and triphenylphosphine (0.478 g, 1.82 mmol) were dissolved in dry THF (40 mL) under a positive pressure of Argon. Diisopropyl azodicarboxylate (0.36 mL, 1.82 mmol) was added to the solution and stirred for ten minutes at room temperature. Diphenylphosphoryl azide (0.41 mL, 1.82 mmol) was added slowly and reaction was allowed to stir overnight at room temperature. The reaction was concentrated in vacuo. Purification by silica gel chromatography (100% Hexanes to 5% Ethyl Acetate/95% Hexanes) yielded compound **2.38a** (0.390 g, 68%) as a tan solid. M.P. = 107.3 -107.7°C. TLC R_f =0.39 (5% Ethyl Acetate/95% Hexanes); IR (ATR, cm^{-1}) 2959, 2933, 2904, 2863, 2108, 2083, 1458, 1272; ^{1}H NMR (400 MHz, $CDCl_3$) δ 3.98 (m, 1H), 2.81 (d, *J* = 4.2 Hz, 1H), 2.32 (dd, *J* = 14.8 ,3.9 Hz, 1H), 1.95 – 1.76 (m, 4H), 1.69 (dt, *J* = 13.7, 3.9 Hz, 1H),1.64 -1.49 (m, 4H), 1.45 – 1.35 (m, 4H), 1.26 (dt, *J* = 14.9 ,2.2 Hz, 1H), 1.20 – 1.12 (m, 3H), 1.10 -1.07 (m, 1H), 1.05 (s, 3H), 1.03 -0.91 (m, 3H), 0.85 (t, *J* = 7.4 Hz, 3H), 0.69 (s, 1H), 0.51 (s, 3H). ^{13}C NMR (100 MHz, $CDCl_3$) δ 63.0, 57.0, 56.9,

56.4, 52.6, 42.7, 42.0, 37.5, 35.4, 33.2, 29.7, 28.8, 28.4, 27.9, 25.7, 24.3, 23.0, 20.1, 15.7, 13.3, 12.4. HRMS (ESI) *m / z* $C_{21}H_{33}N_3ONa$ [M+Na] Exact Mass 366.251584; Observed 366.251626.

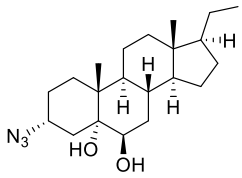

(3α)-3-Azido-pregn-(5α,6β)-diol **(2.39a)**

This compound has been previously made before see, Kerr, W.; Pedicone, C.; Chisholm, J; Dormann, S. Methods of Activating Microglial Cells. WO202028552A1, 2020.

In an oven dried round bottom flask equipped with stir bar, 3α-azido-5,6-epoxy-pregnane (0.760 g, 2.21 mmol) was dissolved in acetone (35 mL). The solution was then cooled to 0°C. Concentrated $HClO_4$(1 mL) was added dropwise and allowed to warm to room temperature after addition. After 18 hours the reaction was concentrated. The organic residue was redissolved in dichloromethane (25 mL) and washed with sodium bicarbonate (1 x 25 mL) and brine (2 x 25 mL). The organic layers were dried over $MgSO_4$ and concentrated in vacuo. Purification by silica gel chromatography (1% MeOH/ 99% DCM) yielded compound **2.39a** (0.523 g, 65%) as a white solid. M.P. = 114.6 -117.2°C. TLC R_f =0.31 (1% Methanol /99% Dichloromethane); IR (ATR, cm^{-1}) 3506, 2918, 2870, 2101, 1453, 1256; ^{1}H NMR (400 MHz, $CDCl_3$) δ 4.11 (m, 1H), 3.58 (m, 1H), 3.49 (s, 1H), 2.43 (dd,*J* = 15.0*,* 4.3 Hz, 1H), 1.99 – 1.86 (m, 3H), 1.78 - 1.62 (m, 5H), 1.58 – 1.40 (m, 6H), 1.36 – 1.17 (m, 5H), 1.15 (s, 3H), 1.13 - 1.02 (m, 3H), 0.89 (t, *J* = 7.4 Hz, 3H), 0.69 (s, 1H), 0.51 (s, 3H). ^{13}C NMR (100 MHz, $CDCl_3$) δ 75.3, 74.2, 58.4, 55.3, 53.0, 45.5, 42.3, 39.1, 38.0, 34.5, 33.9, 30.1, 28.5, 28.1, 25.0, 24.5, 23.1, 20.4, 16.7, 13.3, 12.7.

HRMS (ESI+) *m / z* $C_{21}H_{35}N_3ONa$ [M+Na] Exact Mass 384.262148; Observed 384.262022.

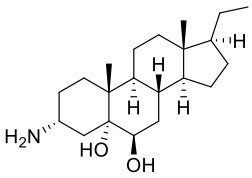

(3α)-3-Amino-pregnane-(5α,6β)-diol **(2.40a)**

This compound has been previously made before see, Kerr, W.; Pedicone, C.; Chisholm, J; Dormann, S. Methods of Activating Microglial Cells. WO202028552A1, 2020.

In an oven dried round bottom flask with stir bar, (3α)-3-azido-pregn-(5α,6β)-diol (0.175 g, 0.484 mmol) was dissolved in dry THF (7 mL) and cooled to 0°C under positive pressure of Argon. A 1.0 M solution of LAH in THF was then added (4.8 mL, 4.8 mmol) to the flask and the reaction was allowed to warm up to room temperature. The reaction was allowed to react over 18 hours. After 18 h, the reaction was diluted with THF (15 mL) and cooled to 0°C. 0.18 mL of DI H_2O and 0.18 mL of 15% NaOH in H_2O were added to the flask and stirred for fifteen minutes. After fifteen minutes, 0.54 mL of DI H_2O and $MgSO_4$ were added to the flask. After ten minutes, the heterogenous mixture was filtered over Celite. After filtering, the crude compound was concentrated in vacuo. Purification by silica gel chromatography (1% triethylamine/ 19% Methanol/ 80% dichloromethane) yielded compound **2.40a** (110 mg, 68% yield) as an off white solid. M.P. = 151.9 -155.2°C. TLC R_f =0.18 (1% triethylamine/ 19% Methanol/ 80% dichloromethane); IR (ATR, cm^{-1}) 3370, 2932, 2866, 1453, 1376, 1037; ^1H NMR (400 MHz, CD_3OD) δ 3.48 -3.45 (m, 2H), 2.26 (m, 1H), 1.97-1.70 (m, 5H), 1.67 – 1.16 (m, 13H), 1.14 (s, 3H),1.12 – 1.01 (m, 2H), 0.79 (t, *J* = 7.3 Hz, 3H), 0.68 (s, 1H), 0.50 (s, 3H). ^{13}C {^1H} NMR (100 MHz, $CDCl_3$) δ 76.0, 75.0, 55.3, 53.0, 46.5, 45.8, 42.3, 39.3, 38.0, 35.0, 34.3, 30.1, 28.7, 28.2, 28.1, 24.5, 23.1,

20.5, 16.6, 13.3, 12.6. HRMS (ESI) *m / z* $C_{21}H_{37}NO_2$ [M+H] Exact Mass 335.2829; Observed 336.2902.

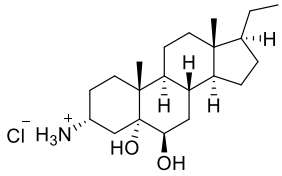

(3α)-3-Amino-pregnane-(5α,6β)-diol hydrochloride (**2.42a)**

(3α)-3-Amino-pregnane-(5α,6β)-diol **2.40a** (131 mg, 0.390 mmol) was suspended in 10 mL of Et_2O and allowed to stir while dry HCl gas was purged into the reaction mixture by the reaction of concentrated sulfuric acid and sodium chloride. During this time the solution turned slightly opaque with some solid precipitation observed. After approx. 15 min the reaction mixture was filtered and the white precipitate was collected and dried under vacuum. The mother liquor was then concentrated to also yield a white solid. Both lots were combined producing the β-amine hydrochloride salt **2.42a** in (125 mg, 86% yield). M.P. = 170.5 – 173.5 °C. TLC Rf =0.18 (1% triethylamine/ 19% Methanol/ 80% dichloromethane); IR (ATR, cm-1) 3245, 2934, 2867, 1450, 1377, 1024; 1H NMR (400 MHz, DMSO-d_6) δ 7.55 (bs, 3H), 4.70 (d, *J = 4.3* Hz, 1H), 4.58 (s, 1H), 3.42-3.41 (m, 2H), 2.29 (dd, *J = 15.3, 3.9* Hz, 1H), 1.91-1.74 (m, 3H), 1.71 – 1.54 (m, 5H), 1.43 – 1.33 (m, 6H),1.23 -1.07 (m, 5H) 1.03 (s, 3H),1.03 – 0.94 (m, 2H), 0.85 (t, *J = 7.3* Hz, 3H), 0.54 (s, 3H). 13C {1H} NMR (100 MHz, DMSO-d_6) δ 75.2, 73.0, 55.6, 53.0, 46.9, 45.4, 42.3, 38.6, 38.2, 34.2, 33.2, 30.2, 28.2, 27.9, 24.6, 24.1, 23.2, 20.6, 16.5, 13.7, 12.9. HRMS (ESI) *m / z* $C_{21}H_{37}NO_2$ [M+H] Exact Mass 335.2829; Observed 336.2902.

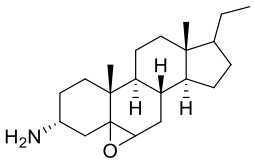

3α-amino-5,6-epoxy-pregnane (**2.44ab**)

In an oven dried round bottom flask, 3α-Azido-5,6-epoxy-pregnane (0.902 g, 3.43 mmol) and triphenyl phosphine (2.25 g, 8.59 mmol) were dissolved in tetrahydrofuran (25 mL). Reaction was heated to 50°C and stirred for one hour. Deionized water (3 mL) was added and the reaction was refluxed overnight. Sodium sulfate was added the following day and reaction mixture was filtered. Organics were concentrated in vacuo and purified through silica gel chromatography using a solvent gradient (10% MeOH/ 90% DCM to 2% triethylamine/ 8% Methanol/ 90% dichloromethane) yielded compound **2.44ab** (0.301 g, 52%) as a white solid. M.P. = 133.7 – 136.4 °C. TLC Rf =0.23(2% triethylamine/ 8% Methanol/ 90% dichloromethane); IR (ATR, cm-1) 3375, 2925, 2862, 2852, 1458, 1374, 929; 1H NMR (400 MHz, DMSO-d_6) δ 3.25 (m, 1H), 2.77 (d, *J* = *3.8* Hz, 1H), 2.30 (dd, *J* = *14.2, 3.8* Hz, 1H), 2.00 – 1.81 (m, 5H), 1.71 – 1.34 (m, 11H), 1.23 – 1.05 (m, 5H), 1.02 (s, 3H), 0.98 – 0.91 (m, 2H), 0.84 (t, *J* = *7.2* Hz, 3H), 0.50 (s, 3H). 13C {1H} NMR (100 MHz, DMSO-d_6) δ 64.9, 56.9, 56.4, 52.6, 47.3, 43.0, 42.0, 37.5, 36.4, 35.6, 29.7, 29.6, 28.6, 28.1, 27.9, 24.3, 23.0, 20.1, 15.5, 13.2, 12.4. HRMS (ESI) *m / z* $C_{21}H_{36}NO$ [M+H] Exact Mass 318.279141; Observed 318.278991.

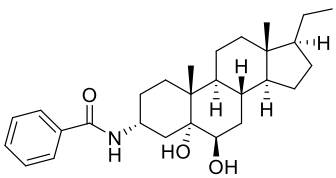

3α-benzoylamino-pregnane-(5α,6β)-diol **(2.43)**

(3α)-3-Amino-pregnane-(5α,6β)-diol (50 mg, 0.149 mmol), benzoyl chloride (0.06 mL, 0.521 mmol), 4-dimethylaminopyridine (6 mg, 0.029 mmol), triethylamine (0.07 mL, 0.521 mmol) were dissolved in dichloromethane (2 mL). The reaction was stirred for 4 hours. After four hours the reaction was diluted with ethyl acetate(5 mL) and quenched with deionized water (5 mL). The organic layer was separated and dried over sodium sulfate. The crude oily solid was purified by flash column chromatography (2% MeOH/98% DCM) to yield compound **2.42** as a white solid (26 mg, 40% yield). M.P. = 136.7 – 140.1°C. TLC Rf =0.68 (2% MeOH/98% DCM); ^{1}H NMR (400 MHz, $CDCl_3$) δ 8.25 (d, *J* = *8.2* Hz, 1H), 7.77 (d, J = 7.0 Hz, 1H), 7.44 (t, *J* = 7.3 Hz, 1H), 7.40 (t, *J* = 7.6 Hz, 2H), 4.55 (m, 1 H), 3.60 (m, 1H), 2.48 (dd, J = 14.7, 5.0 Hz, 1H), 1.95 – 1.77 (m, 6H), 1.71 – 1.56 (m, 6H), 1.52 – 1.38 (m, 3H), 1.36 – 1.30 (m, 2H), 1.21 (s, 3H), 1.18 – 0.97 (m, 6H), 0.88 (t, *J* = *7.4* Hz, 3H), 0.60 (s, 3H). 13C {1H} NMR (100 MHz, $CDCl_3$) δ 165.6, 135.2, 131.0, 128.3, 126.8, 77.2, 75.0, 55.6, 53.0, 47.0, 44.3, 42.4, 39.0, 38.0, 34.4, 34.1, 30.0, 29.0, 28.0, 26.5, 24.4, 23.0, 20.6, 16.8, 13.3, 12.7. HRMS (ESI) *m / z* $C_{28}H_{41}NO_3Na$ [M+Na] Exact Mass 462.297865; Observed 462.297496.

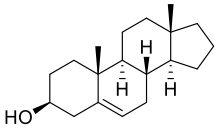

Androst-5-en-3β-ol (**2.36b**)

Lit Reference: Yayla, H. G.; Wang, H.; Tarantino, K. T.; Orbe, H. S.; Knowles, R. R., Catalytic Ring-Opening of Cyclic Alcohols Enabled by PCET Activation of Strong O-H Bonds. *J. Am. Chem. Soc.* **2016,** *138* (34), 10794-10797.

Dehydroepiandrosterone (8.00 g, 27.7 mmol), n-butanol (2 mL), and hydrazine hydrate(5.9 mL, 111 mmol) were dissolved in 180 mL of diethylene glycol. A shortpath

distillation apparatus was attached and heated to reflux. Once temperature reached >200°C, reaction was cooled to approximately 80°C and KOH was added. A reflux condenser was attached and the reaction was heated to reflux. After reacting for 20 h, the reaction was cooled to room temperature and diluted with dichloromethane(100 mL). The reaction contents were transferred to a seperatory funnel, washed with 2M HCl(1 x 75 mL) and brine (2 x 75 mL). Organic layer was seperated, dried over $MgSO_4$ and concentrated in vacuo. Purified by SiO_2 chromatography (25% EA / 75% Hexanes) to yield compound **2.36b** in 97% yield. . M.P: 117.6 – 120.1°C. TLC Rf =0.31 (25% EA / 75% Hexanes); IR(ATR, cm^{-1}) 3224, 2969, 2930, 2895, 2866, 1451, 1375; ^1H NMR (400 MHz, $CDCl_3$) δ 5.36 (m, 1H), 3.55 (m, 1H), 2.32-2.20 (m, 2H), 2.05-1.97 (m, 1H), 1.88 -1.81 (m, 2H), 1.75 (dt, J=12.4, 3.9 Hz, 1H), 1.70-1.56 (m, 4H), 1.52 – 1.50 (m, 1H), 1.48 (d, *J* = 3.9 Hz, 1H), 1.46 – 1.36 (m, 3H), 1.20-1.04 (m, 4H), 1.01 (s, 3H), 1.00 – 0.86 (m, 2H), 0.72 (s, 3H). ^{13}C {^1H} NMR (100 MHz, $CDCl_3$) δ 140.8, 121.7, 71.8, 54.9, 50.5, 42.3, 40.6, 40.3, 38.7, 37.3, 36.7, 32.2, 31.6, 25.6, 21.1, 20.5, 19.4, 17.2.

*Alcohol proton is missing due to deuterium exchange from water in $CDCl_3$

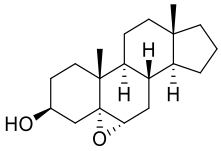

(5α.6α)-Epoxy-androstan-3β-ol (**2.37b**)

This compound has been previously reported see: (Mori, K.; Nakayama, T.; Sakuma, M. Synthesis of some analogues of blattellastanoside A, the steroidal aggregation pheromone of the German cockroach. *Bioorganic & Medicinal Chemistry* **1996,** *4*, 401-408.)

In an oven dried round bottom flask equipped with stir bar, androst-5-en-3β-ol (5.00 g, 18.2 mmol) was dissolved in dry DCM (180 mL). The solution was then cooled to 0°C. meta-Chloroperoxybenzoic acid (7.85 g, 45.5 mmol) was then added. The solution was reacted for 3 h at 0°C. After 3 h the reaction was quenched by adding 100 mL of saturated sodium sulfite solution. The organic layer was separated and the aqueous layer was extracted with DCM (2 x 50 mL). The organic extracts were combined and washed with sodium sulfite (1 x 50 mL), sodium bicarbonate (1 x 50 mL) and brine (1 x 50 mL), dried over sodium sulfate, filtered and concentrated in vacuo. Purification by silica gel chromatography (5% Methanol/ 95% Dichloromethane) afforded compound **2.37b** (3.19 g, 60%) as a white solid. TLC Rf = 0.24 (5% methanol/ 95% DCM); ^{1}H NMR (400 MHz, $CDCl_3$) δ 3.91 (m, 1H), 2.90 (d, *J* = 4.4 Hz, 1H), 2.11 – 1.88 (m, 3H), 1.72-1.56 (m, 6H), 1.46-1.36 (m, 5H), 1.34 -1.24 (m, 4H), 1.15 – 1.08 (m, 3H), 1.06 (s, 3H), 0.90 – 0.82 (m, 1H), 0.65 (s, 3H).

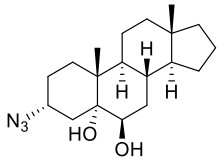

(3α)-Azido-5α-androstane-5a,6β-diol (**2.39b**)

In an oven dried round bottom flask equipped with stir bar, (5α.6α)-Epoxy-androstan-3β-ol (3.19 g, 11.0 mmol) and triphenylphosphine (3.17 g, 12.1 mmol) were dissolved in dry THF (80 mL) under a positive pressure of Argon. Diisopropyl azodicarboxylate (2.37 mL, 12.1 mmol) was added to the solution and stirred for ten minutes at room temperature. Diphenylphosphoryl azide (2.60 mL, 12.1 mmol) was added slowly and reaction was allowed to stir for 20 h at room temperature. The reaction was concentrated in vacuo. The

crude mixture was taken forward and dissolved in acetone. The solution was then cooled to 0°C. Concentrated (stock) $HClO_4$ was added dropwise (2 mL) and the reaction was stirred for 1 h. After 1 h, the reaction was quenched with saturated sodium bicarbonate (50 mL). The organic layer was extracted with DCM (2 x 25 mL). The combined organic layers were washed with sodium bicarbonate (1 x 25 mL) and brine (2 x 25 mL). The organic layers were dried over $MgSO_4$ and concentrated in vacuo. Purification by silica gel chromatography (1% MeOH/ 99% DCM) yielded compound **2.39b** (0.720 g, 19%) as a white solid. M.P. = 121.0 – 122.5°C. TLC Rf =0.55 (10% Methanol/ 90% Dichloromethane); IR (ATR, cm-1) 3535, 3471, 2978, 2936, 2865, 2103, 1451, 1376; ^{1}H NMR (400 MHz, $CDCl_3$) δ 4.08 (m, 1H), 3.56 (d, *J= 2.8* Hz, 1H), 3.46 (s, 1H), 2.41 (dd, J= 15.0, 4.2 Hz, 1H), 1.95-1.87 (m, 1H), 1.85 – 1.78 (m, 2H), 1.76 – 1.69 (m, 2H), 1.67 – 1.55 (m, 5H), 1.51 – 1.39 (m, 4H), 1.34 – 1.13 (m, 6H), 1.12 (s, 3H), 1.07-1.00 (m, 1H), 0.72 (s, 3H). 13C {1H} NMR (100 MHz, $CDCl_3$) δ 75.3, 74.1, 58.4, 53.9, 45.4, 41.0, 40.4, 39.1, 38.8, 34.7, 33.9, 30.5, 28.5, 25.4, 25.1, 20.7, 20.5, 17.6, 16.7. HRMS (ESI) *m / z* $C_{19}H_{31}N_3O_2Na$ [M+Na] Exact Mass 356.230848; Observed 356.231026.

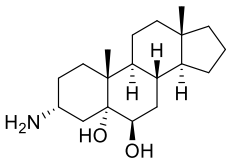

3α-Amino-5α-androstane-5a,6β-diol (**2.40b**)

(3a)-Azido-5a-cholestane-5a,6β-diol (1.450 g, 3.14 mmol) was dissolved in THF (4 mL) and cooled to 0°C under Argon. A 1.0 M soultion of LAH in THF was added slowly over fifteen minutes(20 mL, 20 mmol). Once added reaction was allowed to warm to room temperature and stir overnight for 20 h. Reaction was once again cooled to 0°C and worked up by adding 0.79 mL H_2O slowly, followed by 0.79 mL of 15% soidum hydroxide

solution. After fifteen minutes 1.51 mL of H_2O was added along with some $MgSO_4$. Mixture was then filtered through a pad of celite and concentrated in vacuo. Purification by SiO_2 chromatography (2% NH_4OH/ 18% Methanol/ 80% dichloromethane) yielded compound **2.40b** (0.663 g, 90%) as a white solid. M.P: 143.5-147.4°C; TLC Rf =0.10 (2% NH_4OH/ 18% Methanol/ 80% dichloromethane); IR(ATR, cm^{-1}) 3287, 2931, 2868, 2843, 1637, 1452, 1376; ^1H NMR (400 MHz, CD_3OD) δ 3.49 – 3.46 (m, 2H), 2.26 (dd, *J* = 14.6, 3.8 Hz, 1H), 1.94 (tt, *J* =14.2, 4.3 Hz, 1H), 1.81 – 1.54 (m, 10H), 1.49-1.15 (m, 9H), 1.15 (s, 3H), 1.01 (m, 1H), 0.76 (s, 3H). ^{13}C {^1H} NMR (100 MHz, CD_3OD) δ 75.9, 74.6, 54.1, 46.3, 45.8, 40.7, 40.1, 38.9, 38.8, 34.4, 33.7, 30.4, 28.4, 27.2, 25.1, 20.5, 20.0, 16.6, 15.6. HRMS (ESI) *m / z* $C_{19}H_{34}NO_2$ [M+H] Exact Mass 308.258406; Observed 308.258141.

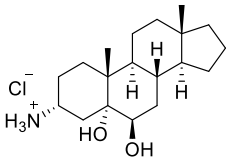

3α-Amino-5α-androstane-5a,6β-diol hydrochloride (**2.42b**)

3α-Amino-5α-androstane-5a,6β-diol (204 mg, 0.66 mmol) was suspended in 15 mL of Et_2O and allowed to stir while dry HCl gas was purged into the reaction mixture by the reaction of concentrated sulfuric acid and sodium chloride. The solution started to turn cloudy/opaque after a few seconds of addition. After approximately 15 minutes, the reaction mixture was filtered and the white precipitate was collected and dried under vacuum producing **2.42b** (70 mg, 31%) as a white solid. M.P: 211.6-213.2°C. TLC Rf =0.10 (2% NH_4OH/ 18% Methanol/ 80% dichloromethane); IR(ATR, cm^{-1}) 3272, 3237, 3162, 2996, 2979, 2966, 2896, 1473, 1377; ^1H NMR (400 MHz, DMSO-d_6) δ 7.61 (bs,3H), 4.69 (d, *J* = 4.4 Hz, 1H), 4.61 (bs, 1H), 3.44-3.42 (m, 2H), 2.28 (dd, *J* = 15.3, 4.8 Hz, 1H),

1.91 – 1.81 (m, 1H), 1.73 – 1.53 (m, 8H), 1.43-1.34 (m, 5H), 1.27 – 1.08 (m, 5H), 1.03 (s, 3H), 0.96 - 0.86 (m, 1H), 0.69 (s, 3H). ^{13}C {^{1}H} NMR (100 MHz, CD_3OD) δ 75.1, 73.0, 54.2, 46.9, 45.3, 41.0, 40.1, 39.0, 38.7, 34.5, 33.2, 30.6, 27.8, 25.5, 24.1, 20.8, 20.6, 17.8, 16.4. HRMS (ESI) *m / z* $C_{19}H_{34}NO_2$ [M+H] Exact Mass 308.258406; Observed 308.258141.

*one carbon peak is obscured by DMSO solvent peak

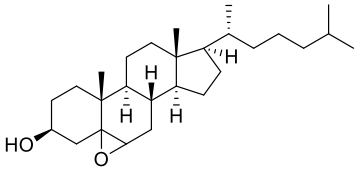

(3β)-Hydroxy-5,6-epoxy-cholestan-3-ol (**2.37c**)

This compound has been previously reported see: (Mori, K.; Nakayama, T.; Sakuma, M. Synthesis of some analogues of blattellastanoside A, the steroidal aggregation pheromone of the German cockroach. *Bioorganic & Medicinal Chemistry* **1996,** *4*, 401-408.)

In an oven dried round bottom flask equipped with stir bar, cholesterol (10.00 g, 25.9 mmol) was dissolved in dry DCM (200 mL). The solution was then cooled to 0°C. meta-Chloroperoxybenzoic acid (11.16 g, 64.9 mmol) was then added. The solution was reacted for 3 h at 0°C. After 3 h the reaction was quenched by adding 100 mL of saturated sodium sulfite solution. The organic layer was separated and the aqueous layer was extracted with DCM (2 x 50 mL). The organic extracts were combined and washed with sodium sulfite (1 x 50 mL), sodium bicarbonate (1 x 50 mL) and brine (1 x 50 mL), dried over sodium sulfate, filtered and concentrated in vacuo. Purification by silica gel chromatography (20% EA / 80% Hexanes) afforded compound **2.37c** (8.3 g, 80%) as a white solid. TLC Rf = 0.39 (30% EA / Hexanes); ^{1}H NMR (400 MHz, $CDCl_3$) δ 3.93 – 3.83

(m, 1H), 2.89 (d, *J* = 4.4 Hz, 1H), 2.08 – 2.02 (m, 1H),1.96 – 1.86 (m, 3H), 1.83 – 1.63 (m, 5H), 1.61 – 1.43 (m, 4H), 1.39 – 1.27 (m, 7H), 1.27 – 1.17 (m, 4H), 1.14 – 1.07 (m, 4H), 1.04 (s, 3H), 1.02 – 0.98 (m, 1H), 0.96 - 0.91 (m, 1H), 0.87(d, J = 6.6 Hz, 3H), 0.84 (dd, J = 6.6, 1.8 Hz, 6H), 0.67 (s, 3H).0.59 (s, 3H).

*mixture of epoxides so integrations may not equal exact number of hydrogens

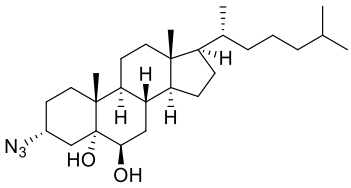

(3a)-Azido-5a-cholestane-5a,6β-diol (**2.39c**)

In an oven dried round bottom flask equipped with stir bar, (3β)-hydroxy-5,6-epoxycholestan-3-ol (10.71 g, 26.6 mmol) and triphenylphosphine (7.33 g, 27.9 mmol) were dissolved in dry THF (150 mL) under a positive pressure of Argon. Diisopropyl azodicarboxylate (5.77 mL, 29.3 mmol) was added to the solution and stirred for ten minutes at room temperature. Diphenylphosphoryl azide (6.32 mL, 29.3 mmol) was added slowly and reaction was allowed to stir for 20 h at room temperature. The reaction was concentrated in vacuo. The crude mixture was taken forward and dissolved in acetone. The solution was then cooled to 0°C. Concentrated(stock) $HClO_4$ was added dropwise(2 mL) and the reaction was stirred for 1 h. After 1 h, the reaction was quenched with saturated sodium bicarbonate (50 mL). The organic layer was extracted with DCM (2 x 25 mL). The combined organic layers were washed with sodium bicarbonate (1 x 25 mL) and brine (2 x 25 mL). The organic layers were dried over $MgSO_4$ and concentrated in

vacuo. Purification by silica gel chromatography (1% MeOH/ 99% DCM) yielded compound **2.39c** (1.50 g, 17%) as a white solid. M.P: 177.8 – 180.1°C. TLC Rf =0.18 (5% Methanol/ 95% Dichloromethane); IR(ATR, cm^{-1}) 3509, 2931, 2865, 2103, 1465, 1375; ^{1}H NMR (400 MHz, $CDCl_3$) δ 4.08 (m, 1H), 3.55 (t, *J* = 2.4 Hz, 1H), 3.44 (s, 1H), 2.40 (dd, *J* = 15.0, 4.3 Hz, 1H), 2.02 – 1.77 (m, 4H) 1.75 – 1.44 (m, 8H), 1.40 – 1.22(m, 7H), 1.21 – 1.13 (m, 4H), 1.11 (s, 3H), 1.11 – 0.94 (m, 5H), 0.90 (d, *J* = 6.5 Hz, 3H), 0.86 (dd, *J* = 6.6, 1.8 Hz, 6H), 0.67 (s, 3H).^{13}C NMR (100 MHz, $CDCl_3$) δ 75.3, 74.2, 58.4, 56.2, 55.7,45.1, 42.7, 39.9, 39.5, 38.9, 36.2, 35.8, 34.4, 33.9, 30.1, 28.5, 28.2, 28.0, 25.0, 24.1, 23.9, 22.8, 22.6, 20.7, 18.7, 16.7, 12.2. HRMS (ESI) *m / z* $C_{27}H_{47}N_3O_2Na$ [M+Na] Exact Mass 468.356049; Observed 468.355677.

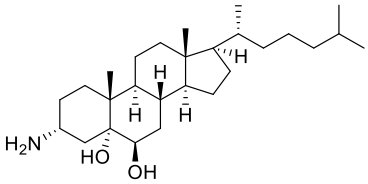

3a-Amino-5a-cholestane-5a,6β-diol (**2.40c**)

Lit Ref: Witiak, D. T.; Parker, R. A.; Dempsey, M. E.; Ritter, M. C. Inhibitors and stimulators of cholesterolgenesis enzymes. Structure-activity study in vitro of amino and selected nitrogen-containing analogs of 5.alpha.-cholestane-3.beta.,5.alpha.,6.beta.-triol. *Journal of Medicinal Chemistry* **1971,** *14*, 684-693.

(3a)-Azido-5a-cholestane-5a,6β-diol (1.450 g, 3.14 mmol) was dissolved in THF (4 mL) and cooled to 0°C under Argon. A 1.0 M soultion of LAH in THF was added slowly over fifteen minutes(32 mL, 32 mmol). Once added reaction was allowed to warm to room temperature and stir overnight for 20 h. Reaction was once again cooled to 0°C and worked up by adding 1.2 mL H_2O slowly, followed by 1.2 mL of 15% soidum hydroxide solution. After fifteen minutes 3.6 mL of H_2O was added along with some $MgSO_4$. Mixture

was then filtered through a pad of celite and concentrated in vacuo. Purification by SiO_2 chromatography (1% NH4OH/ 9% Methanol/ 90% dichloromethane) yielded compound **2.40c** (1.36 g, 99%) as a white solid. M.P: 140.1 – 141.2°C. TLC Rf =0.08 (1% NH_4OH/ 9% methanol/ 90% DCM); IR(ATR, cm^{-1}) 3369, 2929, 2864. 1465, 1380; ^1H NMR (400 MHz, $CDCl_3$) δ 3.59 - 3.56 (m, 2H), 2.22 (dd, *J* = 14.3, Hz, 3.7, 1H), 1.99 -1.77 (m, 4H), 1.75 – 1.44 (m, 7H), 1.38-1.16 (m, 8H), 1.17 – 1.11 (m, 2H), 1.11 (s, 3H), 1.10-0.96 (m, 4H), 0.90 (d, *J* = 6.5 Hz, 3H), 0.86 (dd, *J* = 6.6, 1.6 Hz, 6H), 0.67 (s, 3H).^{13}C NMR (75 MHz, $CDCl_3$) δ 76.1, 74.9, 56.3, 55.8, 46.5, 45.4, 42.7, 40.1, 39.5, 39.2, 36.2, 35.9, 35.0, 34.2, 30.2, 28.7, 28.3, 28.2, 28.0, 24.2, 23.9, 22.8, 22.6, 20.7, 18.7, 16.6, 12.1. HRMS (ESI) *m / z* $C_{27}H_{50}NO_2$ [M+H] Exact Mass 420.383606; Observed 420.383340.

*four exhangeable protons due to water in $CDCl_3$

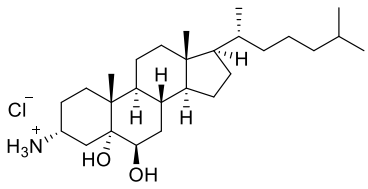

3a-Amino-5a-cholestane-5a,6β-diol hydrochloride (**2.42c**)

3a-Amino-5a-cholestane-5a,6β-diol was suspended in 5 mL of EtOH. To this suspension, 3M HCl(1.2 mL) was added. The heterogenous mixture was stirred for 1 h at room temperature. MeOH(30 mL) was then added to the reaction mixture and concentrated in vacuo. This step was repeated two more times and then placed on a high vacuum pump overnight. This yielded compound **2.42c** as a white solid (618 mg, 87%). M.P: 163.7-166.5°C. TLC Rf =0.11 (1% triethylamine/ 9% methanol/ 90% DCM); IR(ATR, cm^{-1}) 3296, 2932, 2866, 1466, 1381; ^1H NMR (400 MHz, CD_3OD) δ 7.71 (bs, 1H), 3.57 – 3.51 (m, 2H), 2.49 (dd, *J* = 15.4, 4.6 Hz, 1H), 2.11 – 2.01 (m, 2H), 1.87-1.69 (m, 4H), 1.66 – 1.51 (m, 4H), 1.46-1.29 (m, 9H), 1.21-1.00 (m, 7H), 1.16 (s, 3H), 0.94 (d, *J* = 6.5 Hz, 3H), 0.88

(d, *J* = 6.4, 6H), 0.73 (s, 3H). ^{13}C NMR (100 MHz, DMSO-d_6) δ 75.1, 73.0, 56.2, 56.1, 46.9, 45.0, 42.7, 38.5, 36.1, 35.7, 34.1, 33.1, 30.2, 28.3, 27.9, 24.3, 24.1, 23.7, 23.1, 22.9, 20.8, 19.0, 16.4, 12.4. HRMS (ESI) m / z $C_{27}H_{49}NO_2$ H^+ Exact Mass 420.383606; Observed 420.383340.

*some peaks are obscured by solvent in carbon NMR

**Some protons are missing due to deuterium exhange

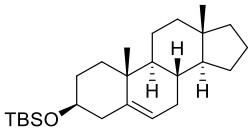

5-androsten-3β-ol- tert-butyldimethylsilyl ether (**2.69**)

This compound has been previously reported, see: (Dungan, O. M.; Dormann, S.; Fernandes, S.; Duffy, B. C.; Effiong, D. G.; Kerr, W. G.; Chisholm, J. D. Synthetic studies on the indane SHIP1 agonist AQX-1125. *Organic & Biomolecular Chemistry* **2022,** *20*, 4016-4020.)

Alcohol **2.35** (4.00 g, 13.7 mmol) was added to a 250 mL oven dried round-bottom flask. 44 mL of DMF and 44 mL of DCM were added to dissolve the ketal. Imidazole (2.25 g, 33.1 mmol) and tert-butyldimethyl silyl chloride (3.11 g, 20.6 mmol) were then added to the reaction. This reaction mixture was allowed to stir at rt for 20 hours under argon. The excess solvent was removed under reduced pressure. The remaining contents were diluted with diethyl ether (150 mL) and washed successively with 5% aqueous HCl (2 x 75 mL), saturated $NaHCO_3$ (2 x 75 mL) and saturated NaCl (75 mL). The organic layer was dried with anhydrous Na_2SO_4 and removed under reduced pressure to yield the silyl ether **2.69** as a white colored solid (5.51 g, 95%). M.P: 117.8 – 118.5°C. TLC R_f = 0.89 (10% Ethyl Acetate/90% hexanes); ^{1}H NMR (400 MHz, $CDCl_3$) δ 5.33 -5.31 (m, 1H), 3.55

(septet, *J* = 4.8 Hz, 1H), 2.30 - 2.24 (m, 1H), 2.17 (qd, *J* = 10.4, 2.8 Hz, 1H), 2.05 -1.97 (m, 1H), 1.82 (dt, J=13.2, 3.4 Hz, 1H), 1.77-1.57 (m, 6H), 1.55-1.35 (m, 5H), 1.23 -1.07 (m, 4H), 1.01 (s, 3H), 0.98 - 0.86 (m, 2H), 0.89 (s, 9H), 0.71 (s, 3H), 0.00 (s, 6H); ^{13}C {^{1}H} NMR (100 MHz, $CDCl_3$) δ 141.6, 121.2, 72.6,54.9, 50.5, 42.8, 40.6, 40.3, 38.7, 37.5, 36.7, 32.2, 32.2, 32.1, 26.0 (3C), 25.6, 21.1, 20.5, 19.5, 18.3, 17.3, -4.57.

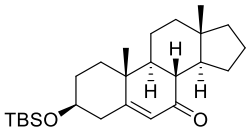

5-Androsten-7-one-3β-ol tert-butyldimethylsilyl ether (**2.70**)

This compound has been previously reported, see: (Dungan, O. M.; Dormann, S.; Fernandes, S.; Duffy, B. C.; Effiong, D. G.; Kerr, W. G.; Chisholm, J. D. Synthetic studies on the indane SHIP1 agonist AQX-1125. *Organic & Biomolecular Chemistry* **2022,** *20*, 4016-4020.)

5-androsten-3β-ol- tert-butyldimethylsilyl ether **2.69** (0.250 g, 0.64 mmol) was added to an oven dried test tube along with Bis[rhodium(α,α,α′,α′-tetramethyl-1,3-benzenedipropionic acid)](0.005 g, 0.0064 mmol). The solids were dissolved in n-heptane (2 mL) and 70 wt % tert-butyl hydroperoxide(0.40 mL, 3.2 mmol) was added slowly. The test tube was equipped with a purge needle and allowed to stir at room temperature for 16 hours. After stirring for 16 hours the reaction mixture diluted with ethyl acetate (5 mL) and was quenched with a saturated sodium thiosulfate solution(10 mL). The organic layer was extracted and subsequently washed with deionized water (2 x 5 mL). The combined aqueous layers were extracted once more with ethyl acetate (5 mL). The combined organic layers were dried over sodium sulfate and concentrated in vacuo. Further purification was done through flash column chromatography (10% Ethyl

Acetate/Hexanes). This yielded compound **2.70** as a white solid in 63% yield. M.P: 146.9 – 148.7°C. TLC R_f = 0.47 (10% Ethyl Acetate in hexanes); ^{1}H NMR (400 MHz, $CDCl_3$) δ 5.68 (s, 1H), 3.60 (sept, *J* = 5.3 Hz, 1H), 2.52- 2.34 (m, 3H), 2.12 (t, *J* = 11.2 Hz, 1H), 1.92 (dt, J=13.7, 3.4 Hz, 1H), 1.86 – 1.47 (m, 9H), 1.45 -1.30 (m, 2H), 1.28 – 1.20 (m, 1H), 1.19 (s, 3H), 1.11 – 1.01 (m, 2H), 0.89 (s, 9H), 0.72 (s, 3H), 0.06 (s, 6H); ^{13}C {^{1}H} NMR (100 MHz, $CDCl_3$): δ 202.3, 166.2, 125.7, 71.3, 50.3, 48.0, 45.8, 42.6, 41.3, 39.2, 38.5, 37.8, 36.5, 31.8, 27.6, 25.8, 21.3, 20.6, 18.2, 17.4, 17.2, -4.64, -4.67.

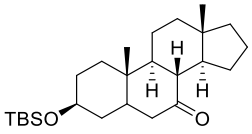

5-Androsta-7-one-3β-ol tert-butyldimethylsilyl ether **(2.71)**

This compound has been previously reported, see: (Dungan, O. M.; Dormann, S.; Fernandes, S.; Duffy, B. C.; Effiong, D. G.; Kerr, W. G.; Chisholm, J. D. Synthetic studies on the indane SHIP1 agonist AQX-1125. *Organic & Biomolecular Chemistry* **2022,** *20*, 4016-4020.)

To a 250 mL oven-dried round bottom flask, tert-butyldimethylsilyl ether **2.70** (2.22g, 5.51 mmol) was dissolved in 154 mL of ethyl acetate. 10% Pd/C (58 mg, 0.551 mmol) was added to the reaction. The reaction was placed under vacuum until bubbling was observed. The reaction was removed from vacuum and placed under a hydrogen atmosphere using a hydrogen balloon. The reaction was allowed to stir for 20 hours at room temperature. The reaction was then filtered through celite, rinsing with ethyl acetate. This was concentrated under reduced pressure to yield ketone **2.71** as a white colored solid (2.1 g, 99%). M.P: 104.3 – 105.4°C. TLC R_f = 0.67 (15% EA /85% hexanes); ^{1}H NMR (400 MHz, $CDCl_3$) δ 3.56 – 3.45 (m, 1H), 2.35 -2.16 (m, 3H), 2.00 -1.94 (m, 1H),

1.72 -1.58 (m, 5H), 1.50 -1.19 (m, 9H), 1.12 – 1.04 (m, 2H), 1.04 (s, 3H), 1.02 – 0.92 (m, 2H), 0.83 (s, 9H), 0.64 (s, 3H), 0.00 (s, 6H).

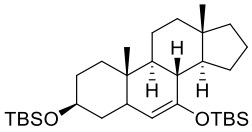

5-Androsta -7– tert-butyldimethyl oxysilane -3β-ol tert-butyldimethylsilyl ether (**2.72**)

This compound has been previously reported, see: (Dungan, O. M.; Dormann, S.; Fernandes, S.; Duffy, B. C.; Effiong, D. G.; Kerr, W. G.; Chisholm, J. D. Synthetic studies on the indane SHIP1 agonist AQX-1125. *Organic & Biomolecular Chemistry* **2022,** *20*, 4016-4020.)

Ketone **2.71** (1.04 g, 2.47 mmol) was dissolved in 30.0 mL of CH_2Cl_2. 9.0 mL of triethylamine (49.4 mmol) was added drop wise at 0 °C. This was allowed to stir at this temperature for 15 minutes. tert-butyldimethylsilyl trifluoromethane sulfonate (1.70 mL, 7.41 mmol) was then slowly added to the reaction, while maintaining 0°C. This reaction mixture was placed at rt and allowed to stir for 20 hours under argon. The next day the reaction was once more placed at 0°C and isopropyl alcohol (1.1 mL) was then added. The reaction was then diluted with DCM (100 mL) and saturated $NaHCO_3$ (50 mL). The aqueous phase was extracted 2x with DCM (100 mL) collected and the organic layer was washed with saturated $NaHCO_3$ (1x 50 mL) and brine (1x 50 mL) and dried over $MgSO_4$ (This was concentrated under reduced pressure and subjected to column chromatography (5% TEA/95% hexanes) to yield silyl enol ether **2.72** as a pale yellowish-white colored solid (0.85 g, 88%). M.P: 104.9 – 108.9°C. TLC R_f = 0.58 (1% EA /99% hexanes); ^{1}H NMR (400 MHz, $CDCl_3$) δ 4.41 (s, 1H), 3.59 (m, 1H), 2.01-

1.79 (m, 2H), 1.76 - 1.56 (m, 5H), 1.51 - 1.15 (m, 9H), 1.14 – 1.07 (m, 2H), 1.06 – 0.98 (m, 2H), 0.92 (s, 9H), 0.89 (s, 9H), 0.87 (s, 3H) 0.74 (m, 3H), 0.12 (m, 6H), 0.06 (m, 6H).

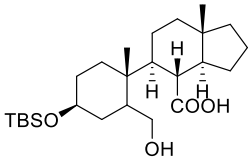

(7a*S*)-5-[(1*R*,4*S*)-4-((tert-butyldimethylsilyl)oxy)-1-methylcyclohexyl]-7a-methylperhydro-1*H*-indene-4-carboxylic acid (**2.73**)

This compound has been previously reported, see: (Dungan, O. M.; Dormann, S.; Fernandes, S.; Duffy, B. C.; Effiong, D. G.; Kerr, W. G.; Chisholm, J. D. Synthetic studies on the indane SHIP1 agonist AQX-1125. *Organic & Biomolecular Chemistry* **2022,** *20*, 4016-4020.)

Silyl enol ether, **2.72** (1.12 g, 2.09 mmol) was dissolved in methanol (50 mL) and DCM (50 mL) and was treated with excess O_3 at -78 °C until the solution turned a light blue. The reaction was purged with Argon until the blue color had dissipated. The reaction was then placed at 0 °C and sodium borohydride (0.316 g, 8.38 mmol) was added in one portion. This was then placed at room temperature and allowed to stir for 20 hours. Reaction was concentrated and then diluted with DCM (50 mL) and water (50 mL). The DCM layer was removed and the aqueous layer extracted with DCM (2 × 50 mL). The organic layers were collected and washed with saturated NaCl (2x 50 mL). The organic layer was dried with anhydrous $MgSO_4$ and removed under reduced pressure to yield acid **2.73** as a white solid (0.240 g, 25%). M.P: 140.1 -143.5°C. TLC R_f = 0.49 (10% MeOH/ 90% DCM); IR (ATR) 3314, 2932, 1669, 1245, 1209; ^{1}H NMR (300 MHz, CD_3OD) δ 3.75 (dd, *J* = 10.3, 2.4 Hz, 1H), 3.54 (m, 1H), 3.09 (t, *J* = 10.4 Hz, 1H), 2.24 (t, 11.2 Hz, 1H), 2.07 (d, *J* = 14.4 Hz, 1H), 1.97-1.89 (m, 1H), 1.80-1.39 (m, 14H), 1.33-1.18 (m, 5H), 0.90

(bs, 12H), 0.73 (s, 3H), 0.07 (s, 6H). ^{13}C {^{1}H} NMR (75 MHz, CD_3OD) δ 179.9, 71.5, 60.9, 51.4, 46.0, 44.8, 42.3, 39.6, 39.4, 38.0, 37.2, 34.2, 31.2, 29.9, 25.8, 24.9, 20.9, 19.5, 18.2, 17.6, 15.6, -5.8. Mass Spec *m/z* $C_{25}H_{46}NaO_4Si$ Exact Mass 461.305758; Observed 461.305346.

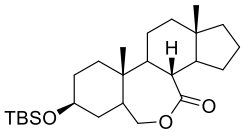

(2*R*,5*S*,16*S*)-5-((tert-butyldimethylsilyl)oxy)-2,16-dimethyl-9-oxatetracyclo[9.7.0.0^{2,7}.0^{12,16}] octadecan-10-lactone (**2.74**)

This compound has been previously reported, see: (Dungan, O. M.; Dormann, S.; Fernandes, S.; Duffy, B. C.; Effiong, D. G.; Kerr, W. G.; Chisholm, J. D. Synthetic studies on the indane SHIP1 agonist AQX-1125. *Organic & Biomolecular Chemistry* **2022,** *20*, 4016-4020.)

Carboxylic acid **2.73** (0.160 g, 0.38 mmol) was dissolved in 5.0 mL of DCM inside a 25 mL round bottom flask and DMAP (0.005 g, 0.038 mmol) was added to the flask. After stirring for 5 minutes, 1-ethyl-3-(3-dimethylaminopropyl)carbodiimide (0.139 g, 0.72 mmol) was then added. The reaction was then stirred for 24 hours. The reaction was diluted with DCM (50 mL) and washed successively with saturated $NaHCO_3$ (2 x 20 mL), 10% aqueous HCl (2 x 20 mL), and sat. aq. NaCl (20 mL). The organic layer was dried with anhydrous $MgSO_4$ and solvent removed under reduced pressure. Purification by silica gel column chromatography using (20% EA/80% hexanes) yielded lactone **2.74** as a white solid (0.090 g, 92%). M.P: TLC R_f = 0.42 (10% EA /90% hexanes); ^{1}H NMR (300 MHz, $CDCl_3$) δ 4.33 (dd, *J* = 12.0, 4.0 Hz, 1H), 3.61 (d, *J* = 12.0 Hz, 1H), 3.57-3.48 (m,

1H), 2.50 (t, 10.8 Hz, 1H), 1.94-1.61 (m, 8H), 1.48-1.12 (m, 9H), 1.11 – 1.04 (m, 1H), 1.02 (s, 3H), 0.98 – 0.91 (m, 1H), 0.87 (s, 9H), 0.70 (s, 3H), 0.04 (s, 6H).

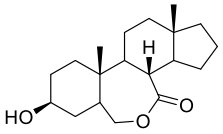

(2*R*,5*S*,16*S*)-5-Hydroxy-2,16-dimethyl-9-oxatetracyclo[9.7.0.$0^{2,7}$.$0^{12,16}$]octadecan-10-one (**2.75**)

This compound has been previously reported, see: (Dungan, O. M.; Dormann, S.; Fernandes, S.; Duffy, B. C.; Effiong, D. G.; Kerr, W. G.; Chisholm, J. D. Synthetic studies on the indane SHIP1 agonist AQX-1125. *Organic & Biomolecular Chemistry* **2022,** *20*, 4016-4020.)

Protected Lactone **2.74** (0.090 g, 0.214 mmol) was dissolved in 10 mL of methanol inside a round bottom flask equipped with stir bar. 10% aq. HCl (3 mL) was added dropwise and the solution was stirred for 4 hours. Reaction was diluted with methanol (20 mL) and concentrated under reduced pressure. Reaction was purified by flash column chromatography (50% Ethyl Acetate/ 50% Hexanes) to yield compound **2.75** as a white solid (0.060 g, 92%). M.P: 125.7 - 129.3°C. TLC R_f = 0.39 (50% EA /50% hexanes); ^{1}H NMR (400 MHz, $CDCl_3$) δ 4.34 (dd, *J* = 12.8, 8.0 Hz, 1H), 3.64- 3.55 (m, 2H), 3.48 (s, 1H), 2.50 (t, 10.4 Hz, 1H), 1.94-1.84 (m, 2H), 1.83 – 1.53 (m, 12H), 1.48 -1.16 (m, 7H), 1.12 -1.04 (m, 1H), 1.03 (s, 3H), 1.02 – 1.00 (m, 1H), 0.71 (s, 3H). ^{13}C {^{1}H} NMR (100 MHz, $CDCl_3$) δ 177.1, 77.2, 70.0, 68.1, 48.4, 47.2, 46.4, 41.8, 39.8, 38.7, 37.3, 37.2, 36.6, 30.7, 27.5, 22.2, 19.8, 16.6, 13.2.

2.8 References

1) Whisstock, J. C.; Wiradjaja, F.; Waters, J. E.; Gurung, R. The Structure and Function of Catalytic Domains Within Inositol Polyphosphate 5-Phosphatases. *IUBMB Life* **2002,** *53*, 15-23.
2) Tsutakawa, S. E.; Shin, D. S.; Mol, C. D.; Izumi, T.; Arvai, A. S.; Mantha, A. K.; Szczesny, B.; Ivanov, I. N.; Hosfield, D. J.; Maiti, B.; Pique, M. E.; Frankel, K. A.; Hitomi, K.; Cunningham, R. P.; Mitra, S.; Tainer, J. A. Conserved Structural Chemistry for Incision Activity in Structurally Non-homologous Apurinic/Apyrimidinic Endonuclease APE1 and Endonuclease IV DNA Repair Enzymes*. *Journal of Biological Chemistry* **2013,** *288*, 8445-8455.
3) Aboelnga, M. M.; Wetmore, S. D. Unveiling a Single-Metal-Mediated Phosphodiester Bond Cleavage Mechanism for Nucleic Acids: A Multiscale Computational Investigation of a Human DNA Repair Enzyme. *Journal of the American Chemical Society* **2019,** *141*, 8646-8656.
4) Pedicone, C.; Meyer, S. T.; Chisholm, J. D.; Kerr, W. G. Targeting SHIP1 and SHIP2 in Cancer. *Cancers* **2021,** *13*, 890.
5) Mills, S. J.; Silvander, C.; Cozier, G.; Trésaugues, L.; Nordlund, P.; Potter, B. V. L. Crystal Structures of Type-II Inositol Polyphosphate 5-Phosphatase INPP5B with Synthetic Inositol Polyphosphate Surrogates Reveal New Mechanistic Insights for the Inositol 5-Phosphatase Family. *Biochemistry* **2016,** *55*, 1384-1397.
6) Kerr, W. G.; Pedicone, C.; Kerr, W. G.; Dormann, S.; Pacherille, A.; Chisholm, J. D.; Kerr, W. G.; Pedicone, C. Small molecule targeting of SHIP1 and SHIP2. *Biochem Soc Trans* **2020,** *48*, 291-300.
7) Trésaugues, L.; Silvander, C.; Flodin, S.; Welin, M.; Nyman, T.; Gräslund, S.; Hammarström, M.; Berglund, H.; Nordlund, P. Structural Basis for Phosphoinositide Substrate Recognition, Catalysis, and Membrane Interactions in Human Inositol Polyphosphate 5-Phosphatases. *Structure* **2014,** *22*, 744-755.
8) Mills, S. J.; Persson, C.; Cozier, G.; Thomas, M. P.; Trésaugues, L.; Erneux, C.; Riley, A. M.; Nordlund, P.; Potter, B. V. L. A Synthetic Polyphosphoinositide Headgroup Surrogate in Complex with SHIP2 Provides a Rationale for Drug Discovery. *ACS Chemical Biology* **2012,** *7*, 822-828.
9) Hsu, F.; Mao, Y. The structure of phosphoinositide phosphatases: Insights into substrate specificity and catalysis. *Biochimica et Biophysica Acta (BBA) - Molecular and Cell Biology of Lipids* **2015,** *1851*, 698-710.
10) Bradshaw, W. J., Williams, E.P., Fernandez-Cid, A., Burgess-Brown, N., von Delft, F., Arrowsmith, C.H., Edwards, A., Bountra, C., Gileadi, O. The Phosphatase and C2 domains of Human SHIP1. https://www.rcsb.org/structure/6IBD
11) Brooks, R.; Fuhler, G. M.; Iyer, S.; Smith, M. J.; Park, M.-Y.; Paraiso, K. H. T.; Engelman, R. W.; Kerr, W. G. SHIP1 Inhibition Increases Immunoregulatory Capacity and Triggers Apoptosis of Hematopoietic Cancer Cells. *The Journal of Immunology* **2010,** *184*, 3582.
12) Fuhler, G. M.; Brooks, R.; Toms, B.; Iyer, S.; Gengo, E. A.; Park, M.-Y.; Gumbleton, M.; Viernes, D. R.; Chisholm, J. D.; Kerr, W. G. Therapeutic Potential of SH2 Domain-Containing Inositol-5′-Phosphatase 1 (SHIP1) and SHIP2 Inhibition in Cancer. *Molecular Medicine* **2012,** *18*, 65-75.

13) Ecker, V.; Stumpf, M.; Brandmeier, L.; Neumayer, T.; Pfeuffer, L.; Engleitner, T.; Ringshausen, I.; Nelson, N.; Jücker, M.; Wanninger, S.; Zenz, T.; Wendtner, C.; Manske, K.; Steiger, K.; Rad, R.; Müschen, M.; Ruland, J.; Buchner, M. Targeted PI3K/AKT-hyperactivation induces cell death in chronic lymphocytic leukemia. *Nature Communications* **2021,** *12*, 3526.
14) Stacchini, A.; Aragno, M.; Vallario, A.; Alfarano, A.; Circosta, P.; Gottardi, D.; Faldella, A.; Rege-Cambrin, G.; Thunberg, U.; Nilsson, K.; Caligaris-Cappio, F. MEC1 and MEC2: two new cell lines derived from B-chronic lymphocytic leukaemia in prolymphocytoid transformation. *Leukemia Research* **1999,** *23*, 127-136.
15) Russo, C. M.; Adhikari, A. A.; Wallach, D. R.; Fernandes, S.; Balch, A. N.; Kerr, W. G.; Chisholm, J. D. Synthesis and initial evaluation of quinoline-based inhibitors of the SH2-containing inositol 5′-phosphatase (SHIP). *Bioorganic & Medicinal Chemistry Letters* **2015,** *25*, 5344-5348.
16) Sosič, I.; Anderluh, M.; Sova, M.; Gobec, M.; Mlinarič Raščan, I.; Derouaux, A.; Amoroso, A.; Terrak, M.; Breukink, E.; Gobec, S. Structure–Activity Relationships of Novel Tryptamine-Based Inhibitors of Bacterial Transglycosylase. *Journal of Medicinal Chemistry* **2015,** *58*, 9712-9721.
17) Hoekstra, E. Lipid phosphatase SHIP2 functions as oncogene in colorectal cancer by regulating PKB activation. *Oncotarget* **2016,** *7*, 73525-73540.
18) Pedicone, C.; Fernandes, S.; Dungan, O. M.; Dormann, S. M.; Viernes, D. R.; Adhikari, A. A.; Choi, L. B.; De Jong, E. P.; Chisholm, J. D.; Kerr, W. G. Pan-SHIP1/2 inhibitors promote microglia effector functions essential for CNS homeostasis. *Journal of Cell Science* **2020,** *133*,
19) Suwa, A.; Yamamoto, T.; Sawada, A.; Minoura, K.; Hosogai, N.; Tahara, A.; Kurama, T.; Shimokawa, T.; Aramori, I. Discovery and functional characterization of a novel small molecule inhibitor of the intracellular phosphatase, SHIP2. *Br J Pharmacol* **2009,** *158*, 879-87.
20) Suwa, A.; Kurama, T.; Yamamoto, T.; Sawada, A.; Shimokawa, T.; Aramori, I. Glucose metabolism activation by SHIP2 inhibitors via up-regulation of GLUT1 gene in L6 myotubes. *European Journal of Pharmacology* **2010,** *642*, 177-182.
21) Bell, G. I.; Kayano, T.; Buse, J. B.; Burant, C. F.; Takeda, J.; Lin, D.; Fukumoto, H.; Seino, S. Molecular biology of mammalian glucose transporters. *Diabetes Care* **1990,** *13*, 198-208.
22) Ghosh, S.; Scozzaro, S.; Ramos, A. R.; Delcambre, S.; Chevalier, C.; Krejci, P.; Erneux, C. Inhibition of SHIP2 activity inhibits cell migration and could prevent metastasis in breast cancer cells. *Journal of Cell Science* **2018,** *131*,
23) Jaladanki, C. K.; Taxak, N.; Varikoti, R. A.; Bharatam, P. V. Toxicity Originating from Thiophene Containing Drugs: Exploring the Mechanism using Quantum Chemical Methods. *Chemical Research in Toxicology* **2015,** *28*, 2364-2376.
24) Lim, J. W.; Kim, S. K.; Choi, S. Y.; Kim, D. H.; Gadhe, C. G.; Lee, H. N.; Kim, H.-J.; Kim, J.; Cho, S. J.; Hwang, H.; Seong, J.; Jeong, K.-S.; Lee, J. Y.; Lim, S. M.; Lee, J. W.; Pae, A. N. Identification of crizotinib derivatives as potent SHIP2 inhibitors for the treatment of Alzheimer's disease. *European Journal of Medicinal Chemistry* **2018,** *157*, 405-422.

25) Ichihara, Y.; Fujimura, R.; Tsuneki, H.; Wada, T.; Okamoto, K.; Gouda, H.; Hirono, S.; Sugimoto, K.; Matsuya, Y.; Sasaoka, T.; Toyooka, N. Rational design and synthesis of 4-substituted 2-pyridin-2-ylamides with inhibitory effects on SH2 domain-containing inositol 5′-phosphatase 2 (SHIP2). *European Journal of Medicinal Chemistry* **2013,** *62*, 649-660.
26) Berg, M. E. A.; Naams, J.-B.; Hautala, L. C.; Tolvanen, T. A.; Ahonen, J. P.; Lehtonen, S.; Wähälä, K. Novel Sulfonanilide Inhibitors of SHIP2 Enhance Glucose Uptake into Cultured Myotubes. *ACS Omega* **2020,** *5*, 1430-1438.
27) Andersen, R. J. Sponging off nature for new drug leads. *Biochem. Pharmacol.* **2017,** *139*, 3-14.
28) Yang, L.; Williams, D. E.; Mui, A.; Ong, C.; Krystal, G.; van Soest, R.; Andersen, R. J. Synthesis of Pelorol and Analogs: Activators of the Inositol 5-Phosphatase SHIP. *Org. Lett.* **2005,** *7*, 1073-1076.
29) Kennah, M.; Yau, T. Y.; Nodwell, M.; Krystal, G.; Andersen, R. J.; Ong, C. J.; Mui, A. L. F. Activation of SHIP via a small molecule agonist kills multiple myeloma cells. *Exp. Hematol. (N. Y., NY, U. S.)* **2009,** *37*, 1274-1283.
30) Ong, C. J.; Ming-Lum, A.; Nodwell, M.; Ghanipour, A.; Yang, L.; Williams, D. E.; Kim, J.; Demirjian, L.; Qasimi, P.; Ruschmann, J.; Cao, L.-P.; Ma, K.; Chung, S. W.; Duronio, V.; Andersen, R. J.; Krystal, G.; Mui, A. L. F. Small-molecule agonists of SHIP1 inhibit the phosphoinositide 3-kinase pathway in hematopoietic cells. *Blood* **2007,** *110*, 1942-1949.
31) Chamberlain, T. C.; Cheung, S. T.; Yoon, J. S. J.; Ming-Lum, A.; Gardill, B. R.; Shakibakho, S.; Dzananovic, E.; Ban, F.; Samiea, A.; Jawanda, K.; Priatel, J.; Krystal, G.; Ong, C. J.; Cherkasov, A.; Andersen, R. J.; McKenna, S. A.; Van Petegem, F.; Mui, A. L. F. Interleukin-10 and Small Molecule SHIP1 Allosteric Regulators Trigger Anti-inflammatory Effects through SHIP1/STAT3 Complexes. *iScience* **2020,** *23*, 101433.
32) Whitfield, H.; Hemmings, A. M.; Mills, S. J.; Baker, K.; White, G.; Rushworth, S.; Riley, A. M.; Potter, B. V. L.; Brearley, C. A. Allosteric Site on SHIP2 Identified Through Fluorescent Ligand Screening and Crystallography: A Potential New Target for Intervention. *J Med Chem* **2021,** *64*, 3813-3826.
33) Meimetis, L. G.; Nodwell, M.; Yang, L.; Wang, X.; Wu, J.; Harwig, C.; Stenton, G. R.; Mackenzie, L. F.; MacRury, T.; Patrick, B. O.; Ming-Lum, A.; Ong, C. J.; Krystal, G.; Mui, A. L.-F.; Andersen, R. J. Synthesis of SHIP1-Activating Analogs of the Sponge Meroterpenoid Pelorol. *European Journal of Organic Chemistry* **2012,** *2012*, 5195-5207.
34) Stenton, G. R.; MacKenzie, L. F.; Tam, P.; Cross, J. L.; Harwig, C.; Raymond, J.; Toews, J.; Wu, J.; Ogden, N.; MacRury, T.; Szabo, C. Characterization of AQX-1125, a small-molecule SHIP1 activator. Part 1. Effects on inflammatory cell activation and chemotaxis in vitro and pharmacokinetic characterization in vivo. *Br. J. Pharmacol.* **2013,** *168*, 1506-1518.
35) Stenton, G. R.; Mackenzie, L. F.; Tam, P.; Cross, J. L.; Harwig, C.; Raymond, J.; Toews, J.; Chernoff, D.; MacRury, T.; Szabo, C. Characterization of AQX-1125, a small-molecule SHIP1 activator: Part 2. Efficacy studies in allergic and pulmonary inflammation models in vivo. *Br J Pharmacol* **2013,** *168*, 1519-29.

36) Williams, D. E.; Andersen, R. J. Biologically active marine natural products and their molecular targets discovered using a chemical genetics approach. *Nat. Prod. Rep.* **2020,** *37*, 617-633.
37) Nickel, J. C.; Egerdie, B.; Davis, E.; Evans, R.; Mackenzie, L.; Shrewsbury, S. B. A Phase II Study of the Efficacy and Safety of the Novel Oral SHIP1 Activator AQX-1125 in Subjects with Moderate to Severe Interstitial Cystitis/Bladder Pain Syndrome. *J Urol* **2016,** *196*, 747-54.
38) Stewart, S. Aquinox Pharma AQX-1125 fails Phase 3 Trial. https://biotuesdays.com/2018/06/27/2018-6-27-aquinox-pharma-aqx-1125-fails-phase-3-trial/ (3/14/2021),
39) Leaker, B. R.; Barnes, P. J.; O'Connor, B. J.; Ali, F. Y.; Tam, P.; Neville, J.; Mackenzie, L. F.; MacRury, T. The effects of the novel SHIP1 activator AQX-1125 on allergen-induced responses in mild-to-moderate asthma. *Clin Exp Allergy* **2014,** *44*, 1146-53.
40) Gross, N. The COPD Pipeline XXVII. *Chronic Obstr Pulm Dis* **2015,** *2*, 191-194.
41) Kennah, M.; Yau, T. Y.; Nodwell, M.; Krystal, G.; Andersen, R. J.; Ong, C. J.; Mui, A. L. Activation of SHIP via a small molecule agonist kills multiple myeloma cells. *Exp Hematol* **2009,** *37*, 1274-83.
42) Lemm, E. A.; Valle-Argos, B.; Smith, L. D.; Richter, J.; Gebreselassie, Y.; Carter, M. J.; Karolova, J.; Svaton, M.; Helman, K.; Weston-Bell, N. J.; Karydis, L.; Williamson, C. T.; Lenz, G.; Pettigrew, J.; Harwig, C.; Stevenson, F. K.; Cragg, M.; Forconi, F.; Steele, A. J.; Cross, J.; Mackenzie, L.; Klener, P.; Packham, G. Preclinical Evaluation of a Novel SHIP1 Phosphatase Activator for Inhibition of PI3K Signaling in Malignant B Cells. *Clinical Cancer Research* **2020,** *26*, 1700-1711.
43) Le Coq, J.; Camacho-Artacho, M.; Velázquez, J. V.; Santiveri, C. M.; Gallego, L. H.; Campos-Olivas, R.; Dölker, N.; Lietha, D. Structural basis for interdomain communication in SHIP2 providing high phosphatase activity. *eLife* **2017,** *6*, e26640.
44) Pedicone, C.; Fernandes, S.; Matera, A.; Meyer, S. T.; Loh, S.; Ha, J.-H.; Bernard, D.; Chisholm, J. D.; Paolicelli, R. C.; Kerr, W. G. Discovery of a novel SHIP1 agonist that promotes degradation of lipid-laden phagocytic cargo by microglia. *iScience* **2022,** *25*, 104170.
45) Brooks, R.; Iyer, S.; Akada, H.; Neelam, S.; Russo, C. M.; Chisholm, J. D.; Kerr, W. G. Coordinate expansion of murine hematopoietic and mesenchymal stem cell compartments by SHIPi. *Stem Cells* **2015,** *33*, 848-58.
46) Srivastava, N.; Iyer, S.; Sudan, R.; Youngs, C.; Engelman, R. W.; Howard, K. T.; Russo, C. M.; Chisholm, J. D.; Kerr, W. G. A small-molecule inhibitor of SHIP1 reverses age- and diet-associated obesity and metabolic syndrome. *JCI Insight* **2016,** *1*,
47) Kam, T.-I.; Park, H.; Gwon, Y.; Song, S.; Kim, S.-H.; Moon, S. W.; Jo, D.-G.; Jung, Y.-K. FcγRIIb-SHIP2 axis links Aβ to tau pathology by disrupting phosphoinositide metabolism in Alzheimer's disease model. *eLife* **2016,** *5*, e18691.
48) Ando, K.; Erneux, C.; Homa, M.; Houben, S.; de Fisenne, M.-A.; Brion, J.-P.; Leroy, K. Dysregulation of Phosphoinositide 5-Phosphatases and Phosphoinositides in Alzheimer's Disease. *Frontiers in Neuroscience* **2021,** *15*,

49) Panitch, R.; Hu, J.; Xia, W.; Bennett, D. A.; Stein, T. D.; Farrer, L. A.; Jun, G. R. Blood and brain transcriptome analysis reveals APOE genotype-mediated and immune-related pathways involved in Alzheimer disease. *Alzheimer's Research & Therapy* **2022,** *14*, 30.
50) Huang, M. Reduction of steroid ketones and other carbonyl compounds by modified Wolff-Kishner method. *J. Am. Chem. Soc.* **1949,** *71*, 3301-3.
51) Staudinger, H.; Meyer, J. Über neue organische Phosphorverbindungen III. Phosphinmethylenderivate und Phosphinimine. *Helvetica Chimica Acta* **1919,** *2*, 635-646.
52) Choi, L. B. Synthesis of SHIP-1 Antagonists and their Analogues. Syracuse University, 2011.
53) Munawar, S.; Zahoor, A. F.; Ali, S.; Javed, S.; Irfan, M.; Irfan, A.; Kotwica-Mojzych, K.; Mojzych, M. Mitsunobu Reaction: A Powerful Tool for the Synthesis of Natural Products: A Review. *Molecules* **2022,** *27*,
54) Cross, A. D. Steroids. CC. 1 Spectra and Stereochemistry, Part III. 2 Steroidal 5, 6-Epoxides. *Journal of the American Chemical Society* **1962,** *84*, 3206-3207.
55) Paillasse, M. R.; Saffon, N.; Gornitzka, H.; Silvente-Poirot, S.; Poirot, M.; de Medina, P. Surprising unreactivity of cholesterol-5,6-epoxides towards nucleophiles. *J Lipid Res* **2012,** *53*, 718-25.
56) Poirot, M.; Silvente-Poirot, S. Cholesterol-5,6-epoxides: Chemistry, biochemistry, metabolic fate and cancer. *Biochimie* **2013,** *95*, 622-631.
57) Wu, X.; Fan, W.; Pan, Y.; Zhai, Y.; Niu, Y.; Li, C.; Mei, Q. Synthesis, Crystal Structure and Anti-Fatigue Effects of Some Benzamide Derivatives. *Molecules* **2014,** *19*, 1034-1046.
58) Polo, E.; Morales-Bayuelo, A.; Orozco-Ugarriza, M. E.; Henao, J. A.; Galdámez, A.; Gutierrez, M. Crystal structure and theoretical studies of 2-bromo-N-(2,4-difluorobenzyl)benzamide; intermediate for the synthesis of phenanthridinone. *Chemical Data Collections* **2019,** *21*, 100218.
59) Gomes, A. R.; Varela, C. L.; Tavares-da-Silva, E. J.; Roleira, F. M. F. Epoxide containing molecules: A good or a bad drug design approach. *European Journal of Medicinal Chemistry* **2020,** *201*, 112327.
60) Brotzel, F.; Mayr, H. Nucleophilicities of amino acids and peptides. *Org Biomol Chem* **2007,** *5*, 3814-20.
61) Varela, C.; Tavares da Silva, E. J.; Amaral, C.; Correia da Silva, G.; Baptista, T.; Alcaro, S.; Costa, G.; Carvalho, R. A.; Teixeira, N. A. A.; Roleira, F. M. F. New Structure–Activity Relationships of A- and D-Ring Modified Steroidal Aromatase Inhibitors: Design, Synthesis, and Biochemical Evaluation. *Journal of Medicinal Chemistry* **2012,** *55*, 3992-4002.
62) Harwig, C.; Seenisamy, J.; Keregadde, M. N.; Chetia, L. Synthesis of a substituted indene derivative. US20170204048A1, 2017.
63) Raymond, J. R.; Han, K.; Zhou, Y.; He, Y.; Noren, B.; Yee, J. G. K. Preparation of seco-steroidal indene derivatives for use as antiinflammatory pharmaceutical agents. WO2004092100A1, 2004.
64) MacKenzie, L. F.; Harwig, C.; Bogucki, D.; Raymond, J. R.; Pettigrew, J. D. Preparation of secosteroids as SHIP1 modulators. WO2014143561A1, 2014.

65) Zaidlewicz, M., 45.5 - Hydroboration of Functional Derivatives of Alkenes. In *Comprehensive Organometallic Chemistry*, Wilkinson, G.; Stone, F. G. A.; Abel, E. W., Eds. Pergamon: Oxford, 1982; pp 229-254.
66) Klein, J.; Dunkelblum, E. Trans directive effect of an allylic hydroxyl in hydroboration. A method for preparation of diequatorial diols. *Tetrahedron Letters* **1966,** *7*, 6047-6049.
67) Dungan, O. M.; Dormann, S.; Fernandes, S.; Duffy, B. C.; Effiong, D. G.; Kerr, W. G.; Chisholm, J. D. Synthetic studies on the indane SHIP1 agonist AQX-1125. *Organic & Biomolecular Chemistry* **2022,** *20*, 4016-4020.
68) Wang, Y.; Kuang, Y.; Zhang, H.; Ma, R.; Wang, Y. Recyclable Dirhodium(II) Catalyst Rh2(esp)2 for the Allylic Oxidation of Δ5-Steroids. *J. Org. Chem.* **2017,** *82*, 4729-4736.

Chapter 3: Studies towards the Design and Synthesis of a SHIP PROTAC

Abstract

Proteolysis Targeting Chimera's or PROTACs have become an emerging tool in the world of drug discovery. They leverage the power of the Ubiquitin-Proteasome System (UPS) by directing ligases (E1/E2/E3) towards targeted proteins which eventually leads to their degradation. This process is accomplished through the synthesis of a bifunctional molecule that binds the targeted protein and the corresponding E3 ligases. By binding both simultaneously this leads to the eventual ubiquitin labelling of the protein which leads to recognition and rapid degradation by the 26S Proteasome. This new wave of potential therapeutics allows for modulation of protein levels inside the cell. This method is also not limited to traditional protein targets allowing for the targeting of potential "undruggable targets" such as GTPases, scaffolding proteins and transcription factors. This work details the synthesis of two SHIP based PROTACs of differing linker sizes with the hope that these molecules can be used for lowering of SHIP protein levels inside the cell. These studies could also provide valuable knowledge of SHIP's scaffolding role and its function in human disease.

3.1 The Ubiquitin-Proteasome System and Targeted Protein Degradation

The Ubiquitin-Proteasome System (UPS) is a distinct feature of eukaryotic cells that helps to label, signal and degrade proteins that no longer have a use or have lost their function. This capability of eukaryotic cells is a necessary biological function that helps maintain the health of the cell and ensures the overall longevity of the organism. A key component of the UPS is the 26S Proteasome, a large protein (mass of ~2000 kDa) that consists of two subunits that both have distinct functionalities.[1] The first subunit is called the core protease, which houses six catalytically active peptidase sites capable of cleaving peptide bonds through a number of different cleavage mechanisms including trypsin, chymotrypsin and caspase-like cleavage.[1] The other subunit is called the regulatory particle and this is the recognition portion of the protease. This complex recognizes proteins which have been covalently attached to the small (~8.6 kDa) regulatory protein ubiquitin, a process referred to as ubiquitylation. The 26S Proteasome identifies mono or poly-ubiquitinated proteins and sequesters them near the core particle for degradation.[2] Ubiquitin possesses seven lysine residues that can be covalently modified (usually converted to an amide) to accommodate another ubiquitin or to amino acid residues on a protein that is going to be marked for degradation. In this way the addition of ubiquitin acts as a degron for proteases.[3] Protein ubiquitylation requires a number of other enzymes, categorized as E1 (ubiquitin-activating enzymes), E2 (ubiquitin-conjugating enzymes), and E3 (ubiquitin ligases, often just referred to as E3 ligases), which all can facilitate the transfer of ubiquitin to targeted proteins.[4,5] The process of ubiquitylation is often repeated, with multiple ubiquitins being linked to assemble a polyubiquitin chain that helps aid in recognition by the 26S Proteasome. Based off a study conducted by Thrower

and co-workers it was determined that in order to be effectively recognized by the 26S Proteasome, a minimum of four ubiquitin or ubiquitin like proteins is necessary for recognition. The K_i of a target of the 26S Proteasome undergoes nearly a 100-fold increase when the ubiquitin chain length increases from two to four with diminishing returns as the chain length increases eventually reaching a plateau after around 12 ubiquitins in the chain.

Protein degradation by the Ubiquitin-Proteasome System is responsible for keeping protein levels in check and maintaining cell homeostasis. This system also provides an opportunity to control protein levels in cells, which has evolved into the field of targeted protein degradation.[6] Researchers have developed a number of strategies for small molecules to interact with the enzymes of the UPS to enhance protein degradation, as utilizing the cells existing machinery provides a novel strategy for target proteins that are difficult to regulate using standard drug discovery methods.[6] The best known strategy which targets the UPS is the PROTAC method (short for Proteolysis Targeting Chimeras).

3.2 Proteolysis Targeting Chimeras (PROTACs)

A Proteolysis Targeting Chimera (PROTAC) is a small molecule-based approach to targeted protein degradation that involves the ubiquitin-proteasome system. This approach is based on the principle that a small molecule that is capable of binding to a protein degradation target (protein of interest, or POI) can be covalently linked to another ligand that is capable of binding to an E3 ligase, bringing the protein degradation target in proximity to the E3 ligase and facilitating ubiquitylation.[7-9] The binding of both ends of the bifunctional molecule results in the formation of a ternary complex between the E3-ligase, POI, and PROTAC. The formation of this ternary complex helps facilitate the

transfer of the polyubiquitin strand from the E3-ligase to the POI, which labels the POI for degradation by the proteasome. Unlike other current inhibitory models, in theory a PROTAC can act effectively in less than stoichiometric quantities and does not need to stay bound in order to be effective. This model has been described by many as event-driven where the event refers to the initial binding and subsequent polyubiquitination of substrate. This is in contrast to typical models of enzyme inhibition, which are often referred to as occupancy driven, as the small molecule needs to occupy a binding site to be effective. Sometimes, the occupancy driven model can lead to off-target side effects due to the need to increase dosage in order to maximize the amount of inhibitor that is bound to target protein. The PROTAC approach may minimize the risk for those side effects since these small molecule chimeras do not need to be dosed at the same concentrations as a typical inhibitor.

Proof of Principle of first PROTAC

The first successful PROTAC based molecule was reported in 2001 by Crews and Deshaies.[10] Using phosphopeptide ligands capable of binding methionine amino-peptidase-2 (MetAP-2) they attached a ligand designed to recruit the F-box protein, Skp-1-Cullin F-box complex, which is a RING class E3 ligase (**Figure 3.1**).[10]

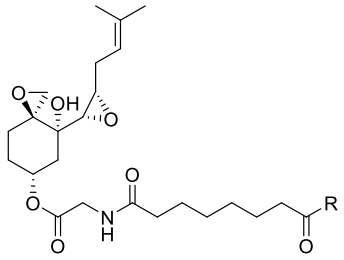

3.1

R = GGGGGGRAEDS*GNES*EGE-COOH or GGGGGGDRHDS*GLDS*M-COOH
S* = phosphorylated serine

Figure 3.1: First Protac targeting MetAP-2

Analysis of the amount of protein after dosing cells with the PROTAC via western blot showed that the levels of MetAP-2 did in fact decrease. This early proof of concept revealed the potential of this strategy and has since led to studies involving many variables in these systems such as what leads to the formation of the ternary complex, different linker lengths between the POI and E3 ligase binding small molecules, as well as which potential E3 ligases could be targeted.

When developing a PROTAC one important factor to consider is the ligand that binds to the E3 ligase. This ligand depends on the desired E3 ligase and there are a wide variety of E3 ligases that can be targeted. However, out of the nearly six hundred plus E3 ligases only a few have been successfully targeted and incorporated into PROTAC designs. Screening for new ligands that bind to underutilized E3 ligases as well as optimization of current ligands are ongoing efforts in the field of targeted protein degradation.[7] Some of the more common E3 ligases are von Hippel-Lindau (VHL), Cereblon (CRBN), cellular inhibitor of apoptosis proteins (cIAP), and mouse double minute 2 homologue (MDM2).[11] There have also been others targeted with PROTACs such as Skp1-Cullin-F-Box complex (SCF), kelch like ECH associated protein 1 (KEAP1), DNA binding protein 1-CUL4 associated factor 16 (DCAF16) and DNA binding protein 1-CUL4 associated factor 11 (DCAF11).[12]

Discovery of VHL Ligands and their Application to PROTACs

The von Hippel-Lindau protein first garnered attention for its association with hypoxia-inducing factor 1 alpha (HIF-1α). Under normal metabolic conditions, the alpha subunit of HIF-1 undergoes rapid degradation by the proteasome.[13] However, when the cells are undergoing hypoxia, HIF-1α becomes activated which leads to increased

glucose transport, metabolism and angiogenesis, all of which are considered to be factors that facilitate the growth of epithelial cancer. In the absence of the von Hippel-Lindau protein (pVHL), hypoxia induced mRNA signaling appears to be upregulated which led researchers to investigate the connection between the two proteins.[13,14] When VHL deficient cells were introduced to exogenous pVHL, HIF-α induction was prevented.[13] In an effort to investigate the relationship between the two proteins, they were targeted with immunoprecipitating antibodies which led to the co-precipitation of VHL with HIF1α in both hypoxia and normal systems, indicating that these two proteins interact closely regardless of the conditions. In an effort to design a HIF-1α PROTAC based off the VHL complex, Crews and Ciulli hypothesized that a ligand could be synthesized for VHL using a hydroxyproline core. One of key recognition elements that recruits the VHL complex to the alpha subunit of HIF is the presence of a hydroxylated proline residue (Hyp564). Using computational studies to build around a hydroxyproline core, they were able to design the first VHL ligand (**3.2 in Figure 3.2**).[15] Further studies involving co-crystallization of the ligand fragment helped to further elucidate key structural elements and specific interactions between subpockets on the active site of the pVHL.[16,17] Through these studies the identification of key structural elements that would be implemented in the second generation VHL ligand (**3.3 in Figure 3.2**) were identified, such as the tert-butyl groups and thiazolyl group in the molecule.[16-18] The hydroxyproline core was found to have the greatest impact on binding affinity with respect to the other fragments with a measured ligand efficiency of 0.53 kcal per mol per non heavy atom despite possessing only a 10 mM affinity. The *tert*-butyl group was found to have a stabilizing interaction inside a binding pocket on the molecule near the active site which is evidenced by its

increase in ligand efficiency of 0.2 kcal per mol per non heavy atom by isothermal titration calorimetry (ITC).[17] This was nearly a two-fold increase over the methyl-isoxazole moiety which contributed only 0.08 kcal per mol per non heavy atom. The addition of the tert-butyl group also helped offset some of the hydrophilic nature of the hydroxyproline core.[17] The *tert*-butyl group was found to have negative interactions when placed on the core or the right hand side of the molecule. A methyl thiazolyl group could also be used in place in the methyl isoxazole, and led to a more potent ligand with similar binding modes.

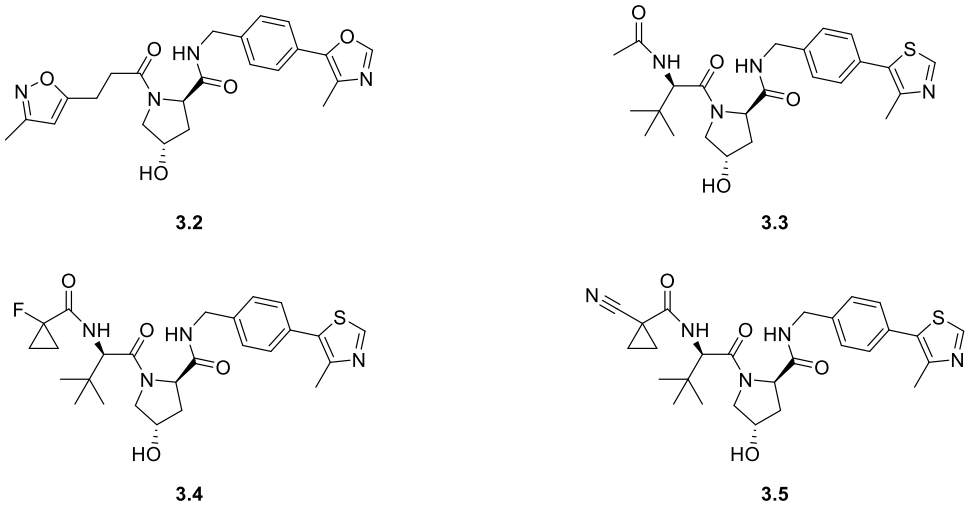

Figure 3.2: VHL Ligands

Both **3.2** and **3.3** were cocrystallized with VHL protein, and the comparison of the two crystal structures revealed that the methyl-thiazolyl group inhabits the same pocket under the P99 residue of the pVHL that the methyl-isoxazole normally does.[18] The researchers proposed that the increase in K_d was a result of the larger more hydrophobic sulfur atoms filling the pocket more adequately then the oxygen atoms in the previous ligand.[18] Ciulli and co-workers further optimized the dipeptide of **3.3** by incorporating different amide capping groups such as the fluorocyclopropane (**3.4**) and a cyanocyclopropane (**3.5**).[19] The incorporation of a cyclopropyl on the alpha carbon of the

amide fits into a hydrophobic pocket on the left-hand side of the VHL ligand.[19] However, the cyclopropane moiety could only access hydrophobic pocket as long as it was on the opposite side of the amide carbonyl which led them to incorporate a fluorine (**3.4**). The incorporation of fluorine insured that the amide would stay the in the active trans amide conformation.[20,21] This compound showed greatly improved activity in both FP assays and ITC experiments with IC_{50} values of 90 and 44 nM in each but also demonstrated significant cytotoxic effects. After multiple iterations of the dipeptide side of the molecule, the cyanocyclopropane **3.5** proved to be a suitable replacement for **3.4**. While the observed ligand efficiency and binding affinity was less than that of the fluorine, the cyano group still provided the electron withdrawing capability to preserve the amide in the trans conformation without any of the cytotoxic effects. This newfound ligand (**3.5**) can be used as a probe for future PROTAC based studies in order to improve on existing protein degraders.

VHL-based PROTACs

VHL based PROTACs have also been deployed to great success using a number of these ligands.[21] In 2019, the research groups of Alessi and Ciulli were able to design and synthesize a Serum/Glucocorticoid Regulated Kinase Family Member 3 (SGK3) based PROTAC using the VHL ligand **3.3**.[22] SGK3 is a part of the PI3K signaling pathway, often compensating for the loss of Akt by upregulating adjacent pathways such as mTORC1 and contributing to resistance against Akt/PI3K inhibitors. The ligand for SGK3 was chosen from a previous SAR study involving SGK3 inhibitors and was ultimately chosen due to the fact that the morpholine group served as a good attachment point for the incorporation of a linker.[23] After synthesizing four potential SGK3 based PROTACs

they discovered that only compound **3.6** had the ability to effectively degrade SGK3, with greater then 50% degradation at 10 µM concentrations. A CRBN E3 based PROTAC was also tested but those compounds performed poorly in initial screening. In addition to the ability of compound **3.6** to degrade SGK3, it was also isoform selective, showing no degradation of the other SGK isoforms. In an effort to improve lipophilicity, compound **3.7** was developed replacing some of the PEG linker with alkyl chains.

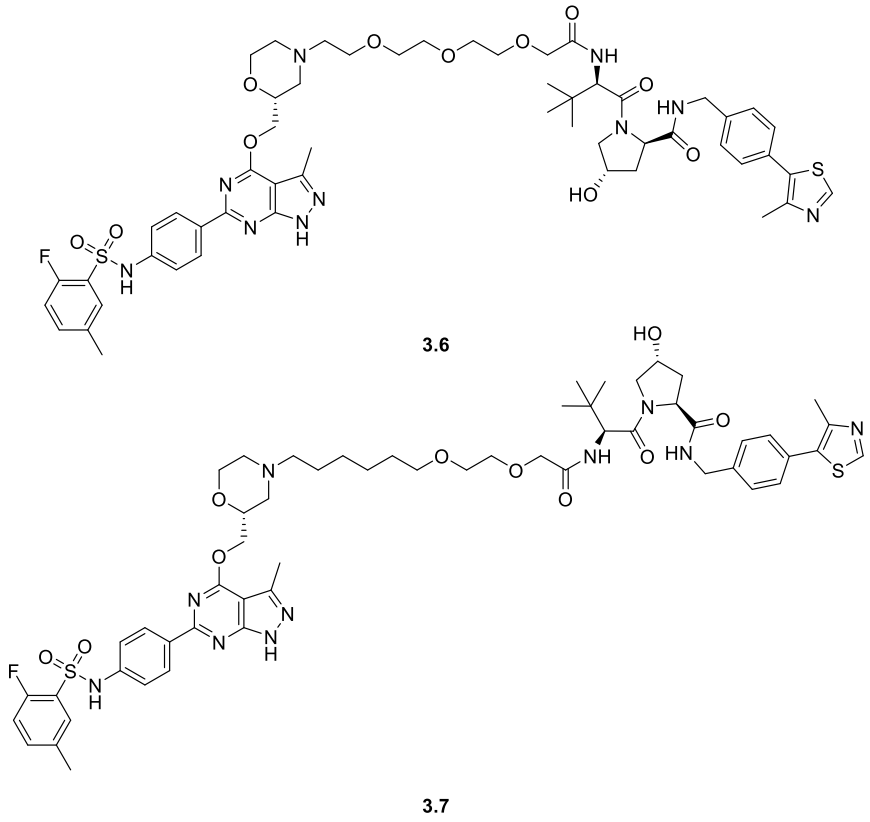

3.6

3.7

Figure 3.3: SGK3 based PROTAC Degraders

Replacement of the linker had a marked improvement on the PROTAC showing degradation levels of greater then 60% 0.1 µM. Interestingly, the study found that in certain breast cancer cells lines like CAMA-1 and ZR-75-1, combination treatment of both the PROTAC and Akt/PI3K inhibitors showed a substantial effect on cancer cell proliferation. This would suggest that in cases of drug resistance a combination of the

PROTAC along with the other inhibitors of PI3K signaling could be a potentially useful strategy.[22]

Crews and co-workers also had significant success using the VHL ligand along with a Brd4 inhibitor for the treatment of castration resistant prostate cancer developing ARV-771 (**3.8** in **Figure 3.4**).[24] Bromo domain and extra-terminal proteins (BET) like Brd4 have been the target of many PROTAC and inhibitor-based strategies due to their role in attenuating AR signaling. In this particular study, the dosage of ARV-771 (**3.8**) resulted in the apoptosis of cancer cells in a variety of castration resistant prostate cancer lines such as VCaP and 22Rv1. ARV-771 dosage induced Brd4 degradation in both 22Rv1 and VCaP mice xenografts, showing efficacy in vivo with minimal side effects.

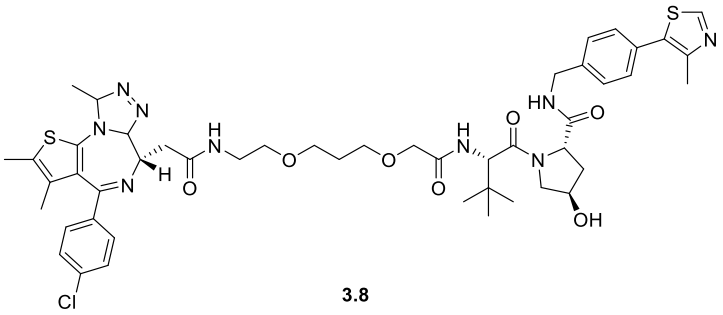

3.8

Figure 3.4: ARV-771 Brd4 PROTAC

Another example of a successful and potent VHL based PROTAC is the compound designed and synthesized by the Crews lab targeting TANK-binding kinase 1 (TBK1). TBK1 is a serine/threonine kinase and believed to be involved in innate immune response.[25] TBK1 also appears to be closely linked to oncogenic KRas mutation which was proven through multiple RNA screening methods. These mRNA screens revealed that TBK1 is upregulated in KRas mutated lung cancer cell lines and subsequent silencing of TBK1 led to tumor growth inhibition.[26] The idea that TBK1 could potentially serve as an anticancer therapeutic was the initial driving factor for the design and elucidation of a

TBK1 based PROTAC. The Crews lab first needed a ligand that could bind TBK1 and found a crystal structure of TBK1 with an inhibitor (**3.9** in Figure 6) bound.[25,27] Through Structure Activity (SAR) analysis, an improved ligand was assembled (**3.10**) removing the morpholine for a phenolic ether and replacing the cyclopropyl group off the pyrimidine ring. These modifications provided multiple vectors for the attachment of a linker and were easily modifiable. The incorporation of the tertiary amide end cap instead of the secondary amide removed a hydrogen bond donor allowing for better drug like properties without having any negative effects on binding.[27]

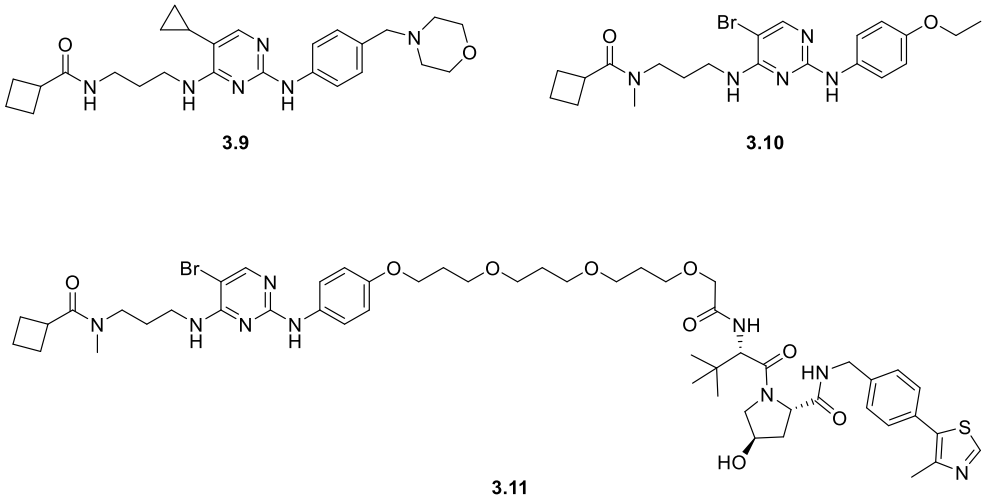

Figure 3.5: TBK1 ligands and TBK1 PROTAC

After undergoing several iterations of linkers, PROTAC **3.11** was identified a useful PROTAC in this system, showing TBK1 degradation with a DC_{50} (concentration needed to degrade 50% of POI) of 12 nM.[27] Other PROTAC iterations had increased potency but also possessed more polar surface area which can lead to decreased membrane permeability. Longer linker lengths were more tolerable to the ternary system then shorter linker lengths with linkers less then 12 atoms showing little to no degradation at all. Furthermore, the parent ligand for the TBK1 kinase showed little selectivity for TBK1 over

its close protein homolog IKKε but the PROTAC showed increased selectivity degrading only TBK1 in the presence of IKKε which had been an area of concern. In vitro testing against variety of KRas dependent cancer cell lines, mutant and wild-type, demonstrated the broad applicability of **3.11**.

These are just a few of the successful VHL PROTACs, over 750 reported VHL PROTAC's exist with a wide variety of cellular targets.[21] The ease of modification of the VHL ligand and relatively rapid incorporation of the ligand into many systems make it an appealing choice. Unfortunately, these VHL based PROTAC molecules often have poor membrane permeability when compared to the standalone VHL ligand. Current research in this area is tied to improving the VHL ligand with the hopes of improving its membrane permeability.[28]

Discovery of CRBN and associated ligands

Another major development in the field of PROTACs has been the discovery of Cereblon (CRBN) which is a protein recognition subunit of a Cullin 4- Ring-Box 1-damaged DNA protein-Cereblon (Cul4-Rbx1-DDB1-CBN) E3 ligase complex.[29] Thalidomide and other immunomodulatory imide drugs were discovered as potential ligands for CRBN by Ito and co-workers in 2010.[30] Many years prior to this discovery, thalidomide and other immunomodulatory imide drugs (IMiDs) were the subject of controversy due the teratogenic effects observed by their first administration as a sedative eventually leading to their withdrawal from the market.[31,32] Several years later in the 1960's, thalidomide was discovered as a potential treatment for complications that arise from lepromatous leprosy commonly referred to as erythema nodosum leprosum or ENL.[33] This led to the FDA lifting the ban on the sale and prescription of thalidomide but

only for the treatment of ENL complications. Further investigation of these IMiD's eventually led to the discovery that thalidomide and other IMiD's inhibited angiogenesis which could potentially be therapeutic for cancer treatment.[34] Thalidomide (**3.12**), pomalidomide (**3.14**) and lenalidomide **(3.13)** all exhibited the ability in some capacity to induce apoptosis and reduce cell proliferation of multiple myeloma and leukemia cell lines.[35-38] The mechanism was poorly understood since these IMiD's can interact with a number of downstream targets such as TNFα, NF-κB in addition to upregulating NK and T cell proliferation, all of which can have a profound effect on multiple myeloma cells.[35] In 2014, both lenalidomide and thalidomide were proven to bind to CRBN and were shown to cause selective degradation of IKZF1 and IKZF3.[37,38] Both IKZF1 and IKZF3 are transcription factors and their upregulation is often associated with unfavorable progression in multiple myeloma.[39,40]

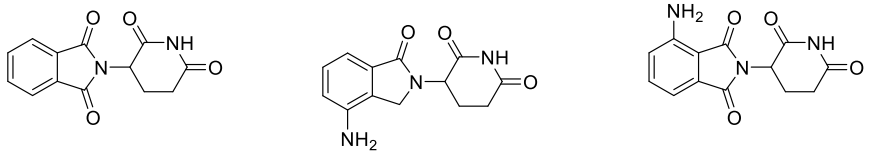

Figure 3.6: CRBN Ligands

CRBN-based PROTACs

The first CRBN based PROTAC (**3.15, Figure 3.7**) was developed by Bradner and co-workers who were targeting BET protein Brd4.[41] Brd4 silencing has been shown to downregulate the MYC oncogene in multiple myeloma and acute myeloid leukemia. The downregulation of the MYC oncogene is believed to contribute towards the antiproliferation of cancer cells. Brd4 along with other BET related proteins has been shown to play a part in DNA repair and damage response.[42] The newly synthesized PROTAC (**3.15**) exhibited a profound ability to degrade Brd4 with over 85% degradation

at 100 nM doses. PROTAC **3.15** when compared to the standalone Brd4 inhibitor induced a stronger pro-apoptotic response in acute myeloid leukemia cell line MV4;11. The proposed PROTAC also performed well during in vivo studies using murine MV4;11 xenografts, demonstrating decreased tumor volume and tumor weight after fourteen days of dosage at 50 mg/kg. The hook effect that is commonly seen in in vivo studies with these bifunctional molecules was also observed after fourteen days.

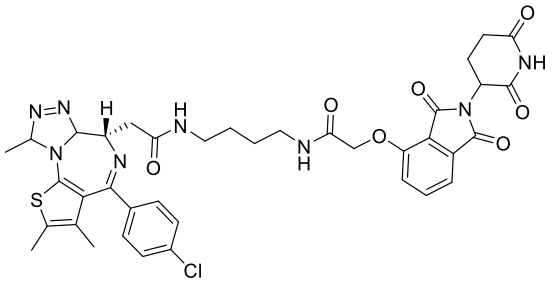

3.15

Figure 3.7: CRBN based Brd4 PROTAC

After the first CRBN based PROTAC was produced with favorable pharmacological properties, more CRBN based PROTAC's were introduced into the fold. The relative ease of modification of the phthalimide ring and straightforward synthesis of the CRBN ligand made adapting existing inhibitors to the PROTAC modality an achievable goal. Shown in **Figure 3.8** are some of the more recently reported PROTAC degraders along with their associated POI ligand. One example is triazole **3.16**, a pan class 1 PI3K inhibitor which has been utilized to target PI3K signaling for the treatment of tumors.[43] Compound **3.16** has had some success in clinical trials, with nine of thirty-nine patients observing a prolonged stable disease state.[43] In addition to clinical settings, promising pre-clinical studies involving **3.16** have been reported in the treatment of human sarcoma cell lines such as HT-1080, SW684 among others.[44] After examination

of the X-ray structures of compound **3.16** docked inside the active site of PI3K, Jiang and co-workers proposed and synthesized protein degraders of PI3K using a modified **3.16** linked to pomalidomide.[45] Compound **3.17** was the most efficient at degrading PI3Kα which was chosen as the model system since out of all PI3K isoforms it is the most ubiquitously expressed throughout the body. One of the morpholines had been changed to a piperazine after structural analysis revealed that only one of the two morpholines on the original inhibitor had favorable protein interactions.[45] The piperazine was then used to incorporate an eleven-atom polyamide linker to pomalidomide. The newly synthesized PROTAC exhibited a ClogP value of 0.64 while also binding to PI3Kα with an IC_{50} 24 nM. Interestingly, compound **3.17** was not the most efficient at binding to PI3Kα but degraded PI3K at a higher rate. Their data seemed to suggest that PROTAC **3.17** was slightly more lipophilic then their more potent analogs, which could have led to increased uptake in cells.[45] When tested in vivo on HepG2 cells, **3.17** demonstrated an ability to inhibit cell proliferation as well as decreased cell viability. The mechanisms for the diminished proliferation and viability were investigated and it was proven that neither apoptosis or cell cycle arrest was induced by **3.17**.[45] Instead autophagosome production was significantly increased upon dosage with **3.17** which resulted in cancer growth inhibition. Since the PI3K axis is one of the most commonly implicated pathways in carcinogenesis, targeted protein degradation of other key enzymes in the PI3K pantheon offers another therapeutic approach to influence signaling this key pathway.

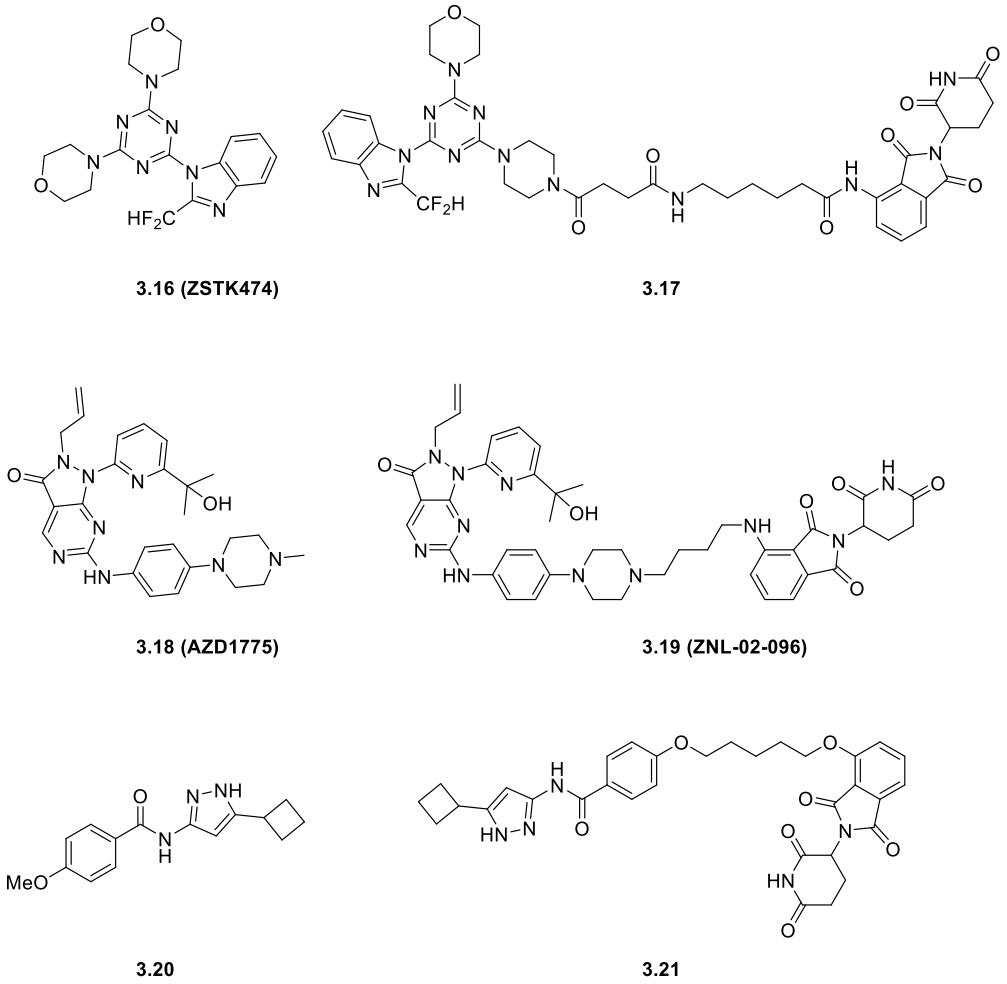

Figure 3.8: CRBN PROTACs with their associated POI ligand

Wee1 has also been the target of cellular protein degradation for its role in the G2/M cell cycle checkpoint. The second gap phase in the cell cycle often serves as the last barrier to preventing mitosis which is a process that is often mediated by cyclin dependent kinase 1 (CDK1).[46] Wee1 is a tyrosine kinase that can inhibit CDK1 activation through the phosphorylation of a tyrosine residue.[46] Typically, this enzymatic event is catalyzed in the presence of DNA damage which essentially pauses the cell cycle for DNA repair.[47] Wee1 is an interesting target for potential cancer treatments in that it can be used to sensitize tumors to DNA crosslinking agents such as cisplatin.[47] Compound **3.18** is an effective Wee1 inhibitor that has been demonstrated to reduce CDK1

phosphorylation and subsequent proliferation of cancer cells.[48,49] Unfortunately, **3.18** has exhibited many side effects despite showing efficacy in clinical a clinical setting.[50] This provided the inspiration for the Gray lab to synthesize a WeeI based protein degradation probe since PROTACs can often avoid problems associated with high dosage toxicities.[51] PROTAC **3.19** was designed through computational studies and became the clear lead out of five designed degradation probes. Maximal protein degradation was achieved at 100 nM in MOLT4 cells and was confirmed to be CRBN dependent as CRBN knockout cell lines exhibited no effects.[51] Furthermore, PROTAC **3.19** exhibited antiproliferative and similar decreased CDK1 phosphorylation levels at a ten-fold lower concentration then the parent compound **3.18**.[51] These results were promising since it provides a potential solution to dose related toxicities and also could serve as an example for the adaptation of other systems that are affected with dose related toxicities.

Cyclin dependent Kinases (CDK's) have also been the target of frequent protein modulation due to their impact in transcription and cell cycle transitions.[52-57] PROTACs targeting CDK2/4/6/9 have been reported with some having the capability to degrade multiple CDK's. One CDK PROTAC was developed by the Rana lab at University of Nebraska, who based their PROTAC on an aminopyrazole CDK inhibitor.[52] Aminopyrazoles are well documented for their ability to mimic ATP binding to CDKs.[58] Through optimization, the Rana lab came up with compound **3.20** which had comparable binding affinity for both CDK5 and CDK9. Subsequent development of **3.20** linked to thalidomide provided **3.21** which functioned to their surprise as a selective CDK9 protein degrader, with CDK9 levels being reduced in HCT116 cells by 65% at 20 μM concentrations of **3.21**. Often families of proteins that share similar enzymatic substrates

are difficult to attack with selectivity.[57] CDK inhibitors tend to suffer from this trait and often designing selective inhibitors is challenging.[57] In the case of compound **3.21**, it was believed that the sudden increase in selectivity for CDK9 is due to the location of the lysine residues in the ternary complex which leads to preferential ubiquitination over other CDK isoforms.[52]

The use of CRBN based PROTAC's continue to expand as the field of targeted protein degradation grows. However, there is still room for improvement in the bioavailability of these ligands as well as the expansion of the protein degradation targets. CRBN based degradation continues to push the envelope with recent advances demonstrating that dual degradation (degradation of two protein targets with one small molecule) is possible with the first trifunctional PROTAC being reported as of 2021.[59]

PROTACs Employing IAP/KEAP1/MDM2 Ligands

Both the von Hippel Lindau and CRBN E3 ligase complexes have contributed a great deal to the study of bifunctional TPD systems. However, in order to combat drug resistance other E3 ligases should be investigated and, as mentioned previously, some other E3 ligases have been used in successful PROTAC's.[60-62] Some examples of non-VHL/CRBN PROTAC's are shown below in **Figure 3.9**. One example of this type employs Inhibitor of Apoptosis Proteins (IAP) such as cIAP1/2 and XIAP in the design of bifunctional degraders. These are referred to as SNIPERs (Specific and Non-genetic Protein Erasers). SNIPERs have used to degrade BCR-ABL and ERα proteins with a great deal of success.[60,61] Compound **3.22** in addition to degrading ERα, also degraded XIAP and cIAP1 which appears to be specific to these class of protein degraders. This provided added utility in tumor cells where XIAP and cIAP1 are overexpressed.[61]

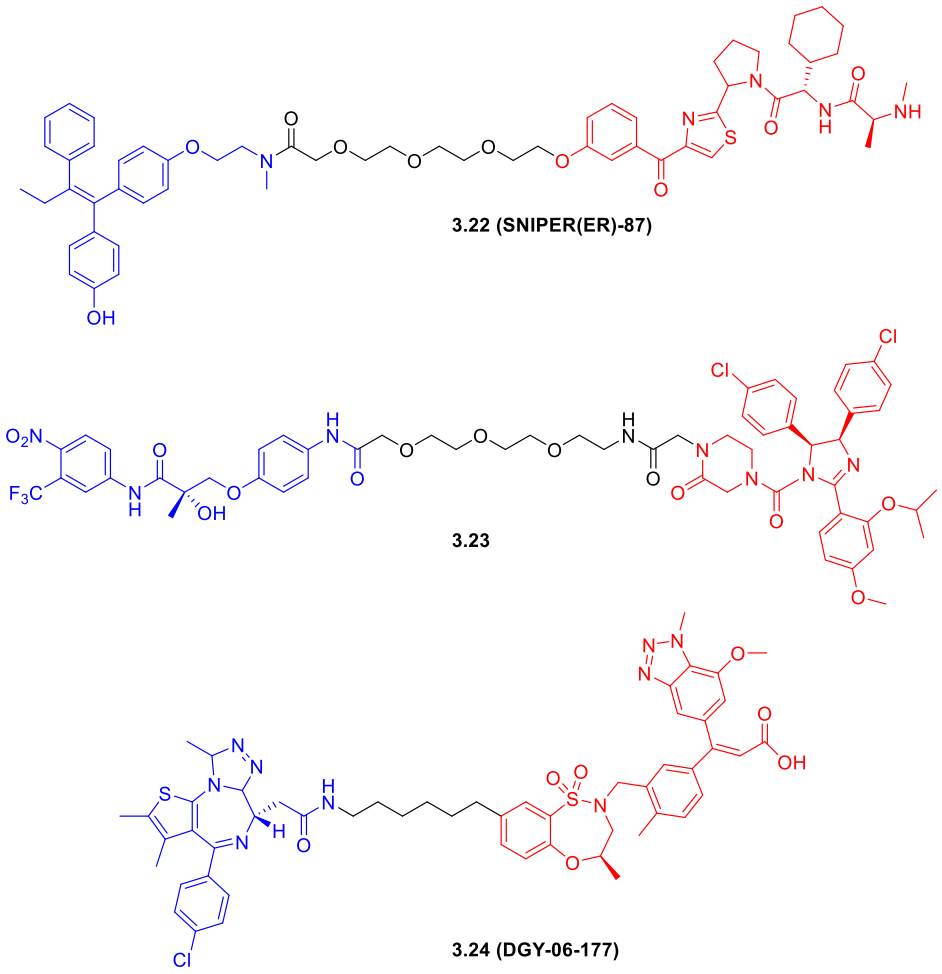

*E3 ligand highlighted in red, and POI ligand highlighted in blue

Figure 3.9: IAP (**3.22**), MDM2 (**3.23**) and KEAP1 PROTAC's (**3.24**)

Compound **3.23** utilizes a Nutlin based ligand that binds to MDM2, which is a RING based E3 ligase, and the POI ligand was a selective androgen receptor modulator (SARM).[62] MDM2 PROTACs often lack effectiveness when compared to other E3 ligases like CRBN with lower degradation levels.[63] Future optimization of MDM2 based PROTACs are ongoing with the goal of improving pharmacological properties of the E3 ligand itself.[11] A few KEAP1 or Kelch-like ECH Associating protein 1 PROTACs have also been introduced in the last couple years, demonstrating the ability to degrade proteins with another E3 ligase.[64,65] Keap1 has been studied for years and there are several well-

known ligands, but unfortunately few have translated well into PROTAC development. Compound **3.24** is a Keap1 recruiting Brd4 protein degrader, adding to list of several iterations of PROTACs targeting the Brd4 protein.[64] Compound **3.24** exhibited the ability to diminish Brd4 protein levels with selectivity compared to the other BET isoforms although no antiproliferative effect was observed when tested on MM.1S cells.

Linker Effects on PROTAC Efficacy

While choosing the appropriate E3 ligase and POI ligand is important, studies have shown that linker can also contribute to the efficacy of a given PROTAC. In some cases, linker composition and linker location even were able to dictate isoform specificity in the POI. For instance, p38 Mitogen activated protein kinases (MAPK) possess four isoforms all of which have been shown to respond to activate under stress and upregulate expression of proinflammatory cytokines.[66] Some isoforms have secondary roles as well such as p38δ which appears to have a role in cytoskeleton rearrangements.[66] Targeting these isoforms with traditional inhibitors strategies has proved to be an issue since the close structural similarity between isoforms often leads to pan-inhibition. The Crews lab hypothesized that a PROTAC utilizing a non-selective POI ligand could be made selective by differing linker compositions and length.[67] Additionally, varying the point of attachment (amide linkage vs phenyl ether linkage) might also lead to selectivity. They produced eight different PROTACS, four amide and four phenyl ethers, all of which contained foretinib a promiscuous kinase inhibitor and tested them against p38α and p38δ. In doing so, they discovered **3.25** (p38α) and **3.26** (p38δ) as isoform selective PROTACs.[67] Interestingly, in the amide series p38α selectivity was lost when linkers of 10 and 11 atoms were used but was nearly 5-fold selective when the linker length was 13 atoms long (**3.25**). A similar

effect was observed in the phenyl ether series where the 10 atom linker (**3.26**) selectively targeted p38δ but lost all selectivity when one extra carbon was added.[67]

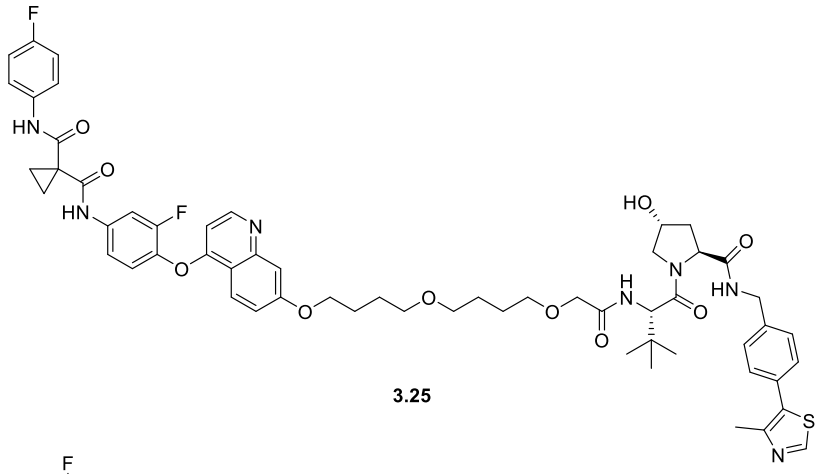

3.25

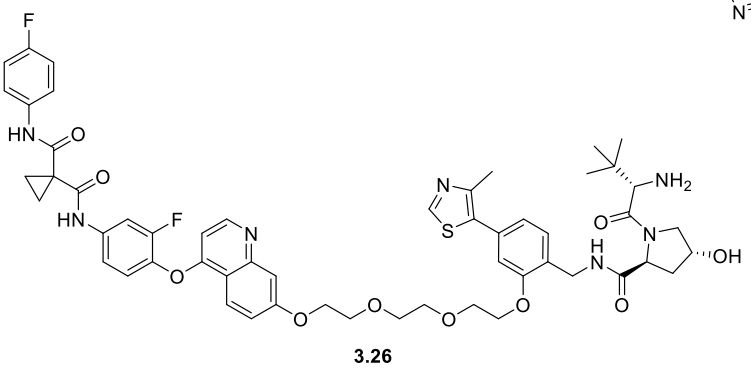

3.26

Figure 3.10: p38 isoform selective MAPK PROTACs

Linker length has always been a concern incorporated into the design of the PROTACs and several statistical analysis studies have been reported in attempts to define the optimal number of atoms for a linker for optimal protein degradation.[68] The results are seemingly inconclusive in many of these studies because most proteins have very different ternary structures and optimal linker lengths tend to vary greatly between POI.[68] One takeaway from a design point of these studies is that more often a linker length of around 9-12 is a good starting point as most of the POIs that were surveyed seemed to have some binding capability with linkers of those lengths. Should no binding or degradation capability be observed than that could indicate that the ligand of the POI has

been modified in an unfavorable manner and has lost the ability to bind to the POI. One study targeting estrogen receptors found that the optimal linker for a PROTAC was 16 atoms long and linker lengths greater then sixteen resulted in a drop off in protein degradation.[69] Presumably, the increase in linker length can be detrimental if it impacts the ability of the ligase to transfer the ubiquitin to the target protein. Chain lengths less then sixteen were also effective with lengths of nine and twelve atoms also showing similar activity.[69] Some research groups have attempted linkers starting as low as 6 atoms against other proteins such as Brd4 and the results have shown that shorter linker lengths can lead to negative cooperativity in some cases.[70] When Ciulli and coworkers tested PROTAC's containing two PEG unit linkers they were significantly less potent than ones containing three or four PEG units. The three-unit PEG linked compound MZ1 (**3.27**) was by far the most potent which had a linker length of approximately ten atoms.[70] When tested for its anticancer properties in HL-60 cell lines(acute myeloid leukemia), MZ1 demonstrated comparable activity to ARV-825 (**3.28)** which is another small molecule Brd4 protein degrader. A crystal structure of **3.27** bound to the von-Hippel Lindau E3 ligase and Brd4 was reported.[71] The flexibility in the linker as well as proximity to both ends allowed for the PROTAC to fold in on itself which led to greater protein-protein interactions. The increase in stabilizing interactions also was believed to have a profound effect on the cooperativity between the E3 ligase and the Brd4 protein.

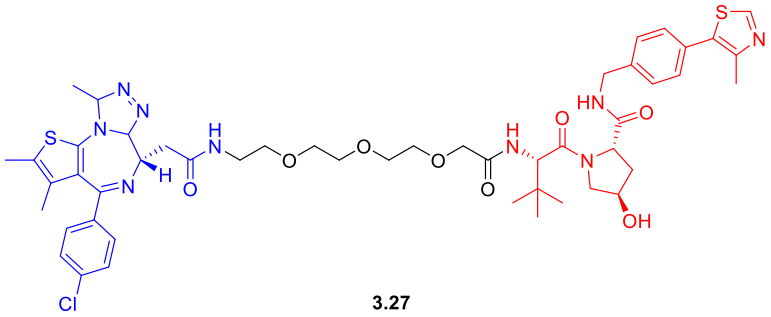

3.27

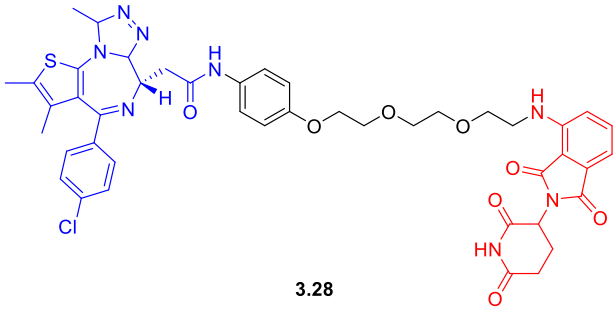

3.28

Figure 3.11: MZ1 BET Protein Degrader (BET ligand is shown in blue and E3 ligand in red)

Linker composition can also have a profound effect on membrane permeability, as well as the dissociation and formation of ternary complexes, typically through manipulation of hydrogen bond donors and polarity of the linker.[72-74] Some linkers that allow for structure plasticity can induce folding of the PROTAC which can increase membrane permeability. For example, when the polyether linker in compound **3.27** was substituted for an alkyl chain, the PROTAC demonstrated less flexibility but also greater lipophilicity. The polyethylene glycol linker when folded in the ternary complex also generated more shielded hydrogen bonds in aqueous medium while the alkyl chain allowed the PROTAC to more quickly dissociate from the POI/E3 due to the lack of shielded hydrogen bonds.[72] Both PROTACs were able to degrade Brd4 efficiently, but the **3.27** dissociated at a much slower rate than the alkyl linker.

Linker design is just another facet of the PROTAC system and linker composition must work in concert with the two ligands in order to facilitate protein degradation. If the PROTAC is too lipophilic, it may have difficulty passing through cell membranes. On the other hand, if the molecule is too hydrophilic, the two warheads could end up in folded conformations instead of forming the desired ternary complex. Multiple research groups have developed computer software to help aid the design of these PROTACs, however they are constrained by one key limitation. They require crystal data of the POI ligand bound to the active site of the POI and the E3 ligase ligand bound to the active site of the ligase in order to simulate ternary complex formation.[75,76]

Ternary Complex Formation and Association of the POI Ligand

The formation of the ternary complex is integral to the degradation of the protein, this has led many groups to study the important interactions in this area. The factors that influence the formation of the ternary complex have been probed using methods such as native mass spectrometry.[77,78] These studies show that at higher concentrations of PROTAC there appears to be a drop off in the relative rate of ternary complex formation.[79] The observed drop off in ternary complex formation at higher concentrations is believed to be the cause of the hook effect or high dosage hook effect.[80] The hook effect refers to the often false drop off in activity reported by assays typically due to reaching the detector limit or from competing interactions. In addition to the effects of concentration, it appears that the ternary complex forms preferentially over the possible binary complexes (PROTAC-POI or PROTAC-E3) when the two proteins have positive cooperativity ($\alpha > 1$), where α is the quotient of the K_d of the binary system over the K_d of the ternary system.[71,78,81] In the event that the two proteins have negative cooperativity inside the

ternary complex then binary complex formation is believed to predominate.[7,78] Protein cooperativity is influenced by protein-protein interactions, typically a hydrogen bond between nearby residues or hydrophobic interactions. These interactions are important to take into consideration when designing a PROTAC since sometimes ligands that have lower affinity are more effective over ligands with higher affinity as long as they contribute to better protein-protein interactions. For example, Bondeson and co-workers discovered that their PROTAC, which was capable of degrading p38α with a DC_{50} of 210 nM, was derived from a ligand that had a standalone IC_{50} of 11 μM.[82] This also demonstrates that as long as a ligand can impart some specificity on a POI, an effective PROTAC may be developed.

Using the PROTAC approach for "undruggable" targets

Another benefit to this sort of therapeutic strategy is in targeting proteins that were once considered undruggable due to the lack of active site, enzymatic activity, or high affinity endogenous ligands. This category of targets includes transcription factors, scaffolding proteins and RAS GTPases.[83,84] As an example, one such target that was once considered undruggable is Signal Transducer and Activator of Transcription 3 (STAT3). This transcription factor is an integral part to many key processes involved in cell survival, cell proliferation, angiogenesis and chemotherapy resistance.[85] STAT3 is suggested to have a role in oncogenesis in prostate and breast cancer which has made it a target in the pharmaceutical industry along with other STAT transcription factors.[85] To target STAT3, Researchers at the University of Michigan in Shaomeng Wang's lab designed SD-36 (**3.29, Figure 3.12**), a STAT3 based PROTAC.[86,87] Initially, they had discovered a small molecule that was capable of binding to the SH2 domain of STAT3

but after discovering that the molecule had poor efficacy in vivo they adapted the structure to accommodate a linker. Using the linker, they attached lenalidomide/pomalidomide, which are both Cereblon (CRBN) E3 ligase ligands. This newly synthesized molecule (**3.29**) was capable of reducing tumor growth in a variety of cell lines such as MOLM-16 (acute myeloid leukemia) and SU-DHL-1 (anaplastic large cell lymphoma).

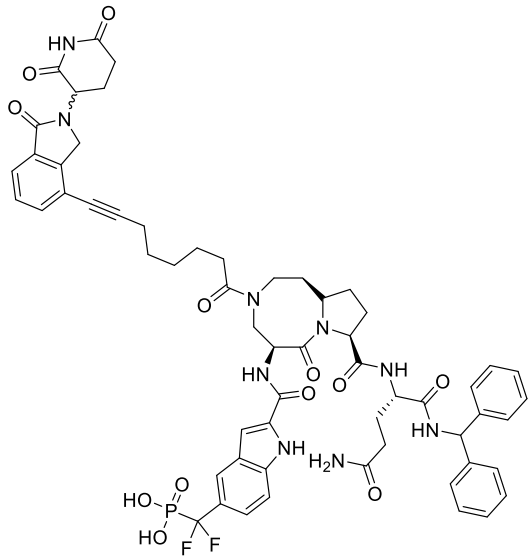

3.29 (SD-36)

Figure 3.12: SD-36, STAT3 PROTAC

Western blot analysis revealed that treatment of cells with SD-36 led to selective degradation of STAT3 with respect to other STAT proteins and also a significant drop in STAT3 protein levels after four hours. The efficacy of SD-36 to turn an otherwise ineffective standalone inhibitor into an effective protein degrader is promising for the development of new therapeutics.

Another system that was widely viewed as an undruggable has been the cupin superfamily of proteins. While some of these proteins have enzymatic activities others such as the protein pirin have no enzymatic activity.[88,89] Pirin, despite the lack of enzymatic activity, is overexpressed in many epithelial cancers and is an important

transcription factor regulator protein forming complexes with NF-κB.[88] A protein degradation probe of pirin was synthesized using the CRBN ligand pomalidomide, further demonstrating the ability of PROTAC like systems to degrade proteins that lack enzymatic activity.[89] After going through several iterations of the degradation probe they landed on CCT367766 (**3.30, Figure 3.13**) which optimized the linker joining the two halves.

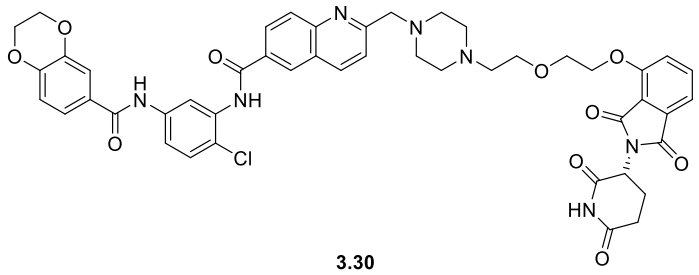

3.30

Figure 3.13: CCT367766 Pirin degradation probe

The design of CCT367766 (**3.30**) was aided through the use of molecular modeling which helped in the design of the linker. Linker interactions are often underrated when it comes to designing an effective PROTAC but computational studies have revealed that linkers play a significant role in protein-protein interactions and often times help stabilize the ternary structure.[90] In the case of pirin, the piperazine motif of the linker was key in providing stabilizing interactions. The initial molecule also had an amide bond in the linker which introduced a rigidity to the structure which was replaced in an effort to remove a hydrogen bond donor as well as introduce flexibility to accommodate the ternary structure formation. It was discovered that the modification of the linker had little to no impact on the binding of the E3 ligase but did demonstrate a 4.2-fold increase in binding of the warhead to the POI.

The use of PROTACs continue to expand as the field of targeted protein degradation grows. In this next section we discuss attempts to develop a PROTAC for use on the SHIP enzyme.

3.3 Synthesis and Design of a Proteolysis Targeting Chimera for SHIP

The SH2-Domain Containing Inositol 5'-Phosphatase (SHIP) and its role in the PI3K pathway has been extensively studied leading to the belief that the manipulation of SHIP could be beneficial in certain disease states like Alzheimer's and cancer. SHIP1 inhibition has previously been shown to induce apoptotic effects against multiple myeloma cell line (OPM2).[91] Targeting SHIP1 along with its isoform SHIP2 has also shown promise as a potential Alzheimer's target.[92] This is due to the finding that SHIP inhibition has led to increased microglial proliferation and increased microglial compartment size leading to an increase in phagocytosis of dead neurons and amyloid-beta protein. Previous research in the Chisholm lab has demonstrated the inhibitory capabilities of a number of aminosteroid, tryptamine and quinoline inhibitors.[93] Unfortunately, the binding affinity of these small molecules are limited in potency with the most potent inhibitors being in the low micromolar range. This led to the inspiration behind a SHIP based PROTAC, since for a molecule to be an effective protein degrader it does not necessarily need to have high binding affinity. Rather the most important aspect is the ability to induce and stabilize ternary complex formation through protein-protein interactions.[94] SHIP also has several non-enzymatic scaffolding roles which also makes it an intriguing target for a PROTAC since protein concentration levels are being modulated, not just enzymatic activity. The role that SHIP scaffolding plays in human disease is not well understood but it is known that SHIP can associate with other proteins such as Dok1 through the binding of its SH2

domain.[95-97] SHIP1 and Dok1 complexation is believed to also have an effect on calcium mobilization which could impact cytoskeleton rearrangements. Nonetheless, a SHIP based PROTAC would allow for the probing of these interactions by offering a way to lower protein levels inside the cell. This could then be compared to the effects of the enzyme inhibitor directly. Utilizing an aminosteroid scaffold it was believed that C17 substitution could be well tolerated for the accommodation of a linker so an initial retrosynthetic analysis was proposed based on linking the E3 ligase ligand to the C17 alkyl chain of the steroid (**Scheme 3.1**). CRBN based ligand pomalidomide had been used before in the targeting of PI3K and was lower in molecular weight when compared to other E3 ligase ligands so it was chosen for the initial exploration.[45] A vinyl iodide could be installed at C17 of the aminosteroid (**3.32**) for use in a Sonagashira reaction with a alkyne linker attached pomalidomide (**3.33**). The alkynyl pomalidomide derivative (**3.33**) could then be accessed through the acylation with the corresponding acid chloride. The necessary pomalidomide based structure for coupling could be synthesized according to literature procedures starting from 3-nitrophthalic anhydride (**3.35**) and *L*-glutarimide hydrochloride (**3.36**).

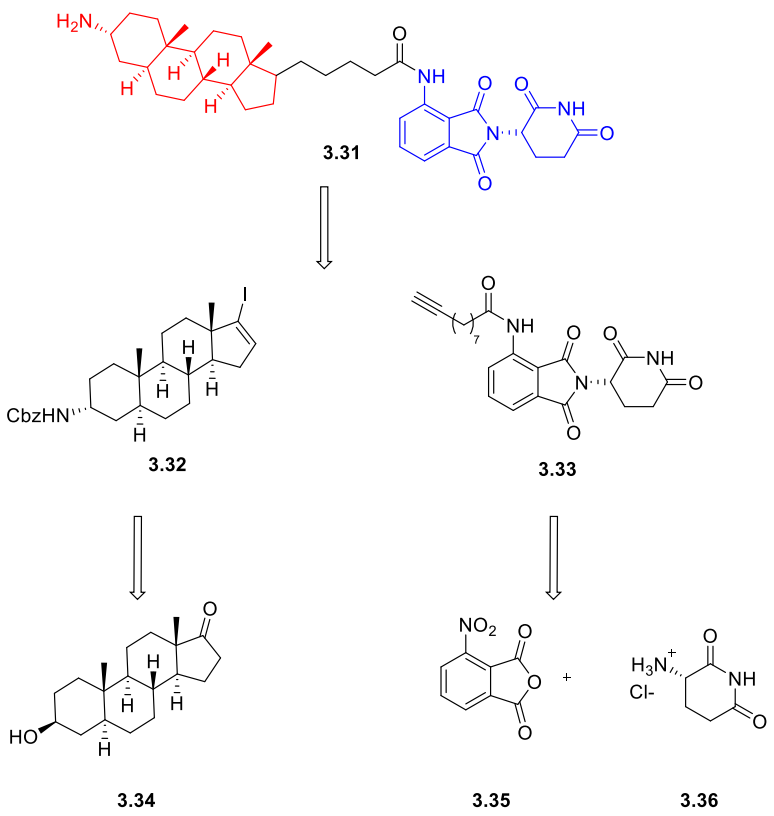

Scheme 3.1: Retrosynthetic Analysis of First SHIP PROTAC

In order to assemble the E3 ligase ligand section of the molecule, literature procedures were used as references.[98,99] The synthesis (**Scheme 3.2**) starts with the Boc-protection of L-glutamine (**3.38**) which is then cyclized using *N,N*-carbonyldiimidazole to form imide **3.39**. These first two steps have been performed multiple times and the yields seem to remain around the same, with the formation of the imide usually being around 36%. Some reasons for this lower yield could be the purity of my starting material since usually the Boc-glutamine is used crude and there usually is some leftover boc anhydride or *tert*-butanol present even after acidic workup which impacts the starting mass and impacts the yield. Secondly, most procedures often let the reaction sit at room temperature for hours or even days after the reaction in order to let the product precipitate out. Typically, majority of the initial precipitate is of high purity and

rather than wait for several days for the rest of the precipitate(which is typically less pure), the filtrate is discarded and the material is carried forward to the next step. However, it is possible that the filtrate could be manipulated to possibly isolate more of the cyclized product. Fortunately, the next three steps all proceed in excellent yields. Making the HCl salt of the glutarimide is accomplished in 99% yield, and the salt is then used to open the anhydride and form the phthalimide in the next step resulting in a 90% yield of compound **3.40**. Compound **3.40** is then hydrogenated to reduce the nitro group to the amine (**3.41**) in 95% yield. The main issue encountered while making these compounds was the poor solubility of the intermediates. Both compounds **3.40** and **3.41** are insoluble in most solvents making purification by chromatography nearly impossible. However, the impurities in both of those reactions can be separated by trituration and filtration. The next step was to attach a linker to compound **3.41** that contained an alkyne. The amine of thalidomide **3.41** could be acylated using the acid chloride of 10-undecynoic acid to install the crucial alkyne needed for cross coupling. It was decided that it would be used as the first linker, since linker length could always be optimized later if the PROTAC proved to have some binding activity and this would serve as a good starting point with a linker length of 11 atoms. The carboxylic acid was converted to the corresponding acid chloride through the reaction of thionyl chloride in dichloromethane and then the crude acid chloride was used in the next step. The amine was then combined with the flask containing crude acid chloride and dissolved and refluxed in dry tetrahydrofuran which gave a yield of 37% of the desired alkyne (**3.33**). This provided the alkyne needed for the desired coupling reaction and attention was then focused on the synthesis of the steroid portion of the PROTAC.

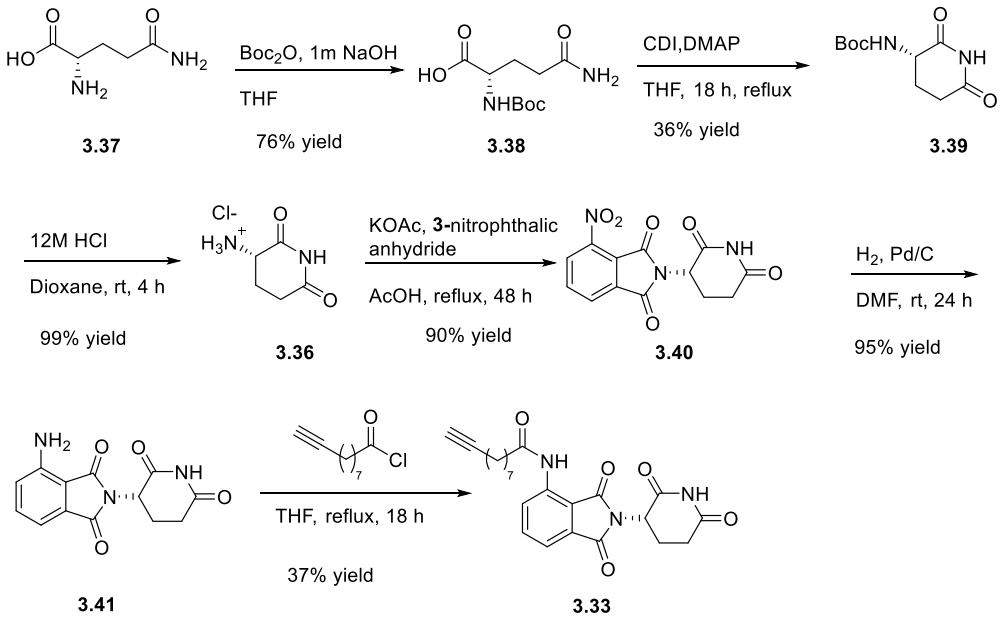

Scheme 3.2: Synthesis of E3 Ligase ligand

Based off literature precedent, it was believed that we could install a vinyl iodide at the C17 position of the steroid.[100] The procedure for making a vinyl iodide would have to be adapted, since the molecule that is being used here possessed an alcohol functional group at the C3 position of the steroid instead of the Cbz protected amine. Also, since the stability of the vinyl iodide was in question (vinyl iodides are often light sensitive), it was decided that introducing that group should be towards the end of the synthesis. Shown below in **Scheme 3.3** is the route used to make desired steroid. The first step is formation of the mesylate (**3.42**) from readily available epiandrosterone **3.34,** followed by the displacement of the mesylate using sodium azide to give the C3 azide (**3.43**). This transformation was also attempted with a Mitsunobu reaction using diisopropylazodicarboxylate and diphenylphosphorylazide but the reaction did not go cleanly. The byproducts from the Mitsunobu reaction were hard to separate from product and the overall yield was lower.

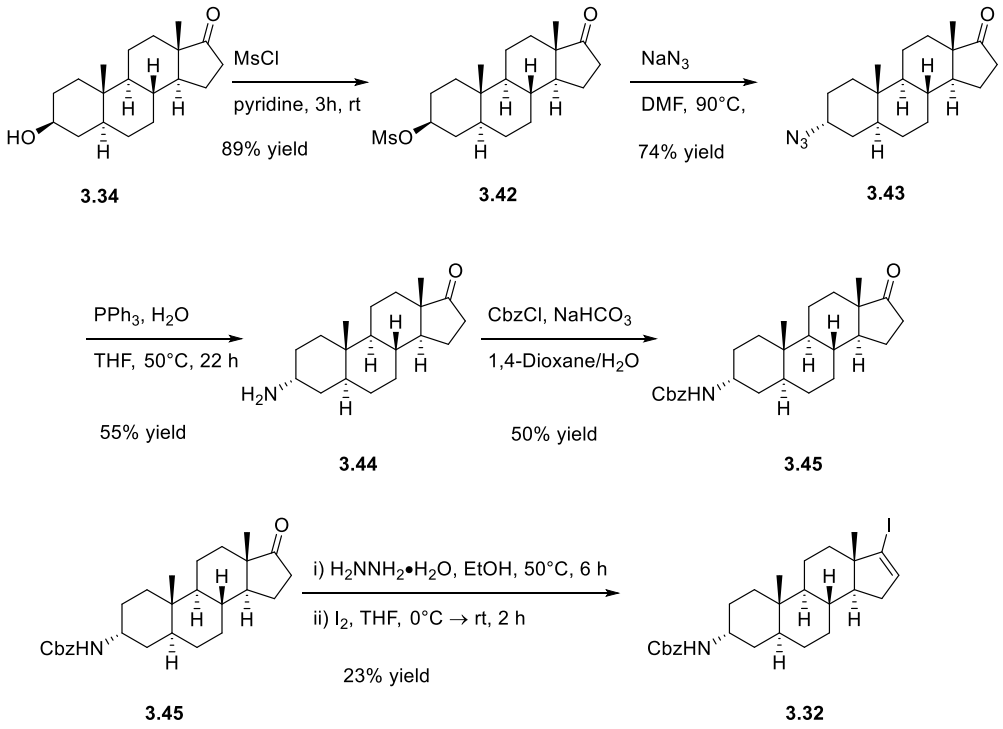

Scheme 3.3: Synthesis of the SHIP Ligand

The azide (**3.43**) was then converted to an amine (**3.44**) through a Staudinger reduction and then protected using benzyl chloroformate (**3.45**). Once the amine was protected, the next step was to make the vinyl iodide which was accomplished over two steps. First the ketone (**3.45**) was converted to the hydrazone in situ using hydrazine hydrate. This hydrazone was then subjected to iodine while placed in an ice bath wrapped in aluminum foil to generate the vinyl iodide whilst shielding it from external light sources that may lead to the degradation of the product (**3.32**). This was accomplished in 23% yield and then was immediately used in the next step shown in **Scheme 3.4.** Unfortunately, the Sonogashira coupling proved to be an issue as neither of the initial conditions attempted resulted in coupled product and one resulted in the recovery of pure vinyl iodide **(Entry 1).** This may be due to the hindered nature of the vinyl iodide, which is next to a quaternary carbon center.

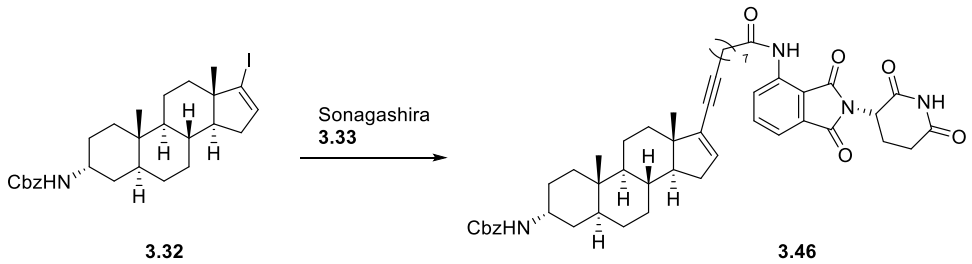

3.32 3.46

Entry	Catalyst	Copper %	Phosphine %	Alkyne	Base (eq)	Time	Yield
1	$Pd(PPh_3)_2Cl_2$	10%	0	1.2 eq.	Et_3N (10 eq.)	16 h	N.R.*
2	$Pd(PPh_3)_2Cl_2$	10%	10%	1.2 eq.	Et_3N (10 eq.)	16 h	N.R

*denotes that starting material(iodide) was recovered
Scheme 3.4: Attempted Sonogashira Reactions (N.R = No Reaction)

Next the synthesis was redesigned to move the attachment point of the phthalidomide away from any hindered centers. An initial retrosynthesis (**Scheme 3.5**) was proposed with that would bring the two halves together with azide-alkyne click chemistry. Click chemistry had also been used previously in the synthesis of CRBN based PROTACs.[45] Previous research efforts by the Chisholm lab had demonstrated the synthesis of an aminosteroid SHIP inhibitor K212 (**3.53, Scheme 3.6**) which possessed an alkyne tethered to the C17 position of the steroid. The free amine could potentially lead to purification difficulties due to polarity so it was proposed that protecting the amine with a boc group (**3.48**) would lead to an overall smoother purification process post coupling reaction. Pomalidomide (**3.41**) could be modified to accommodate the azide linker (**3.49**), which would be needed for the click coupling reaction. The alkyne could be attached to the steroid through the etherification of the C17 alcohol (**3.50**) which would have to be reduced from the ketone. Pomalidomide (**3.41**) could once again be made through the coupling of the glutarimide hydrochloride salt (**3.36**) and 3-nitrophthalic

anhydride (**3.35**). The last step post coupling would be the removal of the protecting group generating the salt (**3.47**).

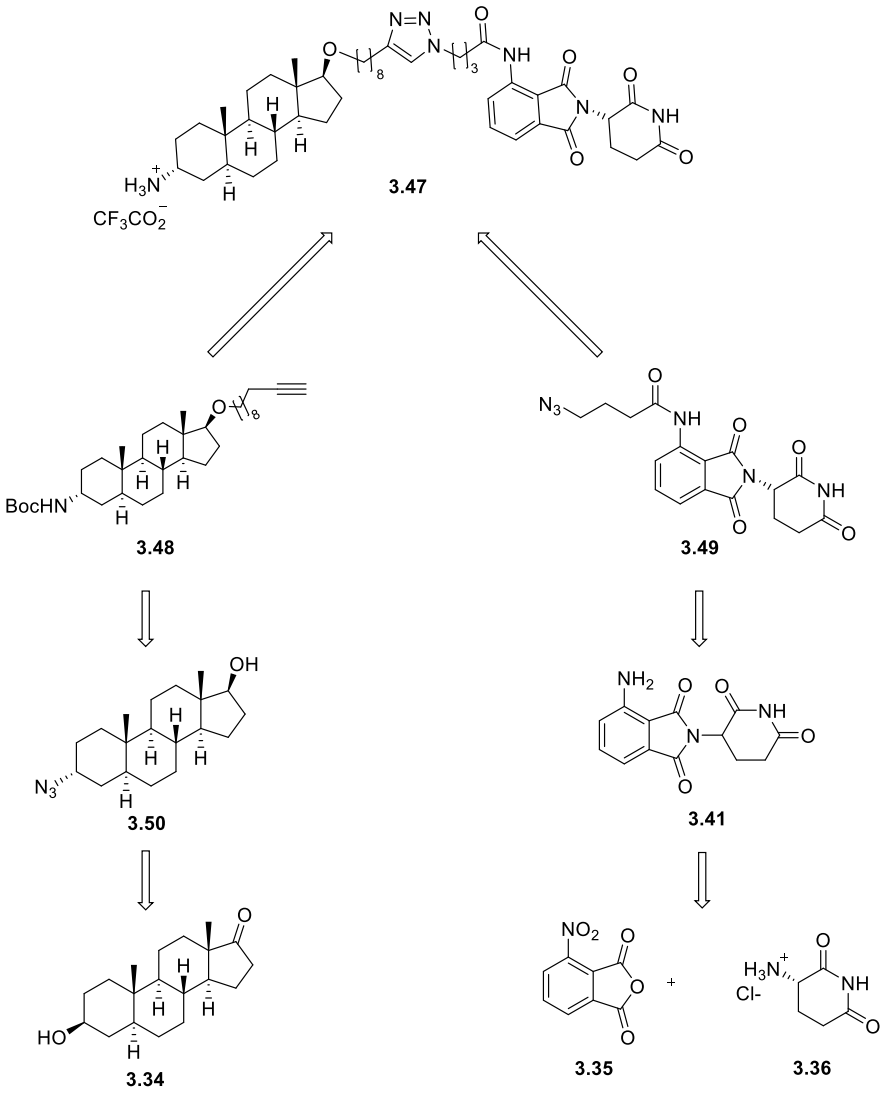

Scheme 3.5: Second Retrosynthetic Analysis

The synthesis (**Scheme 3.6**) of the steroid begins with epiandrosterone (**3.34**) and follows the same initial set of transformations as the previous to generate the azido ketone **3.43.** The ketone at C17 was then reduced with sodium borohydride to generate the alcohol **3.50** which was alkylated with a tosylate (**3.51**). Staudinger conditions resulted in

the formation of the free amine (**3.52**) which was then protected with di-*tert*-butyl dicarbonate to generate the Boc protected amine (**3.48**).

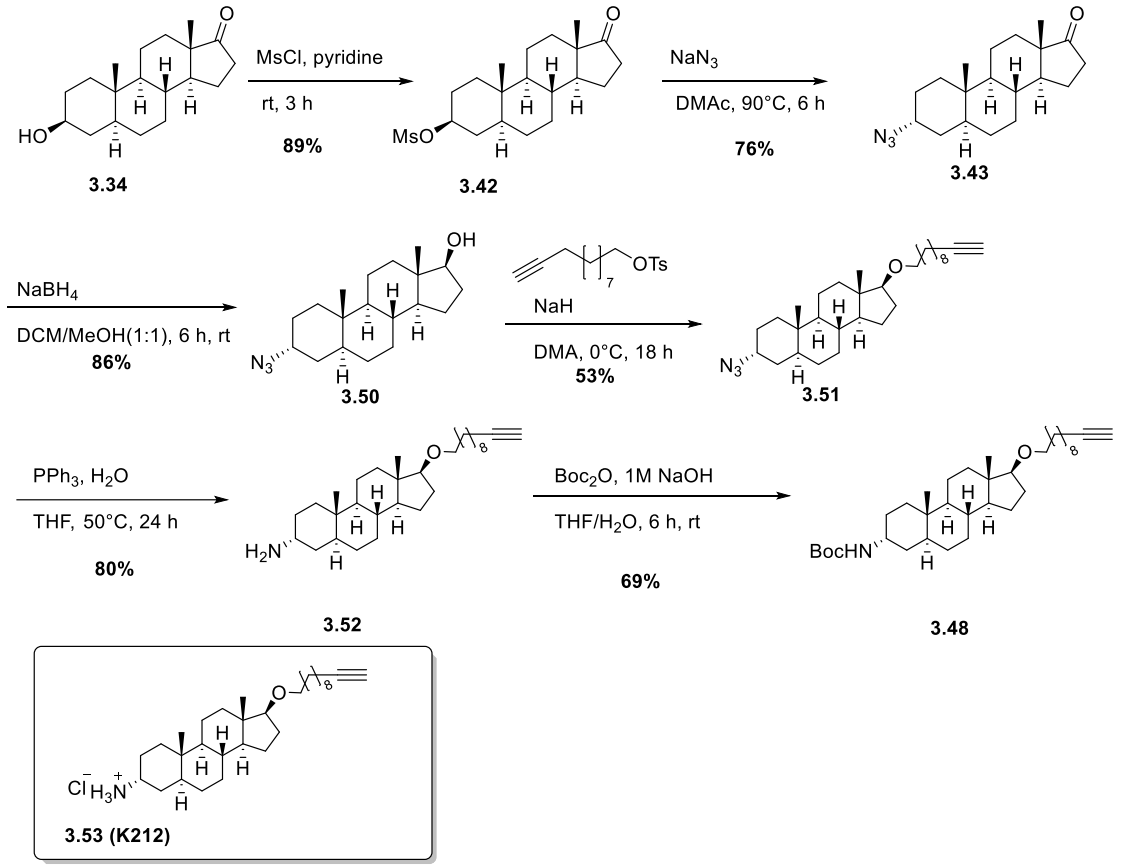

Scheme 3.6: Synthesis of Steroid Alkyne

The pomalidomide ligand had to be adapted as well to accommodate the needed azide, and this molecule was synthesized according to a literature procedure to incorporate linker lengths of four and six carbons respectively. The synthesis starts with the acylation of **3.41** with either 4-bromobutyryl chloride (**3.54**) or 6-bromohexanoyl chloride (**3.55**). The newly formed alkyl bromides were then displaced with sodium azide to generate azides **3.49** and **3.56,** in 47% and 59% yields respectively. A copper catalyzed click reaction was then carried out using 40 mol % copper sulfate and 80 mol % sodium ascorbate. Initial yields during these reactions were low but after changing the solvent to

DMF and using brand new sodium ascorbate, the yield increased nearly four-fold, generating both **3.57** and **3.58** in 56% yield. Sodium ascorbate is necessary for the reduction of copper (II) to the catalytically active copper (I).[101] The previously used sodium ascorbate had already been partially oxidized which could have greatly affected the ability to turn over the copper catalyst.

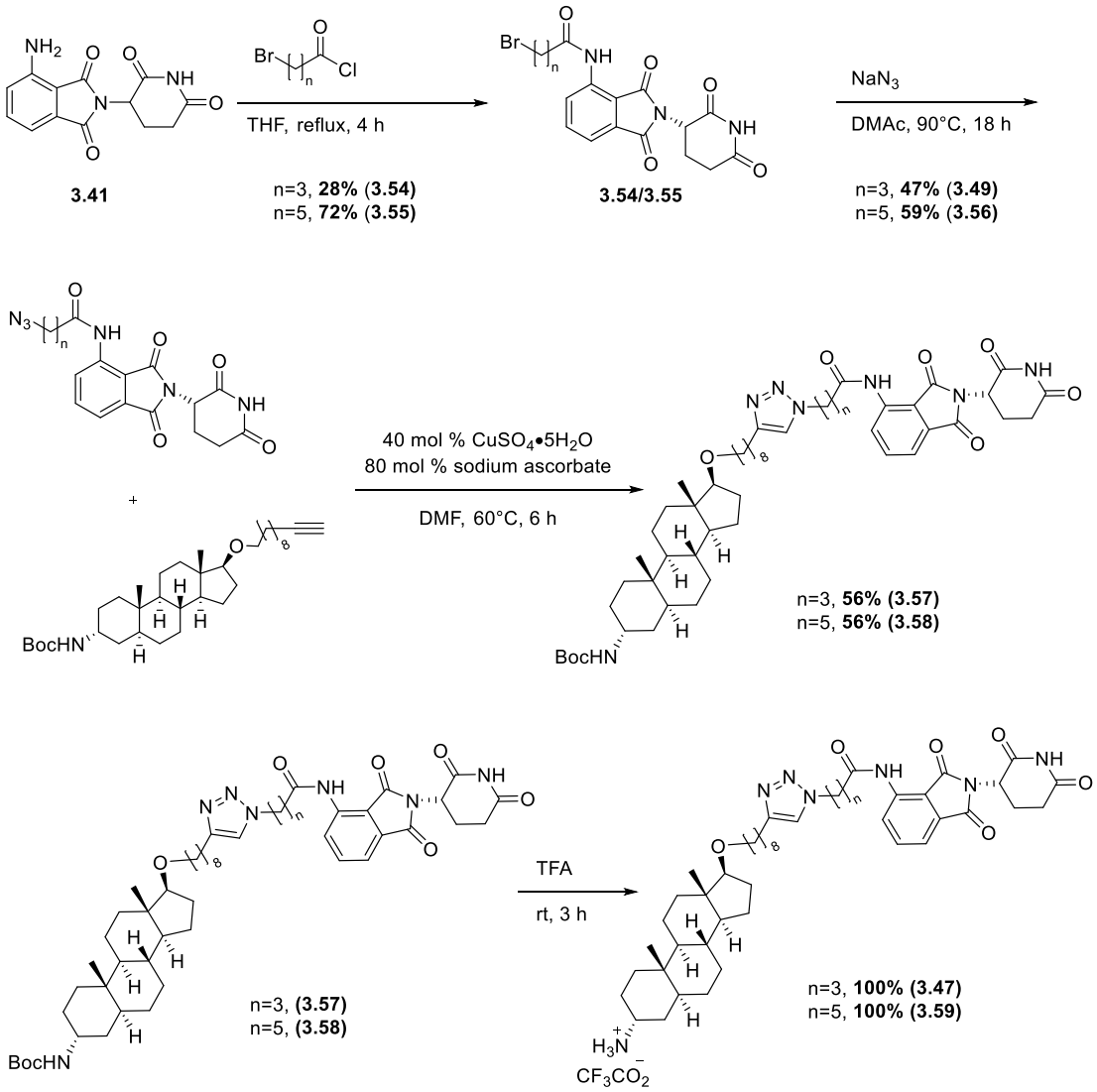

Scheme 3.7: Synthesis of SHIP Based PROTACs

Once the click product was isolated a trifluoroacetic acid mediated Boc deprotection was carried out to yield SHIP based PROTACs **3.47** and **3.59** (**Scheme 3.7**).

3.4 Testing Strategy and Preliminary Data

In order to determine whether or not these molecules would be effective as SHIP protein degraders, their ability to bind SHIP needed to be assessed. This was addressed by evaluating both **3.47** and **3.59** in the malachite green assay. The malachite green assay is a colorimetric assay used to quantify free phosphate generated from hydrolysis of PIP3. Preliminary testing data of the six-carbon linked PROTAC **3.59** revealed that the molecule was a SHIP1 Inhibitor exhibiting a 65% inhibition of SHIP1 in the malachite green assay at 125 µM. Testing data compound on **3.47,** revealed that it is a SHIP1 selective inhibitor, as no inhibition of SHIP2 was observed at 125 µM. The lowest concentration that compound **3.47** demonstrated effective inhibition was at 31.25 µM where it showed a 66% inhibition, so likely the molecules can inhibit SHIP1 at even lower concentrations. From this data, we can conclude that these molecules can bind to SHIP. The next step is to quantify the ability of these PROTACs to degrade SHIP. This will be evaluated through cell based assays using specific cell lines such as BV2 (Alzheimer's) or OPM2 (Multiple Myeloma) cell lines which both express SHIP. After dosage, the cell lysates will be evaluated by western blot analysis which will reveal the amount of degradation induced by the PROTAC should the molecule be capable of degrading the protein.

3.5 Conclusion and Future Directions

In conclusion, a SHIP based PROTAC was designed and synthesized. This required modification of an aminosteroid scaffold that bound to SHIP to accommodate a linker and a CRBN ligand for an E3 ligase. Initial evaluation of this PROTAC shows that inhbition of SHIP1 has been preserved. Studies are now commencing to determine if the

compound can cross cell membranes and degrade the SHIP protein in cells. This PROTAC could prove to be valuable for the modulation of the PI3K cell signaling pathway. As SHIP also has a scaffolding role separate from its enzymatic activities, the PROTAC provides a way to probe this role which has not yet been investigated for its impact in a number of malignancies. In addition to further testing, other PROTACS can also be envisioned that can both bind SHIP and accommodate an E3 ligase ligand. Previous workers in the Chisholm laboratory have synthesized molecules of other structural classes, including tryptamines and quinolines, that act as SHIP inhibitors. These other inhibitors may also be modified into SHIP PROTACs. Tryptamines in particular would be interesting to adapt to this strategy, as they could potentially address cell permeability problems that might be occurring with the aminosteroid based compounds. Additionally, some of these molecules bind to SHIP1 and SHIP2, so the differences in a selective SHIP1 PROTAC or a pan-SHIP1/2 PROTAC could be explored. These molecules may provide insights on the role of SHIP in PI3K signaling, leading to a better understanding of the this important signaling nexus.

3.6 EXPERIMENTAL

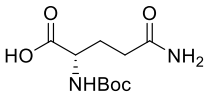

N-(tert-butoxycarbonyl)-*L*-glutamine **(3.38)**

Lit Ref: REDDY, Bathula Surendar; RAO, V.K.K Durga; SHARMA, Komal; REDDY, M. Prathap; BANERJEE, Dibyendu; SINGH, Deependra Kumar (COUNCIL OF SCIENTIFIC & INDUSTRIAL RESEARCH, IN). CATIONIC LIPID CORDIARIMIDE HYBRID

COMPOUNDS AND A PROCESS FOR PREPARATION THEREOF. WO2015189856A1, 2015.

Inside a 500 mL round bottom flask equipped with a magnetic stir bar, *L*-glutamine(8.736 g, 59.7 mmol) was added. The solid was suspended in 1M NaOH (90 mL) and placed in a 0°C ice bath. A solution of di-tert-butyl dicarbonate(19.56 g, 89.0 mmol) in 90 mL of tetrahydrofuran was added slowly over the course of fifteen minutes. The solution went from a milky white color to a clear color and was allowed to react for 24 hours. After 24 hours, the organic solvent was concentrated leaving behind just an aqueous layer. The aqueous layer was washed with hexanes (60 mL) and the organic layer was discarded. The remaining aqueous layer was then acidified using 1M HCl until a pH of 1 was reached. The aqueous layer was then extracted with ethyl acetate (3 x 60 mL). The organic layers were combined and washed once with brine (90 mL). The organic layer was dried over sodium sulfate and concentrated to yield compound **3.38** as an oily white solid (11.39 g, 76%). ^{1}H NMR (400 MHz, C_3D_6SO): δ 7.27 (bs, 1H), 7.01 (d, *J* = 7.8, 1H), 6.75 (bs, 1H), 3.86 -3.83 (m, 1H), 2.12 (t, J = 2.12, 2H), 1.90 (quint, *J* = 7.7 Hz, 1H), 1.72 (quint, *J* = 7.3 Hz, 1H), 1.38 (s, 9H). ^{13}C (100 MHz, C_3D_6SO): δ 176.4, 174.2, 156.7, 79.1, 31.3, 27.4, 13.1.

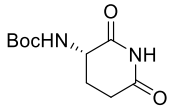

(3S)-3-tert-butoxycarbonylamino-2,6-dioxopiperidine **(3.39)**

This compound has been made previously, for reference: (Teng, B.; Zheng, J.; Huang, H.; Huang, P. Enantioselective Synthesis of Glutarimide Alkaloids Cordiarimides A, B, Crotonimides A, B, and Julocrotine. Chinese Journal of Chemistry **2011**, 29, 1312-1318.)

See Also: Yamaguchi, J.-i.; Noguchi-Yachide, T.; Sakaguchi, Y.; Shibata, C.; Kanuma, S.; Yoshizaki, A.; Takizawa, Y.; Hashimoto, Y. Synthesis of New Hydantoins Bearing Glutarimide or Succinimide Moiety and Their Evaluation for Cell Differentiation-inducing and Anti-angiogenic Activities. HETEROCYCLES **2015**, 91, 764.

Inside an oven-dried 250 mL round bottom flask, Boc-L-Glutamine (9.75 g, 39.5 mmol) was dissolved in THF (72 mL). Dimethylaminopyridine (483 mg, 3.95 mmol) and *N,N*-Carbonyldiimidazole (9.62 g, 59.3 mmol) were added. A reflux condenser was attached and the reaction was heated to reflux for 18 hours. The reaction was cooled to room temperature the next day and then placed in an ice bath. After one hour, the reaction was filtered to yield compound **3.39** as a brown solid (4.02 g, 44%). ^{1}H NMR (400 MHz, $CDCl_3$) δ 7.90 (s, 1H), 5.32 (s, 1H), 4.32 (m, 1H), 2.82-2.72 (m, 1H), 2.71 -2.62 (m, 1H), 2.54-2.51 (m, 1H), 1.86 (dq, *J* = 13.0, 4.6 Hz, 1H), 1.46 (s, 9H).

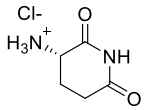

3-aminopiperidine-2,6-dione hydrochloride **(3.36)**

This compound has been made previously, for reference: Yamaguchi, J.-i.; Noguchi-Yachide, T.; Sakaguchi, Y.; Shibata, C.; Kanuma, S.; Yoshizaki, A.; Takizawa, Y.; Hashimoto, Y. Synthesis of New Hydantoins Bearing Glutarimide or Succinimide Moiety and Their Evaluation for Cell Differentiation-inducing and Anti-angiogenic Activities. HETEROCYCLES **2015**, 91, 764.

Inside a 100 mL round bottom flask, (3S)-3-tert-butoxycarbonylamino-2,6-dioxopiperidine (1.60 g, 7.00 mmol) was dissolved in 1,4 -Dioxane(10 mL). Concentrated hydrochloric acid was added and the reaction was stirred for 1 hour. The reaction turned a milky white

color and the reaction was concentrated under reduced pressure. Methanol(50 mL) was added and the suspension was concentrated again. This was repeated three times. After, the off-white solid was placed under high vacuum overnight to yield compound **3.36** (1.15 g, 99%). ^{1}H NMR (400 MHz, DMSO – d_6) δ 8.65 (s, 3H), 4.20 (dd, J = 13.0, 5.3 Hz, 1H), 2.82 – 2.67 (m, 1H), 2.64 – 2.56 (m, 1H), 2.27 – 2.18 (m, 1H), 2.03 (dq, J = 12.9, 4.8 Hz, 1H).

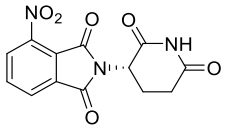

2-(2,6-dioxopiperidin-3-yl)-4-nitroisoindoline-1,3-dione **(3.40)**

This compound has been made previously, please see: Burslem, G. M.; Ottis, P.; Jaime-Figueroa, S.; Morgan, A.; Cromm, P. M.; Toure, M.; Crews, C. M. Efficient Synthesis of Immunomodulatory Drug Analogues Enables Exploration of Structure–Degradation Relationships. ChemMedChem 2018, 13, 1508-1512.

Inside a 250 mL oven-dried round bottom flask equipped with stir bar, 3-nitrophthalic anhydride (3.14 g, 16.5 mmol), 3-aminopiperidine-2,6-dione hydrochloride (1.81 g, 11.0 mmol), and potassium acetate (1.08 g, 11.0 mmol) were measured and placed inside the flask. Acetic acid (40 mL) was added and the reaction was heated to reflux and reacted for 48 hours. The following day the reaction mixture was cooled to room temperature and then diluted with deionized water. The solid precipitate that had formed was collected on a funnel and washed repeatedly with deionized water. The brownish solid was placed on vacuum and dried for 24 hours to yield compound **3.40** (3.02 g, 90%). ^{1}H NMR (400 MHz, DMSO – d_6) δ 8.35 (d, J = 7.5 Hz, 1H), 8.24 (d, J = 6.9 Hz, 1H), 8.12 (t, J= 7.8 Hz, 1H), 5.20 (dd, J = 12.9, 5.4 Hz, 1H), 2.94 – 2.83 (m, 1H), 2.66 -2.50 (m, 2H), 2.10 -2.04 (m,

1H). ^{13}C NMR (100 MHz, DMSO – d_6) δ 173.1, 169.9, 165.6, 163.0, 144.9, 137.3, 133.5, 129.3, 127.7, 123.0, 49.0, 31.3, 22.2.

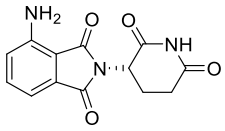

4-amino-2-(2,6-dioxopiperidin-3-yl)isoindoline-1,3-dione **(3.41)**

This compound has been prepared previously, see: Burslem, G. M.; Ottis, P.; Jaime-Figueroa, S.; Morgan, A.; Cromm, P. M.; Toure, M.; Crews, C. M. Efficient Synthesis of Immunomodulatory Drug Analogues Enables Exploration of Structure–Degradation Relationships. ChemMedChem 2018, 13, 1508-1512.

Inside a 250 mL oven-dried round bottom flask equipped with stir bar, 2-(2,6-dioxopiperidin-3-yl)-4-nitroisoindoline-1,3-dione (621 mg, 2.04 mmol) and 10% palladium on carbon (217 mg, 0.204 mmol) were added. The solids were suspended in *N,N*-dimethyl formamide (5 mL) and a rubber septum was used to seal the flask. The reaction flask was put on vacuum until bubbling had occurred, at this point a hydrogen balloon was attached and the reaction was allowed to stir at room temperature for 24 h. The reaction mixture was then filtered through a bed of celite and transferred to a 250 mL round bottom flask. The flask was then diluted with n-heptanes (100 mL) and then concentrated in vacuo. This process was repeated to three times to yield compound **3.41** as a dark yellow-green solid (531 mg, 95% yield). ^{1}H NMR (400 MHz, DMSO – d_6) δ 7.47 (m, 1H), 7.01 (m, 2H), 6.51 (s, 2H), 5.04 (dd, J = 12.6 ,4.9 Hz, 1H), 2.94 – 2.82 (m, 1H), 2.63 -2.53 (m, 2H), 2.04 -1.98 (m, 1H).; ^{13}C NMR (100 MHz, DMSO – d_6) δ 173.3, 170.5, 167.8, 147.2, 135.9, 132.5, 122.2, 111.5, 109.0, 49.0, 31.4, 22.6.

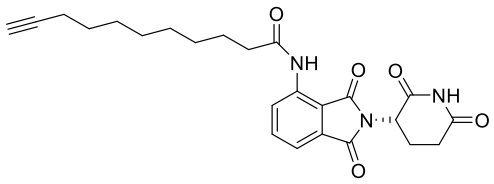

N-(2-(2,6-dioxopiperidin-3-yl)-1,3-dioxoisoindolin-4-yl)undec-10-ynamide **(3.33)**

Inside a 10 mL round bottom flask equipped with stir bar, 10-undecynoic acid (130 mg, 0.705 mmol) was dissolved in dichloromethane (1 mL). Thionyl chloride (0.1 mL, 1.3 mmol) was added and reaction was stirred at reflux for 4 hours. Reaction was then concentrated and put on high vacuum for 2 hours. The crude acid chloride was dissolved with tetrahydrofuran (1.5 mL). 4-amino-2-(2,6-dioxopiperidin-3-yl)isoindoline-1,3-dione (110 mg, 0.36 mmol) was added to the flask and the reaction was heated at reflux for 18 h. Water (5 mL) was added to quench the reaction and the aqueous layer was extracted with ethyl acetate (2 x 10 mL).Organic layers were dried over Na_2SO_4 and concentrated. Purified by flash column chromatography (5% MeOH/DCM) to yield **3.33** as a tan solid (66 mg, 37%). TLC R_f =0.44 (7% Methanol/ 93 % Dichloromethane); M.P = 163.7 – 165.0°C; IR (ATR, cm^{-1}) 3360, 3289, 2928, 2855, 1776, 1702, 1619, 1530, 1479, 1379; ^1H NMR (400 MHz, DMSO – d_6) δ 9.69 (s, 1H), 8.47 (d, J =8.4 Hz, 1H), 7.83 (t, J = 7.9 Hz, 1H), 7.61 (d, J = 7.2 Hz, 1H), 5.14 (dd, J = 12.8, 5.4 Hz, 1H), 2.96 – 2.83 (m, 1H), 2.71 (t, J = 2.6 Hz, 1H), 2.67 -2.55 (m, 2H), 2.48 -2.43 (m, 2H), 2.18 -2.02 (m, 3H), 1.68 - 1.59 (m, 2H), 1.49 – 1.39 (m, 2H), 1.39 -1.22 (m, 8H). ^{13}C {^1H} NMR (100 MHz, $CDCl_3$) δ 172.4, 170.6, 169.2, 167.8, 166.7, 137.9, 136.5, 131.1, 125.3, 118.4, 115.2, 84.7, 68.1, 49.3, 38.0, 31.4, 29.1, 29.1, 28.9, 28.7, 28.4, 25.2, 22.7, 18.4. HRMS (ESI) *m / z* $C_{24}H_{28}N_3O_5$ [M+H] Exact Mass 438.202347; Observed 438.202273.

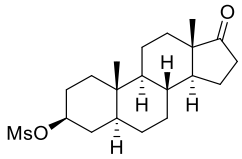

(3β,5α)-3-[(methylsulfonyl)oxy]androstan-17-one **(3.42)**

Lit Ref: Wang, Y. Epiandrosterone-derived prolinamide as an efficient asymmetric catalyst for Michael addition reactions of aldehydes to nitroalkenes. *RSC advances* **2014,** *4*, 30850-30856.

Epiandrosterone (4.04 g, 13.8 mmol) was dissolved in pyridine (14 mL). Methanesulfonyl chloride was added (1.27 mL, 16.5 mmol) and the reaction was stirred at room temperature for 3 h. After 3 hours, a solid precipitate had formed and 1M HCl (60 mL) was added and stirred for fifteen minutes. The reaction mixture was poured into 150 mL of water and the solids were collected onto a filter. The filter solids were washed with water and then transferred to a vial. The vial was placed on high vacuum for 24 hours which gave compound **3.39** as a white solid (4.56 g, 89%). TLC R_f = 0.35 (25% EtOAc/Hexanes); ^{1}H NMR (400 MHz, $CDCl_3$) δ 4.62 (sept, *J* = 5.1 Hz, 1H), 3.00 (s, 3H), 2.46 (dd, J = 19.2, 8.8 Hz, 1H), 2.14 -1.91 (m, 3H), 1.83 – 1.76 (m, 3H), 1.75 – 1.68 (m, 1H), 1.68 – 1.58 (m, 3H), 1.54 – 1.44 (m, 3H), 1.40 – 1.16 (m, 6H), 1.09 – 0. 92 (m, 2H), 0.88 (s, 6H), 0.77 -0.69 (m, 1H).

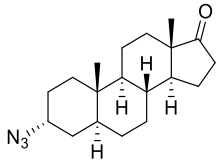

3α-azido-5α-androstan-17-one **(3.43)**

Lit Ref: Wang, Y. Epiandrosterone-derived prolinamide as an efficient asymmetric catalyst for Michael addition reactions of aldehydes to nitroalkenes. *RSC advances* **2014,** *4*, 30850-30856.

(3β,5α)-3-[(methylsulfonyl)oxy]androstan-17-one (3.00 g, 8.13 mmol) and sodium azide (0.793 g, 12.2 mmol) were dissolved in *N,N*-dimethylformamide (24 mL) inside a 100 mL round bottom flask equipped with stir bar. A reflux condenser was attached and the reaction was heated to 90°C for 20 h. Reaction was then cooled to room temperature and diluted with water (120 mL). Organics were extracted with ethyl acetate (60 mL) and dry loaded onto a silica gel column. The product was isolated using a (20% Ethyl Acetate/ Hexanes) system. Fractions were combined and concentrated on reduced pressure to yield compound **3.43** as a tan solid (1.90 g, 74%). TLC R_f =0.68 (20% ethyl acetate/ 80% hexanes); ^{1}H NMR (400 MHz, $CDCl_3$) δ 3.92 (m, 1H), 2.43 (dd, J = 19.1, 8.8 Hz, 1H), 2.13 -2.01 (m, 1H), 1.97 – 1.89 (m, 1H), 1.84 – 1.76 (m, 2H), 1.74 – 1.63 (m, 3H), 1.54 – 1.39 (m, 6H), 1.34 – 1.16 (m, 6H), 1.02 (qd, *J* = 12.4, 4.9 Hz, 1H), 0.87 – 0.74 (m, 1H), 0.86 (s, 3H), 0.82 (s, 3H).

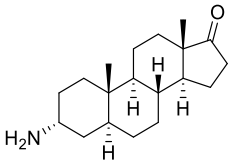

3α-amino-5α-androstan-17-one **(3.44)**

Lit Ref: Wang, Y. Epiandrosterone-derived prolinamide as an efficient asymmetric catalyst for Michael addition reactions of aldehydes to nitroalkenes. *RSC advances* **2014,** *4*, 30850-30856.

3α-azido-5α-androstan-17-one (0.500 g, 1.58 mmol) and triphenylphosphine (0.831 g, 3.16 mmol) were dissolved in tetrahydrofuran (8 mL) and heated in an oil bath at 50°C for thirty minutes. Deionized water (0.5 mL) was then added and the reaction was cooled to room temperature. The reaction was stirred for another 16 hours at room temperature. After 16 hours had passed, silica gel was added and the reaction mixture was dry loaded on a silica gel column. The amine was separated using a gradient solvent system of (10% MeOH/DCM) to (2% triethylamine/8% Methanol/ 90% dichloromethane). This gave compound **3.41** (272 mg, 59%) as a white solid. M.P. = 133.6 - 134.9 °C; TLC R_f =0.05 (1% Et_3N/ 9% Methanol/ 90% Dichloromethane); IR (ATR, cm^{-1}) 3446, 3374, 2962, 2929, 2913, 2885, 1737, 1453, 1399; ^1H NMR (400 MHz, CD_3OD) δ 3.11 (m, 1H), 2.45 (dd, J = 19.2, 8.7 Hz, 1H), 2.14 – 1.92 (m, 2H), 1.89 – 1.46 (m, 10H), 1.40 – 1.23 (m, 7H), 1.16 – 1.03 (m, 1H), 0.93 -0.85 (m, 7H). HRMS (ESI) *m / z* $C_{19}H_{32}NO$ [M+H] Exact Mass 290.247841; Observed 290.247652.

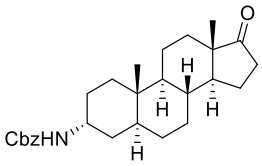

3α-Benzoyloxycarbonylamino-5α-androstan-17-one **(3.45)**

Using a 250 mL round bottom flask equipped with a stir bar, 3α-amino-5α-androstan-17-one (1.00 g, 3.45 mmol) and sodium carbonate (0.549 g, 5.18 mmol) were dissolved in a 1:1 mixture of 1,4-Dioxane and deionized water (20 mL). Benzyl chloroformate (0.73 mL, 5.18 mmol) was added slowly over a few minutes. The reaction was stirred overnight for 16 hours at room temperature. The following day the reaction was diluted with ethyl acetate (50 mL) and the organic layer was separated. The organic layer was then washed

with brine (1 x 25 mL) and deionized water (1 x 25 mL). The organic layers were then dried over sodium sulfate and the solvent was removed under reduced pressure. The crude oil was then dry loaded onto silica gel and purified by flash column chromatography (30% Ethyl Acetate/Hexanes). The fractions containing product were concentrated under reduced pressure to yield **3.42** as a white foamy solid (731 mg, 50%). M.P. =113.7 – 114.7°C; TLC R_f =0.23 (15% ethyl acetate/ 85 % hexanes); IR (ATR, cm^{-1}) 3339, 3061, 2966, 2927, 2851, 1730, 1708, 1526; ^{1}H NMR (400 MHz, $CDCl_3$) δ 7.39 -7.29 (m, 5H), 5.09 (s, 2H), 5.05 – 5.00 (m, 1H), 3.92 (m, 1H), 2.42 (dd, J = 19.2, 8.7 Hz, 1H), 2.12 – 2.01 (m, 1H), 1.96 – 1.89 (m, 1H), 1.83 – 1.76 (m, 2H), 1.73 – 1.61 (m, 3H), 1.59 –1.39 (m, 5H), 1.34 – 1.16 (m, 6H), 1.06 – 0.92 (m, 2H), 0.85 (s, 3H), 0.82 (s, 3H), 0.76 – 0.69 (m, 1H). ^{13}C NMR (100 MHz, $CDCl_3$) δ 155.6, 136.6, 128.6, 128.3, 128.2, 77.2, 66.6, 54.6, 51.5, 47.8, 46.3, 40.7, 36.2, 35.8, 35.0, 33.1, 33.0, 31.5, 30.8, 28.1, 26.2, 21.7, 20.0, 13.8, 11.4. Anal calcd for $C_{27}H_{37}NO_3$: C, 76.56; H, 8.80; N, 3.31 Found: C, 76.40; H, 8.55; N, 3.49.

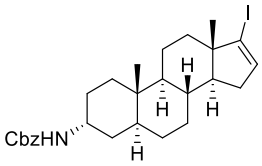

3α- Benzoyloxycarbonylamino-17-iodo-5α-androst-16,17-ene **(3.32)**

Using a 100 mL round bottom flask equipped with a stir bar, 3α-Benzoyloxycarbonylamino-5α-androstan-17-one (0.614 g, 1.44 mmol), hydrazine hydrate (0.56 mL, 7.24 mmol), and triethylamine (1.00 mL, 7.24 mmol) were added and dissolved in ethanol (8 mL). The reaction was heated at 50°C for two hours. At that point the reaction was diluted with ethyl acetate (30 mL) and water (30 mL). The organic layer was separated and then concentrated under reduced pressure. The crude solid was then

placed under high vacuum for 2 hours. The solid was then dissolved in dry tetrahydrofuran (10 mL) and dry triethylamine (2 mL). In a separate flask, Iodine (1.4 g, 5.53 mmol) was dissolved in 10 mL of dry tetrahydrofuran. Both flasks were placed under Argon and inside an ice bath(0°C). The iodine solution was then transferred by cannula to the flask containing the crude hydrazone over forty minutes. Once everything was transferred, the ice baths were removed and the reaction was stirred for another hour at room temperature. After one hour, the reaction was diluted with ethyl acetate (40 mL) and saturated sodium thiosulfate (40 mL) was added. The organic layer was separated and then washed subsequently with sodium bicarbonate (30 mL) and brine (40 mL). The organic layer was then dried over sodium sulfate and then dry loaded onto silica gel. Purification by flash column chromatography (30% Ethyl Acetate/Hexanes) gave compound **3.32** as a brownish-white oily solid (420 mg, 23%). TLC R_f =0.77 (15% ethyl acetate/ 85 % hexanes); ^{1}H NMR (400 MHz, $CDCl_3$) δ 7.42 -7.24 (m, 5H), 6.11 (dd, J = 3.0, 1.5 Hz, 1H), 5.09 (s, 2H), 5.03 (s, 1H), 3.91 (m, 1H), 2.23 – 1.99 (m, 2H), 1.96 – 1.86 (m, 1H), 1.74 – 1.64 (m, 3H), 1.64 – 1.56 (m, 3H), 1.50 – 1.25 (m, 4H), 1.25 – 1.11 (m, 4H), 1.09 – 0.85 (m, 3H), 0.82 (s, 3H), 0.82 – 0.72 (m, 1H), 0.72 (s, 3H).

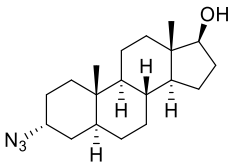

3α-azido-5α-androstan-17β-ol (**3.50)**

This compound has been previously reported, see: (Dungan, O. Synthetic Studies on Small Molecule Modulators of Src Homology 2 (SH2) Domain-Containing Inositol 5'-Phosphatase (SHIP). Syracuse University, 2019.)

Azide **3.43** (0.250 g, 0.7929 mmol) was dissolved in dichloromethane/methanol(1:1, 1.6 mL) and was cooled to 0℃. Sodium borohydride (0.020 g, 0.554 mmol) was added and the reaction was allowed to react for four hours. The reaction was then quenched with the addition of 1 mL 1M HCl, 5 mL NH_4Cl. The methanol was removed by rotary evaporation followed by dilution with dichloromethane (10 mL). The organic layer was washed with NH_4Cl (10 mL) and brine (10 mL) and then dried over Na_2SO_4. Organic layer was concentrated and purified using flash column silica gel chromatography (20% Ethyl Acetate/ 80% Hexanes). Compound **3.50** (0.218 g, 86%) was isolated as a white solid. TLC R*ƒ*= 0.39 (20% Ethyl Acetate/ 80% Hexanes); ^{1}H NMR (400 MHz, $CDCl_3$) δ 3.90 (t, *J* = 2.8 Hz, 1H), 3.66 (t, *J* = 8.6 Hz, 1H), 2.12 – 2.04 (m, 1H), (dt, *J* = 8.9, 3.4 Hz, 1H), 1.76 – 1.65 (m, 3H), 1.64 – 1.54 (m, 3H), 1.53 – 1.47 (m, 2H), 1.47 – 1.37 (m, 4H), 1.33-1.16 (m, 5H), 1.12 – 0.87 (m, 3H), 0.82 (s, 3H), 0.80 - 0.73 (m, 1H), 0.75 (s, 3H).

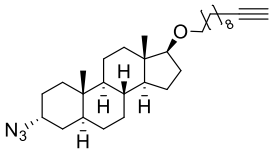

3α-azido-5β-androstan-17-undecyn-ether **(3.51)**

Alcohol **3.50** (0.152 g, 0.478775 mmol) was dissolved in *N,N*-dimethylacetamide (3 mL) and cooled to 0°C under Argon. 60% sodium hydride in mineral oil (0.090 g, 2.39 mmol) was then added slowly and the reaction was stirred for fifteen minutes. 10-undecyn-1-ol tosylate (0.185 g, 0.57453) was added via syringe slowly. Stirred for 18 hours under Argon. Reaction was quenched with 1M HCl (3 mL) and diluted with EtOAc (10 mL). Flask was poured into a separatory funnel and aqueous layer was removed. 2% LiCl solution was used to wash organic layer (3 x 25 mL) to remove any residual *N,N*-dimethylacetamide. Organic layer was then dried over sodium sulfate and then

concentrated to give a crude oil. The crude oil was then purified through flash column silica gel chromatography (5% EtOAc/Hexanes) to yield an oily opaque semi-solid (0.120 g, 53%). M.P = 116.5 - 119.3°C. TLC Rf = 0.72 (10% EtOAc/ 90% Hexanes); IR (ATR, cm^{-1}) 3280, 2969, 2924, 2847, 2102, 2073, 1465, 1379; ^{1}H NMR (400 MHz, $CDCl_3$) δ 3.88 (s, 1H), 3.47 – 3.36 (m, 2H), 3.27 (t, *J* = 8.4 Hz, 1H), 2.18 (td, *J* = 7.2, 2.6 Hz, 2H), 2.01 – 1.95 (m, 1H), 1.93 (t, *J* = 2.6 Hz, 1H), 1.87 (dt, *J* = 12.0, 2.8 Hz, 1H), 1.72 – 1.63 (m, 3H), 1.58 – 1.45 (m, 9H), 1.44 – 1.34 (m, 5H), 1.33 – 1.26 (m, 8H), 1.23 – 1.09 (m, 5H), 0.98 – 0.83 (m, 3H), 0.79 (s, 3H), 0.76 – 0.69 (m, 1H), 0.74 (s, 3H); ^{13}C {^{1}H} NMR (100 MHz, $CDCl_3$) δ 89.1, 84.8, 71.0, 70.2, 68.0, 58.2, 54.3, 51.3, 43.1, 40.1, 38.1, 36.0, 35.3, 32.9, 32.6, 31.5, 30.2, 29.4, 29.1, 28.7, 28.5, 28.2, 28.2, 26.2, 25.6, 23.3, 20.5, 18.4, 11.7, 11.6. HRMS (ESI) *m / z* $C_{30}H_{50}N_3O$ [M+H] Exact Mass 468.394840; Observed 468.394839.

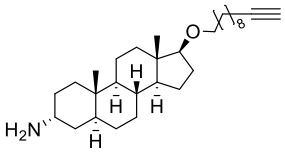

3α-amino-5β-androstan-17-undecyn-ether (**3.52)**

Azide **3.52** (1.020 g, 2.18 mmol) and Triphenyl phosphine (1.143 g, 4.36 mmol were added to a round bottom flask equipped with stir bar. The solids were dissolved with tetrahydrofuran (20 mL) and the reaction was heated to 50°C for thirty minutes. Deionized water (2 mL) was added and then the reaction was heated at 50°C for 24 hours. Reaction was dried with sodium sulfate, filtered into a round bottom flask and concentrated to give a crude oil. The crude oil was then purified through flash column silica gel chromatography by a gradient solvent system (5 to 10% MeOH/Dichloromethane to 2% Et_3N/ 8% Methanol/ 90% Dichloromethane) to yield a white solid (0.773 g, 80%). M.P = 57.7 –

60.1°C. TLC Rf = 0.24 (2% Et_3N/ 8% Methanol/ 90% Dichloromethane); IR (ATR, cm^{-1}) 3366, 3308, 3247, 2929, 2912, 2848, 1446; ^1H NMR (400 MHz, $CDCl_3$) δ 3.49 – 3.39 (m, 2H), 3.35 -3.28 (m, 1H), 3.16 – 3.11 (m, 1H), 2.19 – 2.12 (m, 3H), 2.02 – 1.93 (m, 1H), 1.88 (dt, *J* = *12.2, 3.4* Hz, 1H), 1.83 – 1.74 (m, 1H), 1.73 – 1.46 (m, 15H), 1.36 – 1.12 (m, 14H), 1.04 -0.90 (m, 2H), 0.83 (s, 3H), 0.82 – 0.77 (m, 1H), 0.75 (s, 3H); ^{13}C {^1H} NMR (100 MHz, $CDCl_3$) δ 89.1, 84.8, 70.2, 68.0, 54.6, 51.4, 45.9, 43.1, 39.2, 38.2, 36.4, 36.1, 35.4, 32.1, 31.6, 30.2, 29.4, 29.4, 29.0, 28.9, 28.7, 28.6, 28.5, 28.2, 26.2, 23.3, 20.5, 18.4, 11.7, 11.4. HRMS (ESI) *m / z* $C_{30}H_{52}NO$ [M+H] Exact Mass 442.404342; Observed 442.404255.

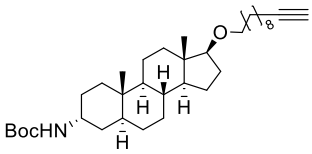

tert-butyl N-[(1S,3aS,3bR,5aS,7R,9aS,9bS,11aS)-9a,11a-dimethyl-1-(undec-10-yn-1-yloxy)-hexadecahydro-1H-cyclopenta[a]phenanthren-7-yl]carbamate (**3.48)**

Amine **3.52** (662 mg, 1.49 mmol) and di-*tert*-butyl dicarbonate (654 mg, 2.997 mmol) were dissolved in tetrahydrofuran (10 mL) and a stir bar was added. Aqueous NaOH (1M, 5 mL) was added and the reaction was stirred for six hours. After six hours, the reaction was diluted with brine (75 mL) and extracted with ethyl acetate (75 mL). The organic layer was dried over sodium sulfate and then purified through flash column silica gel chromatography (5% EtOAc/ 95% Hexanes) to yield Boc-protected amine **3.49** as a white solid(0.564 g, 69%). M.P = 76.9 – 78.5°C. TLC Rf = 0.51 (5% EtOAc/ Hexanes); IR (ATR, cm^{-1}) 3311, 3270, 3134, 2928, 2851, 1692, 1454, 1388; ^1H NMR (400 MHz, $CDCl_3$) δ 4.80 (s, 1H), 3.82 (s, 1H), 3.46 – 3.35 (m, 2H), 3.25 (t, *J* = 8.4 Hz, 1H), 2.16 (td, *J* = 7.0, 2.6

Hz, 2H), 2.00 – 1.93 (m, 1H), 1.92 (t, *J* = 2.6 Hz, 1H) 1.91 – 1.84 (m, 1H), 1.73 – 1.58 (m, 3H), 1.57 – 1.48 (m, 8H), 1.43 (s, 9H), 1.41 – 1.32 (m, 4H), 1.33 – 1.25 (s, 9H), 1.24 – 1.13 (m, 5H), 1.12 – 0.82 (m, 4H), 0.78 (s, 3H), 0.72 (s, 3H), 0.71 – 0.64 (m, 1H).; $^{13}C\{^{1}H\}$ NMR (100 MHz, $CDCl_3$) δ 155.2, 89.1, 84.8, 79.0, 70.2, 68.0, 54.7, 51.4, 45.7, 43.1, 40.8, 38.2, 36.1, 35.3, 33.3, 33.1, 31.6, 30.2, 29.4, 29.4, 29.1, 28.7, 28.5 (3C), 28.4, 28.1, 27.4, 26.4, 26.2, 23.3, 20.5, 18.4, 11.7, 11.5. HRMS (ESI) *m / z* $C_{35}H_{59}NO_3Na$ [M+Na] Exact Mass 564.438716; Observed 564.438378.

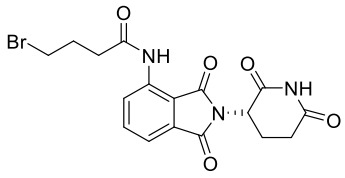

4-Bromo-N-(2-(2,6-dioxopiperidin-3-yl)-1,3-dioxoisoindolin-4-yl)butanamide **(3.54)**

This compound has been made previously, for reference: (Li, W.; Gao, C.; Zhao, L.; Yuan, Z.; Chen, Y.; Jiang, Y. Phthalimide conjugations for the degradation of oncogenic PI3K. *European Journal of Medicinal Chemistry* **2018,** *151*, 237-247.)

4-amino-2-(2,6-dioxopiperidin-3-yl)isoindoline-1,3-dione (0.500 g, 1.829 mmol) was suspended in 8 mL of tetrahydrofuran under Argon inside a round bottom flask equipped with stir bar. 4-bromobutryrl chloride (0.81 mL, 2.744 mmol) was added slowly and then a reflux condenser was attached. Reaction was heated under reflux for four hours under Argon. Reaction was then quenched using sodium bicarbonate (25 mL) and then extracted with dichloromethane (2 x 25 mL). Organic layer was then washed with brine (100 mL) and then organic were dried over Na_2SO_4. Organic layer was then concentrated

and the crude oil was purified by flash column chromatography (1% MeOH/ 99% DCM) to yield compound **3.54** as an off-white solid (215 mg, 28%). TLC R_f =0.53 (1% methanol / 99 % dichloromethane); ^{1}H NMR (400 MHz, $CDCl_3$) δ 9.42 (s, 1H), 8.81 (d, *J* = 8.4 Hz, 1H), 7.97 (s, 1H), 7.72 (t, *J* = 7.6 Hz, 1H), 7.56 (d, *J* = 7.3 Hz, 1H), 4.95 (dd, *J* = 12.4 ,5.4 Hz, 1H), 3.52 (t, *J* = 6.3 Hz, 1H), 2.95 – 2.74 (m, 3H), 2.67 (t, *J* = 7.0 Hz, 1H), 2.30 (quint, *J* = 7.2 Hz, 1H), 2.21 – 2.16 (m, 1H).

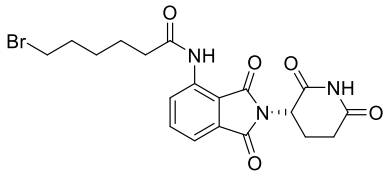

6-Bromo-N-(2-(2,6-dioxopiperidin-3-yl)-1,3-dioxoisoindolin-4-yl)hexanamide **(3.55)**

This compound has been made previously, for reference: (Li, W.; Gao, C.; Zhao, L.; Yuan, Z.; Chen, Y.; Jiang, Y. Phthalimide conjugations for the degradation of oncogenic PI3K. *European Journal of Medicinal Chemistry* **2018,** *151*, 237-247.)

4-amino-2-(2,6-dioxopiperidin-3-yl)isoindoline-1,3-dione (0.101 g, 0.369 mmol) was suspended in 8 mL of tetrahydrofuran under Argon inside a round bottom flask equipped with stir bar. 6-bromohexanoyl chloride (0.11 mL, 0.739 mmol) was added slowly and then a reflux condenser was attached. Reaction was heated under reflux for four hours under Argon. Reaction was then quenched using sodium bicarbonate (10 mL) and then extracted with dichloromethane (2 x 10 mL). Organic layer was then washed with brine (50 mL) and then organic were dried over Na_2SO_4. Organic layer was then concentrated and the crude oil was purified by flash column chromatography (1% MeOH/ 99% DCM) to yield compound **3.55** as an off-white solid (117 mg, 72%). TLC R_f =0.59 (1% methanol / 99 % dichloromethane); ^{1}H NMR (400 MHz, $CDCl_3$) δ 9.41 (s, 1H), 8.82 (d, *J* = 8.5 Hz, 1H), 7.97 (s, 1H), 7.72 (t, *J* = 7.5 Hz, 1H), 7.55 (d, *J* = 7.0Hz, 1H) 4.95 (dd, *J* = 12.4 ,5.6

Hz, 1H), 3.43 (t, *J* = 6.7 Hz, 2H), 2.95 – 2.91 (m, 1H), 2.89- 2.75 (m, 2H), 2.49 (t, *J* = 7.5 Hz, 2H), 2.22 – 2.15 (m, 1H), 1.93 (quint, *J* = 7.2 Hz, 2H), 1.79 (quint, *J* = 7.3 Hz, 2H), 1.56 – 1.52 (m, 2H).

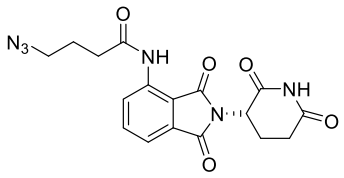

4-Azido-N-(2-(2,6-dioxopiperidin-3-yl)-1,3-dioxoisoindolin-4-yl)butanamide **(3.49)**

This compound has been made previously, for reference: (Li, W.; Gao, C.; Zhao, L.; Yuan, Z.; Chen, Y.; Jiang, Y. Phthalimide conjugations for the degradation of oncogenic PI3K. *European Journal of Medicinal Chemistry* **2018,** *151*, 237-247.)

4-Bromo-N-(2-(2,6-dioxopiperidin-3-yl)-1,3-dioxoisoindolin-4-yl)butanamide (0.165 g, 0.3907 mmol), sodium azide (0.069 g, 0.7815 mmol) and *N,N*-Dimethylacetamide (1.2 mL) were added to a round bottom flask with stir bar under Argon. Reaction was heated to 90°C and allowed to react for eighteen hours. After which the reaction was diluted with ethyl acetate (15 mL) and 2% LiCl solution (100 mL). The organic layer was extracted and then washed with brine (100 mL), The organic layer was then dried over Na_2SO_4 and concentrated in vacuo to yield a crude yellow solid. Following purification by flash column chromatography (20% Acetone/ 80% Dichloromethane) **3.49** was isolated as a tan solid (0.063 g, 47% yield). TLC R_f =0.54 (20% acetone / 80 % dichloromethane); ^{1}H NMR (400 MHz, $CDCl_3$) δ 9.43 (s, 1H), 8.82 (d, *J* = 8.5 Hz, 1H), 7.97 (s, 1H), 7.72 (t, *J* = 7.5 Hz, 1H), 7.55 (d, *J* = 7.2 Hz, 1H), 4.96 (dd, *J* = 12.4 ,5.5 Hz, 1H), 3.44 (t, *J* = 6.5 Hz, 2H), 2.96 – 2.71 (m, 3H), 2.57 (t, *J* = 7.2 Hz, 2H), 2.22 – 2.15 (m, 1H), 2.04 (quint, *J* = 6.8 Hz, 2H).

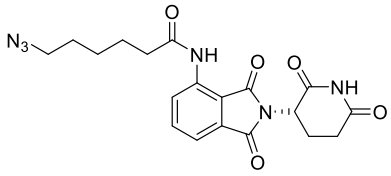

6-Azido-N-(2-(2,6-dioxopiperidin-3-yl)-1,3-dioxoisoindolin-4-yl)hexanamide **(3.56)**

This compound has been made previously, for reference: (Li, W.; Gao, C.; Zhao, L.; Yuan, Z.; Chen, Y.; Jiang, Y. Phthalimide conjugations for the degradation of oncogenic PI3K. *European Journal of Medicinal Chemistry* **2018,** *151*, 237-247.)

6-Bromo-N-(2-(2,6-dioxopiperidin-3-yl)-1,3-dioxoisoindolin-4-yl)hexanamide (0.081 g, 0.184 mmol), sodium azide (0.024 g, 0.368 mmol) and *N,N*-Dimethylacetamide (1.0 mL) were added to a round bottom flask with stir bar under Argon. Reaction was heated to 90°C and allowed to react for eighteen hours. After which the reaction was diluted with ethyl acetate (10 mL) and 2% LiCl solution (100 mL). The organic layer was extracted and then washed with brine (100 mL), The organic layer was then dried over Na_2SO_4 and concentrated in vacuo to yield a crude yellow solid. Following purification by flash column chromatography (20% Acetone/ 80% Dichloromethane) **3.56** was isolated as a tan solid (0.044 g, 59% yield). TLC R_f =0.55 (20% acetone / 80 % dichloromethane); ^{1}H NMR (400 MHz, $CDCl_3$) δ 9.42 (s, 1H), 8.82 (d, *J* = 8.4 Hz, 1H), 7.95 (s, 1H), 7.72 (t, *J* = 7.5 Hz, 1H), 7.55 (d, *J* = 6.9 Hz, 1H), 4.95 (dd, *J* = 12.4 ,5.3 Hz, 1H), 3.43 (t, *J* = 6.7 Hz, 2H), 2.97 – 2.90 (m, 1H), 2.88- 2.71 (m, 2H), 2.49 (t, *J* = 7.4 Hz, 2H), 2.22 – 2.15 (m, 1H), 1.79 (quint, *J* = 7.7 Hz, 2H), 1.66 (quint, *J* = 7.2 Hz, 2H), 1.52– 1.44 (m, 2H).

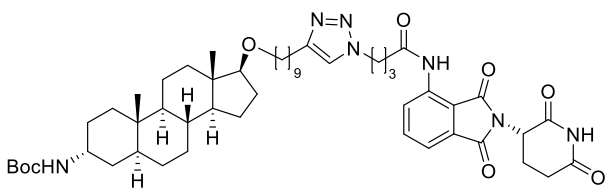

tert-butyl N-[(1S,3aS,3bR,5aS,7R,9aS,9bS,11aS)-1-({9-[1-(3-{[2-(2,6-dioxopiperidin-3-yl)-1,3-dioxo-2,3-dihydro-1H-isoindol-4-yl]carbamoyl}propyl)-2,3-dihydro-1H-1,2,3-triazol-4-yl]nonyl}oxy)-9a,11a-dimethyl-hexadecahydro-1H-cyclopenta[a]phenanthren-7-yl]carbamate (**3.57)**

Alkyne **3.48** (100 mg, 0.18459 mmol)**,** copper sulfate pentahydrate (9 mg, 0.03691 mmol), and sodium ascorbate (14 mg, 0.07382) were dissolved in *N,N*-dimethylformamide (1 mL) inside a round-bottom flask with stir bar. After stirring for ten minutes, Azide **3.49** (63 mg, 0.18459 mmol) was added and then a condenser was attached. The reaction was then heated at 60°C for four hours after which the reaction was cooled to room temperature. Sodium bicarbonate (10 mL) was added and the organics were extracted with ethyl acetate (15 mL). Organic layer was washed once more with sodium bicarbonate (10 mL) and brine (10 mL). Organic layer was then dried over Na_2SO_4 and concentrated to yield a crude oil. Purification by flash column chromatography gradient (10/20/30% Acetone / 90/80/70% Dichloromethane) to yield **3.57** as a white solid (96 mg, 56%). M.P = 88.2-88.8°C. TLC Rf = 0.58 (30% acetone / 70 % dichloromethane); IR (ATR, cm^{-1}) 3357, 3329, 2927, 2853, 1778, 1692, 1662, 1533, 1479, 1396; ^{1}H NMR (400 MHz, $CDCl_3$) δ 9.38 (m, 1H),), 8.75 (d, *J* = 8.5 Hz, 1H), 8.52 (s, 1H), 7.70 (t, *J* = 7.6 Hz, 1H), 7.53 (d, *J* = 7.3 Hz, 1H), 7.30, (s, 1H), 4.94 (m, 1H), 4.82 (m, 1H), 4.42 (t, *J* = 6.4 Hz, 2H), 3.81 (m, 1H), 3.46 – 3.33 (m, 2H), 3.25 (t, *J* = 8.3 Hz, 1H), 2.95 – 2.85 (m, 1H), 2.81 – 2.73 (m, 2H), 2.71 – 2.64 (m, 2H), 2.50 (t, *J* = 6.9 Hz, 2H), 2.31 (quint, *J* = 6.3 Hz, 2H), 2.18 – 2.13 (m, 1H), 1.98 – 1.84 (m, 2H), 1.68 – 1.58 (m, 4H), 1.55 – 1.45 (m, 6H), 1.45 – 1.39 (m, 10H), 1.37 – 1.23 (m, 13H), 1.21 – 1.14 (m, 4H), 1.12 – 0.83 (m, 5H), 0.77 (s, 3H), 0.72 (s, 3H), 0.71 – 0.64 (m, 1H).; ^{13}C {^{1}H} NMR (100 MHz, $CDCl_3$) δ 170.9, 170.7, 169.0,

168.0, 166.6, 155.2, 148.7, 137.5, 136.4, 131.2, 125.3, 120.7, 118.7, 115.5, 89.1, 79.0, 70.2, 69.5, 54.6, 53.8, 51.4, 49.3, 49.0, 45.7, 43.1, 40.8, 38.2, 36.1, 35.3, 33.9, 33.3, 33.1, 31.5, 31.4, 30.2, 29.5, 29.5, 29.3, 29.3, 28.5 (3C), 28.1, 26.4, 26.2, 25.7, 25.5, 23.3, 22.7, 20.5, 11.7, 11.5. HRMS (ESI) *m / z* $C_{52}H_{76}N_7O_8$ [M+H] Exact Mass 926.574989; Observed 926.574831.

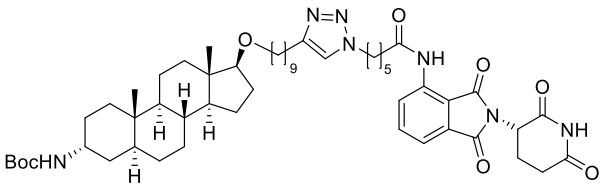

tert-butyl N-[(1S,3aS,3bR,5aS,7R,9aS,9bS,11aS)-1-({9-[1-(5-{[2-(2,6-dioxopiperidin-3-yl)-1,3-dioxo-2,3-dihydro-1H-isoindol-4-yl]carbamoyl}pentyl)-2,3-dihydro-1H-1,2,3-triazol-4-yl]nonyl}oxy)-9a,11a-dimethyl-hexadecahydro-1H-cyclopenta[a]phenanthren-7-yl]carbamate (**3.58)**

Alkyne **3.48** (78 mg, 0.145 mmol)**,** copper sulfate pentahydrate (14mg, 0.058 mmol), and sodium ascorbate (23 mg, 0.116 mmol) were dissolved in *N,N*-dimethylformamide (1 mL) inside a round-bottom flask with stir bar. After stirring for ten minutes, Azide **3.56** (60 mg, 0.145 mmol) was added and then a condenser was attached. The reaction was then heated at 60°C for four hours after which the reaction was cooled to room temperature. Sodium bicarbonate (10 mL) was added and the organics were extracted with ethyl acetate (15 mL). Organic layer was washed once more with sodium bicarbonate (10 mL) and brine (10 mL). Organic layer was then dried over Na_2SO_4 and concentrated to yield a crude oil. Purification by flash column chromatography gradient (10/20/30% Acetone / 90/80/70% Dichloromethane) to yield **3.58** as a white solid (91 mg, 56%). M.P = 93.1 - 94.8°C. TLC Rf = 0.66 (30% acetone / 70 % dichloromethane); IR (ATR, cm^{-1}) 3353,

2925, 2851, 1771, 1697, 1617, 1522, 1478, 1396, 1348; ^{1}H NMR (400 MHz, $CDCl_3$) δ 9.38 (s, 1H), 8.77 (d, *J* = 8.4 Hz, 1H), 8.61 (s, 1H), 7.70 (t, *J* = 7.6 Hz, 1H), 7.52 (d, *J* = 7.2 Hz, 1H), 7.24, (s, 1H), 4.94 (dd, *J* = 12.0, 5.1 Hz, 1H), 4.82 (d, *J* = 7.3 Hz, 1H), 4.42 (t, *J* = 7.1 Hz, 1H), 3.81 (m, 1H), 3.46 – 3.33 (m, 2H), 3.23 (t, *J* = 8.3 Hz, 1H), 2.92 – 2.82 (m, 1H), 2.82 – 2.72 (m, 2H), 2.65 (t, *J* = 7.6 Hz, 2H), 2.44 (t, *J* = 7.3 Hz, 2H), 2.19 – 2.12 (m, 1H), 1.98 – 1.88 (m, 3H), 1.88 – 1.81 (m, 1H), 1.80 – 1.72 (m, 2H), 1.67 – 1.58 (m, 5H), 1.54 – 1.46 (m, 6H), 1.45 – 1.39 (m, 11H), 1.35 – 1.21 (m, 14H), 1.20 – 1.12 (m, 4H), 1.12 – 0.96 (m, 2H), 0.94 – 0.80 (m, 2H), 0.77 (s, 3H), 0.72 (s, 3H), 0.71 – 0.64 (m, 1H).; ^{13}C {^{1}H} NMR (100 MHz, $CDCl_3$) δ 171.8, 170.9, 169.2, 168.0, 166.7, 155.2, 148.4, 137.7, 136.4, 131.2, 125.2, 120.4, 118.5, 115.4, 89.1, 79.0, 77.2, 70.2, 54.6, 51.4, 49.8, 49.3, 45.7, 43.1, 40.7, 38.2, 37.4, 36.1, 35.3, 33.3, 33.1, 31.5, 31.4, 30.2, 30.1, 29.5, 29.5, 29.3, 29.3, 28.5 (3C), 28.4, 28.1, 26.4, 26.2, 26.0, 25.7, 24.4, 23.3, 22.7, 20.5, 11.7, 11.5. HRMS (ESI) *m / z* $C_{54}H_{80}N_7O_8$ [M+H] Exact Mass 954.606289; Observed 954.605861.

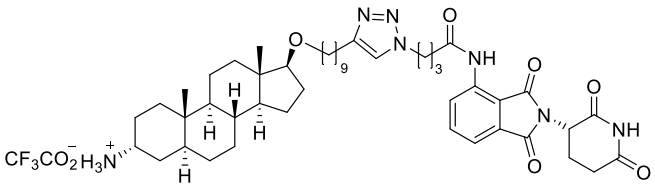

(1S,3aS,3bR,5aS,7R,9aS,9bS,11aS)-1-({9-[1-(3-{[2-(2,6-dioxopiperidin-3-yl)-1,3-dioxo-2,3-dihydro-1H-isoindol-4-yl]carbamoyl}propyl)-2,3-dihydro-1H-1,2,3-triazol-4-yl]nonyl}oxy)-9a,11a-dimethyl-hexadecahydro-1H-cyclopenta[a]phenanthren-7-aminium trifluoroacetate (**3.47)**

Boc protected amine **3.56** (90 mg, 0.097 mmol) was stirred with concentrated trifluoroacetic acid for three hours at room temperature inside a 10 mL round bottom flask with a stir bar. The crude reaction mixture was transferred to a separate 250 mL flask and

the trifluoroacetic acid was azeotroped by addition of methanol (100 mL) followed subsequent concentration by rotary evaporation. This process was repeated three times to yield **3.47** as a hygroscopic white solid (91 mg, 100% yield). M.P = 84.3 – 85.8°C. TLC Rf = 0.00 (30% acetone / 70 % dichloromethane); IR (ATR, cm^{-1}) 3349, 3094, 2979, 2969, 2929, 2855, 1777, 1696, 1619, 1533, 1482, 1393; ^{1}H NMR (400 MHz, CD_3OD) δ 8.77 (d, *J* = 7.2 Hz, 1H), 7.90 - 7.70 (m, 2H), 7.57 (d, *J* = 6.0 Hz, 1H), 5.16 – 5.09 (m, 1H), 4.51 (m, 1H), 3.56 – 3.36 (m, 3H), 3.23 (t, *J* = 8.3 Hz, 1H), 2.96 – 2.62 (m, 5H), 2.55 (m, 2H), 2.32 (m, 2H), 2.19 – 2.11 (m, 1H), 2.04 – 1.84 (m, 3H), 1.78 – 1.40 (m, 14H), 1.40 – 1.13 (m, 18H), 1.05 – 0.92 (m, 2H), 0.85 (s, 3H), 0.74 (s, 3H).; ^{13}C {^{1}H} NMR (100 MHz, CD_3OD) δ 173.1, 171.5, 169.8, 168.4, 166.8, 136.7, 135.7, 131.6, 125.6, 118.1, 116.9, 89.1, 69.8, 54.0, 51.1, 49.3, 49.2, 42.8, 38.9, 37.8, 35.7, 35.1, 33.2, 31.2, 31.1, 30.8, 30.7, 29.8, 29.2, 29.1, 29.0, 28.9, 28.8, 28.1, 27.8, 27.5, 25.9, 25.2, 24.8, 23.9, 22.8, 22.2, 20.1, 10.8, 10.2. HRMS (ESI) *m / z* $C_{47}H_{68}N_7O_6$ [M+H] Exact Mass 826.522559; Observed 826.522737. *some peaks in carbon are obscured by CD_3OD peak

**Some protons have exchanged and are not listed.

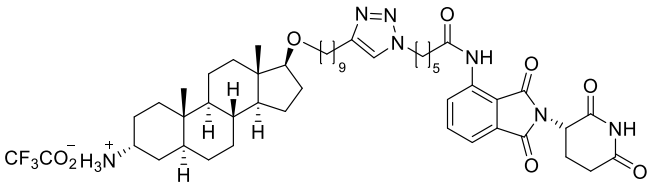

(1S,3aS,3bR,5aS,7R,9aS,9bS,11aS)-1-({9-[1-(5-{[2-(2,6-dioxopiperidin-3-yl)-1,3-dioxo-2,3-dihydro-1H-isoindol-4-yl]carbamoyl}pentyl)-2,3-dihydro-1H-1,2,3-triazol-4-yl]nonyl}oxy)-9a,11a-dimethyl-hexadecahydro-1H-cyclopenta[a]phenanthren-7-aminium trifluoroacetate (**3.59)**

Boc protected amine **3.58** (80 mg, 0.08272 mmol) was stirred with concentrated trifluoroacetic acid for three hours at room temperature inside a 10 mL round bottom flask with a stir bar. The crude reaction mixture was transferred to a separate 250 mL flask and the trifluoroacetic acid was azeotroped by addition of methanol (100 mL) followed subsequent concentration by rotary evaporation. This process was repeated three times to yield **3.59** as a hygroscopic white solid (81 mg, 100% yield). M.P = 129.5 – 131.1°C. TLC Rf = 0.00 (30% acetone / 70 % dichloromethane); IR (ATR, cm^{-1}) 3280, 3249, 2932, 2922, 2851, 2102, 1743, 1700, 1647, 1526, 1478, 1395; ^{1}H NMR (400 MHz, CD_3OD) δ 8.61 (d, *J* = 8.4 Hz, 1H), 7.78 (t, *J* = 7.4 Hz, 1H), 7.73 (s, 1H), 7.58 (d, *J* = 6.8 Hz, 1H), 5.13 (dd, *J* = 12.8, 5.6 Hz, 1H), 4.38 (t, *J* = 7.0 Hz, 2H), 3.50 (m, 1H), 3.42 (m, 2H), 3.28 (m, 1H), 2.93 – 2.71 (m, 3H), 2.65 (t, *J* = 7.6 Hz, 2H), 2.50 (t, *J* = 7.3 Hz, 1H), 2.19 – 2.11 (m, 1H), 2.02 – 1.93 (m, 3H), 1.91 – 1.85 (m, 1H), 1.82 – 1.70 (m, 4H), 1.68 – 1.47 (m, 8H), 1.46 – 1.36 (m, 6H), 1.36 – 1.26 (m, 14H), 1.24 – 1.13 (m, 3H), 1.04 – 0.89 (m, 2H), 0.86 (s, 3H), 0.83 – 0.76 (m, 1H), 0.74 (s, 3H).;^{13}C {^{1}H} NMR (100 MHz, CD_3OD) δ 171.9, 171.3, 169.1, 168.3, 166.7, 137.7, 136.4, 131.1, 125.3, 118.6, 115.4, 89.0, 77.2, 70.2, 53.4, 51.0, 50.5, 49.3, 47.7, 43.0, 38.7, 37.9, 35.8, 35.1, 31.9, 31.3, 31.1, 30.2, 29.8, 29.7, 29.7, 29.4, 29.4, 29.2, 29.2, 28.1, 28.0, 26.1, 25.9, 25.1, 24.4, 24.3, 23.3, 22.7, 22.6, 20.4, 14.1, 11.7, 11.2.; HRMS (ESI) *m / z* $C_{49}H_{72}N_7O_6$ [M+H] Exact Mass 854.553860; Observed 854.553817.

**Some protons have exchanged and are not listed.

3.7 References

1) Marshall, R. S.; Vierstra, R. D. Dynamic Regulation of the 26S Proteasome: From Synthesis to Degradation. *Frontiers in Molecular Biosciences* **2019,** *6*,
2) Bhattacharyya, S.; Yu, H.; Mim, C.; Matouschek, A. Regulated protein turnover: snapshots of the proteasome in action. *Nature Reviews Molecular Cell Biology* **2014,** *15*, 122+.
3) Xu, P.; Duong, D. M.; Seyfried, N. T.; Cheng, D.; Xie, Y.; Robert, J.; Rush, J.; Hochstrasser, M.; Finley, D.; Peng, J. Quantitative Proteomics Reveals the Function of Unconventional Ubiquitin Chains in Proteasomal Degradation. *Cell* **2009,** *137*, 133-145.
4) Kleiger, G.; Mayor, T. Perilous journey: a tour of the ubiquitin–proteasome system. *Trends in Cell Biology* **2014,** *24*, 352-359.
5) Hershko, A.; Ciechanover, A. The ubiquitin system. *Annual review of biochemistry* **1998,** *67*, 425-479.
6) Zhao, L.; Zhao, J.; Zhong, K.; Tong, A.; Jia, D. Targeted protein degradation: mechanisms, strategies and application. *Signal Transduction and Targeted Therapy* **2022,** *7*, 113.
7) Hu, Z. Recent Developments in PROTAC-Mediated Protein Degradation: From Bench to Clinic. *Chembiochem : a European journal of chemical biology* **2022,** *23*.
8) Burslem, G. M.; Crews, C. M. Proteolysis-Targeting Chimeras as Therapeutics and Tools for Biological Discovery. *Cell* **2020,** *181*, 102-114.
9) Toure, M.; Crews, C. M. Small-Molecule PROTACS: New Approaches to Protein Degradation. *Angewandte Chemie International Edition* **2016,** *55*, 1966-1973.
10) Sakamoto, K. M.; Kim, K. B.; Kumagai, A.; Mercurio, F.; Crews, C. M.; Deshaies, R. J. Protacs: Chimeric molecules that target proteins to the Skp1–Cullin–F box complex for ubiquitination and degradation. *Proceedings of the National Academy of Sciences* **2001,** *98*, 8554-8559.
11) Bricelj, A.; Steinebach, C.; Kuchta, R.; Gütschow, M.; Sosič, I. E3 Ligase Ligands in Successful PROTACs: An Overview of Syntheses and Linker Attachment Points. *Frontiers in Chemistry* **2021,** *9*,
12) Kramer, L. T.; Zhang, X. Expanding the landscape of E3 ligases for targeted protein degradation. *Current Research in Chemical Biology* **2022,** *2*, 100020.
13) Maxwell, P. H.; Wiesener, M. S.; Chang, G.-W.; Clifford, S. C.; Vaux, E. C.; Cockman, M. E.; Wykoff, C. C.; Pugh, C. W.; Maher, E. R.; Ratcliffe, P. J. The tumour suppressor protein VHL targets hypoxia-inducible factors for oxygen-dependent proteolysis. *Nature* **1999,** *399*, 271-275.
14) Iliopoulos, O.; Levy, A. P.; Jiang, C.; Kaelin, W. G., Jr.; Goldberg, M. A. Negative regulation of hypoxia-inducible genes by the von Hippel-Lindau protein. *Proc Natl Acad Sci U S A* **1996,** *93*, 10595-9.
15) Buckley, D. L.; Van Molle, I.; Gareiss, P. C.; Tae, H. S.; Michel, J.; Noblin, D. J.; Jorgensen, W. L.; Ciulli, A.; Crews, C. M. Targeting the von Hippel–Lindau E3 Ubiquitin Ligase Using Small Molecules To Disrupt the VHL/HIF-1α Interaction. *Journal of the American Chemical Society* **2012,** *134*, 4465-4468.
16) Buckley, D. L.; Gustafson, J. L.; Van Molle, I.; Roth, A. G.; Tae, H. S.; Gareiss, P. C.; Jorgensen, W. L.; Ciulli, A.; Crews, C. M. Small-Molecule Inhibitors of the

Interaction between the E3 Ligase VHL and HIF1α. *Angewandte Chemie International Edition* **2012,** *51*, 11463-11467.
17) Van Molle, I.; Thomann, A.; Buckley, Dennis L.; So, Ernest C.; Lang, S.; Crews, Craig M.; Ciulli, A. Dissecting Fragment-Based Lead Discovery at the von Hippel-Lindau Protein:Hypoxia Inducible Factor 1α Protein-Protein Interface. *Chemistry & Biology* **2012,** *19*, 1300-1312.
18) Galdeano, C.; Gadd, M. S.; Soares, P.; Scaffidi, S.; Van Molle, I.; Birced, I.; Hewitt, S.; Dias, D. M.; Ciulli, A. Structure-Guided Design and Optimization of Small Molecules Targeting the Protein–Protein Interaction between the von Hippel–Lindau (VHL) E3 Ubiquitin Ligase and the Hypoxia Inducible Factor (HIF) Alpha Subunit with in Vitro Nanomolar Affinities. *Journal of Medicinal Chemistry* **2014,** *57*, 8657-8663.
19) Soares, P.; Gadd, M. S.; Frost, J.; Galdeano, C.; Ellis, L.; Epemolu, O.; Rocha, S.; Read, K. D.; Ciulli, A. Group-Based Optimization of Potent and Cell-Active Inhibitors of the von Hippel-Lindau (VHL) E3 Ubiquitin Ligase: Structure-Activity Relationships Leading to the Chemical Probe (2S,4R)-1-((S)-2-(1-Cyanocyclopropanecarboxamido)-3,3-dimethylbutanoyl)-4-hydroxy-N-(4-(4-methylthiazol-5-yl)benzyl)pyrrolidine-2-carboxamide (VH298). *J Med Chem* **2018,** *61*, 599-618.
20) W. Banks, J.; S. Batsanov, A.; A. K. Howard, J.; O'Hagan, D.; S. Rzepa, H.; Martin-Santamaria, S. The preferred conformation of α-fluoroamides. *Journal of the Chemical Society, Perkin Transactions 2* **1999**, 2409-2411.
21) Diehl, C. J.; Ciulli, A. Discovery of small molecule ligands for the von Hippel-Lindau (VHL) E3 ligase and their use as inhibitors and PROTAC degraders. *Chem Soc Rev* **2022,** *51*, 8216-8257.
22) Tovell, H.; Testa, A.; Zhou, H.; Shpiro, N.; Crafter, C.; Ciulli, A.; Alessi, D. R. Design and Characterization of SGK3-PROTAC1, an Isoform Specific SGK3 Kinase PROTAC Degrader. *ACS Chemical Biology* **2019,** *14*, 2024-2034.
23) Halland, N.; Schmidt, F.; Weiss, T.; Saas, J.; Li, Z.; Czech, J.; Dreyer, M.; Hofmeister, A.; Mertsch, K.; Dietz, U.; Strübing, C.; Nazare, M. Discovery of N-[4-(1H-Pyrazolo[3,4-b]pyrazin-6-yl)-phenyl]-sulfonamides as Highly Active and Selective SGK1 Inhibitors. *ACS Med Chem Lett* **2015,** *6*, 73-8.
24) Raina, K.; Lu, J.; Qian, Y.; Altieri, M.; Gordon, D.; Rossi, A. M.; Wang, J.; Chen, X.; Dong, H.; Siu, K.; Winkler, J. D.; Crew, A. P.; Crews, C. M.; Coleman, K. G. PROTAC-induced BET protein degradation as a therapy for castration-resistant prostate cancer. *Proc Natl Acad Sci U S A* **2016,** *113*, 7124-9.
25) Larabi, A.; Devos, Juliette M.; Ng, S.-L.; Nanao, Max H.; Round, A.; Maniatis, T.; Panne, D. Crystal Structure and Mechanism of Activation of TANK-Binding Kinase 1. *Cell Reports* **2013,** *3*, 734-746.
26) Barbie, D. A.; Tamayo, P.; Boehm, J. S.; Kim, S. Y.; Moody, S. E.; Dunn, I. F.; Schinzel, A. C.; Sandy, P.; Meylan, E.; Scholl, C.; Fröhling, S.; Chan, E. M.; Sos, M. L.; Michel, K.; Mermel, C.; Silver, S. J.; Weir, B. A.; Reiling, J. H.; Sheng, Q.; Gupta, P. B.; Wadlow, R. C.; Le, H.; Hoersch, S.; Wittner, B. S.; Ramaswamy, S.; Livingston, D. M.; Sabatini, D. M.; Meyerson, M.; Thomas, R. K.; Lander, E. S.; Mesirov, J. P.; Root, D. E.; Gilliland, D. G.; Jacks, T.; Hahn, W. C. Systematic RNA

interference reveals that oncogenic KRAS-driven cancers require TBK1. *Nature* **2009,** *462*, 108-12.
27) Crew, A. P.; Raina, K.; Dong, H.; Qian, Y.; Wang, J.; Vigil, D.; Serebrenik, Y. V.; Hamman, B. D.; Morgan, A.; Ferraro, C.; Siu, K.; Neklesa, T. K.; Winkler, J. D.; Coleman, K. G.; Crews, C. M. Identification and Characterization of Von Hippel-Lindau-Recruiting Proteolysis Targeting Chimeras (PROTACs) of TANK-Binding Kinase 1. *Journal of Medicinal Chemistry* **2018,** *61*, 583-598.
28) Klein, V. G.; Townsend, C. E.; Testa, A.; Zengerle, M.; Maniaci, C.; Hughes, S. J.; Chan, K.-H.; Ciulli, A.; Lokey, R. S. Understanding and Improving the Membrane Permeability of VH032-Based PROTACs. *ACS Medicinal Chemistry Letters* **2020,** *11*, 1732-1738.
29) Chamberlain, P. P.; Lopez-Girona, A.; Miller, K.; Carmel, G.; Pagarigan, B.; Chie-Leon, B.; Rychak, E.; Corral, L. G.; Ren, Y. J.; Wang, M.; Riley, M.; Delker, S. L.; Ito, T.; Ando, H.; Mori, T.; Hirano, Y.; Handa, H.; Hakoshima, T.; Daniel, T. O.; Cathers, B. E. Structure of the human Cereblon-DDB1-lenalidomide complex reveals basis for responsiveness to thalidomide analogs. *Nature Structural and Molecular Biology* **2014,** *21*, 803+.
30) Ito, T.; Ando, H.; Suzuki, T.; Ogura, T.; Hotta, K.; Imamura, Y.; Yamaguchi, Y.; Handa, H. Identification of a Primary Target of Thalidomide Teratogenicity. *Science* **2010,** *327*, 1345-1350.
31) Asatsuma-Okumura, T.; Ito, T.; Handa, H. Molecular Mechanisms of the Teratogenic Effects of Thalidomide. *Pharmaceuticals* **2020,** *13*, 95.
32) Bartlett, J. B.; Dredge, K.; Dalgleish, A. G. The evolution of thalidomide and its IMiD derivatives as anticancer agents. *Nature Reviews Cancer* **2004,** *4*, 314+.
33) Sheskin, J. THALIDOMIDE IN THE TREATMENT OF LEPRA REACTIONS. *Clin Pharmacol Ther* **1965,** *6*, 303-6.
34) D'Amato, R. J.; Loughnan, M. S.; Flynn, E.; Folkman, J. Thalidomide is an inhibitor of angiogenesis. *Proceedings of the National Academy of Sciences* **1994,** *91*, 4082-4085.
35) Zhu, Y. X.; Kortuem, K. M.; Stewart, A. K. Molecular mechanism of action of immune-modulatory drugs thalidomide, lenalidomide and pomalidomide in multiple myeloma. *Leuk Lymphoma* **2013,** *54*, 683-7.
36) Awan, F. T. Thalidomide and lenalidomide as new therapeutics for the treatment of chronic lymphocytic leukemia. *Leukemia & Lymphoma* **2010,** *51*, 27-38.
37) Lu, G.; Middleton, R. E.; Sun, H.; Naniong, M.; Ott, C. J.; Mitsiades, C. S.; Wong, K. K.; Bradner, J. E.; Kaelin, W. G., Jr. The myeloma drug lenalidomide promotes the cereblon-dependent destruction of Ikaros proteins. *Science* **2014,** *343*, 305-9.
38) Krönke, J.; Udeshi, N. D.; Narla, A.; Grauman, P.; Hurst, S. N.; McConkey, M.; Svinkina, T.; Heckl, D.; Comer, E.; Li, X.; Ciarlo, C.; Hartman, E.; Munshi, N.; Schenone, M.; Schreiber, S. L.; Carr, S. A.; Ebert, B. L. Lenalidomide causes selective degradation of IKZF1 and IKZF3 in multiple myeloma cells. *Science* **2014,** *343*, 301-5.
39) Pourabdollah, M.; Bahmanyar, M.; Atenafu, E. G.; Reece, D.; Chang, H. IKZF1/3 Protein Expressions Are Associated with a Better Survival in Relapsed/Refractory Multiple Myeloma Patients Treated with Lenalidomide. *Blood* **2016,** *128*, 4506.

40) Fionda, C.; Abruzzese, M. P.; Zingoni, A.; Cecere, F.; Vulpis, E.; Peruzzi, G.; Soriani, A.; Molfetta, R.; Paolini, R.; Ricciardi, M. R.; Petrucci, M. T.; Santoni, A.; Cippitelli, M. The IMiDs targets IKZF-1/3 and IRF4 as novel negative regulators of NK cell-activating ligands expression in multiple myeloma. *Oncotarget* **2015,** *6*,
41) Winter, G. E.; Buckley, D. L.; Paulk, J.; Roberts, J. M.; Souza, A.; Dhe-Paganon, S.; Bradner, J. E. DRUG DEVELOPMENT. Phthalimide conjugation as a strategy for in vivo target protein degradation. *Science* **2015,** *348*, 1376-81.
42) Donati, B.; Lorenzini, E.; Ciarrocchi, A. BRD4 and Cancer: going beyond transcriptional regulation. *Mol Cancer* **2018,** *17*, 164.
43) Lockhart, A. C.; Olszanski, A. J.; Allgren, R. L.; Yaguchi, S.; Cohen, S. J.; Hilton, J. F.; Wang-Gillam, A.; Shapiro, G. I. Abstract B271: A first-in-human Phase I study of ZSTK474, an oral pan-PI3K inhibitor, in patients with advanced solid malignancies. *Molecular Cancer Therapeutics* **2013,** *12*, B271-B271.
44) Namatame, N.; Tamaki, N.; Yoshizawa, Y.; Okamura, M.; Nishimura, Y.; Yamazaki, K.; Tanaka, M.; Nakamura, T.; Semba, K.; Yamori, T.; Yaguchi, S. I.; Dan, S. Antitumor profile of the PI3K inhibitor ZSTK474 in human sarcoma cell lines. *Oncotarget* **2018,** *9*, 35141-35161.
45) Li, W.; Gao, C.; Zhao, L.; Yuan, Z.; Chen, Y.; Jiang, Y. Phthalimide conjugations for the degradation of oncogenic PI3K. *European Journal of Medicinal Chemistry* **2018,** *151*, 237-247.
46) Schmidt, M.; Rohe, A.; Platzer, C.; Najjar, A.; Erdmann, F.; Sippl, W. Regulation of G2/M Transition by Inhibition of WEE1 and PKMYT1 Kinases. *Molecules* **2017,** *22*, 2045.
47) Carrassa, L.; Damia, G. DNA damage response inhibitors: Mechanisms and potential applications in cancer therapy. *Cancer Treatment Reviews* **2017,** *60*, 139-151.
48) Hirai, H.; Iwasawa, Y.; Okada, M.; Arai, T.; Nishibata, T.; Kobayashi, M.; Kimura, T.; Kaneko, N.; Ohtani, J.; Yamanaka, K.; Itadani, H.; Takahashi-Suzuki, I.; Fukasawa, K.; Oki, H.; Nambu, T.; Jiang, J.; Sakai, T.; Arakawa, H.; Sakamoto, T.; Sagara, T.; Yoshizumi, T.; Mizuarai, S.; Kotani, H. Small-molecule inhibition of Wee1 kinase by MK-1775 selectively sensitizes p53-deficient tumor cells to DNA-damaging agents. *Mol Cancer Ther* **2009,** *8*, 2992-3000.
49) Guertin, A. D.; Li, J.; Liu, Y.; Hurd, M. S.; Schuller, A. G.; Long, B.; Hirsch, H. A.; Feldman, I.; Benita, Y.; Toniatti, C.; Zawel, L.; Fawell, S. E.; Gilliland, D. G.; Shumway, S. D. Preclinical Evaluation of the WEE1 Inhibitor MK-1775 as Single-Agent Anticancer Therapy. *Molecular Cancer Therapeutics* **2013,** *12*, 1442-1452.
50) Do, K.; Wilsker, D.; Ji, J.; Zlott, J.; Freshwater, T.; Kinders, R. J.; Collins, J.; Chen, A. P.; Doroshow, J. H.; Kummar, S. Phase I Study of Single-Agent AZD1775 (MK-1775), a Wee1 Kinase Inhibitor, in Patients With Refractory Solid Tumors. *J Clin Oncol* **2015,** *33*, 3409-15.
51) Li, Z.; Pinch, B. J.; Olson, C. M.; Donovan, K. A.; Nowak, R. P.; Mills, C. E.; Scott, D. A.; Doctor, Z. M.; Eleuteri, N. A.; Chung, M.; Sorger, P. K.; Fischer, E. S.; Gray, N. S. Development and Characterization of a Wee1 Kinase Degrader. *Cell Chemical Biology* **2020,** *27*, 57-65.e9.
52) Robb, C. M.; Contreras, J. I.; Kour, S.; Taylor, M. A.; Abid, M.; Sonawane, Y. A.; Zahid, M.; Murry, D. J.; Natarajan, A.; Rana, S. Chemically induced degradation of

CDK9 by a proteolysis targeting chimera (PROTAC). *Chemical Communications* **2017,** *53*, 7577-7580.

53) Su, S.; Yang, Z.; Gao, H.; Yang, H.; Zhu, S.; An, Z.; Wang, J.; Li, Q.; Chandarlapaty, S.; Deng, H.; Wu, W.; Rao, Y. Potent and Preferential Degradation of CDK6 via Proteolysis Targeting Chimera Degraders. *Journal of Medicinal Chemistry* **2019,** *62*, 7575-7582.

54) Riching, K. M.; Schwinn, M. K.; Vasta, J. D.; Robers, M. B.; Machleidt, T.; Urh, M.; Daniels, D. L. CDK Family PROTAC Profiling Reveals Distinct Kinetic Responses and Cell Cycle-Dependent Degradation of CDK2. *SLAS Discov* **2021,** *26*, 560-569.

55) Li, J.; Liu, T.; Song, Y.; Wang, M.; Liu, L.; Zhu, H.; Li, Q.; Lin, J.; Jiang, H.; Chen, K.; Zhao, K.; Wang, M.; Zhou, H.; Lin, H.; Luo, C. Discovery of Small-Molecule Degraders of the CDK9-Cyclin T1 Complex for Targeting Transcriptional Addiction in Prostate Cancer. *Journal of Medicinal Chemistry* **2022,** *65*, 11034-11057.

56) Wei, M.; Zhao, R.; Cao, Y.; Wei, Y.; Li, M.; Dong, Z.; Liu, Y.; Ruan, H.; Li, Y.; Cao, S.; Tang, Z.; Zhou, Y.; Song, W.; Wang, Y.; Wang, J.; Yang, G.; Yang, C. First orally bioavailable prodrug of proteolysis targeting chimera (PROTAC) degrades cyclin-dependent kinases 2/4/6 in vivo. *European Journal of Medicinal Chemistry* **2021,** *209*, 112903.

57) Zhou, F.; Chen, L.; Cao, C.; Yu, J.; Luo, X.; Zhou, P.; Zhao, L.; Du, W.; Cheng, J.; Xie, Y.; Chen, Y. Development of selective mono or dual PROTAC degrader probe of CDK isoforms. *Eur J Med Chem* **2020,** *187*, 111952.

58) Pevarello, P.; Brasca, M. G.; Amici, R.; Orsini, P.; Traquandi, G.; Corti, L.; Piutti, C.; Sansonna, P.; Villa, M.; Pierce, B. S.; Pulici, M.; Giordano, P.; Martina, K.; Fritzen, E. L.; Nugent, R. A.; Casale, E.; Cameron, A.; Ciomei, M.; Roletto, F.; Isacchi, A.; Fogliatto, G.; Pesenti, E.; Pastori, W.; Marsiglio, A.; Leach, K. L.; Clare, P. M.; Fiorentini, F.; Varasi, M.; Vulpetti, A.; Warpehoski, M. A. 3-Aminopyrazole inhibitors of CDK2/cyclin A as antitumor agents. 1. Lead finding. *J Med Chem* **2004,** *47*, 3367-80.

59) Zheng, M.; Huo, J.; Gu, X.; Wang, Y.; Wu, C.; Zhang, Q.; Wang, W.; Liu, Y.; Liu, Y.; Zhou, X.; Chen, L.; Zhou, Y.; Li, H. Rational Design and Synthesis of Novel Dual PROTACs for Simultaneous Degradation of EGFR and PARP. *Journal of Medicinal Chemistry* **2021,** *64*, 7839-7852.

60) Shimokawa, K.; Shibata, N.; Sameshima, T.; Miyamoto, N.; Ujikawa, O.; Nara, H.; Ohoka, N.; Hattori, T.; Cho, N.; Naito, M. Targeting the Allosteric Site of Oncoprotein BCR-ABL as an Alternative Strategy for Effective Target Protein Degradation. *ACS Medicinal Chemistry Letters* **2017,** *8*, 1042-1047.

61) Ohoka, N.; Okuhira, K.; Ito, M.; Nagai, K.; Shibata, N.; Hattori, T.; Ujikawa, O.; Shimokawa, K.; Sano, O.; Koyama, R.; Fujita, H.; Teratani, M.; Matsumoto, H.; Imaeda, Y.; Nara, H.; Cho, N.; Naito, M. In Vivo Knockdown of Pathogenic Proteins via Specific and Nongenetic Inhibitor of Apoptosis Protein (IAP)-dependent Protein Erasers (SNIPERs)*. *Journal of Biological Chemistry* **2017,** *292*, 4556-4570.

62) Schneekloth, A. R.; Pucheault, M.; Tae, H. S.; Crews, C. M. Targeted intracellular protein degradation induced by a small molecule: En route to chemical proteomics. *Bioorganic & Medicinal Chemistry Letters* **2008,** *18*, 5904-5908.

63) Sun, Y.; Zhao, X.; Ding, N.; Gao, H.; Wu, Y.; Yang, Y.; Zhao, M.; Hwang, J.; Song, Y.; Liu, W.; Rao, Y. PROTAC-induced BTK degradation as a novel therapy for

mutated BTK C481S induced ibrutinib-resistant B-cell malignancies. *Cell Research* **2018,** *28*, 779-781.

64) Du, G.; Jiang, J.; Henning, N. J.; Safaee, N.; Koide, E.; Nowak, R. P.; Donovan, K. A.; Yoon, H.; You, I.; Yue, H.; Eleuteri, N. A.; He, Z.; Li, Z.; Huang, H. T.; Che, J.; Nabet, B.; Zhang, T.; Fischer, E. S.; Gray, N. S. Exploring the target scope of KEAP1 E3 ligase-based PROTACs. *Cell Chemical Biology* **2022,** *29*, 1470-1481.e31.

65) Lu, M.; Liu, T.; Jiao, Q.; Ji, J.; Tao, M.; Liu, Y.; You, Q.; Jiang, Z. Discovery of a Keap1-dependent peptide PROTAC to knockdown Tau by ubiquitination-proteasome degradation pathway. *European Journal of Medicinal Chemistry* **2018,** *146*, 251-259.

66) Cuenda, A.; Rousseau, S. p38 MAP-Kinases pathway regulation, function and role in human diseases. *Biochimica et Biophysica Acta (BBA) - Molecular Cell Research* **2007,** *1773*, 1358-1375.

67) Smith, B. E.; Wang, S. L.; Jaime-Figueroa, S.; Harbin, A.; Wang, J.; Hamman, B. D.; Crews, C. M. Differential PROTAC substrate specificity dictated by orientation of recruited E3 ligase. *Nature Communications* **2019,** *10*, 131.

68) Bemis, T. A.; La Clair, J. J.; Burkart, M. D. Unraveling the Role of Linker Design in Proteolysis Targeting Chimeras. *Journal of Medicinal Chemistry* **2021,** *64*, 8042-8052.

69) Cyrus, K.; Wehenkel, M.; Choi, E.-Y.; Han, H.-J.; Lee, H.; Swanson, H.; Kim, K.-B. Impact of linker length on the activity of PROTACs. *Molecular BioSystems* **2011,** *7*, 359-364.

70) Chan, K.-H.; Zengerle, M.; Testa, A.; Ciulli, A. Impact of Target Warhead and Linkage Vector on Inducing Protein Degradation: Comparison of Bromodomain and Extra-Terminal (BET) Degraders Derived from Triazolodiazepine (JQ1) and Tetrahydroquinoline (I-BET726) BET Inhibitor Scaffolds. *Journal of Medicinal Chemistry* **2018,** *61*, 504-513.

71) Gadd, M. S.; Testa, A.; Lucas, X.; Chan, K. H.; Chen, W.; Lamont, D. J.; Zengerle, M.; Ciulli, A. Structural basis of PROTAC cooperative recognition for selective protein degradation. *Nat Chem Biol* **2017,** *13*, 514-521.

72) Weerakoon, D.; Carbajo, R. J.; De Maria, L.; Tyrchan, C.; Zhao, H. Impact of PROTAC Linker Plasticity on the Solution Conformations and Dissociation of the Ternary Complex. *Journal of Chemical Information and Modeling* **2022,** *62*, 340-349.

73) Shah, R. R.; Redmond, J. M.; Mihut, A.; Menon, M.; Evans, J. P.; Murphy, J. A.; Bartholomew, M. A.; Coe, D. M. Hi-JAK-ing the ubiquitin system: The design and physicochemical optimisation of JAK PROTACs. *Bioorganic & Medicinal Chemistry* **2020,** *28*, 115326.

74) Poongavanam, V.; Atilaw, Y.; Siegel, S.; Giese, A.; Lehmann, L.; Meibom, D.; Erdelyi, M.; Kihlberg, J. Linker-Dependent Folding Rationalizes PROTAC Cell Permeability. *Journal of Medicinal Chemistry* **2022,** *65*, 13029-13040.

75) Zaidman, D.; Prilusky, J.; London, N. PRosettaC: Rosetta Based Modeling of PROTAC Mediated Ternary Complexes. *Journal of Chemical Information and Modeling* **2020,** *60*, 4894-4903.

76) Drummond, M. L.; Williams, C. I. In Silico Modeling of PROTAC-Mediated Ternary Complexes: Validation and Application. *Journal of Chemical Information and Modeling* **2019,** *59*, 1634-1644.
77) Song, J. H.; Wagner, N. D.; Yan, J.; Li, J.; Huang, R. Y. C.; Balog, A. J.; Newitt, J. A.; Chen, G.; Gross, M. L. Native mass spectrometry and gas-phase fragmentation provide rapid and in-depth topological characterization of a PROTAC ternary complex. *Cell Chemical Biology* **2021,** *28*, 1528-1538.e4.
78) Beveridge, R.; Kessler, D.; Rumpel, K.; Ettmayer, P.; Meinhart, A.; Clausen, T. Native Mass Spectrometry Can Effectively Predict PROTAC Efficacy. *ACS Central Science* **2020,** *6*, 1223-1230.
79) Pettersson, M.; Crews, C. M. PROteolysis TArgeting Chimeras (PROTACs) - Past, present and future. *Drug Discov Today Technol* **2019,** *31*, 15-27.
80) Miles, L. E. M. Properties, variants, and applications of the immunoradiometric assay method. *Ricerca in clinica e in laboratorio* **1975,** *5*, 59.
81) Hughes, Scott J.; Ciulli, A. Molecular recognition of ternary complexes: a new dimension in the structure-guided design of chemical degraders. *Essays in Biochemistry* **2017,** *61*, 505-516.
82) Bondeson, D. P.; Smith, B. E.; Burslem, G. M.; Buhimschi, A. D.; Hines, J.; Jaime-Figueroa, S.; Wang, J.; Hamman, B. D.; Ishchenko, A.; Crews, C. M. Lessons in PROTAC Design from Selective Degradation with a Promiscuous Warhead. *Cell Chem Biol* **2018,** *25*, 78-87.e5.
83) Coleman, N.; Rodon, J. Taking Aim at the Undruggable. *American Society of Clinical Oncology Educational Book* **2021**, e145-e152.
84) Moore, A. R.; Rosenberg, S. C.; McCormick, F.; Malek, S. RAS-targeted therapies: is the undruggable drugged? *Nature Reviews Drug Discovery* **2020,** *19*, 533-552.
85) Haura, E. B.; Turkson, J.; Jove, R. Mechanisms of Disease: insights into the emerging role of signal transducers and activators of transcription in cancer. *Nature Clinical Practice Oncology* **2005,** *2*, 315+.
86) Zhou, H.; Bai, L.; Xu, R.; Zhao, Y.; Chen, J.; McEachern, D.; Chinnaswamy, K.; Wen, B.; Dai, L.; Kumar, P.; Yang, C.-Y.; Liu, Z.; Wang, M.; Liu, L.; Meagher, J. L.; Yi, H.; Sun, D.; Stuckey, J. A.; Wang, S. Structure-Based Discovery of SD-36 as a Potent, Selective, and Efficacious PROTAC Degrader of STAT3 Protein. *Journal of Medicinal Chemistry* **2019,** *62*, 11280-11300.
87) Bai, L.; Zhou, H.; Xu, R.; Zhao, Y.; Chinnaswamy, K.; McEachern, D.; Chen, J.; Yang, C.-Y.; Liu, Z.; Wang, M.; Liu, L.; Jiang, H.; Wen, B.; Kumar, P.; Meagher, J. L.; Sun, D.; Stuckey, J. A.; Wang, S. A Potent and Selective Small-Molecule Degrader of STAT3 Achieves Complete Tumor Regression In Vivo. *Cancer Cell* **2019,** *36*, 498-511.e17.
88) Perez-Dominguez, F.; Carrillo-Beltrán, D.; Blanco, R.; Muñoz, J. P.; León-Cruz, G.; Corvalan, A. H.; Urzúa, U.; Calaf, G. M.; Aguayo, F., Role of Pirin, an Oxidative Stress Sensor Protein, in Epithelial Carcinogenesis. In *Biology*, 2021; Vol. 10.
89) Chessum, N. E. A.; Sharp, S. Y.; Caldwell, J. J.; Pasqua, A. E.; Wilding, B.; Colombano, G.; Collins, I.; Ozer, B.; Richards, M.; Rowlands, M.; Stubbs, M.; Burke, R.; McAndrew, P. C.; Clarke, P. A.; Workman, P.; Cheeseman, M. D.; Jones, K. Demonstrating In-Cell Target Engagement Using a Pirin Protein

Degradation Probe (CCT367766). *Journal of Medicinal Chemistry* **2018,** *61*, 918-933.
90) Douglass, E. F., Jr.; Miller, C. J.; Sparer, G.; Shapiro, H.; Spiegel, D. A. A Comprehensive Mathematical Model for Three-Body Binding Equilibria. *Journal of the American Chemical Society* **2013,** *135*, 6092-6099.
91) Fuhler, G. M.; Brooks, R.; Toms, B.; Iyer, S.; Gengo, E. A.; Park, M.-Y.; Gumbleton, M.; Viernes, D. R.; Chisholm, J. D.; Kerr, W. G. Therapeutic Potential of SH2 Domain-Containing Inositol-5′-Phosphatase 1 (SHIP1) and SHIP2 Inhibition in Cancer. *Molecular Medicine* **2012,** *18*, 65-75.
92) Pedicone, C.; Fernandes, S.; Dungan, O. M.; Dormann, S. M.; Viernes, D. R.; Adhikari, A. A.; Choi, L. B.; De Jong, E. P.; Chisholm, J. D.; Kerr, W. G. Pan-SHIP1/2 inhibitors promote microglia effector functions essential for CNS homeostasis. *J. Cell Sci.* **2020,** *133*, jcs238030.
93) Pedicone, C.; Meyer, S. T.; Chisholm, J. D.; Kerr, W. G. Targeting SHIP1 and SHIP2 in Cancer. *Cancers (Basel)* **2021,** *13*,
94) Casement, R.; Bond, A.; Craigon, C.; Ciulli, A. Mechanistic and Structural Features of PROTAC Ternary Complexes. *Methods Mol Biol* **2021,** *2365*, 79-113.
95) Waterman, P. M.; Marschner, S.; Brandl, E.; Cambier, J. C. The inositol 5-phosphatase SHIP-1 and adaptors Dok-1 and 2 play central roles in CD4-mediated inhibitory signaling. *Immunol Lett* **2012,** *143*, 122-30.
96) Pauls, S. D.; Marshall, A. J. Regulation of immune cell signaling by SHIP1: A phosphatase, scaffold protein, and potential therapeutic target. *Eur J Immunol* **2017,** *47*, 932-945.
97) Sattler, M.; Verma, S.; Pride, Y. B.; Salgia, R.; Rohrschneider, L. R.; Griffin, J. D. SHIP1, an SH2 domain containing polyinositol-5-phosphatase, regulates migration through two critical tyrosine residues and forms a novel signaling complex with DOK1 and CRKL. *J Biol Chem* **2001,** *276*, 2451-8.
98) Burslem, G. M. Efficient Synthesis of Immunomodulatory Drug Analogues Enables Exploration of Structure–Degradation Relationships. *ChemMedChem 13*, 1508-1512.
99) Rana, S. Selective degradation of CDK6 by a palbociclib based PROTAC. *Bioorganic & medicinal chemistry letters 29*, 1375-1379.
100) Koch, V. Stille and Suzuki Cross-Coupling Reactions as Versatile Tools for Modifications at C-17 of Steroidal Skeletons - A Comprehensive Study. *Advanced synthesis & catalysis 359*, 832-840.
101) Berg, R.; Straub, B. F. Advancements in the mechanistic understanding of the copper-catalyzed azide-alkyne cycloaddition. *Beilstein J Org Chem* **2013,** *9*, 2715-50.

Appendix: ^{1}H and ^{13}C NMR Spectra

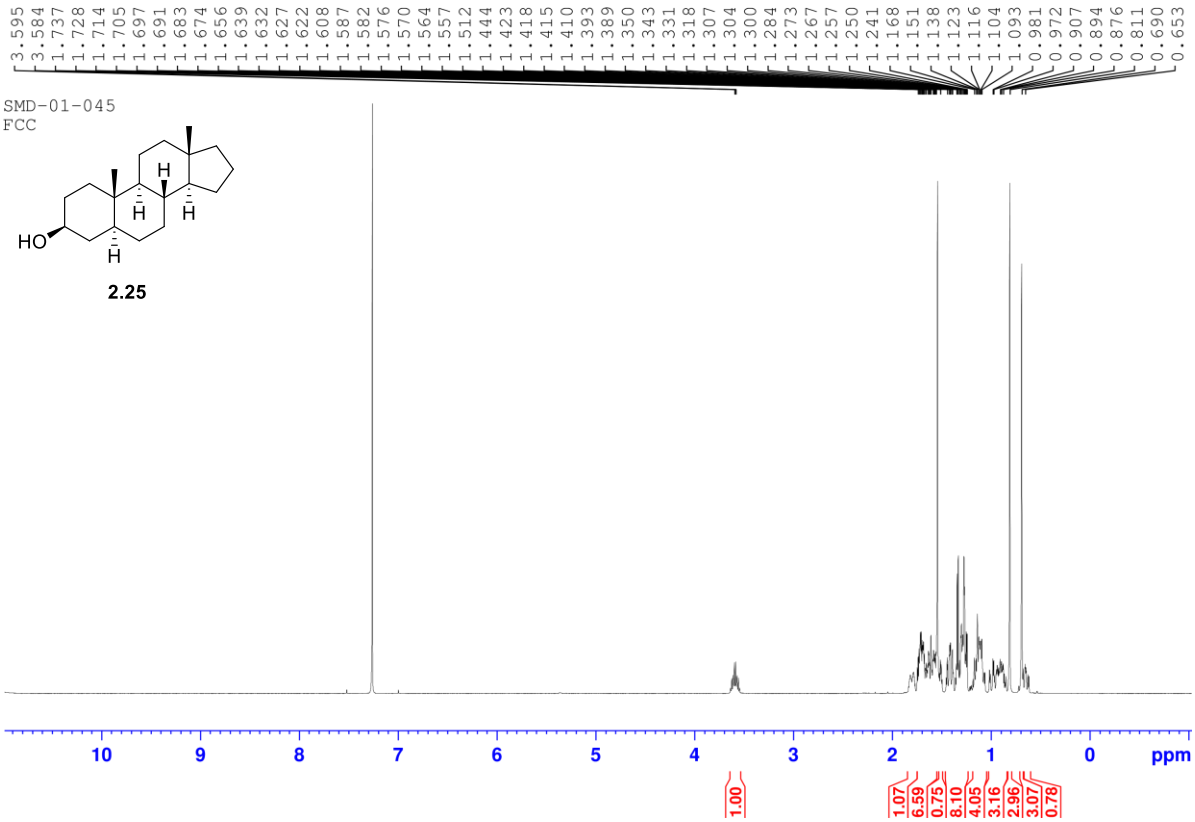

2.25

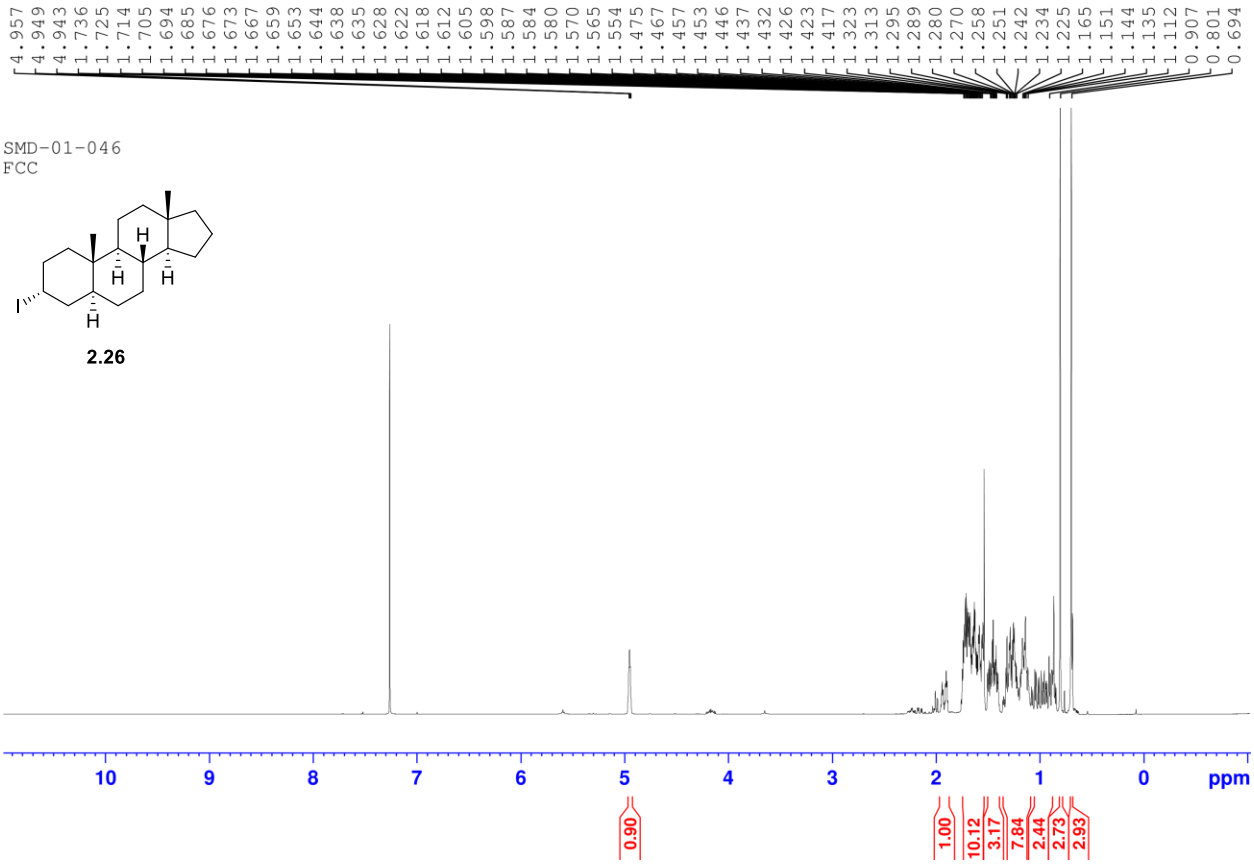
4.957
4.949
4.943
1.736
1.725
1.714
1.705
1.694
1.685
1.676
1.673
1.667
1.659
1.653
1.644
1.638
1.635
1.628
1.622
1.618
1.612
1.605
1.598
1.587
1.584
1.580
1.570
1.565
1.554
1.475
1.467
1.457
1.453
1.446
1.437
1.432
1.426
1.423
1.417
1.323
1.313
1.295
1.289
1.280
1.270
1.258
1.251
1.242
1.234
1.225
1.165
1.151
1.144
1.135
1.112
0.907
0.801
0.694
SMD-01-046
FCC
H
H
H
H
I
2.26
10
9
8
7
6
5
4
3
2
1
0
ppm
0.90
1.00
10.12
3.17
7.84
2.44
2.73
2.93

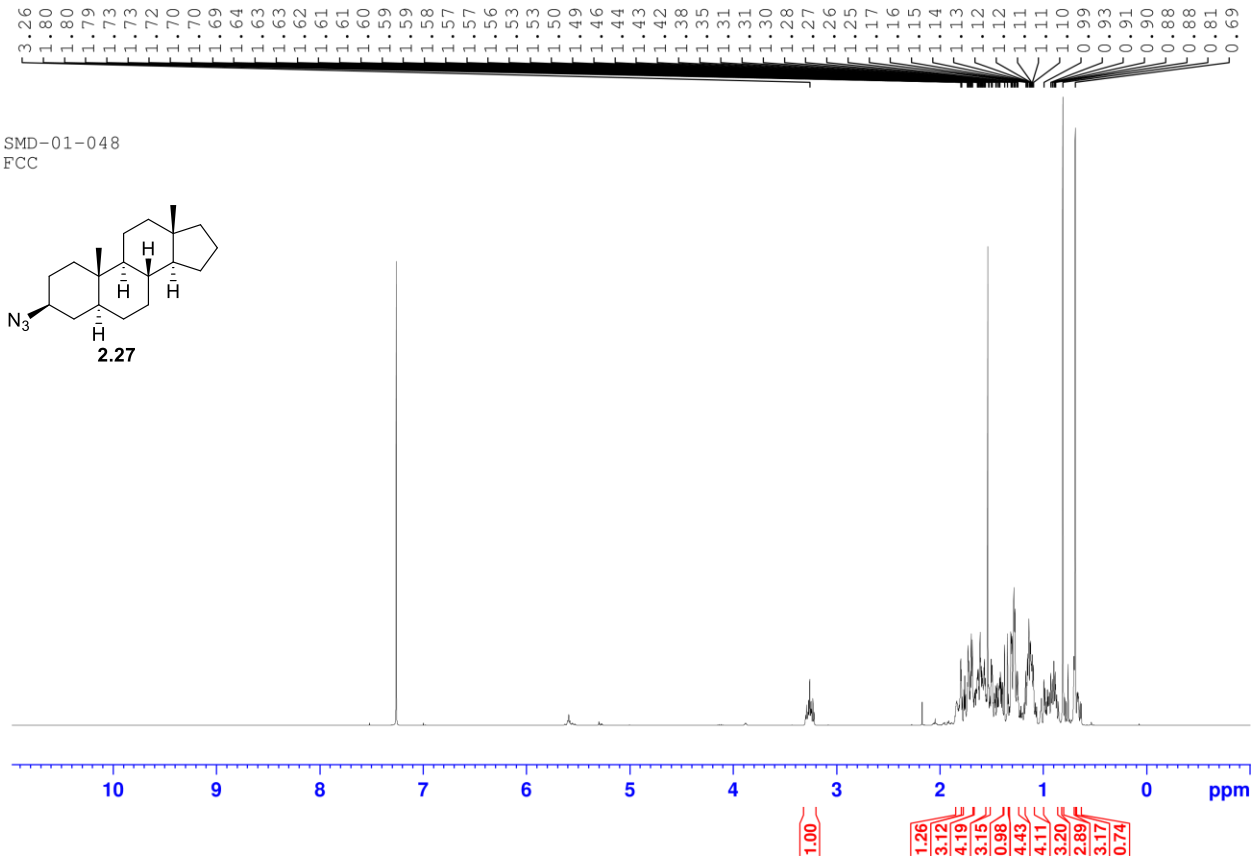
3.26
1.80
1.80
1.79
1.73
1.73
1.72
1.70
1.70
1.69
1.64
1.63
1.63
1.62
1.61
1.61
1.60
1.59
1.59
1.58
1.57
1.57
1.56
1.53
1.53
1.50
1.49
1.46
1.44
1.43
1.42
1.38
1.35
1.31
1.31
1.30
1.28
1.27
1.26
1.25
1.17
1.16
1.15
1.14
1.13
1.12
1.12
1.11
1.11
1.10
0.99
0.93
0.91
0.90
0.88
0.81
0.69
SMD-01-048
FCC
H
H
H
N3
H
2.27
10
9
8
7
6
5
4
3
2
1
0
ppm
1.00
1.26
3.12
4.19
3.15
0.98
4.43
4.11
3.20
2.89
3.17
0.74

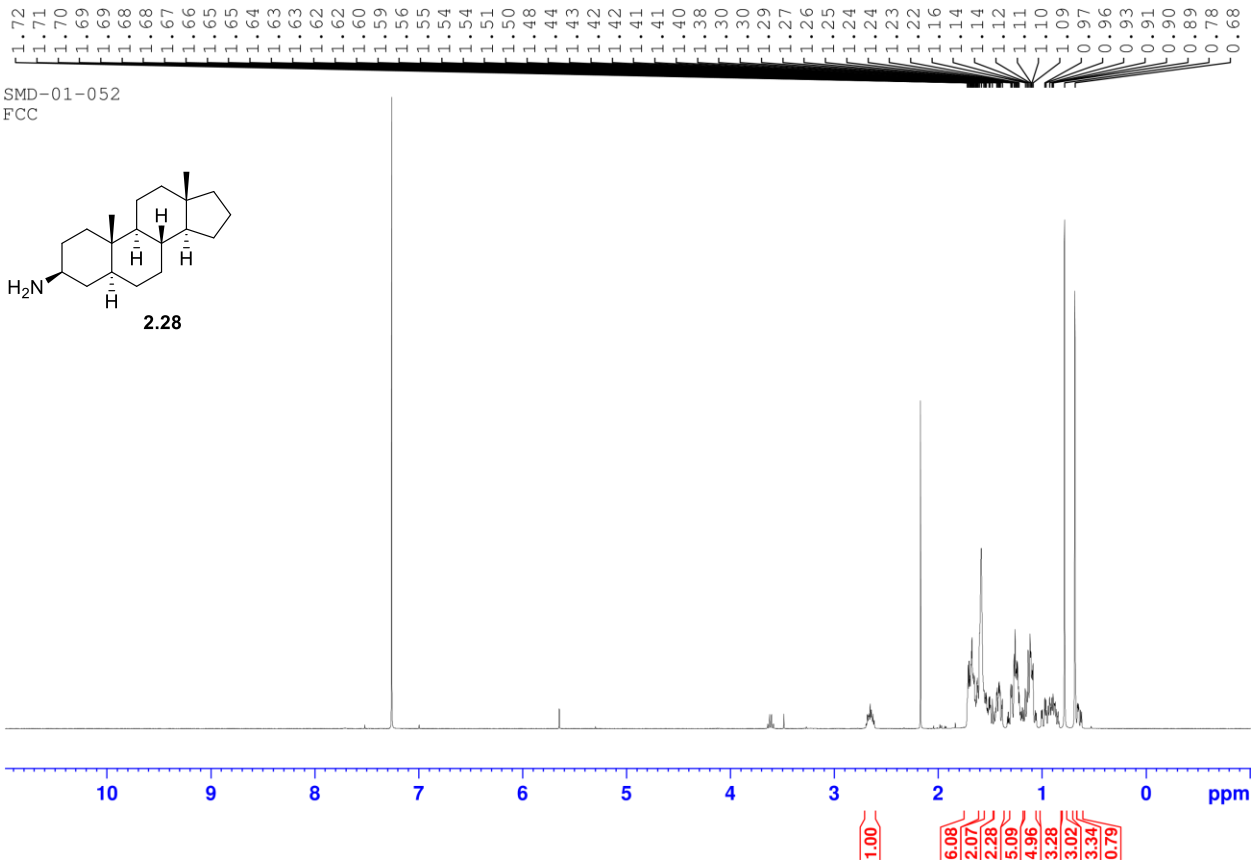
1.72 1.71 1.70 1.69 1.69 1.68 1.68 1.67 1.66 1.65 1.65 1.64 1.63 1.63 1.62 1.62 1.60 1.59 1.56 1.55 1.54 1.54 1.51 1.50 1.48 1.44 1.43 1.42 1.42 1.41 1.41 1.40 1.38 1.30 1.30 1.29 1.27 1.26 1.25 1.24 1.24 1.23 1.22 1.16 1.14 1.14 1.12 1.11 1.10 1.09 0.97 0.96 0.93 0.91 0.90 0.89 0.78 0.68
SMD-01-052
FCC
H
H
H
H2N
H
2.28
10 9 8 7 6 5 4 3 2 1 0 ppm
1.00
6.08
2.07
2.28
5.09
4.96
3.28
3.02
3.34
0.79

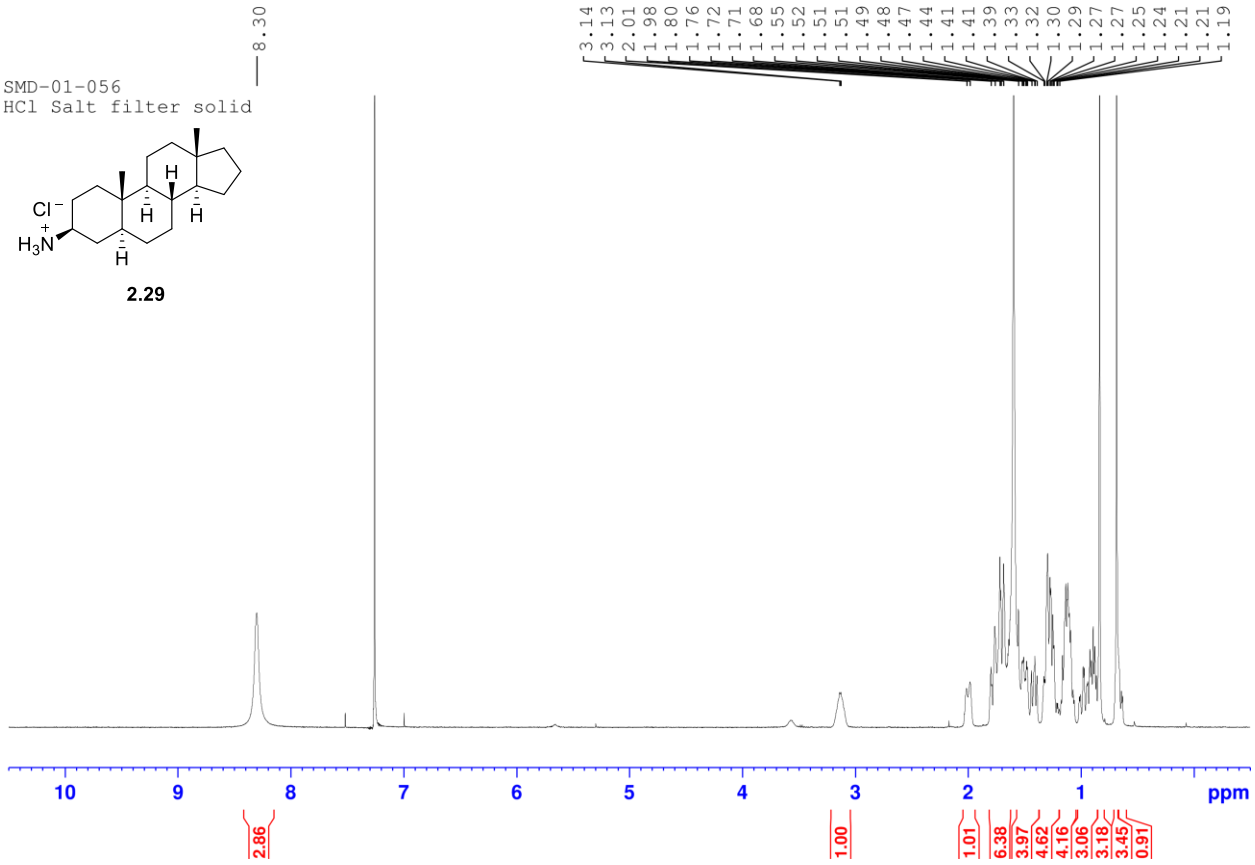
SMD-01-056
HCl Salt filter solid
2.29
8.30
3.14
3.13
2.01
1.98
1.80
1.76
1.72
1.71
1.68
1.55
1.52
1.51
1.51
1.49
1.48
1.47
1.44
1.41
1.41
1.39
1.33
1.32
1.30
1.29
1.27
1.27
1.25
1.24
1.21
1.21
1.19
10
9
8
7
6
5
4
3
2
1
ppm
2.86
1.00
1.01
6.38
3.97
4.62
4.16
3.06
3.18
3.45
0.91

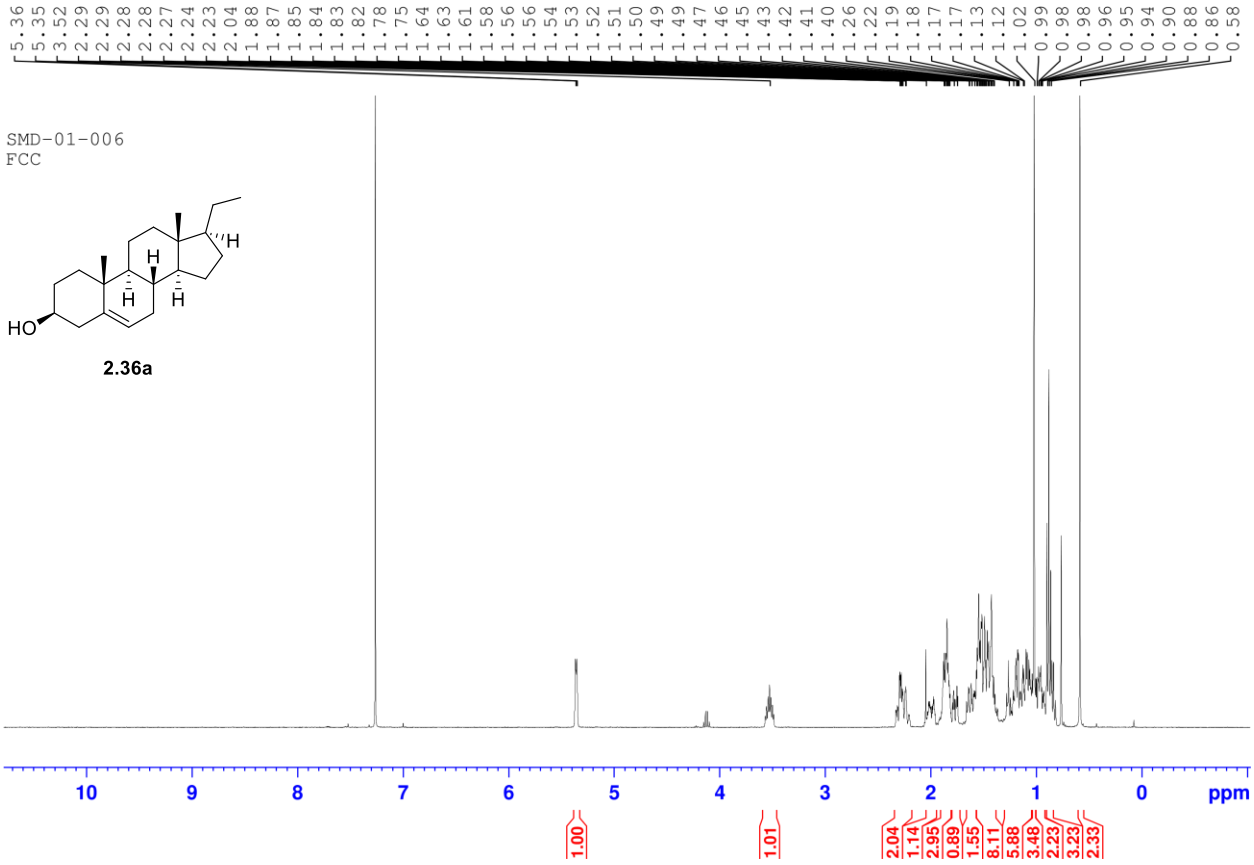
5.36
5.35
3.52
2.29
2.29
2.28
2.28
2.27
2.24
2.23
2.04
1.88
1.87
1.85
1.84
1.83
1.82
1.78
1.75
1.64
1.63
1.61
1.58
1.56
1.56
1.54
1.53
1.52
1.51
1.50
1.49
1.49
1.47
1.46
1.45
1.43
1.42
1.41
1.40
1.26
1.22
1.19
1.18
1.17
1.17
1.13
1.12
1.02
0.99
0.98
0.98
0.96
0.95
0.94
0.90
0.88
0.86
0.58
SMD-01-006
FCC
HO
H
H
H
H
2.36a
10
9
8
7
6
5
4
3
2
1
0
ppm
1.00
1.01
2.04
1.14
2.95
0.89
1.55
8.11
5.88
3.48
2.23
3.23
2.33

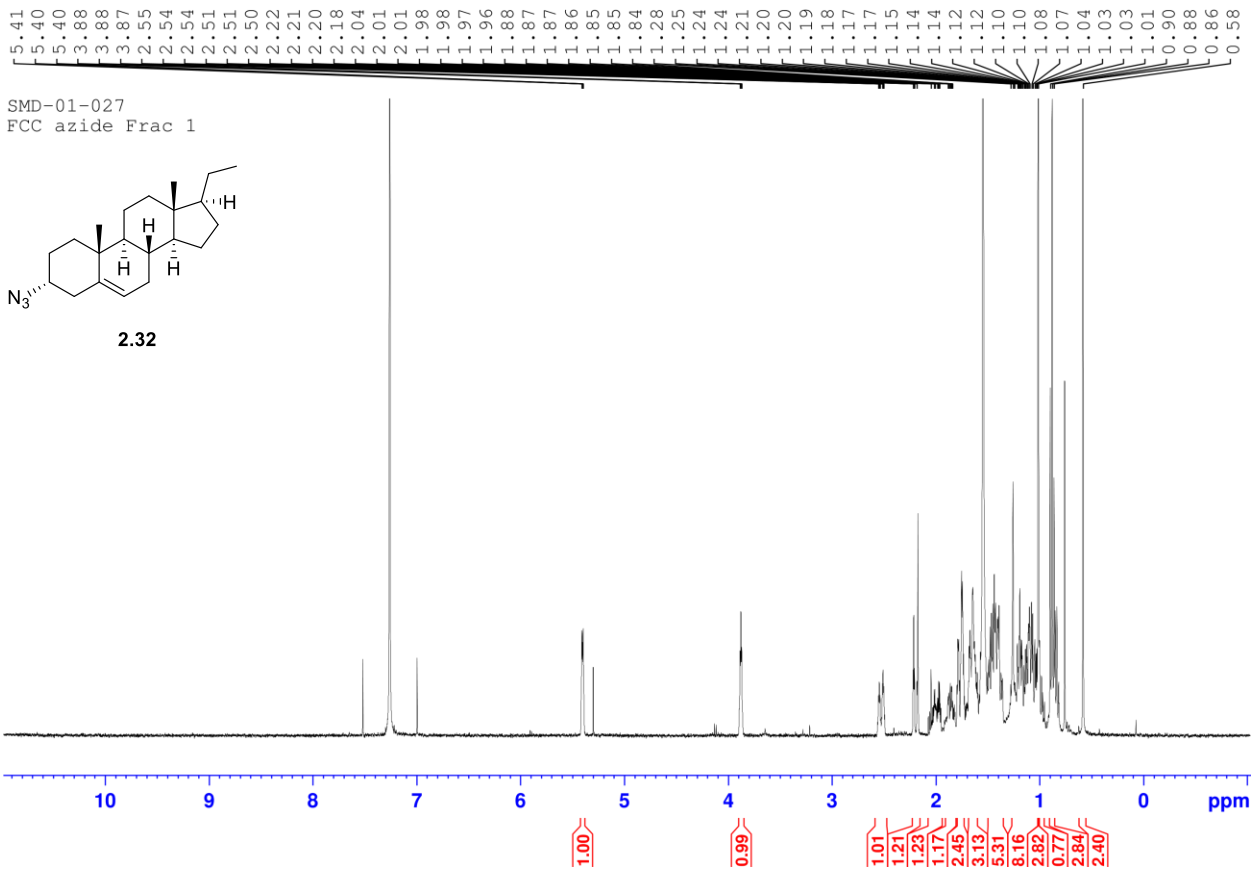
5.41 5.40 5.40 3.88 3.88 3.87 2.55 2.54 2.54 2.51 2.51 2.50 2.22 2.21 2.20 2.18 2.04 2.01 2.01 1.98 1.98 1.97 1.96 1.88 1.87 1.87 1.86 1.85 1.85 1.84 1.28 1.25 1.24 1.24 1.21 1.20 1.20 1.19 1.18 1.17 1.17 1.15 1.14 1.14 1.12 1.12 1.10 1.10 1.08 1.07 1.04 1.03 1.03 1.01 0.90 0.88 0.86 0.58
SMD-01-027
FCC azide Frac 1
H
H
H
H
N3
2.32
10 9 8 7 6 5 4 3 2 1 0 ppm
1.00 0.99 1.01 1.21 1.23 1.17 2.45 3.13 5.31 8.16 2.82 0.77 2.84 2.40

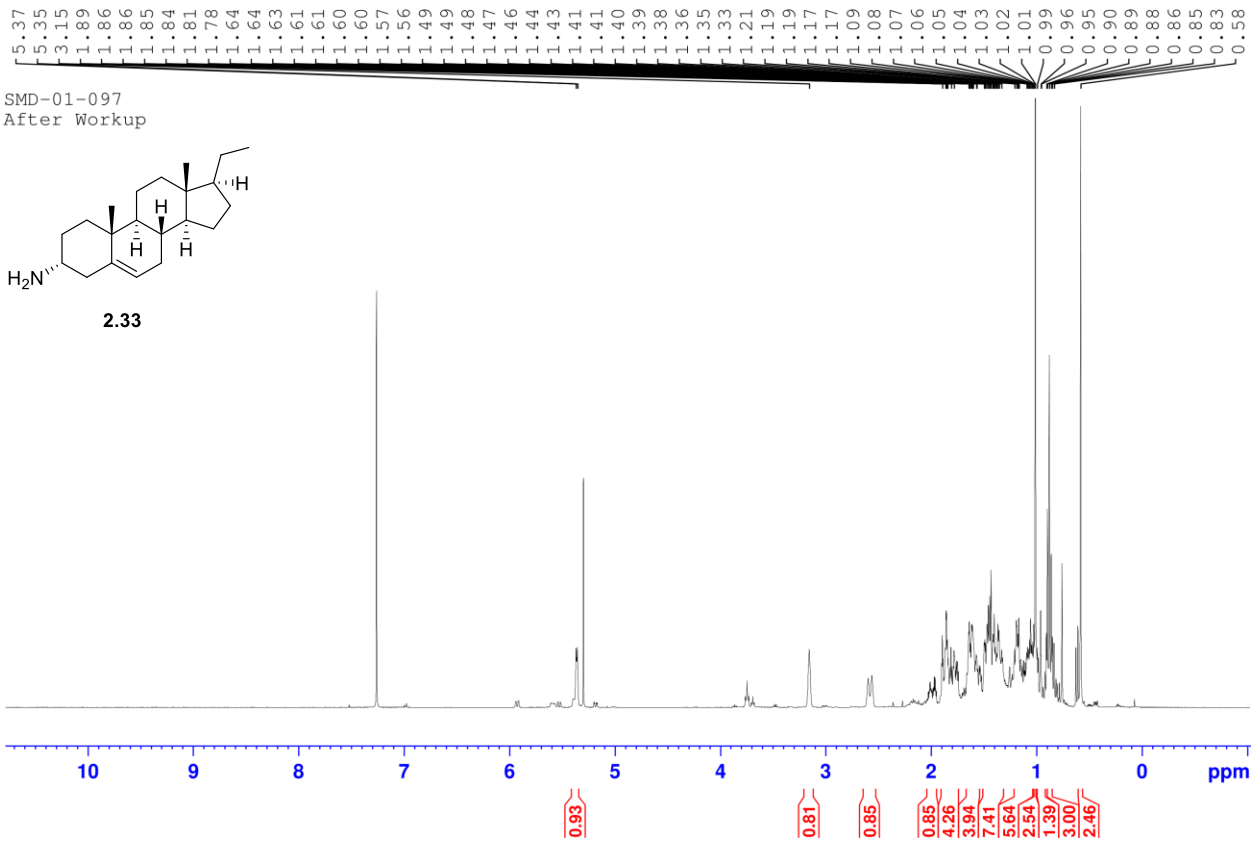
5.37
5.35
3.15
1.89
1.86
1.86
1.85
1.84
1.81
1.78
1.64
1.64
1.63
1.61
1.61
1.60
1.60
1.57
1.56
1.49
1.49
1.48
1.47
1.46
1.44
1.43
1.41
1.41
1.40
1.39
1.38
1.36
1.35
1.33
1.21
1.19
1.19
1.17
1.17
1.09
1.08
1.07
1.06
1.05
1.04
1.03
1.02
1.01
0.99
0.96
0.95
0.90
0.89
0.88
0.86
0.85
0.83
0.58
SMD-01-097
After Workup
H
H
H
H
H2N
2.33
10
9
8
7
6
5
4
3
2
1
0
ppm
0.93
0.81
0.85
0.85
4.26
3.94
7.41
5.64
2.54
1.39
3.00
2.46

SMD-01-100
1H Char

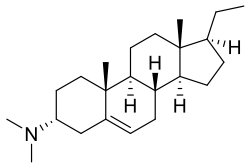

2.34b

SMD-01-100
13C Char

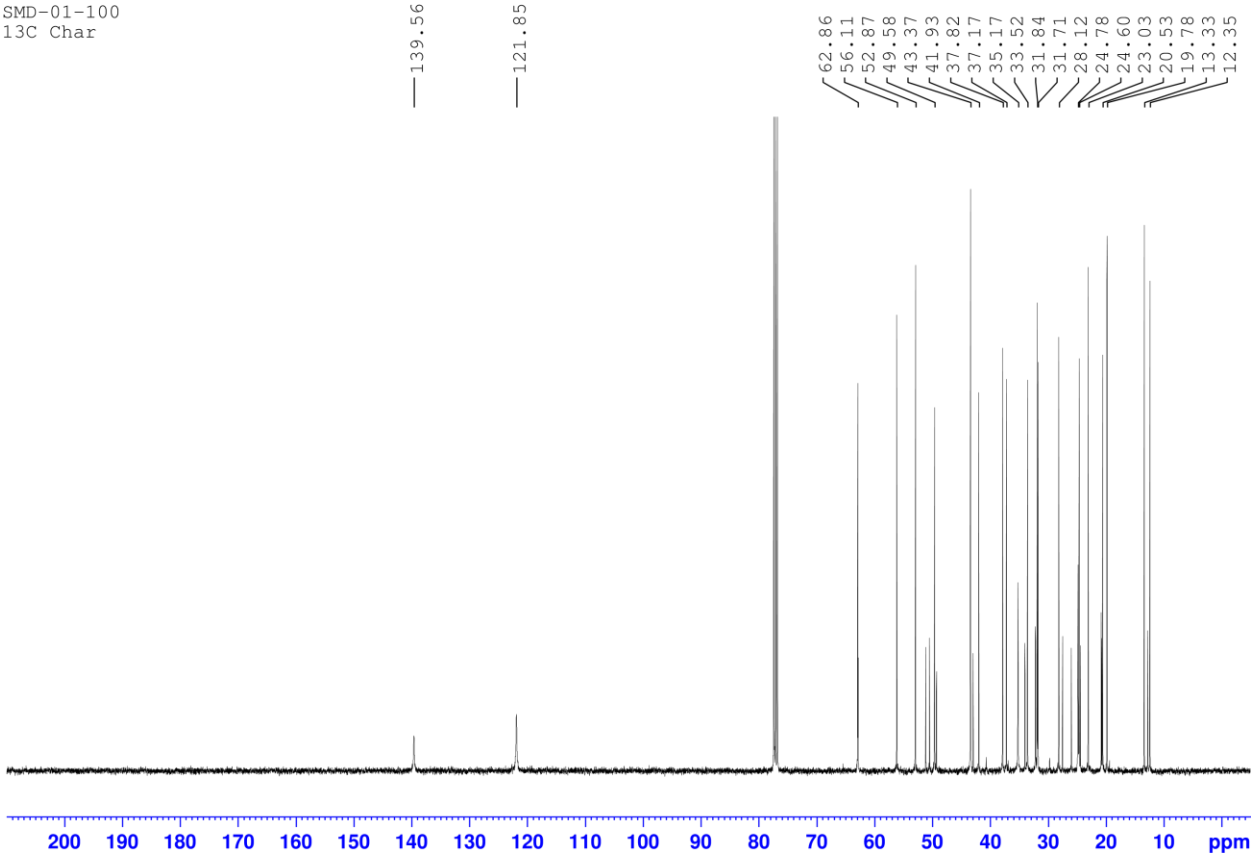

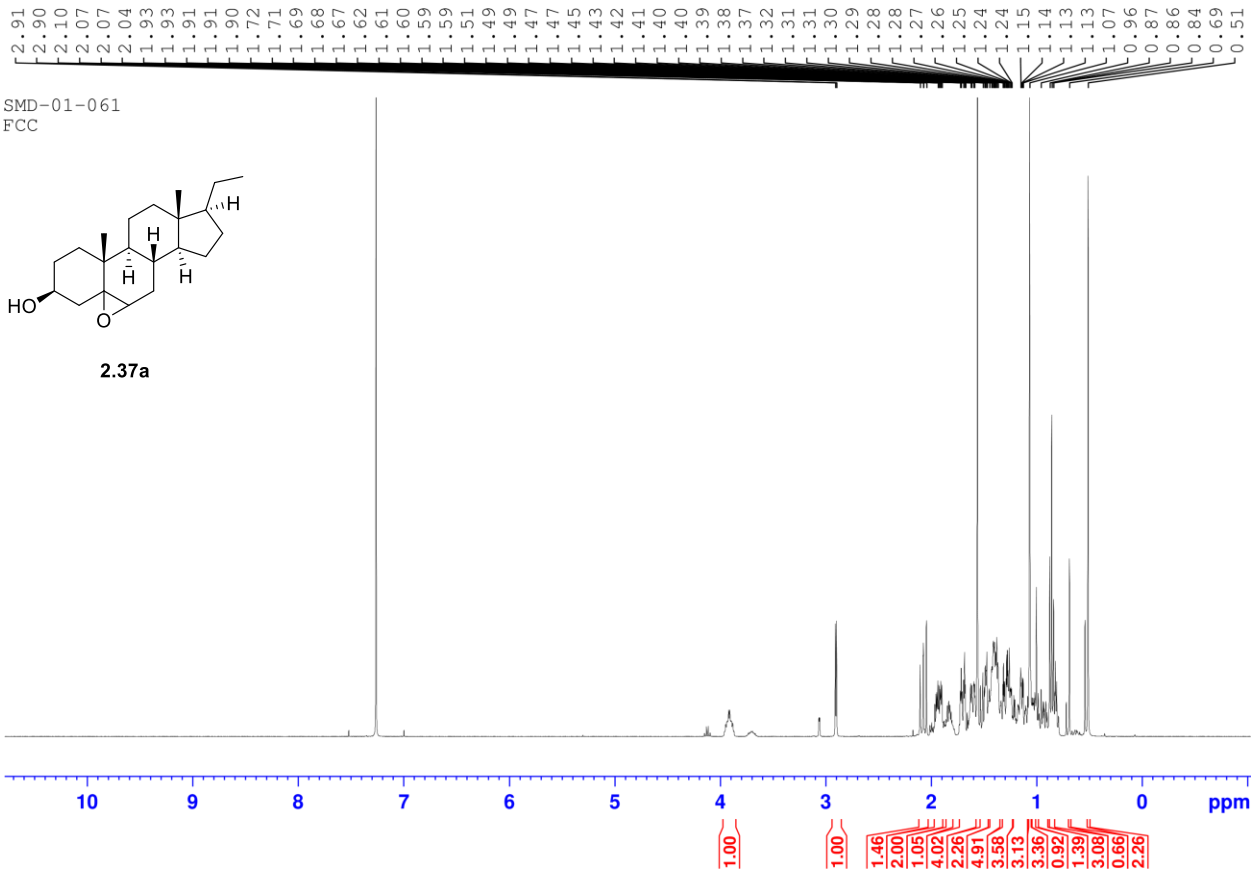
2.91 2.90 2.10 2.07 2.07 2.04 1.93 1.93 1.91 1.91 1.90 1.72 1.71 1.69 1.68 1.67 1.62 1.61 1.60 1.59 1.59 1.51 1.49 1.49 1.47 1.47 1.45 1.43 1.42 1.41 1.40 1.40 1.39 1.38 1.37 1.32 1.31 1.31 1.30 1.29 1.28 1.28 1.27 1.26 1.25 1.24 1.24 1.15 1.14 1.13 1.13 1.07 0.96 0.87 0.86 0.84 0.69 0.51
SMD-01-061
FCC
HO
H
H
H
H
O
10 9 8 7 6 5 4 3 2 1 0 ppm
1.00 1.00 1.46 2.00 1.05 4.02 2.26 4.91 3.58 3.13 3.36 0.92 1.39 3.08 0.66 2.26

2.37a

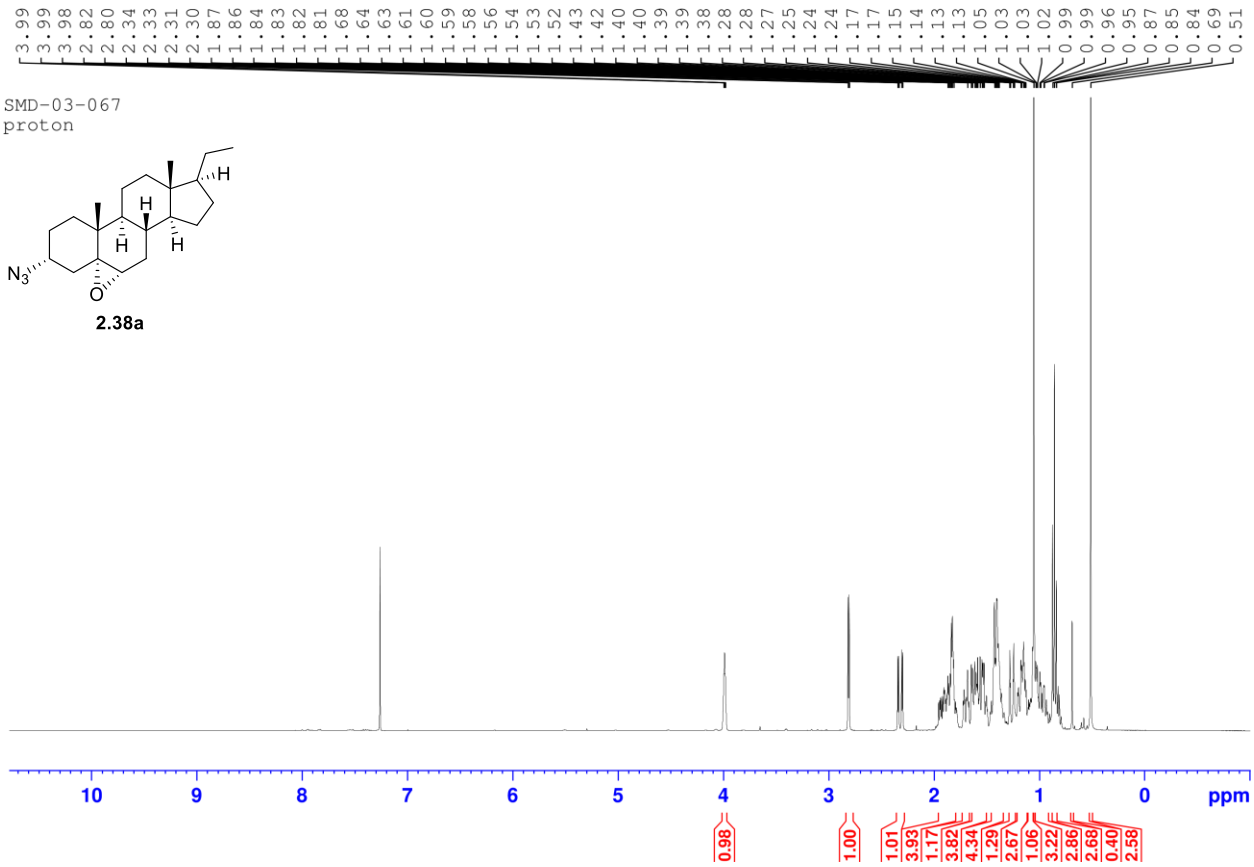
SMD-03-067
proton
2.38a
10 9 8 7 6 5 4 3 2 1 0 ppm

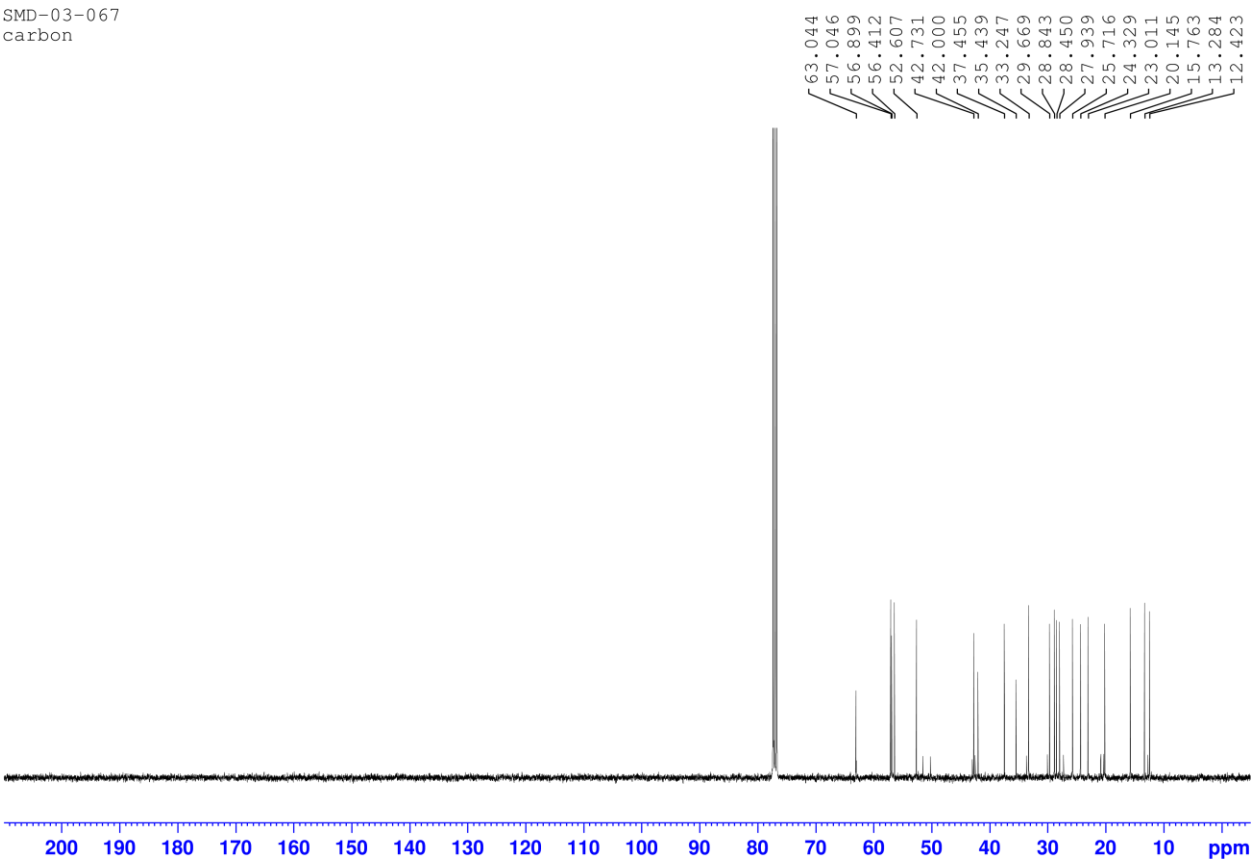
SMD-03-067
carbon
200 190 180 170 160 150 140 130 120 110 100 90 80 70 60 50 40 30 20 10 ppm

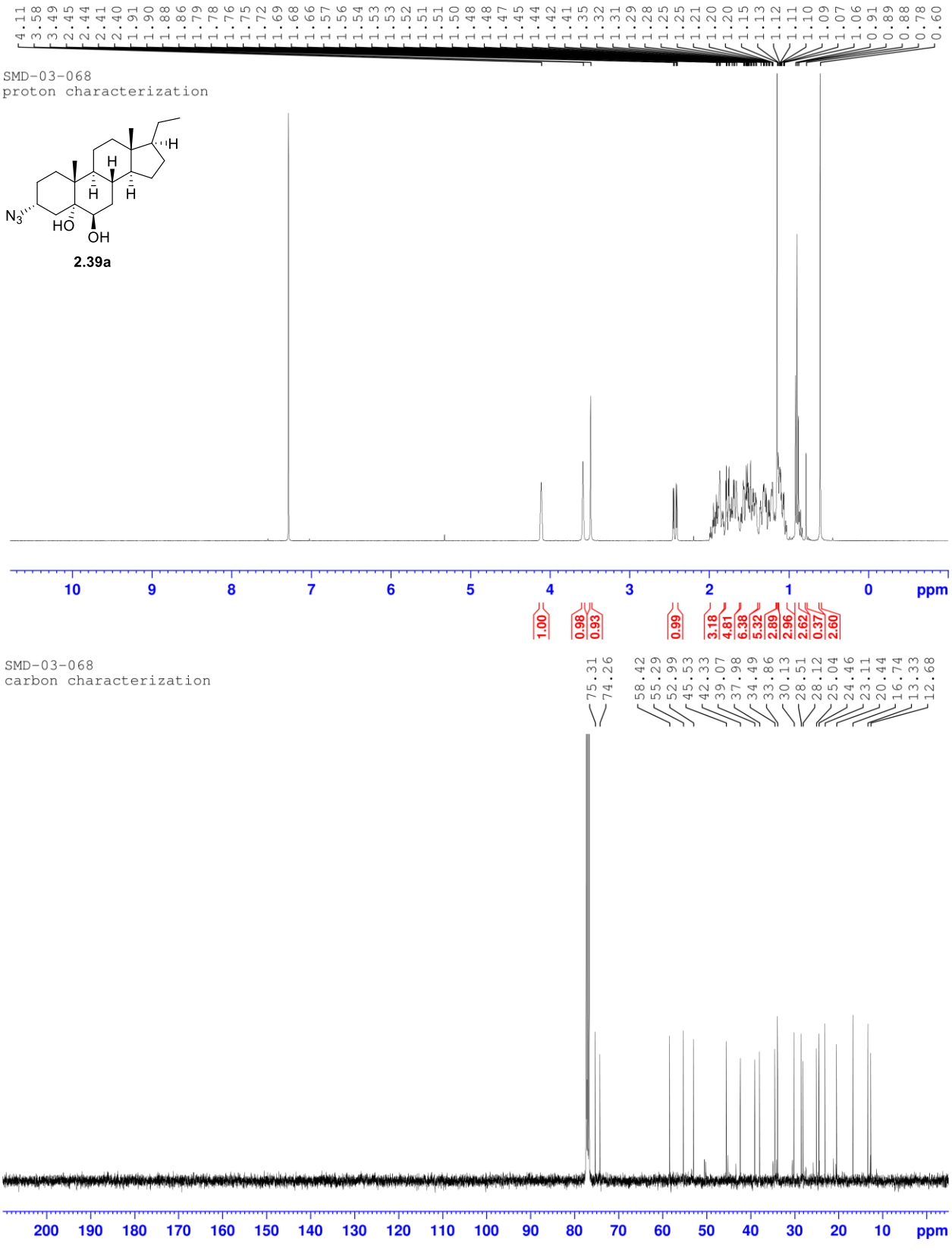
SMD-03-068
proton characterization
2.39a
SMD-03-068
carbon characterization
ppm

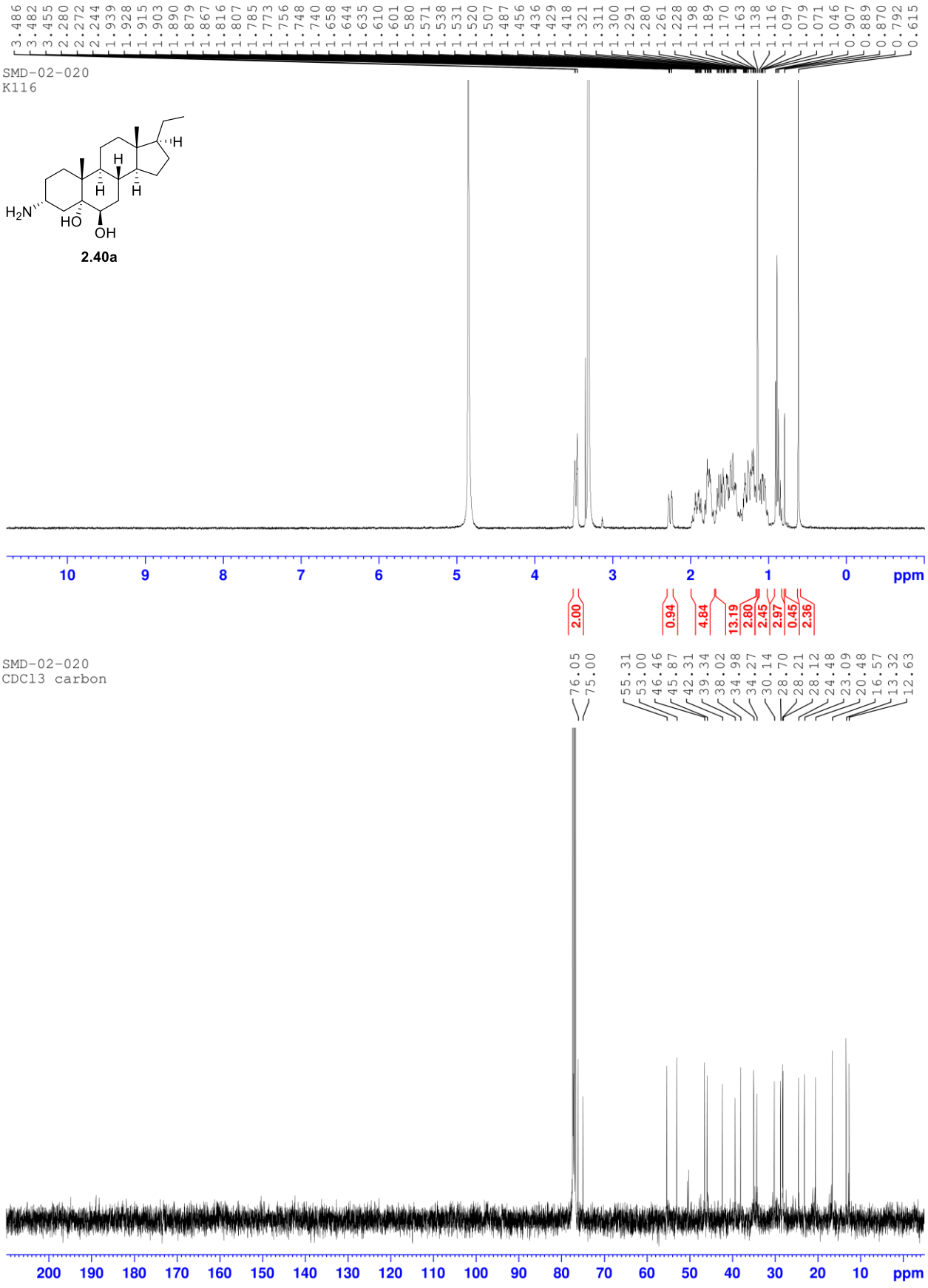
SMD-02-020
K116
2.40a
SMD-02-020
CDCl3 carbon

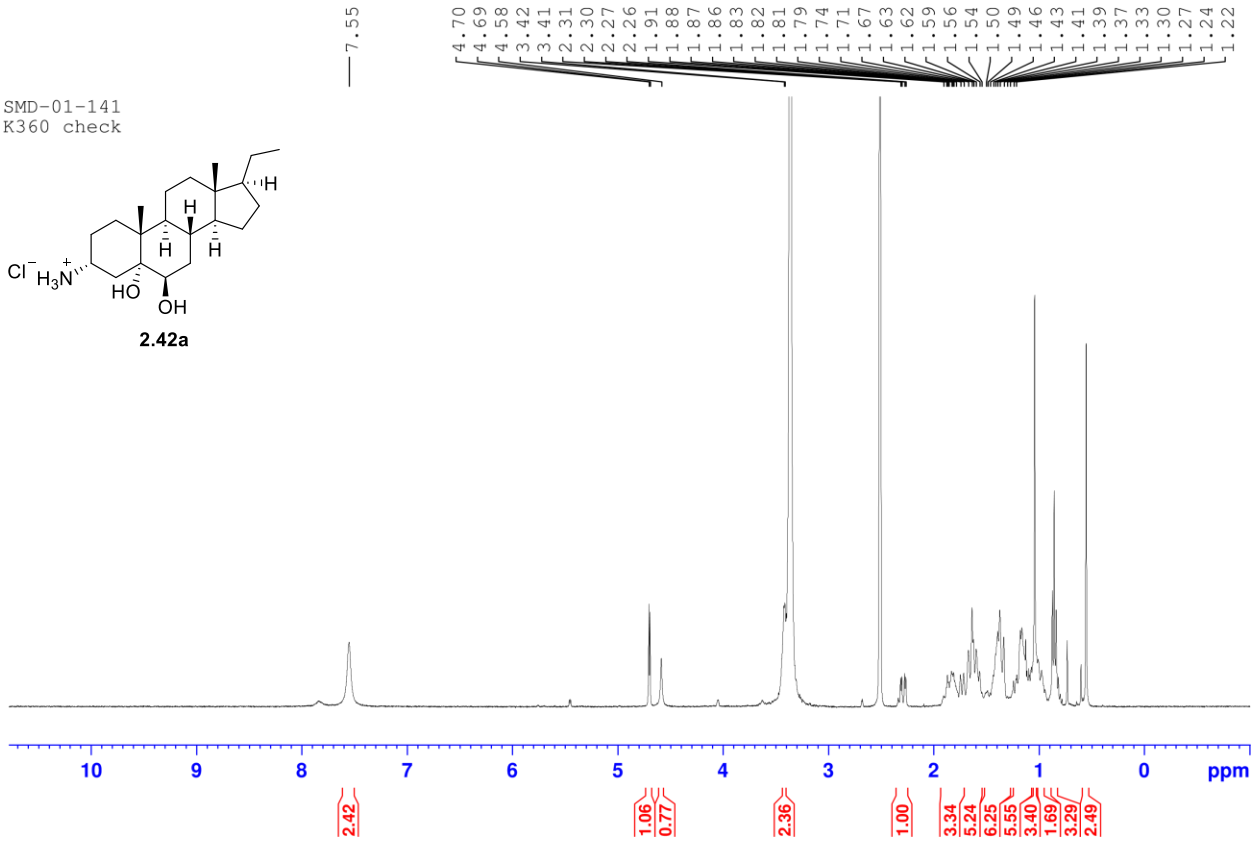
SMD-01-141
K360 check
7.55
4.70
4.69
4.58
3.42
3.41
2.31
2.30
2.27
2.26
1.91
1.88
1.87
1.86
1.83
1.82
1.81
1.79
1.74
1.71
1.67
1.63
1.62
1.59
1.56
1.54
1.50
1.49
1.46
1.43
1.41
1.39
1.37
1.33
1.30
1.27
1.24
1.22
Cl⁻ H3N+
HO
OH
H
H
H
H
2.42a
10 9 8 7 6 5 4 3 2 1 0 ppm
2.42
1.06
0.77
2.36
1.00
3.34
5.24
6.25
5.55
3.40
1.69
3.29
2.49

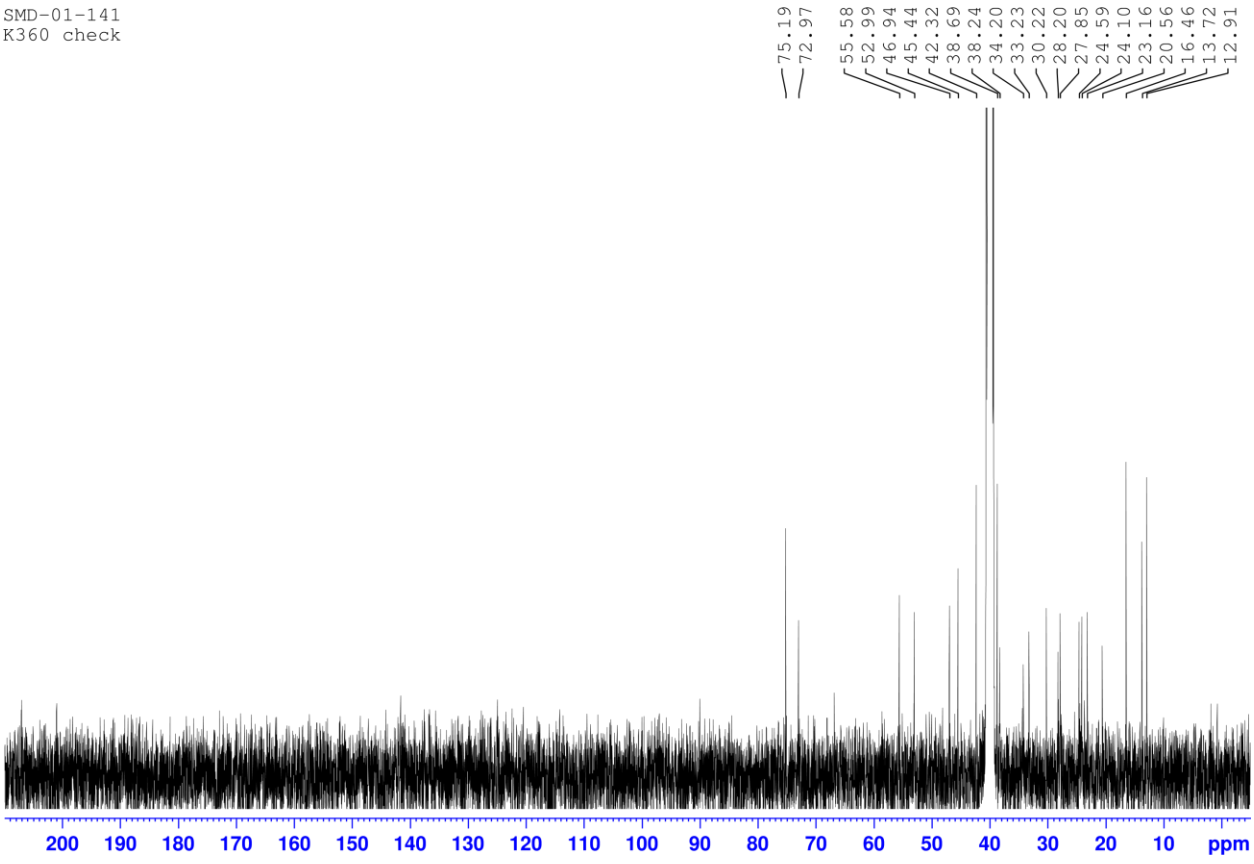
SMD-01-141
K360 check
75.19
72.97
55.58
52.99
46.94
45.44
42.32
38.69
38.24
34.20
33.23
30.22
28.20
27.85
24.59
24.10
23.16
20.56
16.46
13.72
12.91
200 190 180 170 160 150 140 130 120 110 100 90 80 70 60 50 40 30 20 10 ppm

SMD-05-133
proton

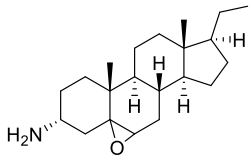

2.44ab

SMD-05-133
carbon

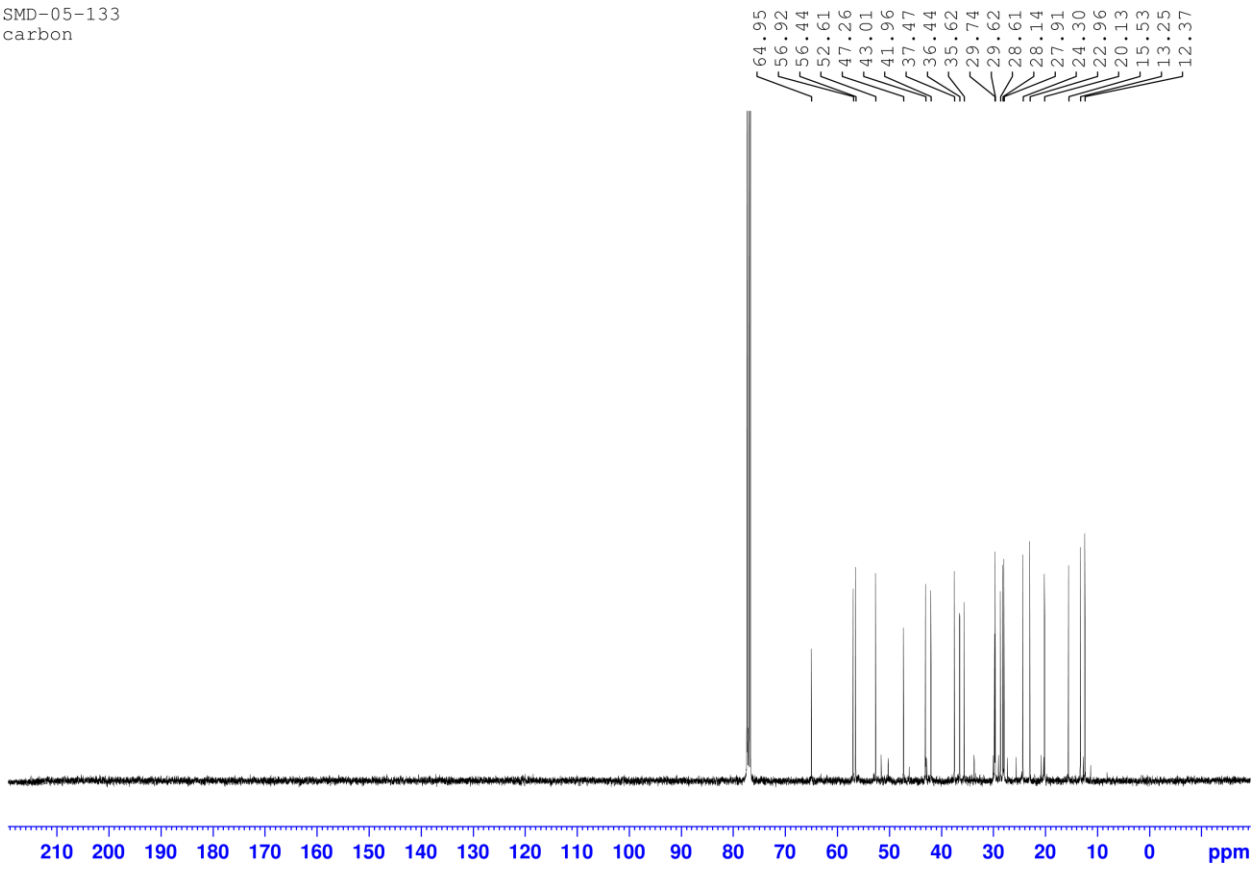

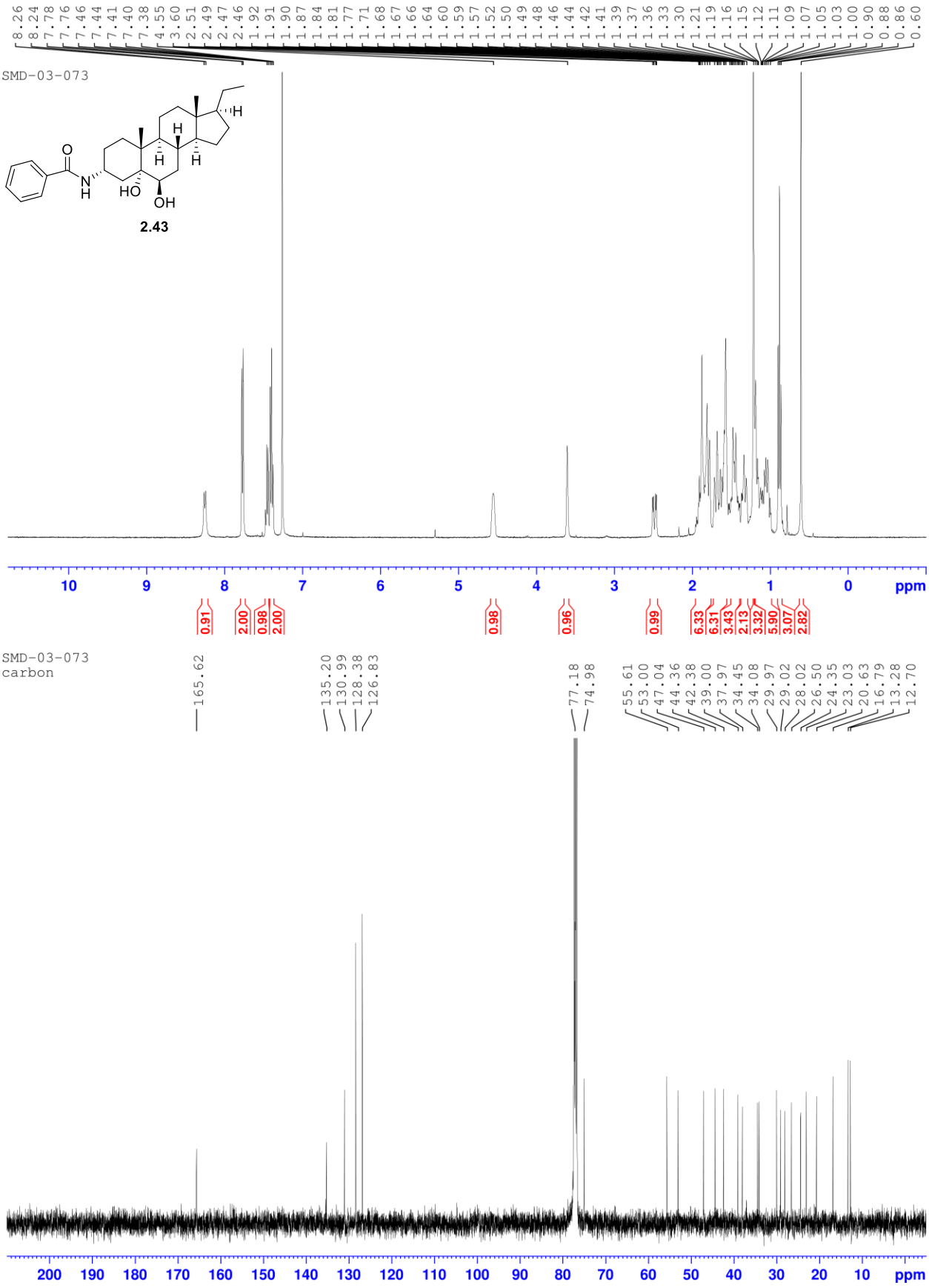
SMD-03-073
2.43
SMD-03-073
carbon
ppm

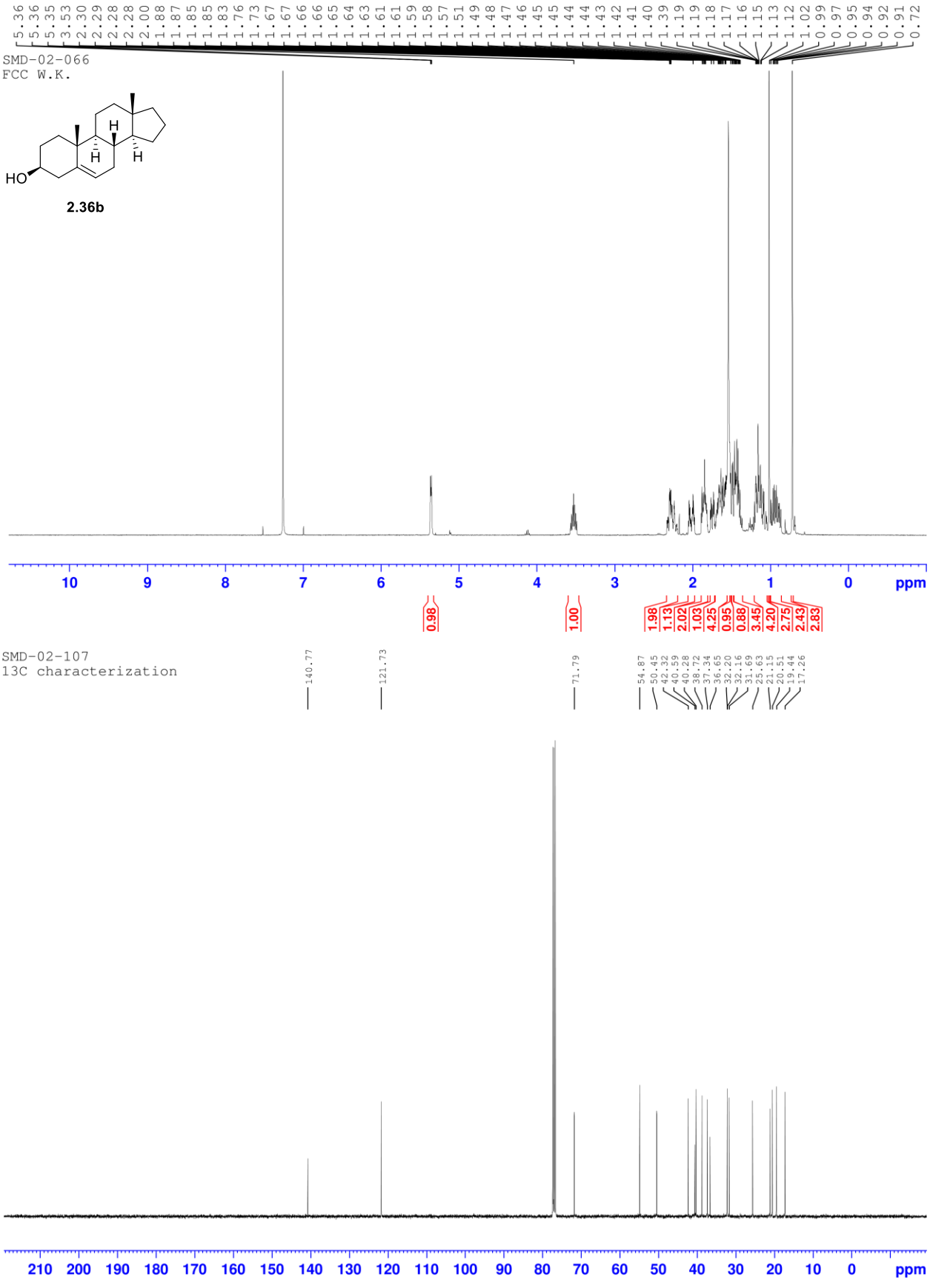
5.36 5.36 5.35 3.53 2.30 2.29 2.28 2.28 2.00 1.88 1.87 1.85 1.85 1.83 1.76 1.73 1.67 1.67 1.66 1.66 1.65 1.64 1.63 1.61 1.61 1.59 1.58 1.57 1.51 1.49 1.48 1.47 1.46 1.45 1.45 1.44 1.44 1.43 1.42 1.41 1.40 1.39 1.19 1.19 1.18 1.17 1.16 1.15 1.13 1.12 1.02 0.99 0.97 0.95 0.94 0.92 0.91 0.72
SMD-02-066
FCC W.K.
HO
H
H
H
2.36b
10 9 8 7 6 5 4 3 2 1 0 ppm
0.98 1.00 1.98 1.13 2.02 1.03 4.25 0.95 0.88 3.45 4.20 2.75 2.43 2.83
SMD-02-107
13C characterization
140.77 121.73 71.79 54.87 50.45 42.32 40.59 40.28 38.72 37.34 36.65 32.20 32.16 31.69 25.63 21.15 20.51 19.44 17.26
210 200 190 180 170 160 150 140 130 120 110 100 90 80 70 60 50 40 30 20 10 0 ppm

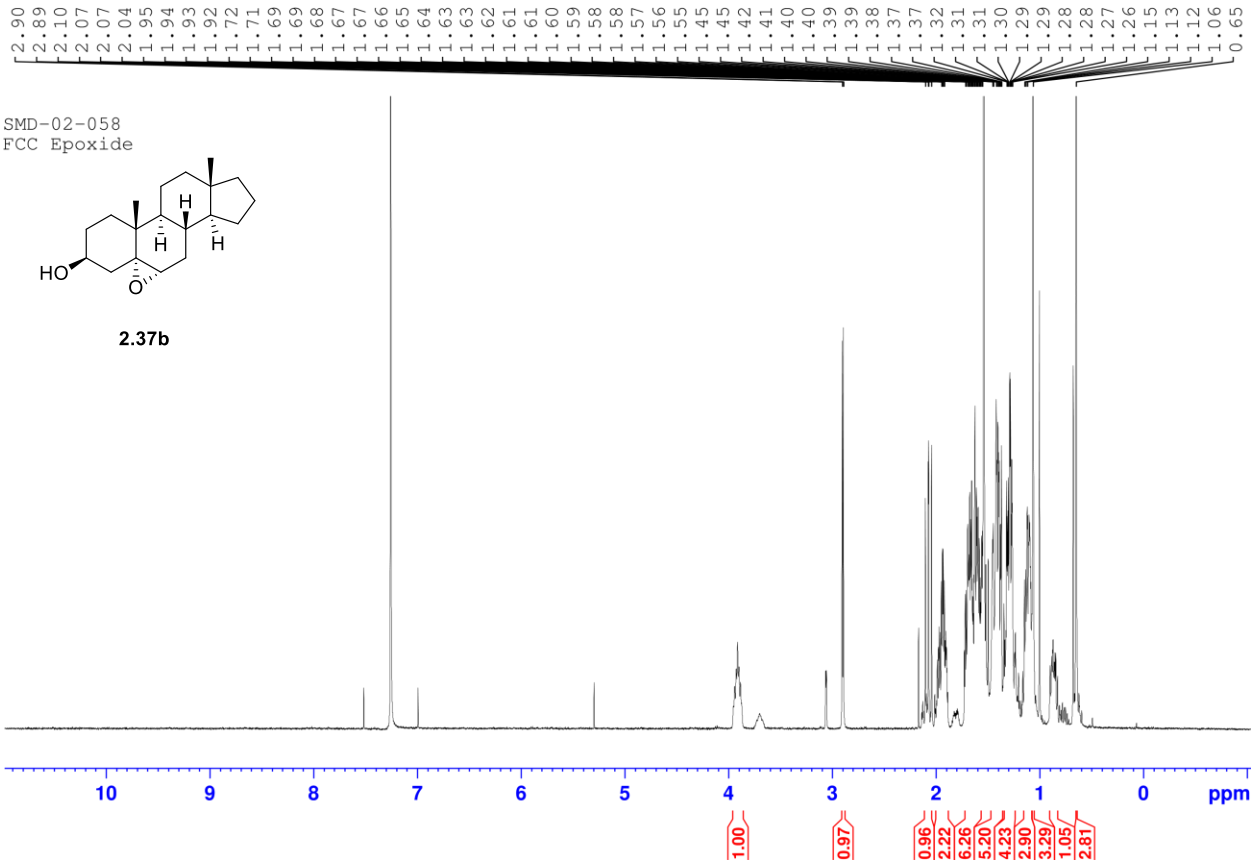
2.90 2.89 2.10 2.07 2.07 2.04 1.95 1.94 1.93 1.92 1.72 1.71 1.69 1.69 1.68 1.67 1.67 1.66 1.65 1.64 1.63 1.63 1.62 1.61 1.61 1.60 1.59 1.58 1.58 1.57 1.56 1.55 1.45 1.45 1.42 1.41 1.40 1.40 1.39 1.39 1.38 1.37 1.37 1.32 1.31 1.31 1.30 1.29 1.29 1.28 1.28 1.27 1.26 1.15 1.13 1.12 1.06 0.65
SMD-02-058
FCC Epoxide
HO
H
H
H
O
2.37b
10 9 8 7 6 5 4 3 2 1 0 ppm
1.00 0.97 0.96 2.22 6.26 5.20 4.23 2.90 3.29 1.05 2.81

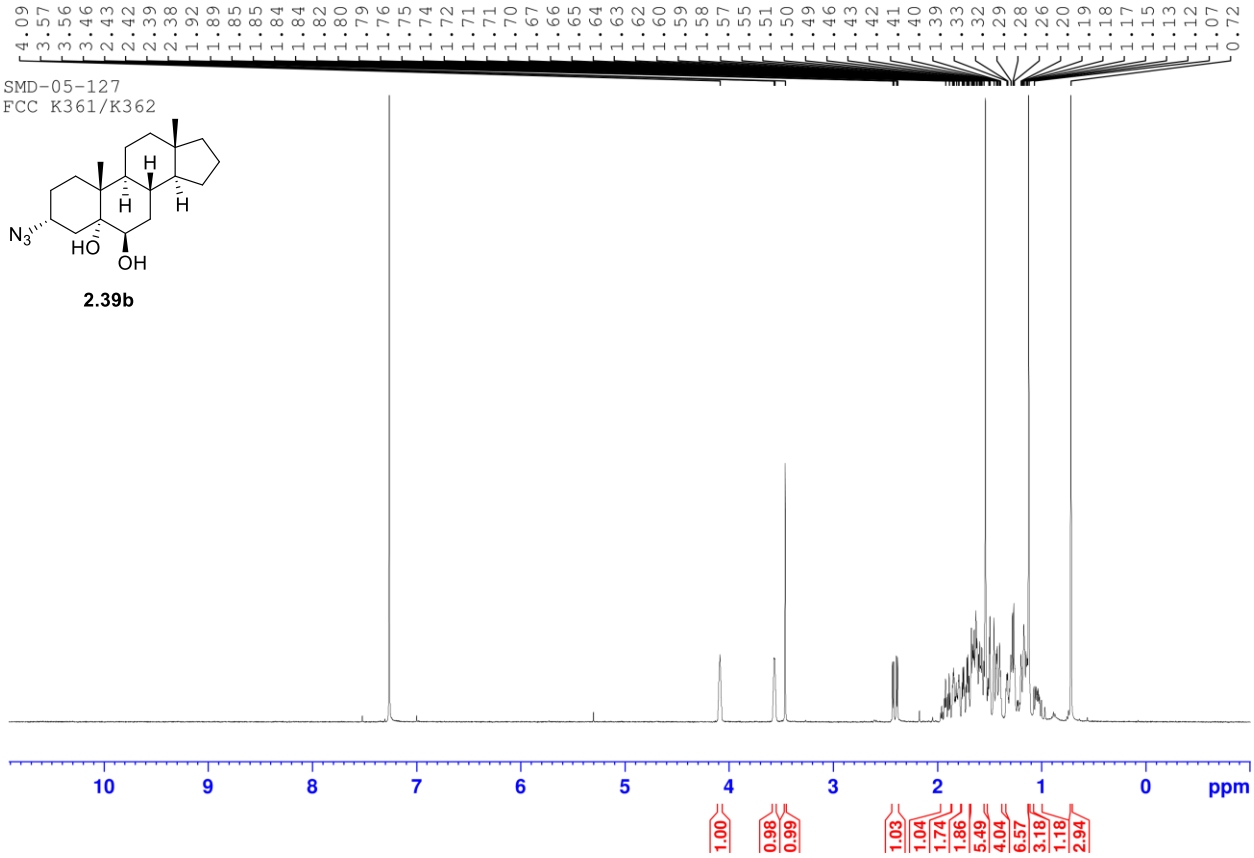
SMD-05-127
FCC K361/K362
2.39b
ppm

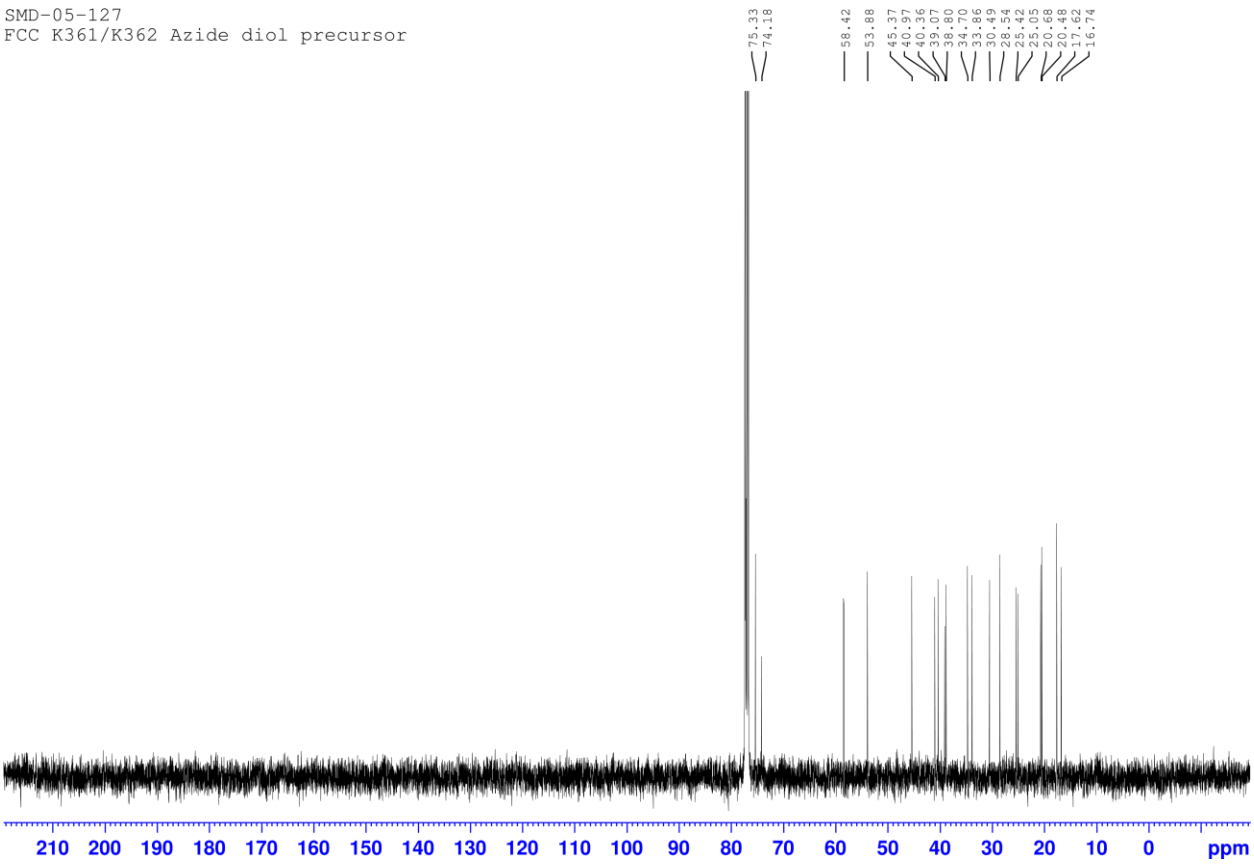
SMD-05-127
FCC K361/K362 Azide diol precursor
ppm

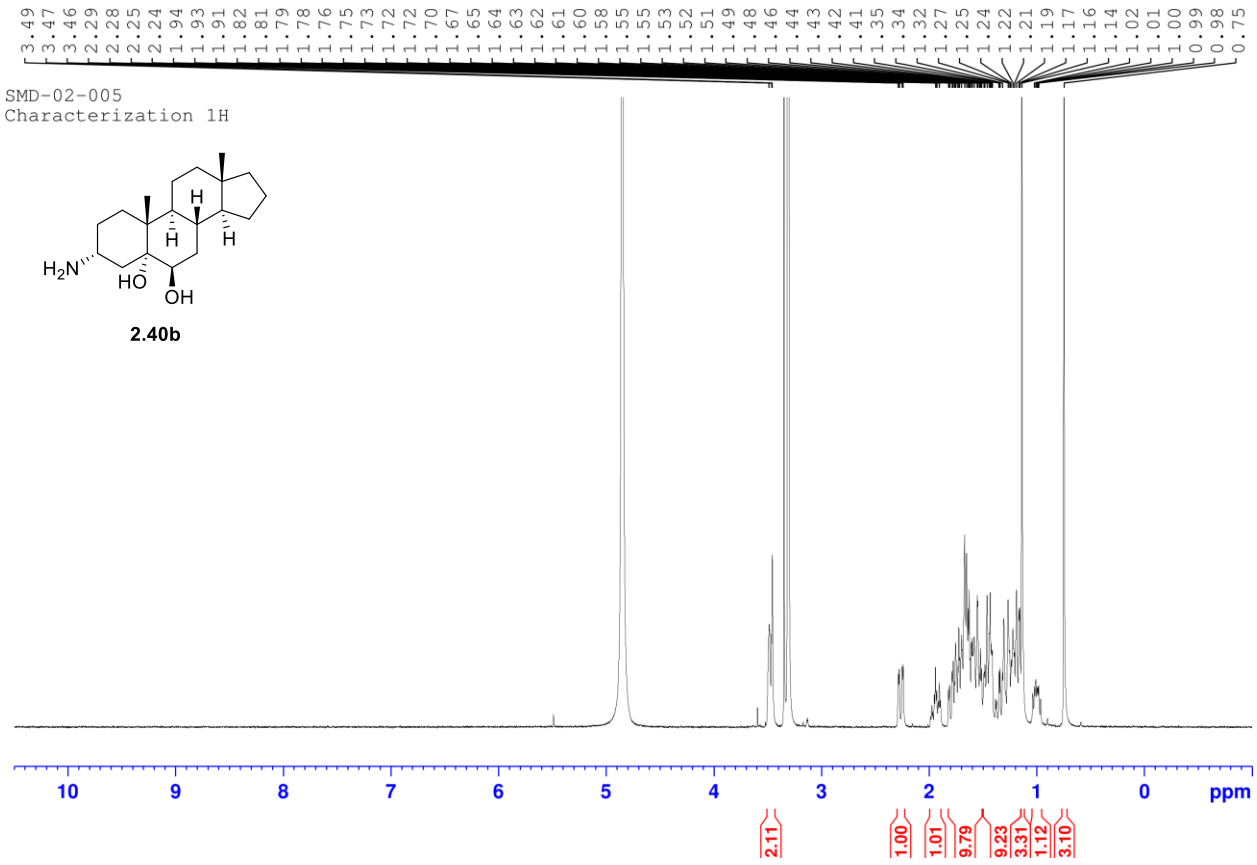
SMD-02-005
Characterization 1H
H
H
H
H2N
HO
OH
2.40b
ppm

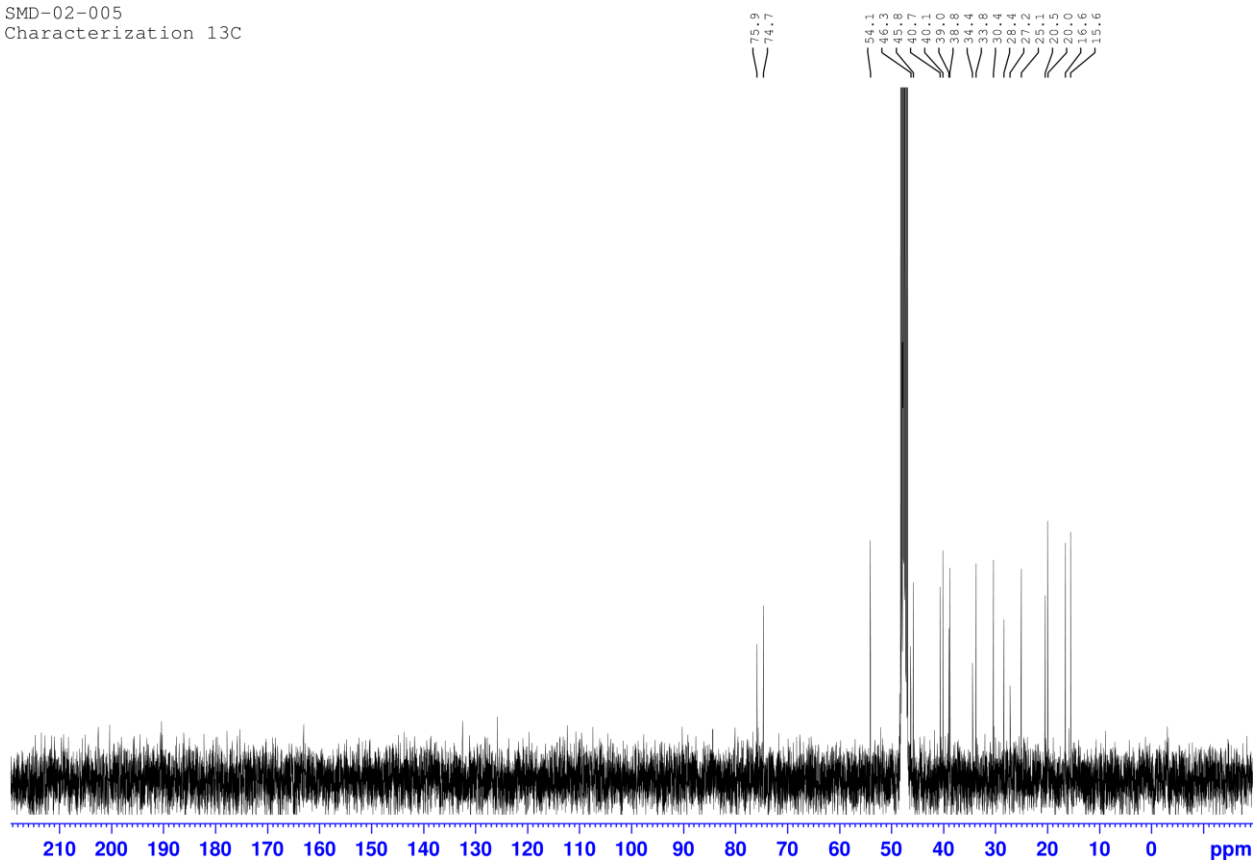
SMD-02-005
Characterization 13C
ppm

SMD-02-008
proton

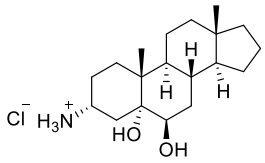

2.42b

SMD-02-008
carbon

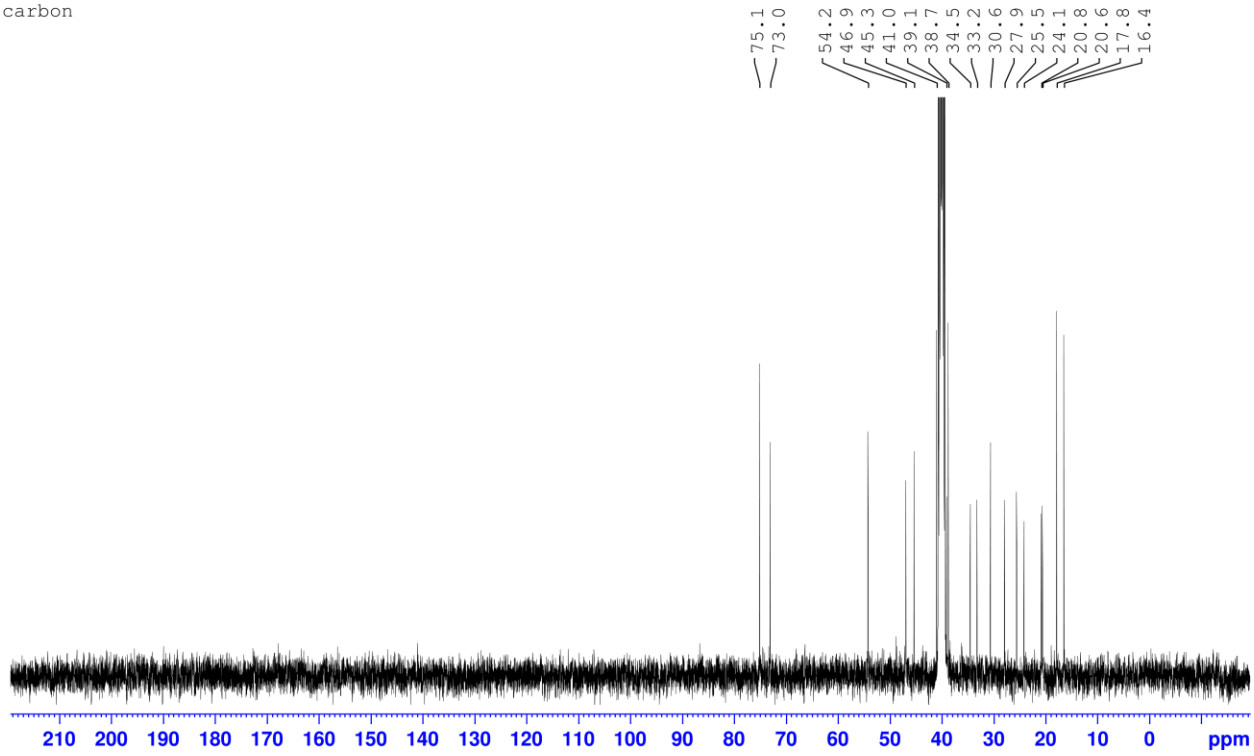

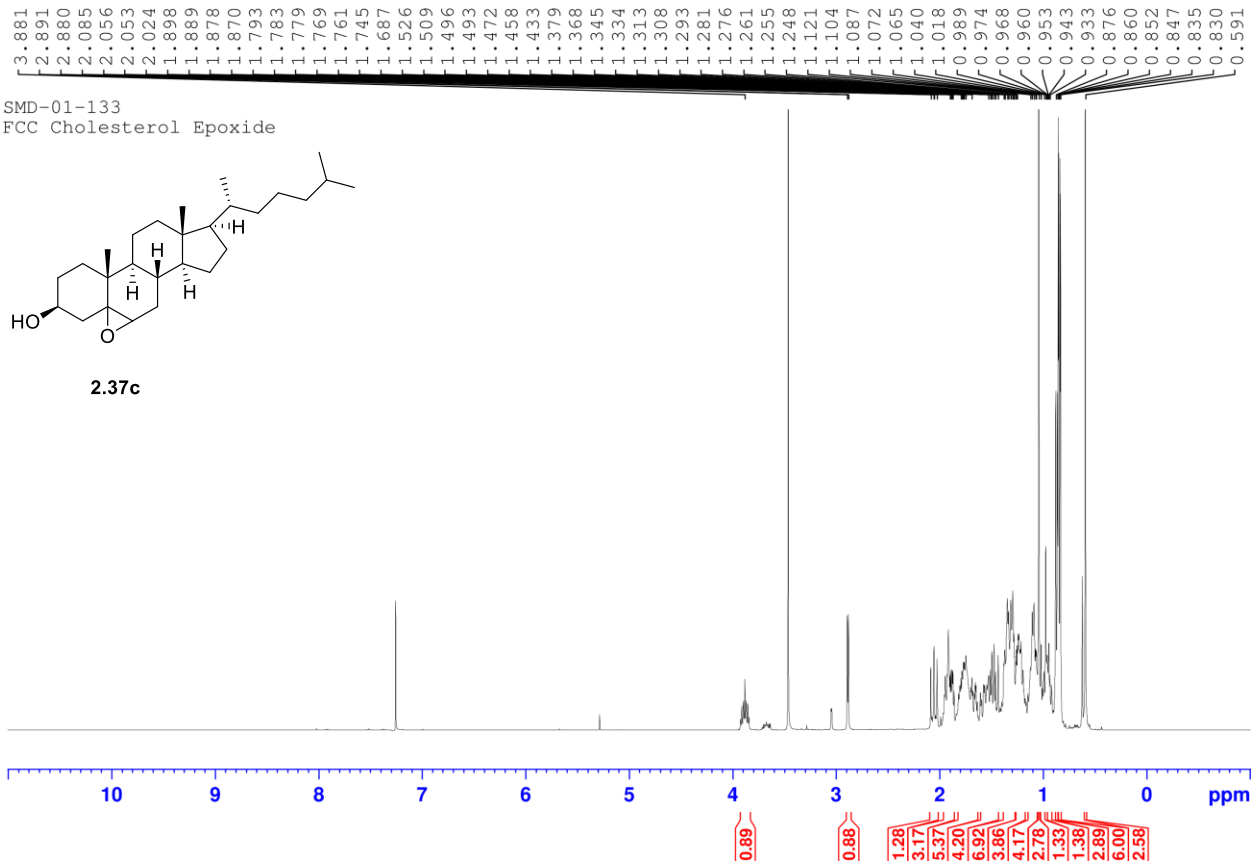
3.881
2.891
2.880
2.085
2.056
2.053
2.024
1.898
1.889
1.878
1.870
1.793
1.783
1.779
1.769
1.761
1.745
1.687
1.526
1.509
1.496
1.493
1.472
1.458
1.433
1.379
1.368
1.345
1.334
1.313
1.308
1.293
1.281
1.276
1.261
1.255
1.248
1.121
1.104
1.087
1.072
1.065
1.040
1.018
0.989
0.974
0.968
0.960
0.953
0.943
0.933
0.876
0.860
0.852
0.847
0.835
0.830
0.591
SMD-01-133
FCC Cholesterol Epoxide
HO
O
H
H
H
H
10
9
8
7
6
5
4
3
2
1
0
ppm
0.89
0.88
1.28
3.17
5.37
4.20
6.92
3.86
4.17
2.78
1.33
1.38
2.89
6.00
2.58

2.37c

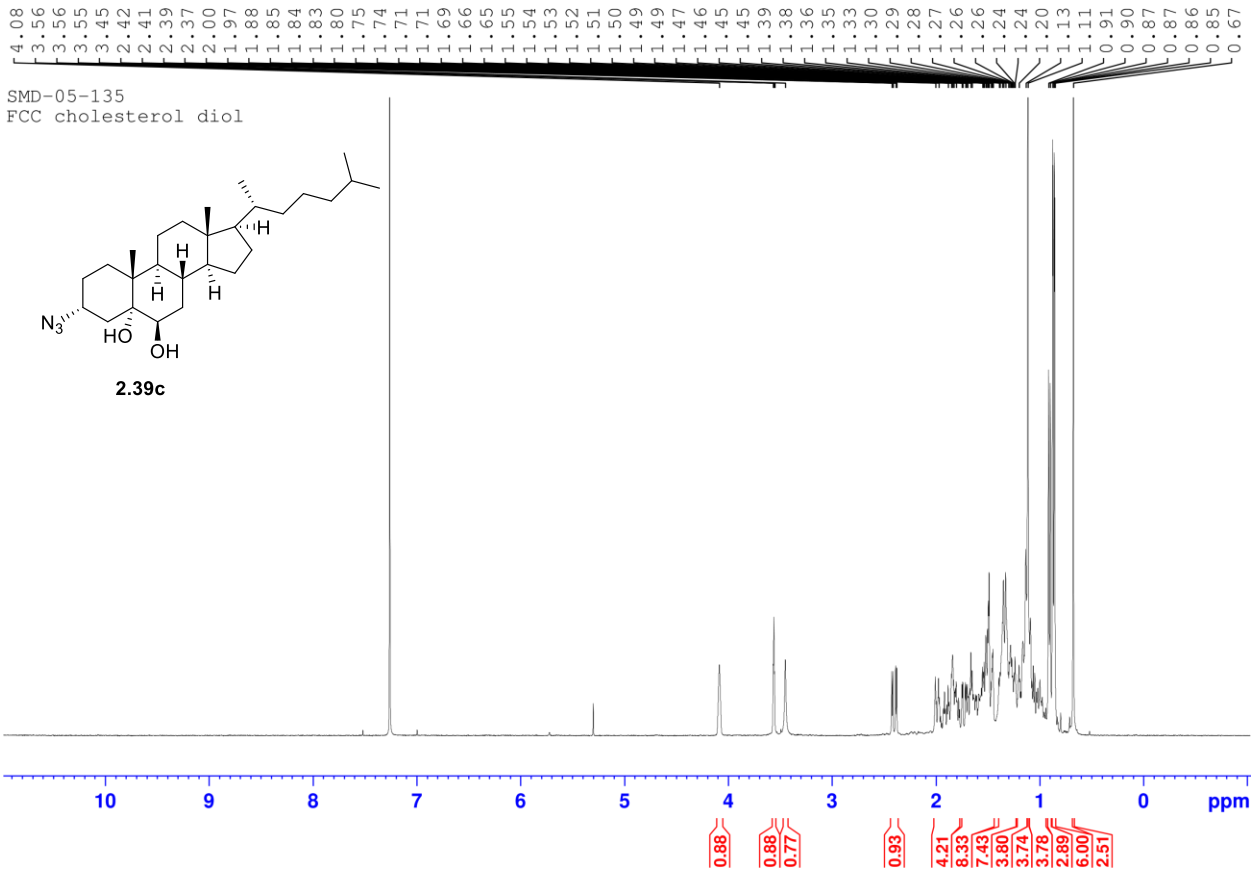
SMD-05-135
FCC cholesterol diol
2.39c
ppm

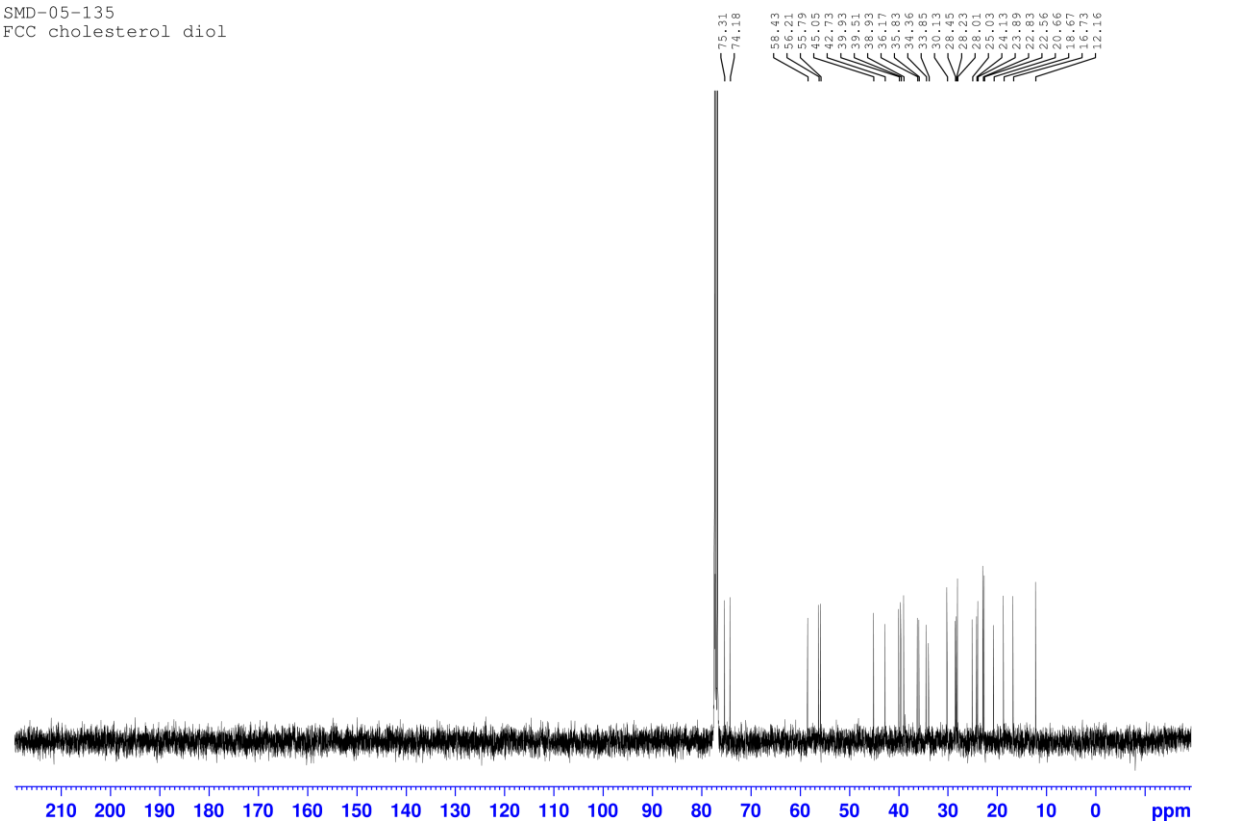
SMD-05-135
FCC cholesterol diol
ppm

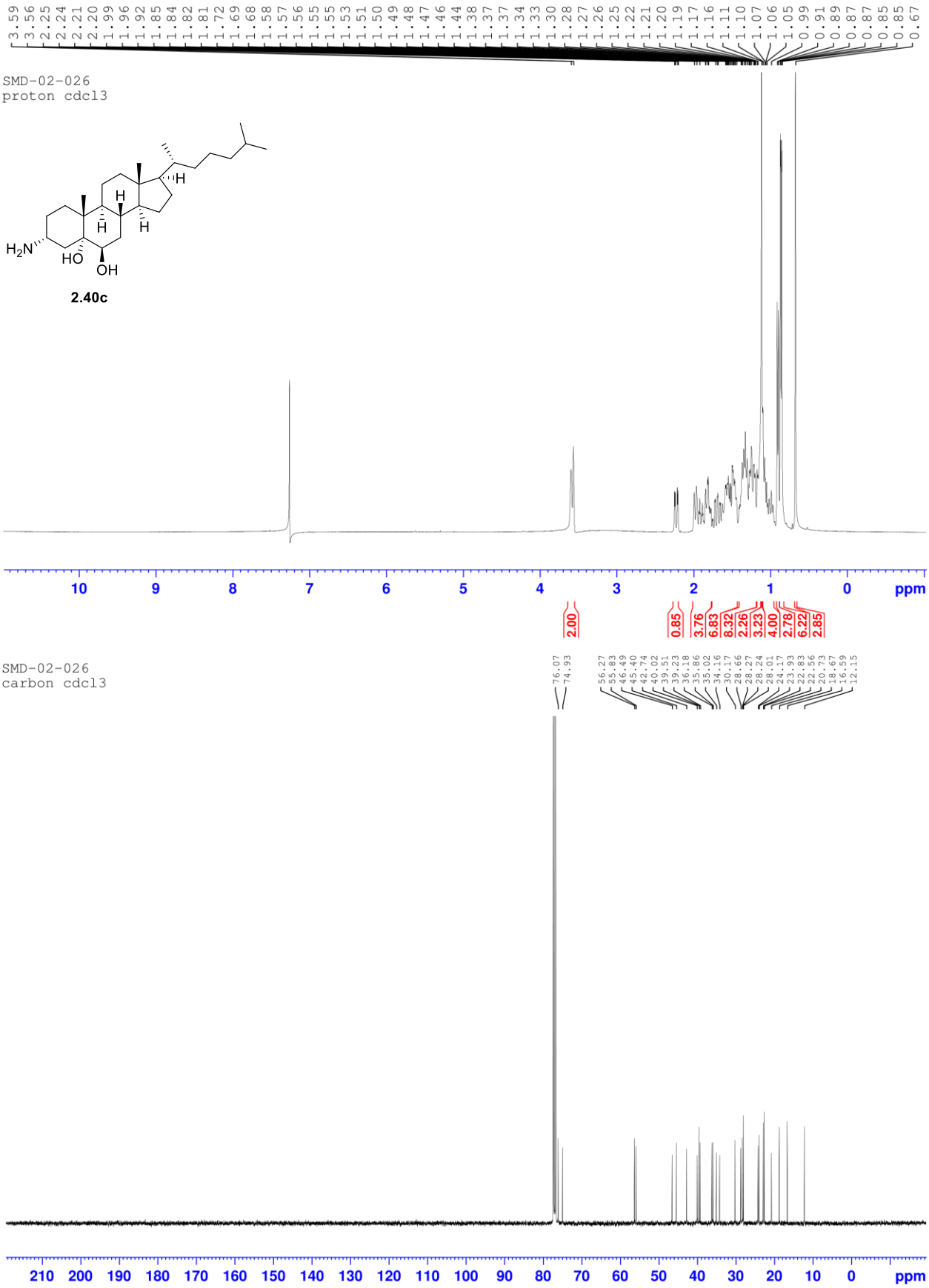
3.59 3.56 2.25 2.24 2.21 2.20 1.99 1.96 1.92 1.85 1.84 1.82 1.81 1.72 1.69 1.68 1.58 1.57 1.56 1.55 1.55 1.53 1.51 1.50 1.49 1.48 1.47 1.46 1.44 1.38 1.37 1.37 1.34 1.33 1.30 1.28 1.27 1.26 1.25 1.22 1.21 1.20 1.19 1.17 1.16 1.11 1.10 1.07 1.06 1.05 0.99 0.91 0.89 0.87 0.87 0.85 0.85 0.67
SMD-02-026
proton cdcl3
H
H
H
H
H2N
HO
OH
2.40c
10 9 8 7 6 5 4 3 2 1 0 ppm
2.00 0.85 3.76 6.83 8.32 2.26 3.23 4.00 2.78 6.22 2.85
SMD-02-026
carbon cdcl3
76.07 74.93 56.27 55.83 46.49 45.40 42.74 40.02 39.51 39.23 36.18 35.86 35.02 34.16 30.17 28.66 28.27 28.24 28.01 24.17 23.93 22.83 22.56 20.73 18.67 16.59 12.15
210 200 190 180 170 160 150 140 130 120 110 100 90 80 70 60 50 40 30 20 10 0 ppm

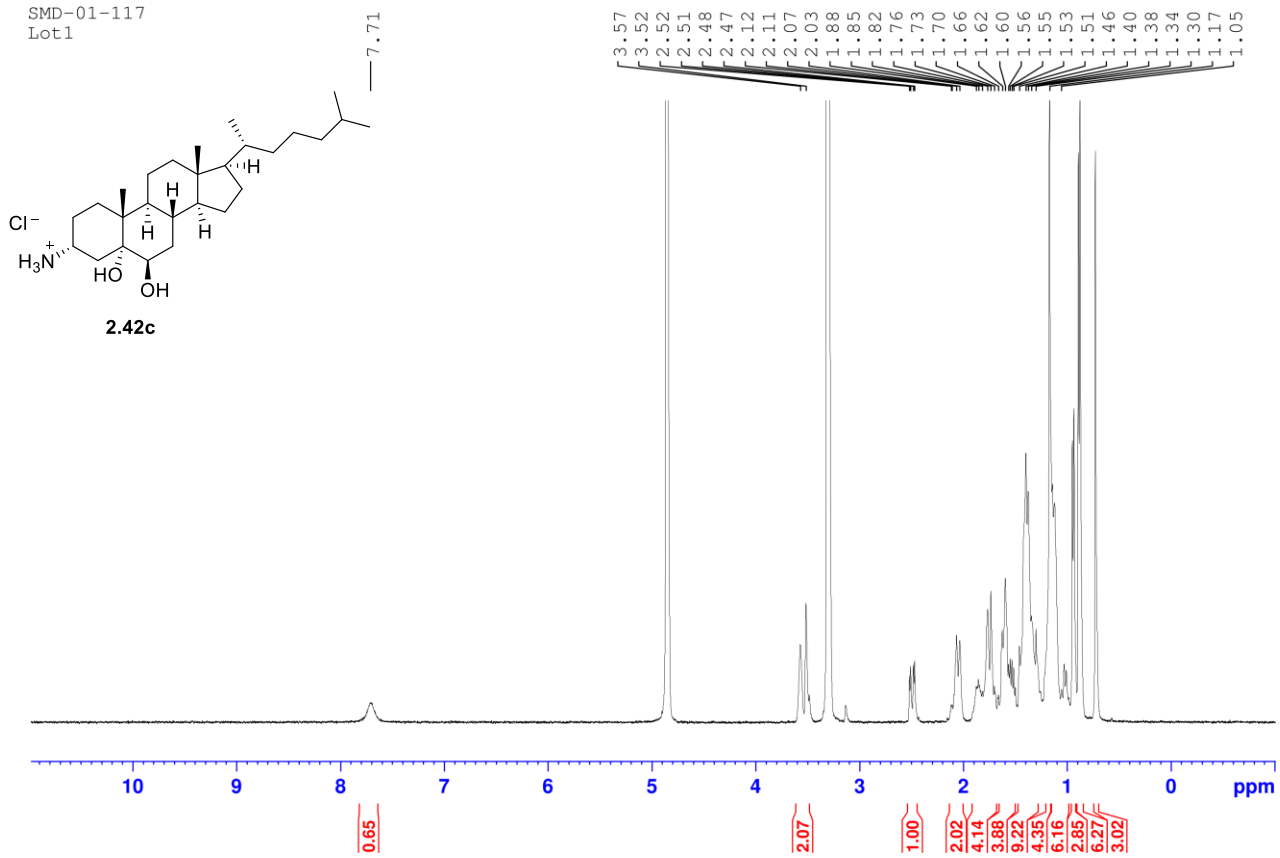
SMD-01-117
Lot1
7.71
3.57
3.52
2.52
2.51
2.48
2.47
2.12
2.11
2.07
2.03
1.88
1.85
1.82
1.76
1.73
1.70
1.66
1.62
1.60
1.56
1.55
1.53
1.51
1.46
1.40
1.38
1.34
1.30
1.17
1.05
Cl⁻
H3N+
HO
OH
H
H
H
H
10
9
8
7
6
5
4
3
2
1
0
ppm
0.65
2.07
1.00
2.02
4.14
3.88
9.22
4.35
6.16
2.85
6.27
3.02

2.42c

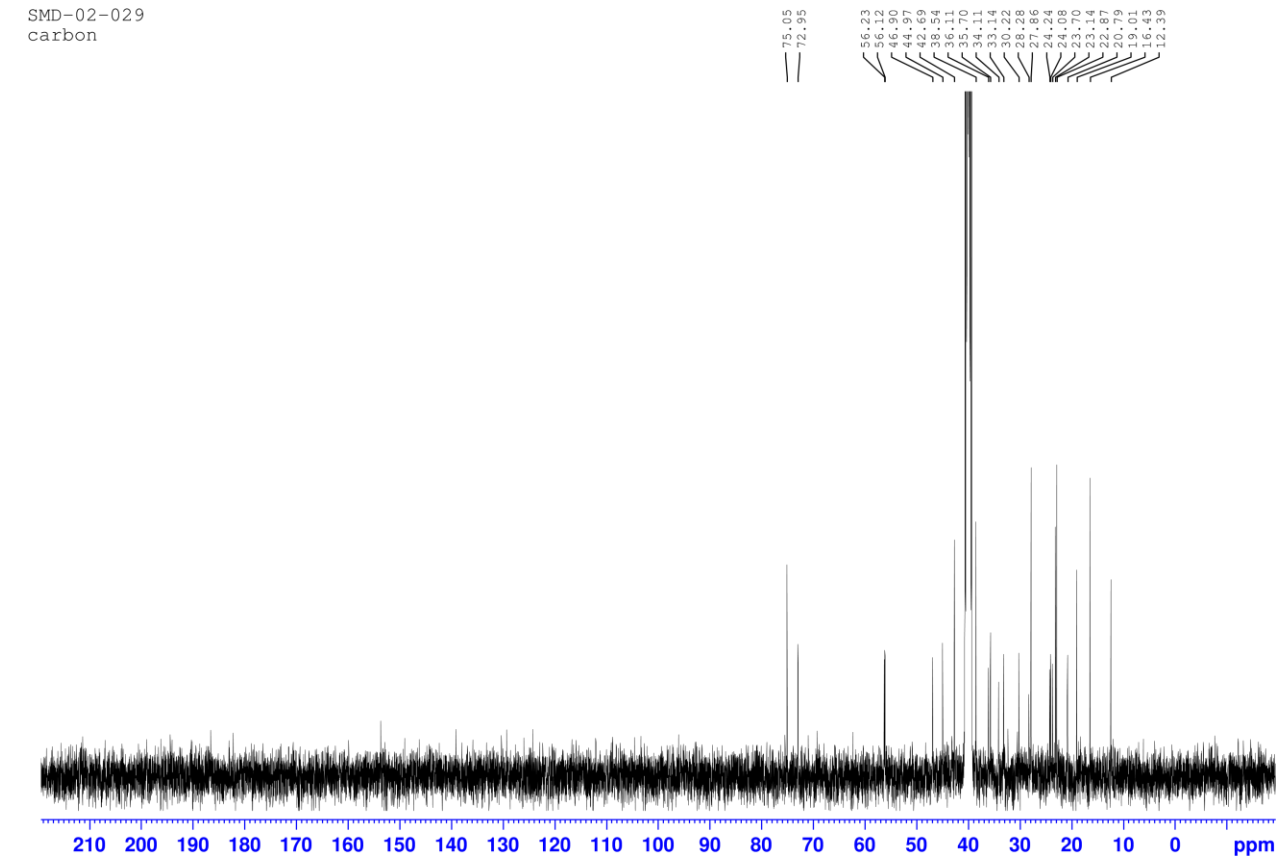
SMD-02-029
carbon
75.05
72.95
56.23
56.12
46.90
44.97
42.69
38.54
36.11
35.70
34.11
33.14
30.22
28.28
27.86
24.24
24.08
23.70
23.14
22.87
20.79
19.01
16.43
12.39
210
200
190
180
170
160
150
140
130
120
110
100
90
80
70
60
50
40
30
20
10
0
ppm

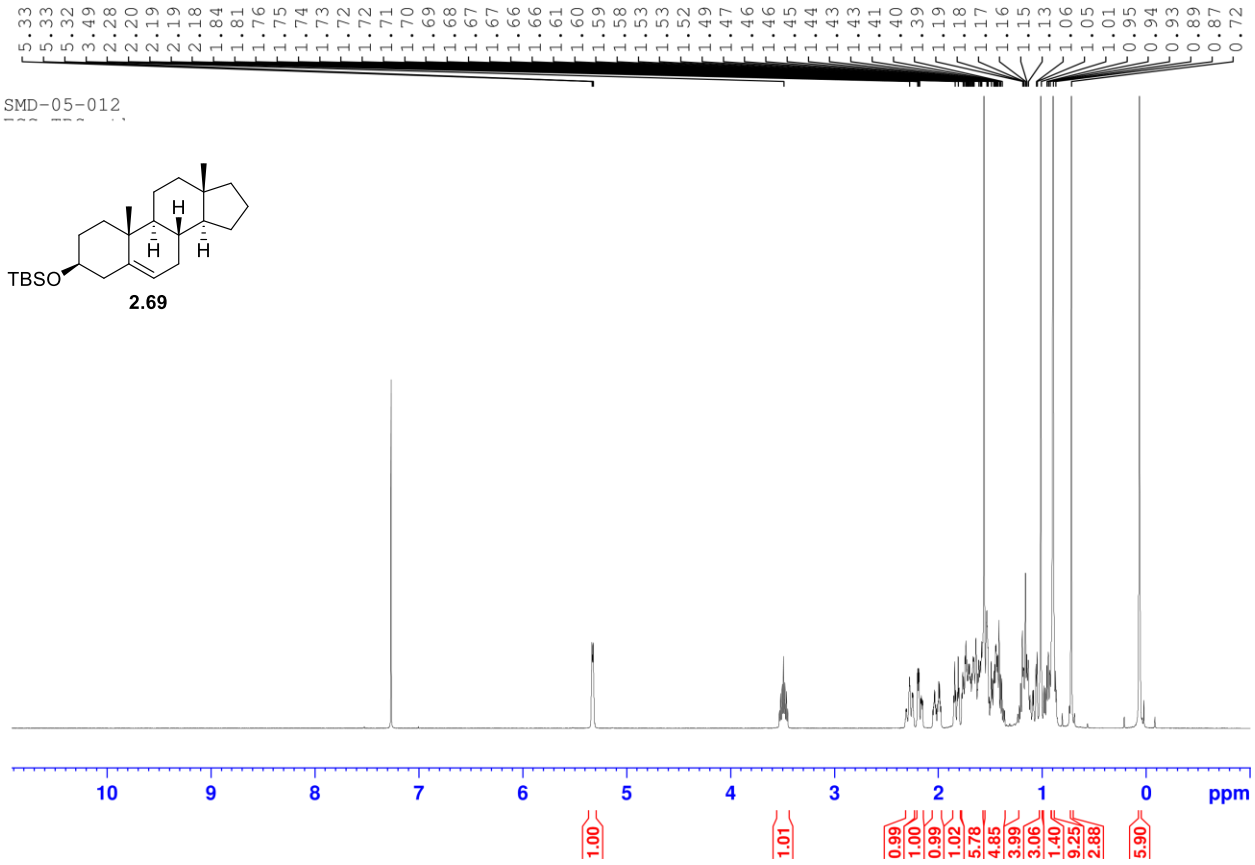
SMD-05-012
TBSO
H
H
H
2.69
ppm

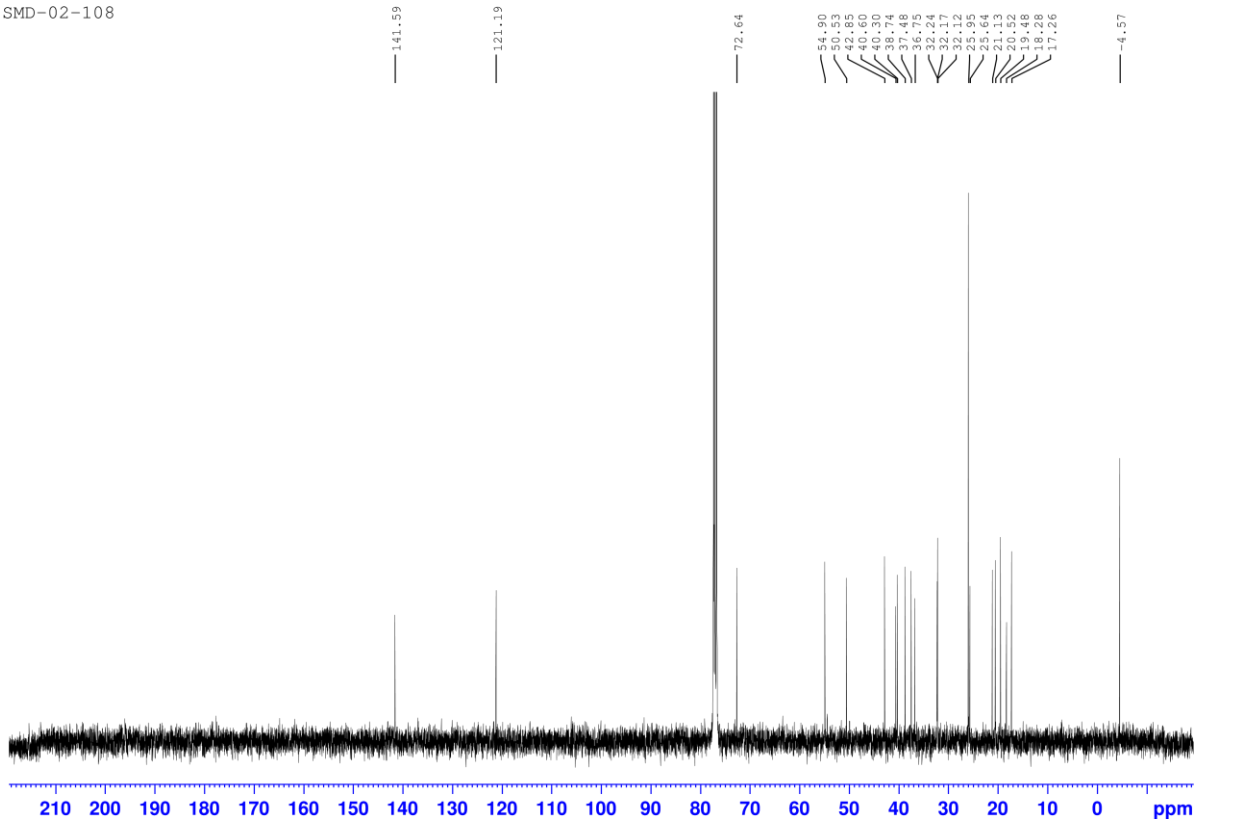
SMD-02-108
ppm

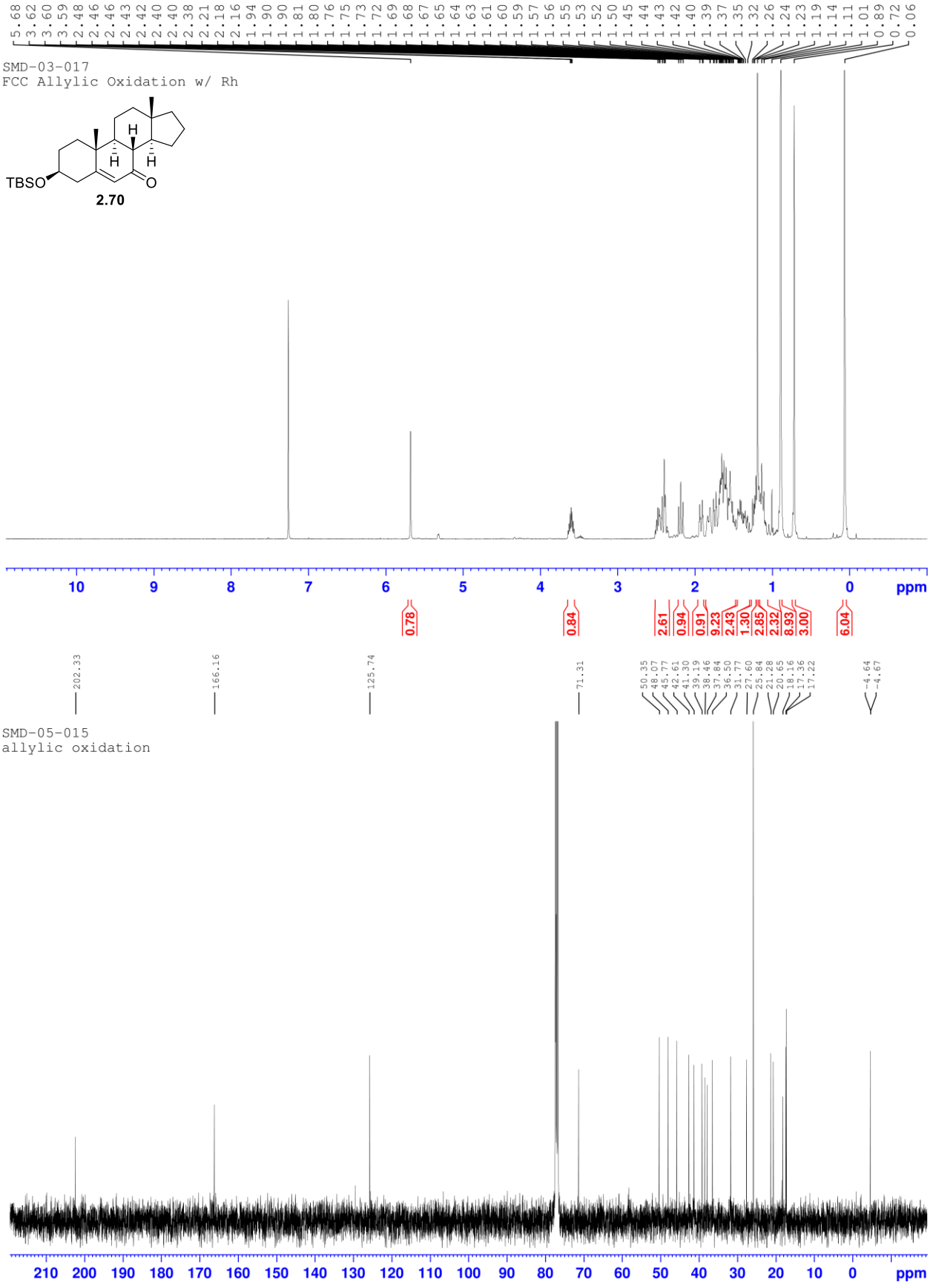
5.68 3.62 3.60 3.59 2.48 2.46 2.46 2.43 2.42 2.40 2.40 2.38 2.21 2.18 2.16 1.94 1.90 1.90 1.81 1.80 1.76 1.75 1.73 1.72 1.69 1.68 1.67 1.65 1.64 1.63 1.61 1.60 1.59 1.57 1.56 1.55 1.53 1.52 1.50 1.45 1.44 1.43 1.42 1.40 1.39 1.37 1.35 1.32 1.26 1.24 1.23 1.19 1.14 1.11 1.01 0.89 0.72 0.06
SMD-03-017
FCC Allylic Oxidation w/ Rh
TBSO
H
H
H
O
2.70
10 9 8 7 6 5 4 3 2 1 0 ppm
0.78 0.84 2.61 0.94 0.91 9.23 2.43 1.30 2.85 2.32 8.93 3.00 6.04
202.33 166.16 125.74 71.31 50.35 48.07 45.77 42.61 41.30 39.19 38.46 37.84 36.50 31.77 27.60 25.84 21.28 20.65 18.16 17.36 17.22 -4.64 -4.67
SMD-05-015
allylic oxidation
210 200 190 180 170 160 150 140 130 120 110 100 90 80 70 60 50 40 30 20 10 0 ppm

SMD-02-119
Hydrogenation

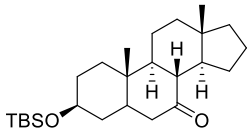

2.71

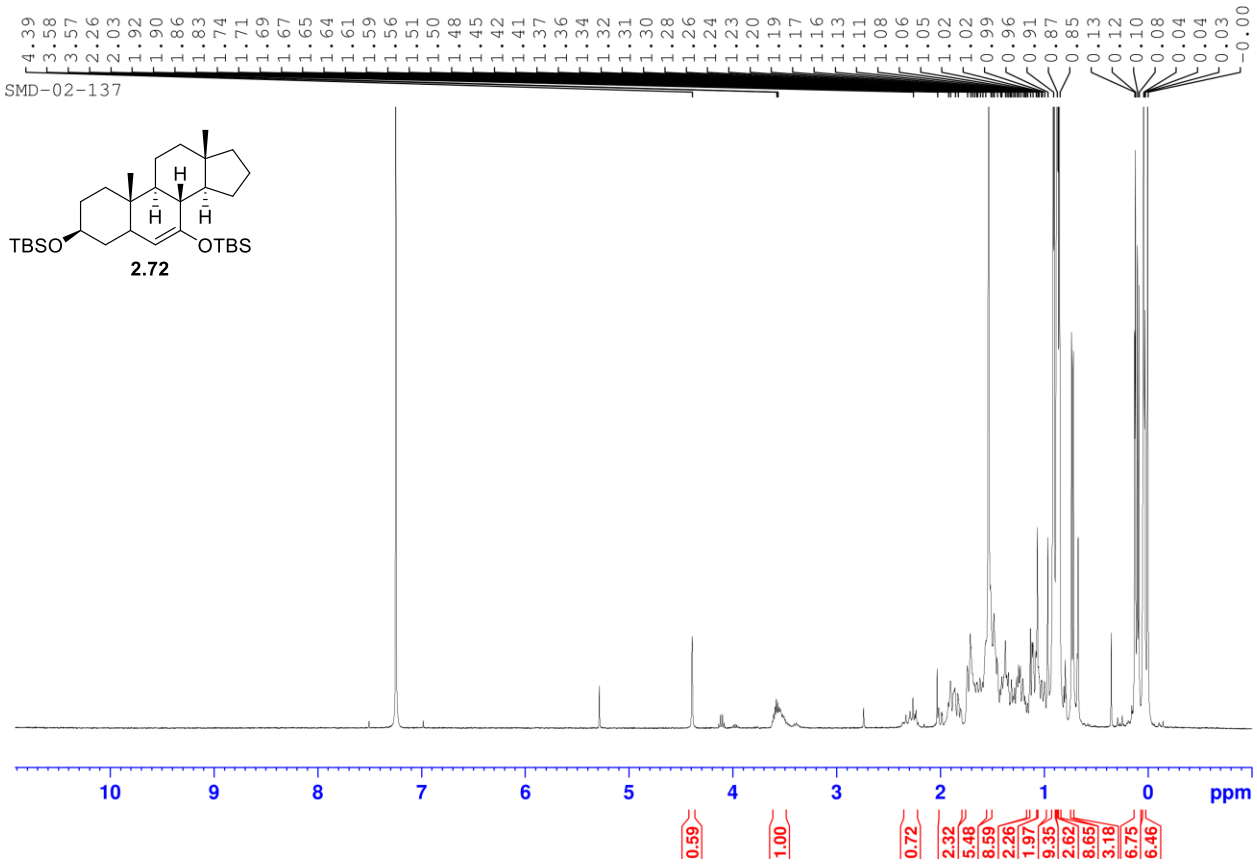
4.39
3.58
3.57
2.26
2.03
1.92
1.90
1.86
1.83
1.74
1.71
1.69
1.67
1.65
1.64
1.61
1.59
1.56
1.51
1.50
1.48
1.45
1.42
1.41
1.37
1.36
1.34
1.32
1.31
1.30
1.28
1.26
1.24
1.23
1.20
1.19
1.17
1.16
1.13
1.11
1.08
1.06
1.05
1.02
1.02
0.99
0.96
0.91
0.87
0.85
0.13
0.12
0.10
0.08
0.04
0.04
0.03
-0.00
SMD-02-137
H
H
H
TBSO
OTBS
2.72
10
9
8
7
6
5
4
3
2
1
0
ppm
0.59
1.00
0.72
2.32
5.48
8.59
2.26
1.97
9.35
2.62
8.65
3.18
6.75
6.46

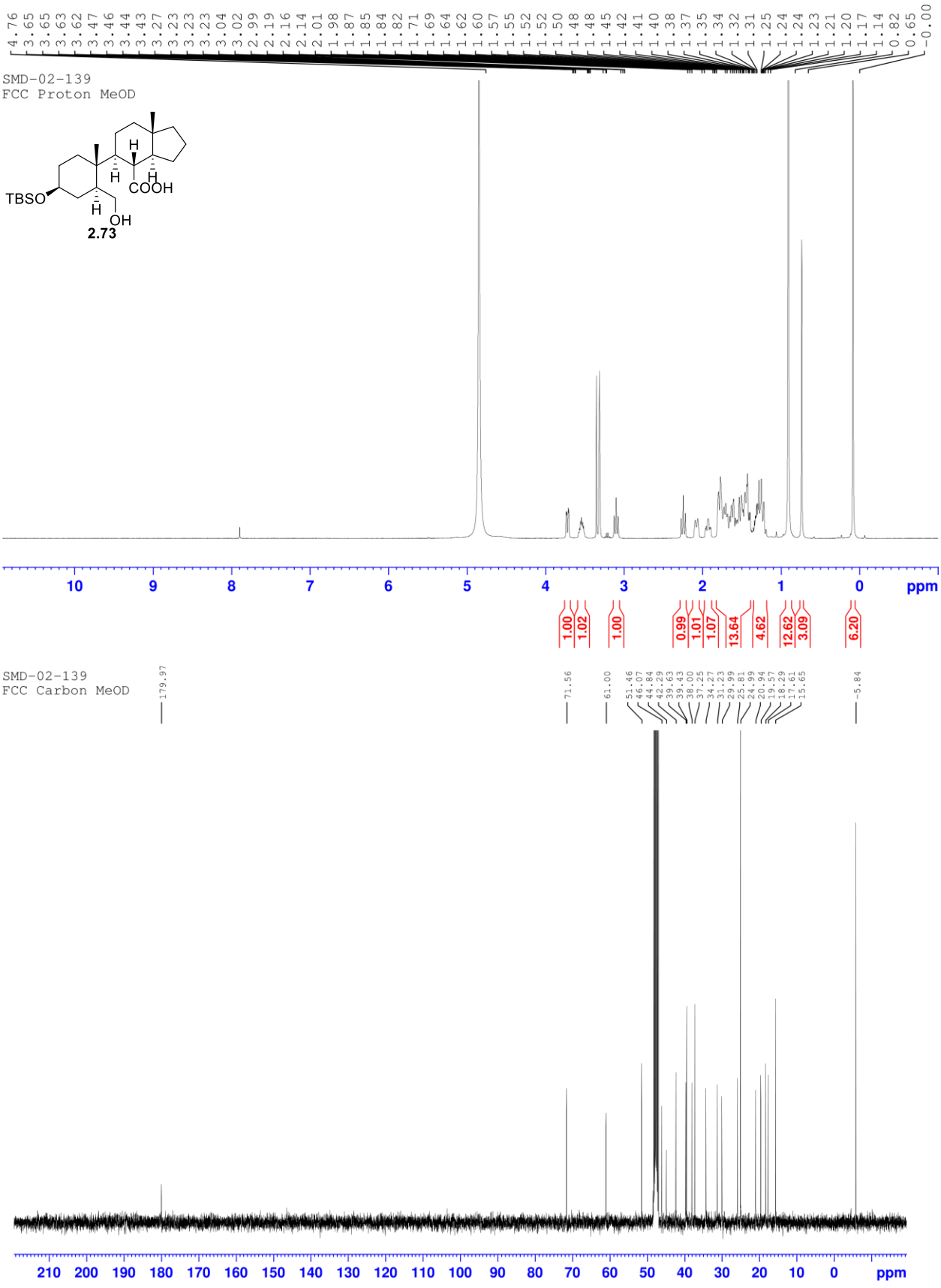
SMD-02-139
FCC Proton MeOD
TBSO
COOH
OH
2.73
SMD-02-139
FCC Carbon MeOD
ppm

SMD-02-141
FCC Protected Lactone

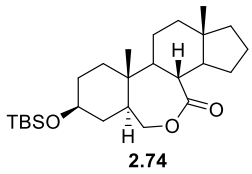

2.74

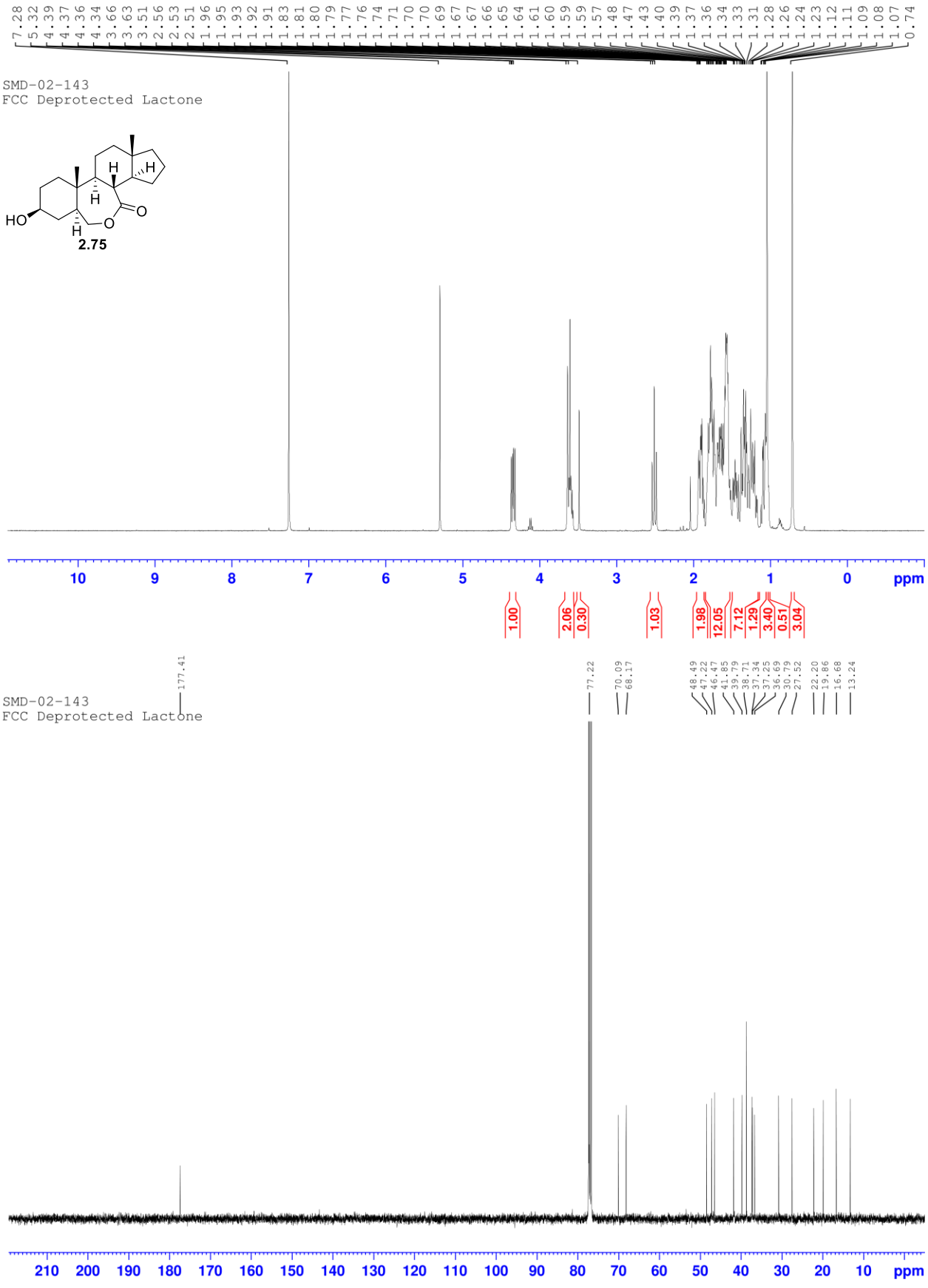
7.28
5.32
4.39
4.37
4.36
4.34
3.66
3.63
3.51
2.56
2.53
2.51
1.96
1.95
1.93
1.92
1.91
1.83
1.81
1.80
1.79
1.77
1.76
1.74
1.71
1.70
1.69
1.67
1.67
1.66
1.65
1.64
1.61
1.60
1.59
1.59
1.57
1.48
1.47
1.43
1.40
1.39
1.37
1.36
1.34
1.33
1.31
1.28
1.26
1.24
1.23
1.12
1.11
1.09
1.08
1.07
0.74
SMD-02-143
FCC Deprotected Lactone
HO
O
O
H
H
H
H
2.75
10
9
8
7
6
5
4
3
2
1
0
ppm
1.00
2.06
0.30
1.03
1.98
12.05
7.12
1.29
3.40
0.51
3.04
177.41
77.22
70.09
68.17
48.49
47.22
46.47
41.85
39.79
38.71
37.34
37.25
36.69
30.79
27.52
22.20
19.86
16.68
13.24
SMD-02-143
FCC Deprotected Lactone
210
200
190
180
170
160
150
140
130
120
110
100
90
80
70
60
50
40
30
20
10
ppm

SMD-03-147

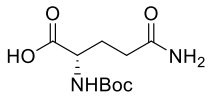

3.38

SMD-05-079
Boc-L-Gln

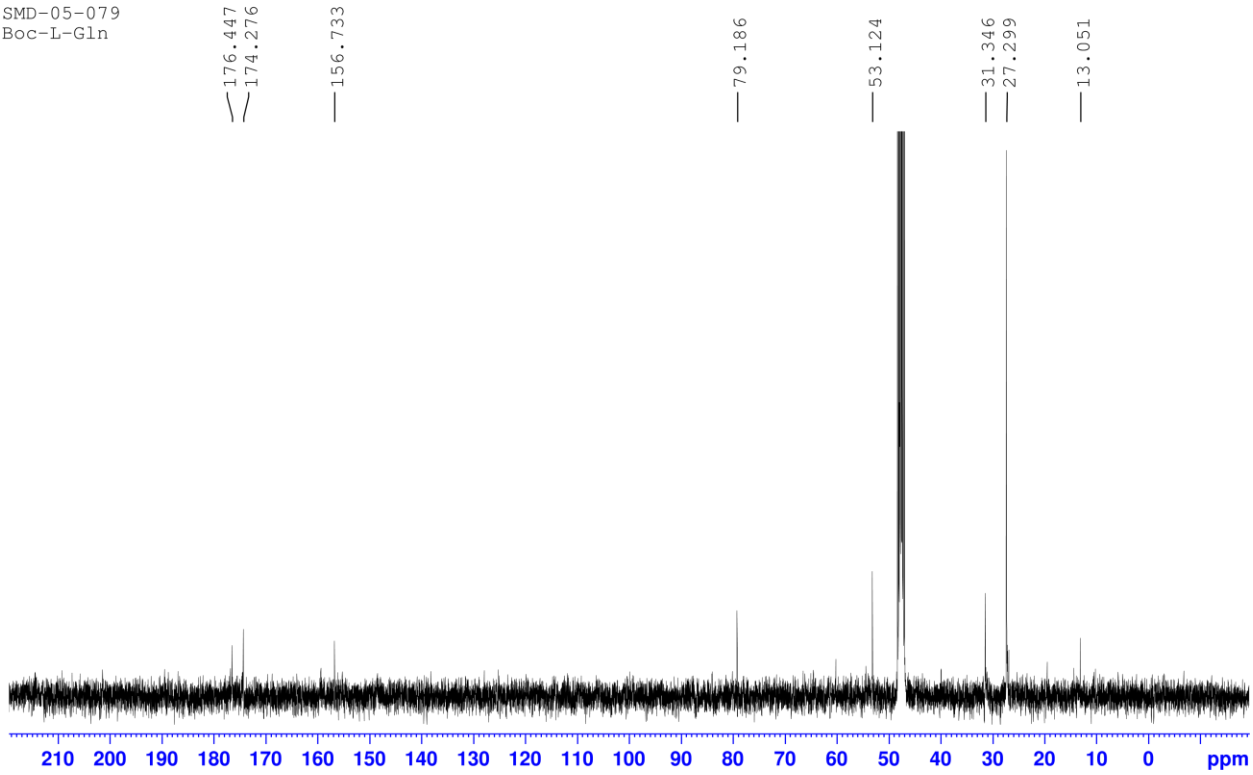

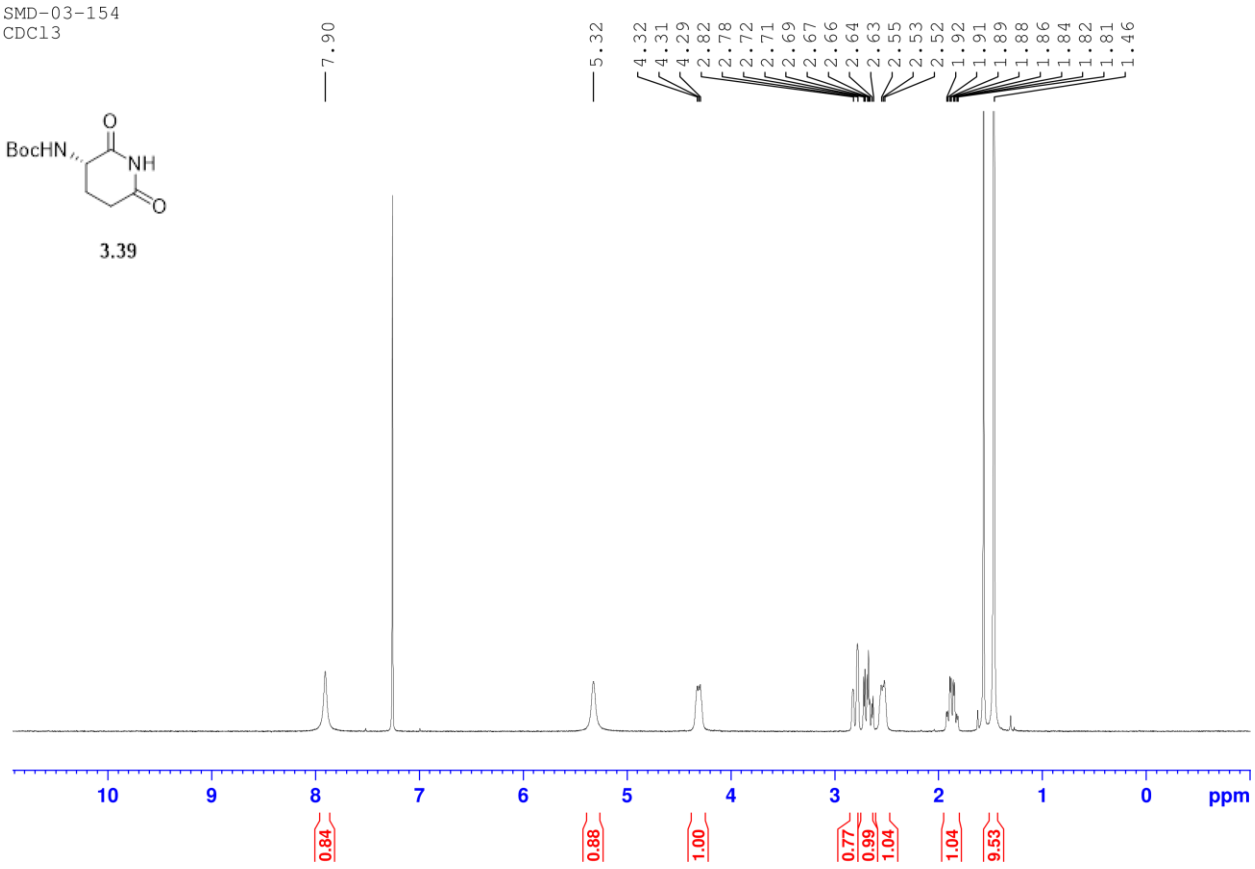
SMD-03-154
CDCl3
7.90
5.32
4.32
4.31
4.29
2.82
2.78
2.72
2.71
2.69
2.67
2.66
2.64
2.63
2.55
2.53
2.52
1.92
1.91
1.89
1.88
1.86
1.84
1.82
1.81
1.46
BocHN
NH
O
O
3.39
10
9
8
7
6
5
4
3
2
1
0
ppm
0.84
0.88
1.00
0.77
0.99
1.04
1.04
9.53

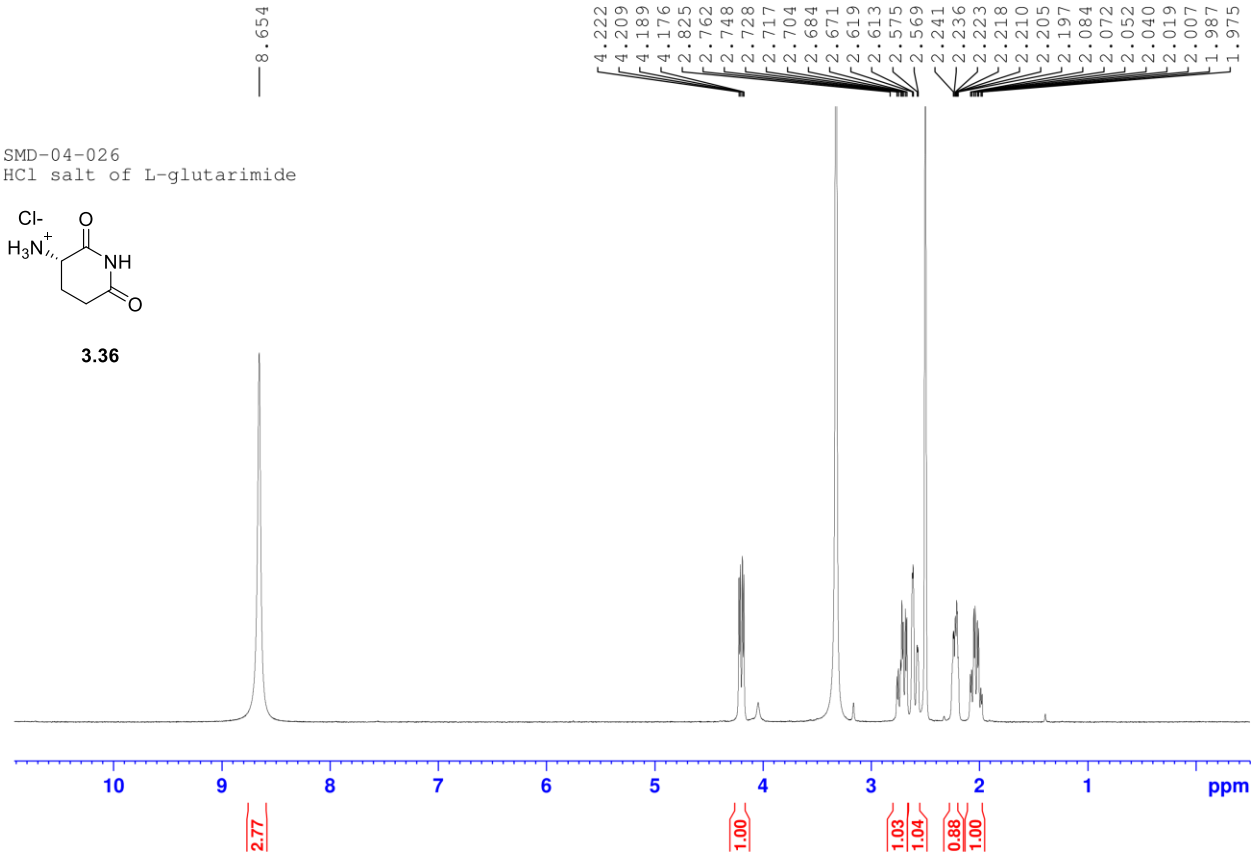
8.654
4.222
4.209
4.189
4.176
2.825
2.762
2.748
2.728
2.717
2.704
2.684
2.671
2.619
2.613
2.575
2.569
2.241
2.236
2.223
2.218
2.210
2.205
2.197
2.084
2.072
2.052
2.040
2.019
2.007
1.987
1.975
SMD-04-026
HCl salt of L-glutarimide
Cl-
H3N+
O
NH
O
3.36
10
9
8
7
6
5
4
3
2
1
ppm
2.77
1.00
1.03
1.04
0.88
1.00

SMD-04-084
E3 w/ NO2

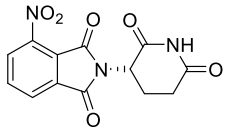

3.40

SMD-04-016
E3 Ligase NO2

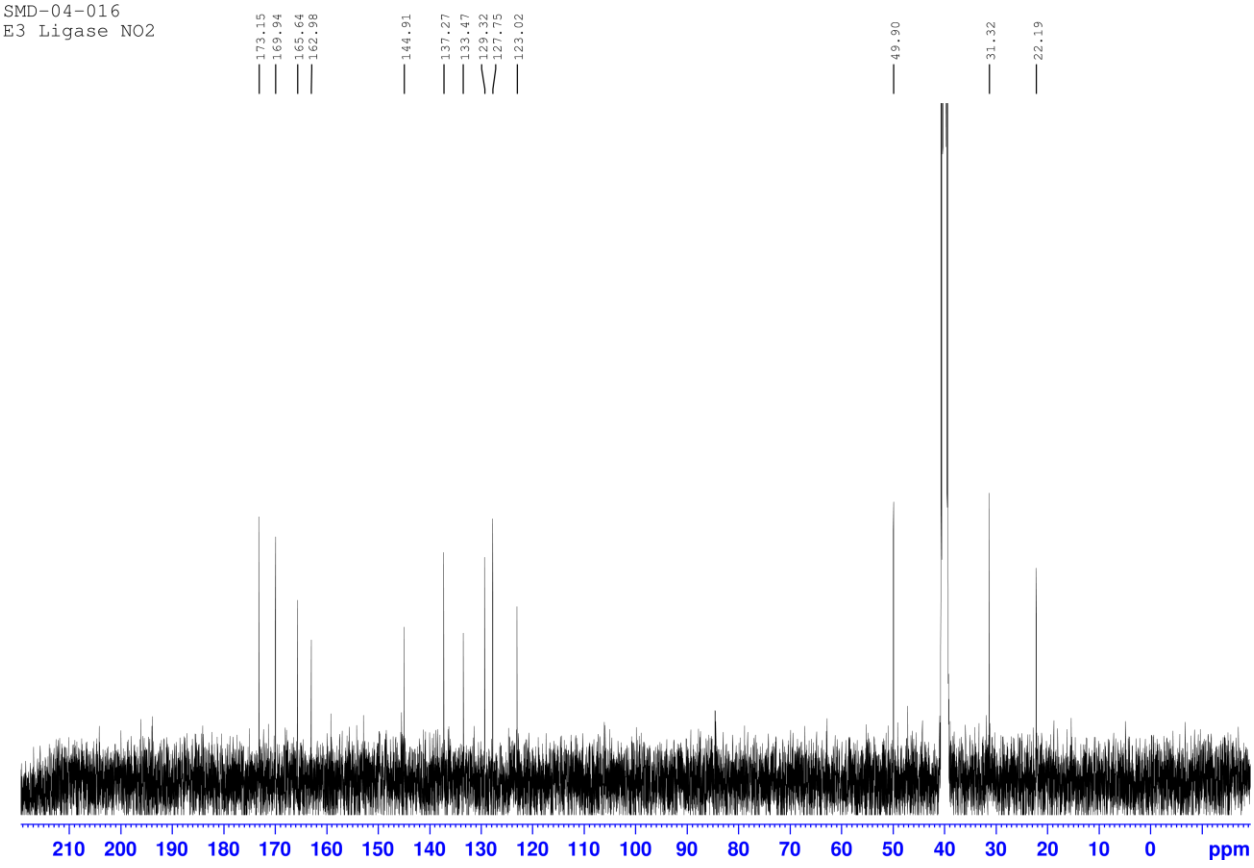

SMD-04-045
Hydrogenation

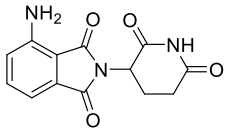

3.41

SMD-04-020
filter solid

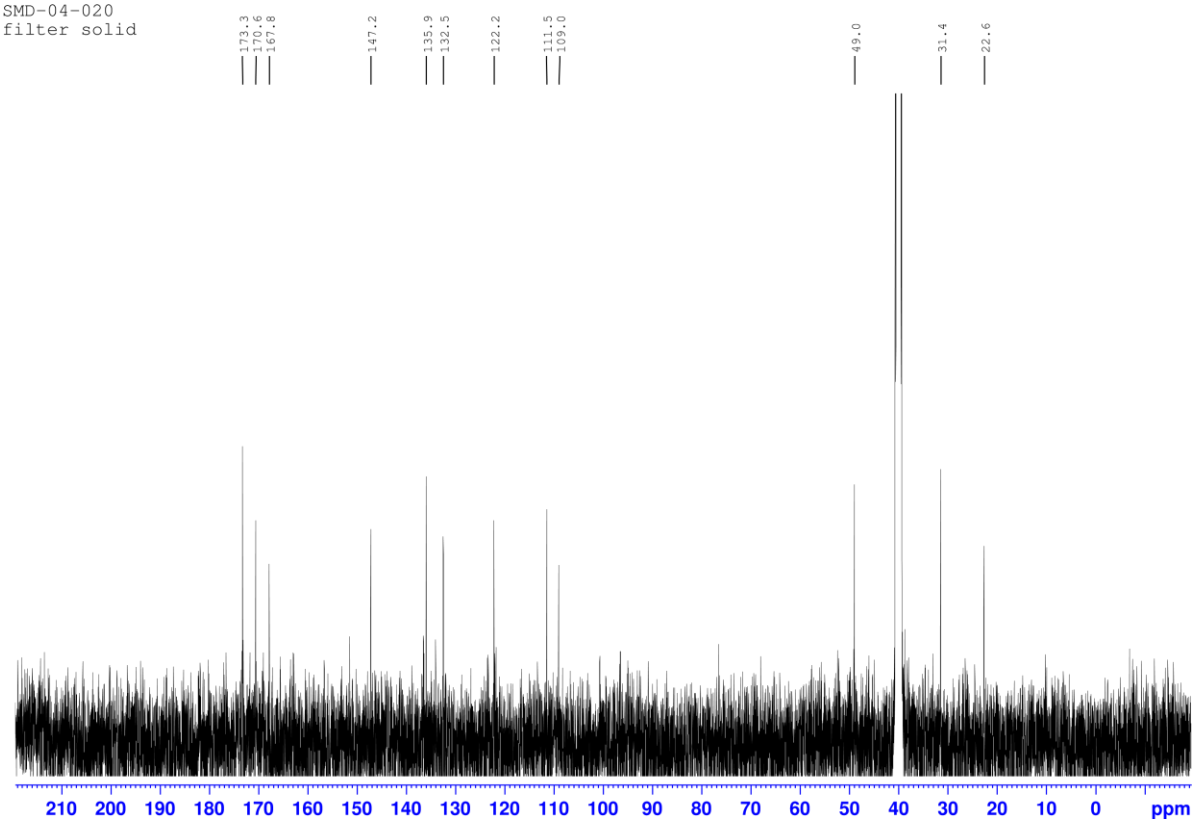

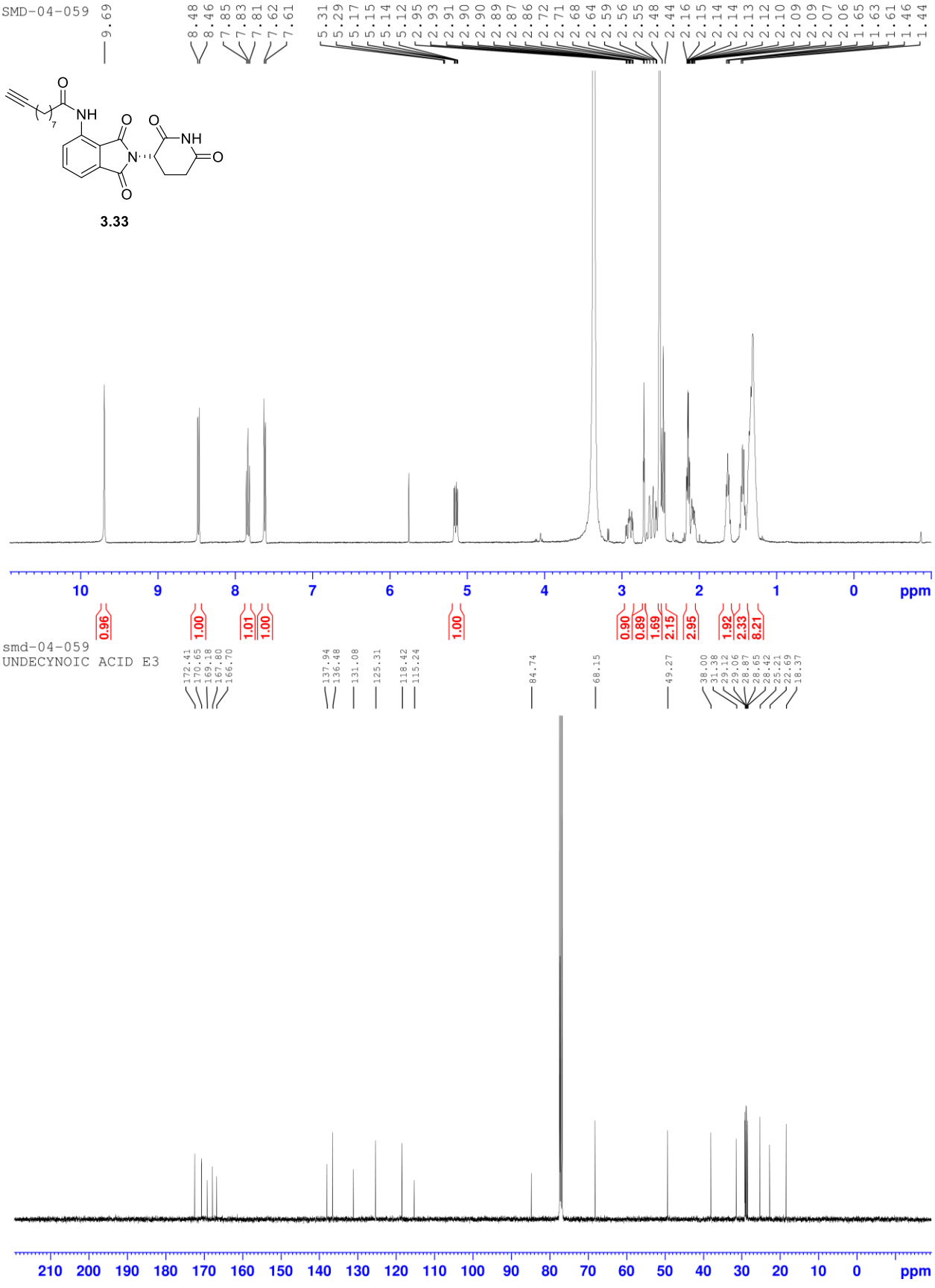
SMD-04-059
9.69
8.48
8.46
7.85
7.83
7.81
7.62
7.61
5.31
5.29
5.17
5.15
5.14
5.12
2.95
2.93
2.91
2.90
2.90
2.89
2.87
2.86
2.72
2.71
2.68
2.64
2.59
2.56
2.55
2.48
2.44
2.16
2.15
2.14
2.14
2.13
2.12
2.10
2.09
2.09
2.07
2.06
1.65
1.63
1.61
1.46
1.44
NH
O
O
NH
O
N
O
O
3.33
10
9
8
7
6
5
4
3
2
1
0
ppm
0.96
1.00
1.01
1.00
1.00
0.90
0.89
1.69
2.15
2.95
1.92
2.33
8.21
smd-04-059
UNDECYNOIC ACID E3
172.41
170.65
169.18
167.80
166.70
137.94
136.48
131.08
125.31
118.42
115.24
84.74
68.15
49.27
38.00
31.38
29.22
29.16
28.87
28.65
28.42
25.21
22.69
18.37
210
200
190
180
170
160
150
140
130
120
110
100
90
80
70
60
50
40
30
20
10
0
ppm

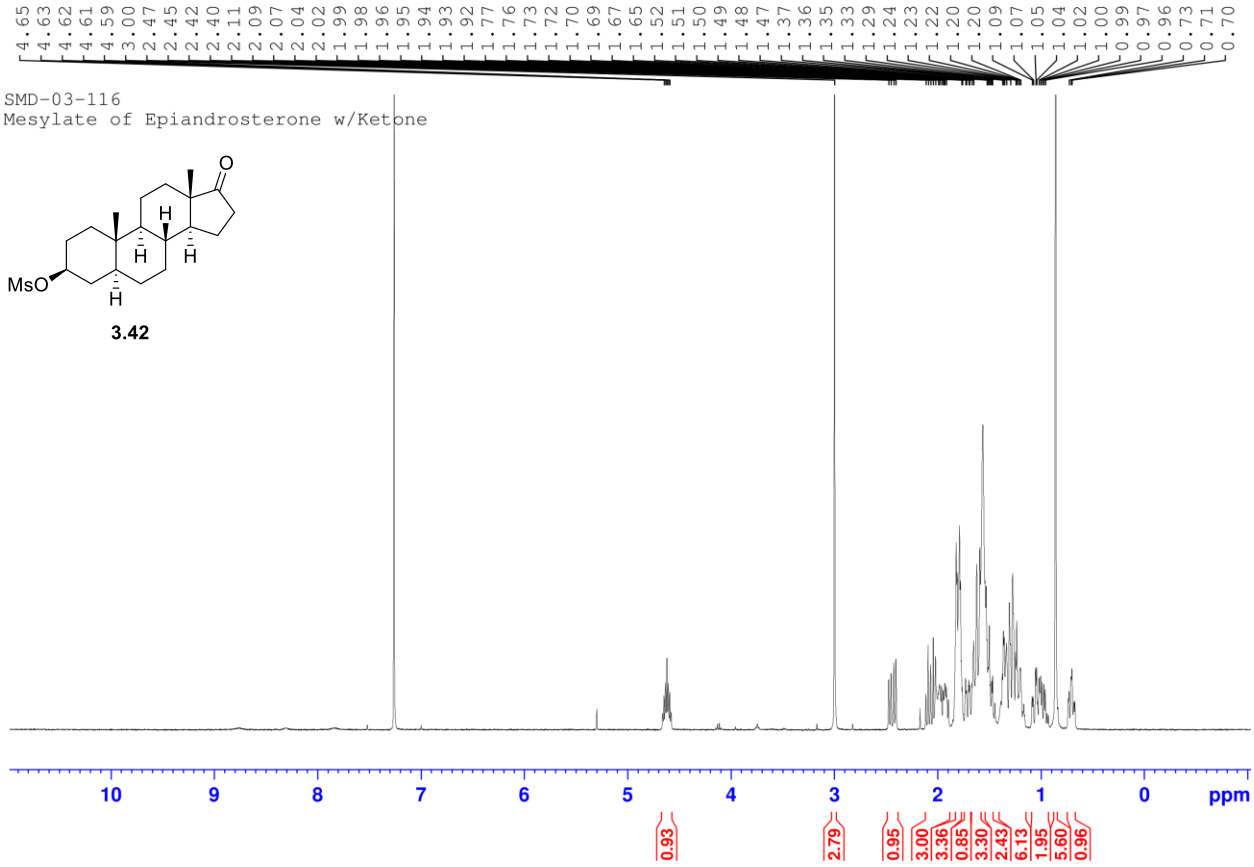
4.65
4.63
4.62
4.61
4.59
3.00
2.47
2.45
2.42
2.40
2.11
2.09
2.07
2.04
2.02
1.99
1.98
1.96
1.95
1.94
1.93
1.92
1.77
1.76
1.73
1.72
1.70
1.69
1.67
1.65
1.52
1.51
1.50
1.49
1.48
1.47
1.37
1.36
1.35
1.33
1.29
1.24
1.23
1.22
1.20
1.20
1.09
1.07
1.05
1.04
1.02
1.00
0.99
0.97
0.96
0.73
0.71
0.70
SMD-03-116
Mesylate of Epiandrosterone w/Ketone
O
H
H
H
MsO
H
3.42
10
9
8
7
6
5
4
3
2
1
0
ppm
0.93
2.79
0.95
3.00
3.36
0.85
3.30
2.43
6.13
1.95
5.60
0.96

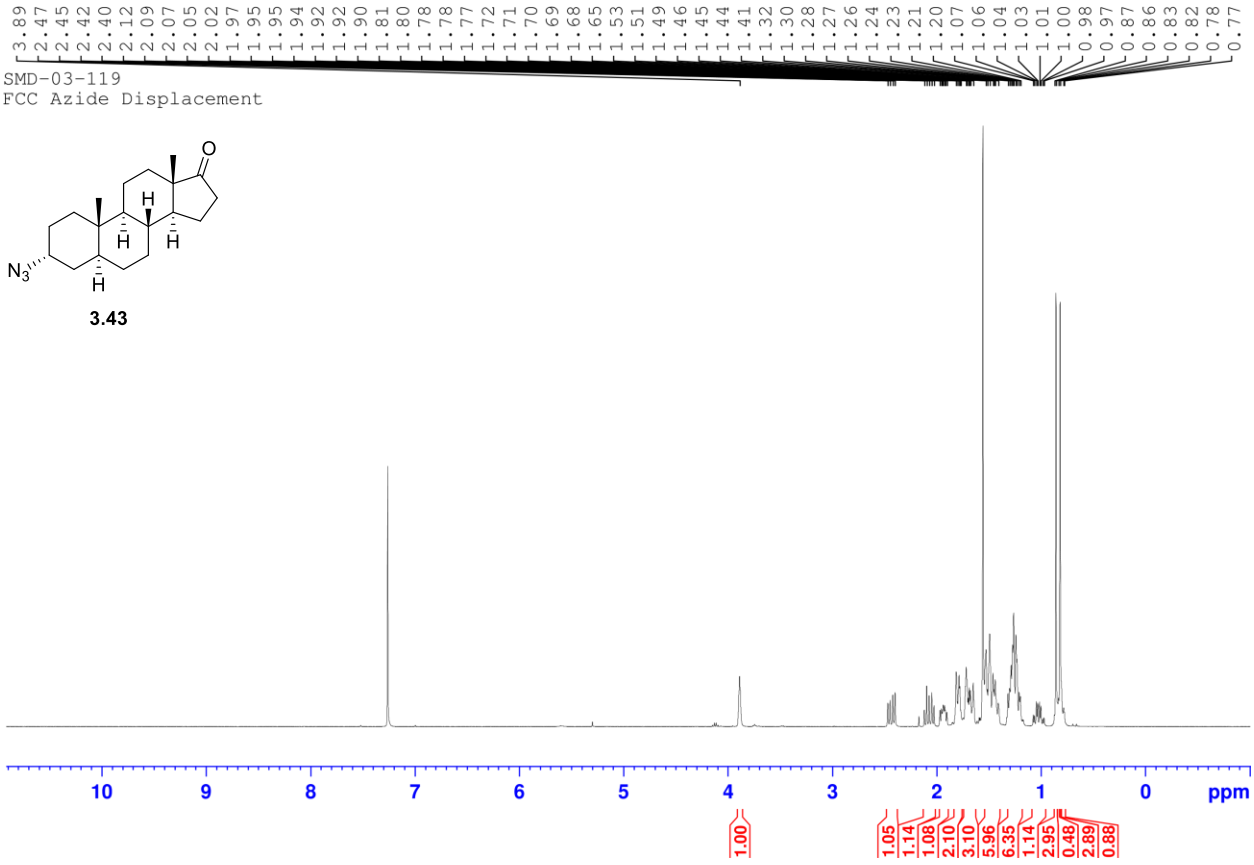
3.89 2.47 2.45 2.42 2.40 2.12 2.09 2.07 2.05 2.02 1.97 1.95 1.95 1.94 1.92 1.92 1.90 1.81 1.80 1.78 1.78 1.77 1.72 1.71 1.70 1.69 1.68 1.65 1.53 1.51 1.49 1.46 1.45 1.44 1.41 1.32 1.30 1.28 1.27 1.26 1.24 1.23 1.21 1.20 1.07 1.06 1.04 1.03 1.01 1.00 0.98 0.97 0.87 0.86 0.83 0.82 0.78 0.77
SMD-03-119
FCC Azide Displacement
O
H
H
H
N3
H
10 9 8 7 6 5 4 3 2 1 0 ppm
1.00
1.05 1.14 1.08 2.10 3.10 5.96 6.35 1.14 2.95 0.48 2.89 0.88

3.43

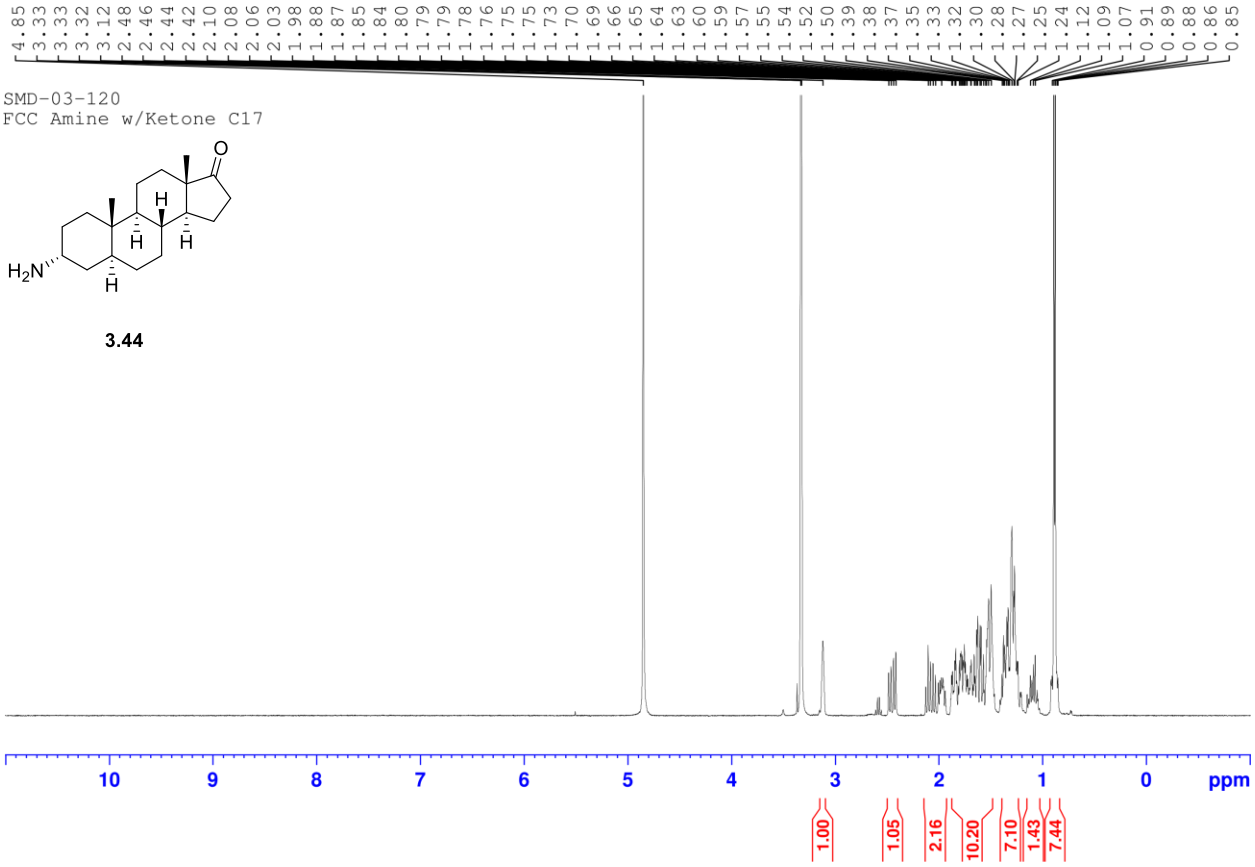
4.85
3.33
3.33
3.32
3.12
2.48
2.46
2.44
2.42
2.10
2.08
2.06
2.03
1.98
1.88
1.87
1.85
1.84
1.80
1.79
1.79
1.78
1.76
1.75
1.75
1.73
1.70
1.69
1.66
1.65
1.64
1.63
1.60
1.59
1.57
1.55
1.54
1.52
1.50
1.39
1.38
1.37
1.35
1.33
1.32
1.30
1.28
1.27
1.25
1.24
1.12
1.09
1.07
0.91
0.89
0.88
0.86
0.85
SMD-03-120
FCC Amine w/Ketone C17
O
H
H
H
H2N
H
3.44
10
9
8
7
6
5
4
3
2
1
0
ppm
1.00
1.05
2.16
10.20
7.10
1.43
7.44

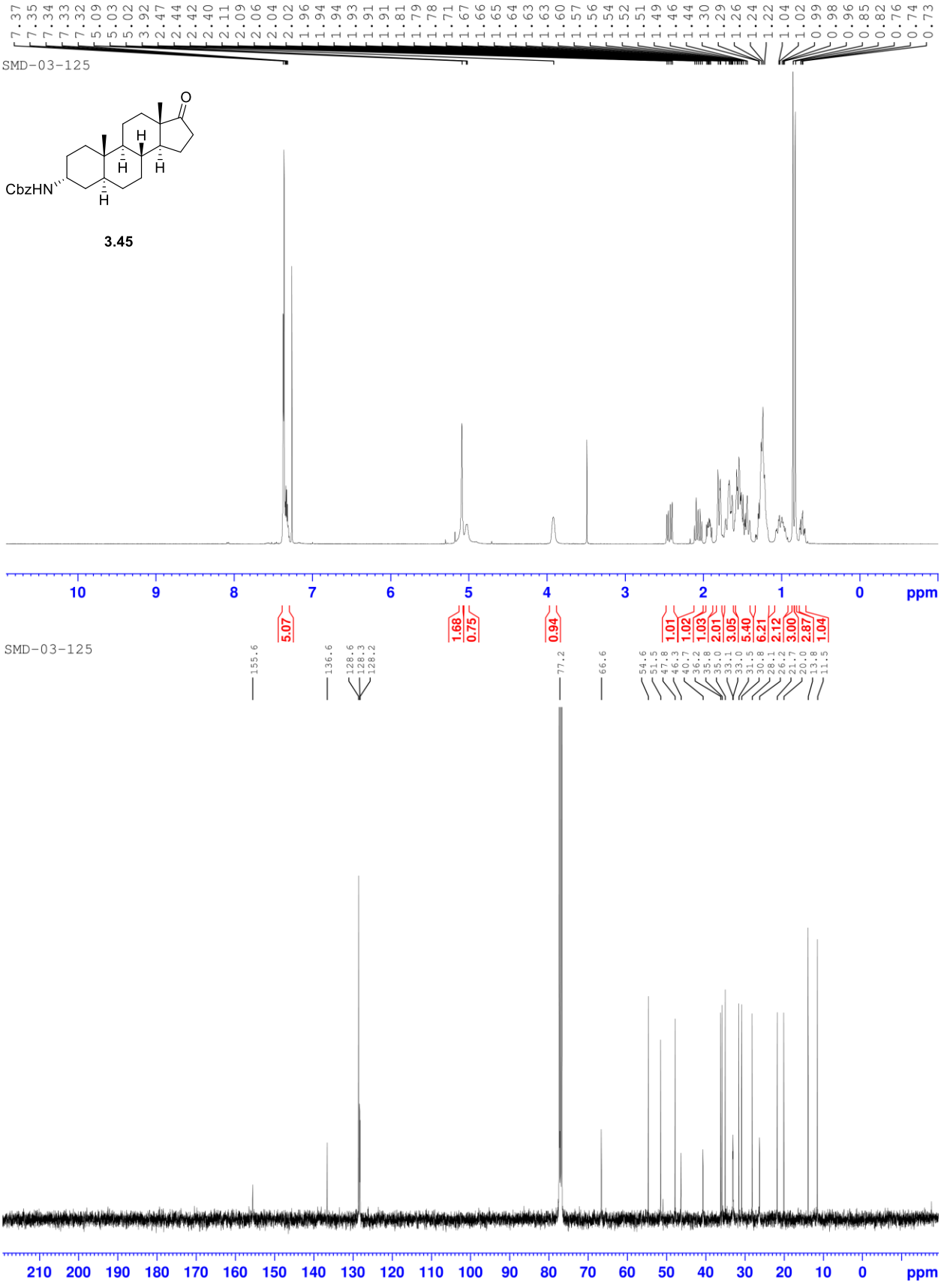
SMD-03-125
7.37 7.35 7.34 7.33 7.32 5.09 5.03 5.02 3.92 2.47 2.44 2.42 2.40 2.11 2.09 2.06 2.04 2.02 1.96 1.94 1.94 1.93 1.91 1.91 1.81 1.79 1.78 1.71 1.67 1.66 1.65 1.64 1.63 1.63 1.60 1.57 1.56 1.54 1.52 1.51 1.49 1.46 1.44 1.30 1.29 1.26 1.24 1.22 1.04 1.02 0.99 0.98 0.96 0.85 0.82 0.76 0.74 0.73
O
H
H
H
CbzHN
H
3.45
10 9 8 7 6 5 4 3 2 1 0 ppm
5.07 1.68 0.75 0.94 1.01 1.02 1.03 2.01 3.05 5.40 6.21 2.12 3.00 2.87 1.04
SMD-03-125
155.6 136.6 128.6 128.3 128.2 77.2 66.6 54.6 51.5 47.8 46.3 40.7 36.2 35.8 35.0 33.1 33.0 31.5 30.8 28.1 26.2 21.7 21.0 13.8 11.5
210 200 190 180 170 160 150 140 130 120 110 100 90 80 70 60 50 40 30 20 10 0 ppm

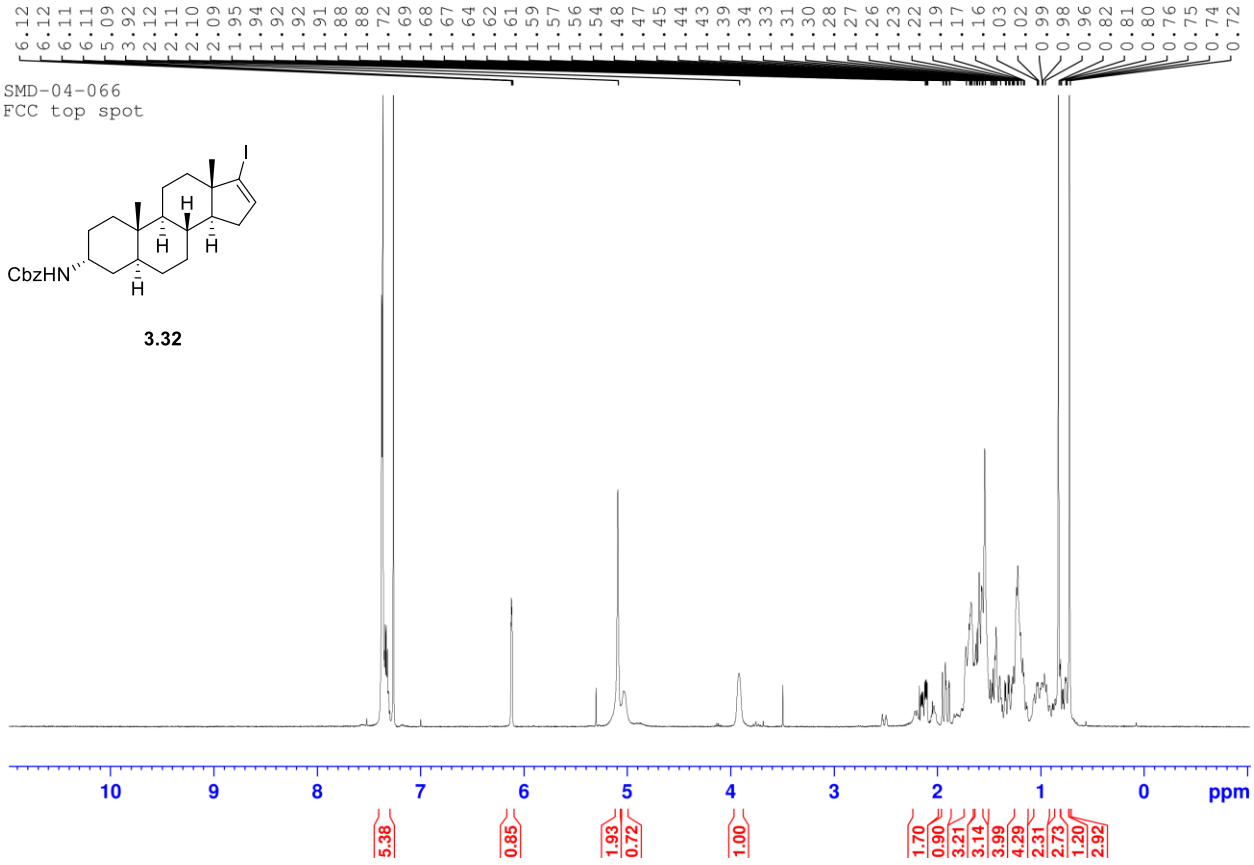
6.12
6.12
6.11
6.11
5.09
3.92
2.12
2.11
2.10
2.09
1.95
1.94
1.92
1.92
1.91
1.88
1.88
1.72
1.69
1.68
1.67
1.64
1.62
1.61
1.59
1.57
1.56
1.54
1.48
1.47
1.45
1.44
1.43
1.39
1.34
1.33
1.31
1.30
1.28
1.27
1.26
1.23
1.22
1.19
1.17
1.16
1.03
1.02
0.99
0.98
0.96
0.82
0.81
0.80
0.76
0.75
0.74
0.72
SMD-04-066
FCC top spot
I
H
H
H
CbzHN
H
10
9
8
7
6
5
4
3
2
1
0
ppm
5.38
0.85
1.93
0.72
1.00
1.70
0.90
3.21
3.14
3.99
4.29
2.31
2.73
1.20
2.92

3.32

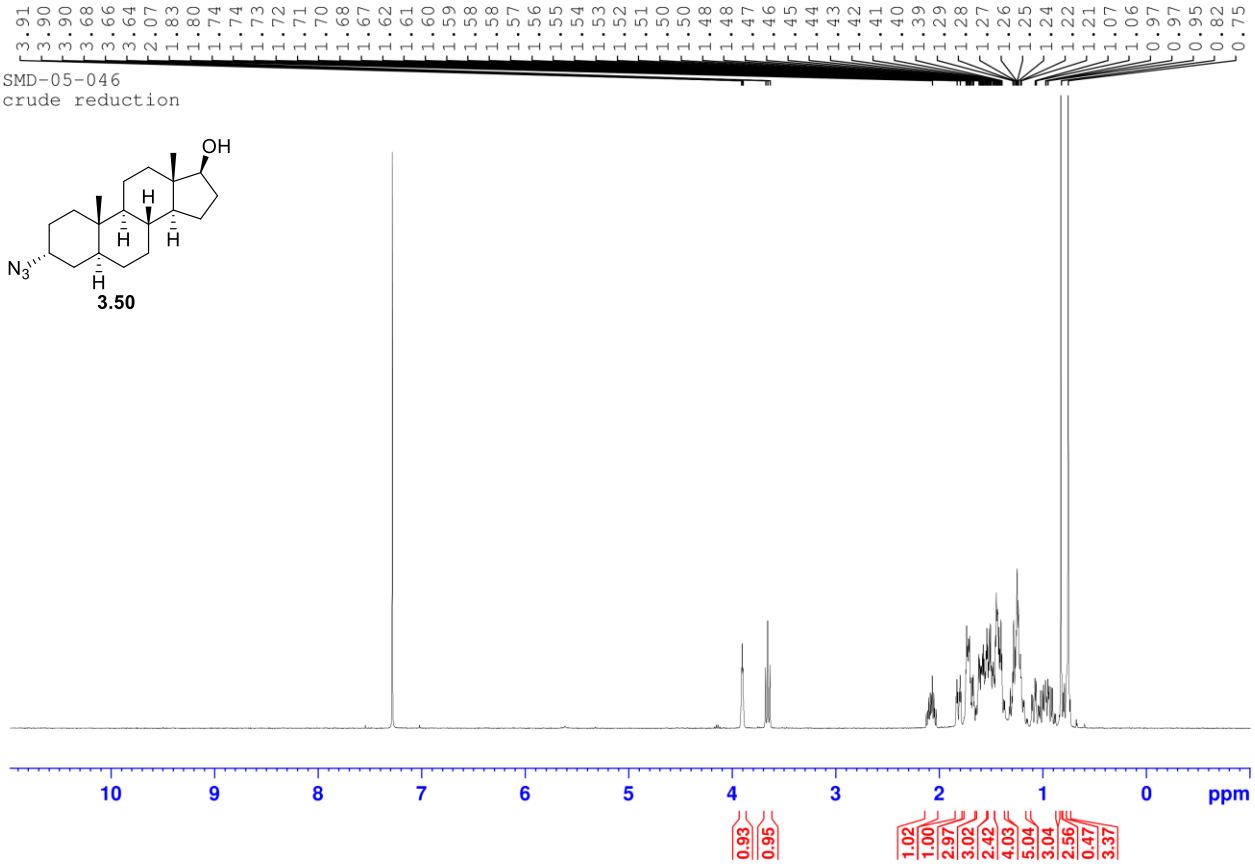
3.91 3.90 3.90 3.68 3.66 3.64 2.07 1.83 1.80 1.74 1.74 1.73 1.72 1.71 1.70 1.68 1.67 1.62 1.61 1.60 1.59 1.58 1.58 1.57 1.56 1.55 1.54 1.53 1.52 1.51 1.50 1.50 1.48 1.48 1.47 1.46 1.45 1.44 1.43 1.42 1.41 1.40 1.39 1.29 1.28 1.27 1.26 1.25 1.24 1.22 1.21 1.07 1.06 0.97 0.97 0.95 0.82 0.75
SMD-05-046
crude reduction
OH
H
H
H
N3
H
3.50
10 9 8 7 6 5 4 3 2 1 0 ppm
0.93 0.95
1.02 1.00 2.97 3.02 2.42 4.03 5.04 3.04 2.56 0.47 3.37

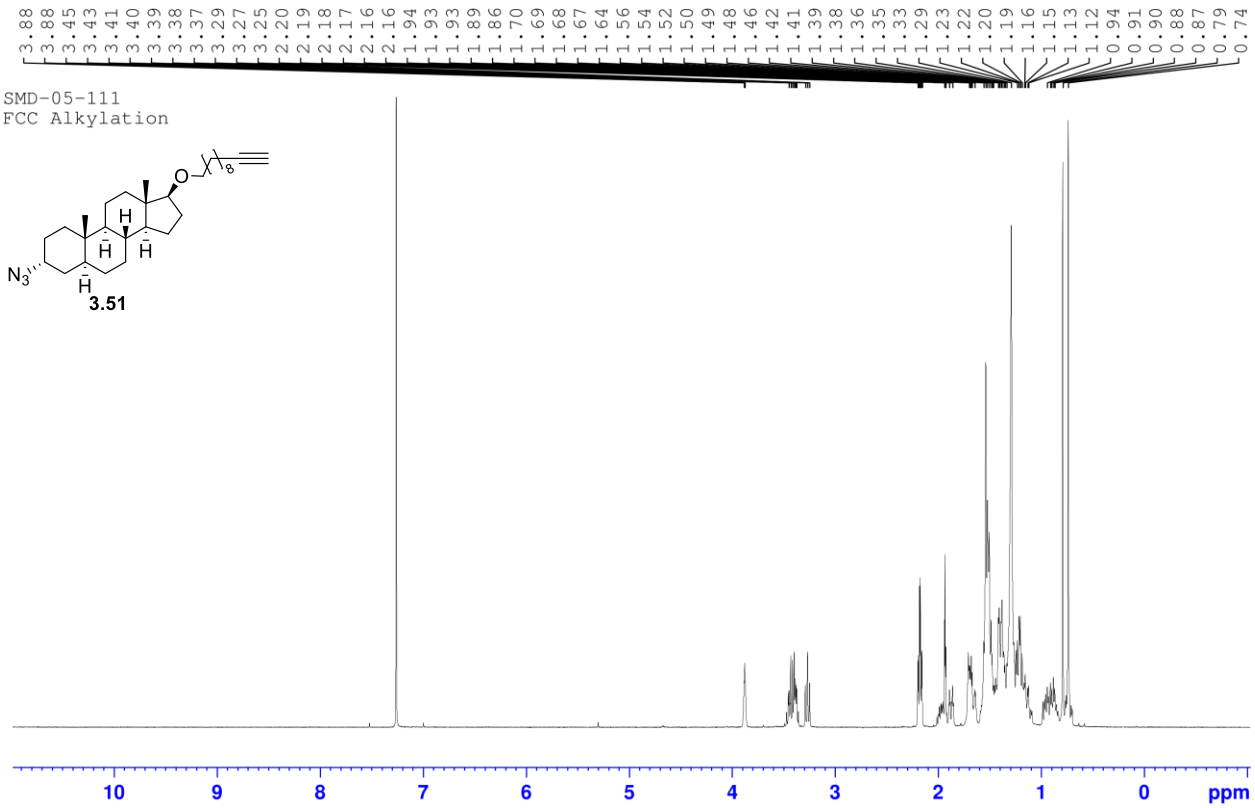
SMD-05-111
FCC Alkylation
3.51
10 9 8 7 6 5 4 3 2 1 0 ppm

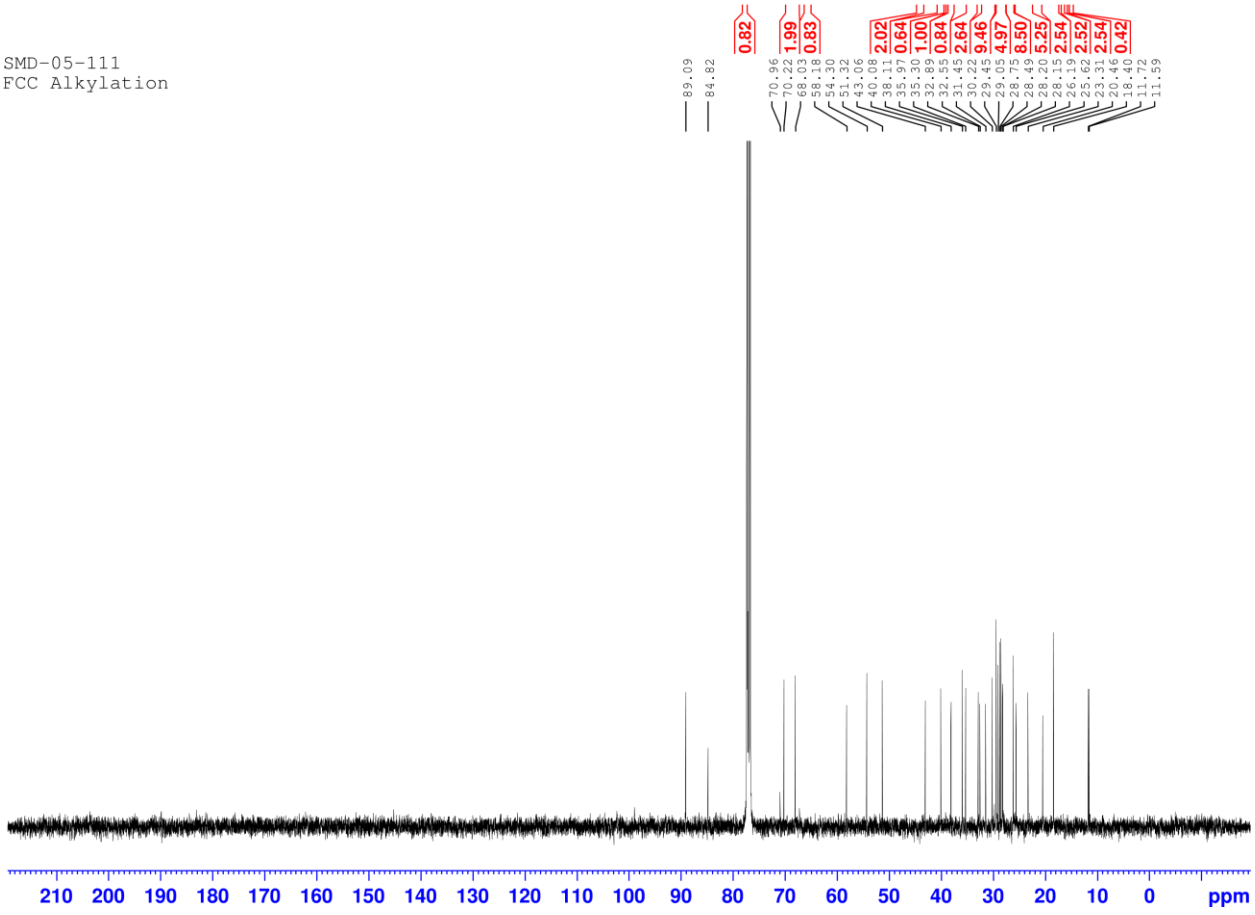
SMD-05-111
FCC Alkylation
210 200 190 180 170 160 150 140 130 120 110 100 90 80 70 60 50 40 30 20 10 0 ppm

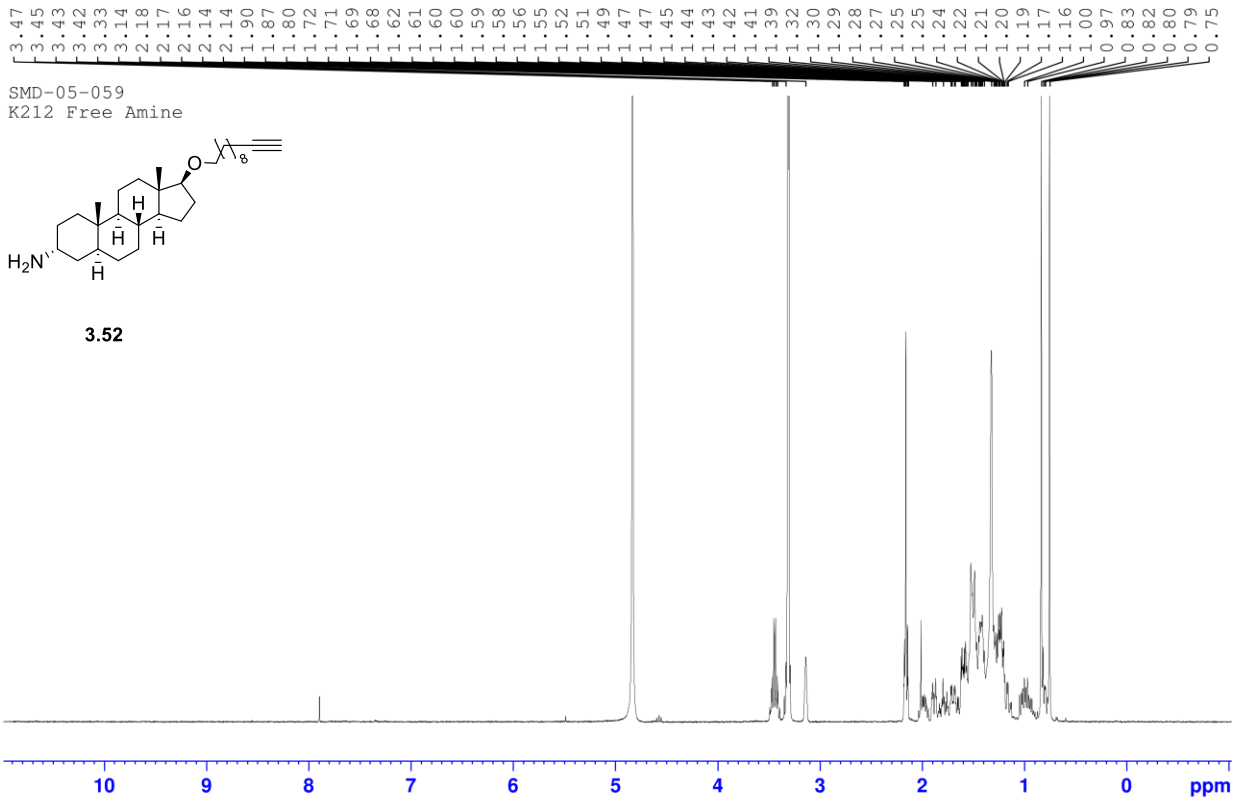
SMD-05-059
K212 Free Amine
3.52
10 9 8 7 6 5 4 3 2 1 0 ppm

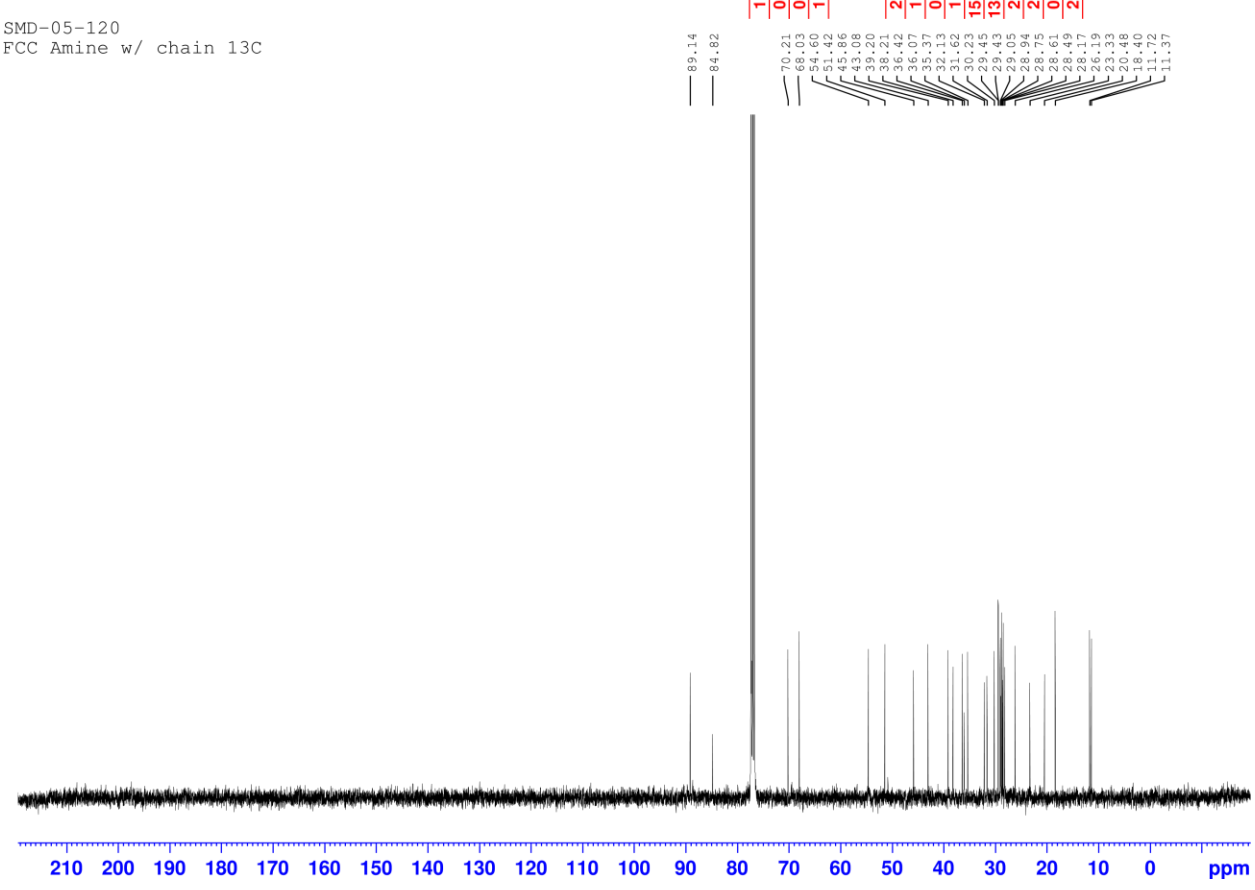
SMD-05-120
FCC Amine w/ chain 13C
210 200 190 180 170 160 150 140 130 120 110 100 90 80 70 60 50 40 30 20 10 0 ppm

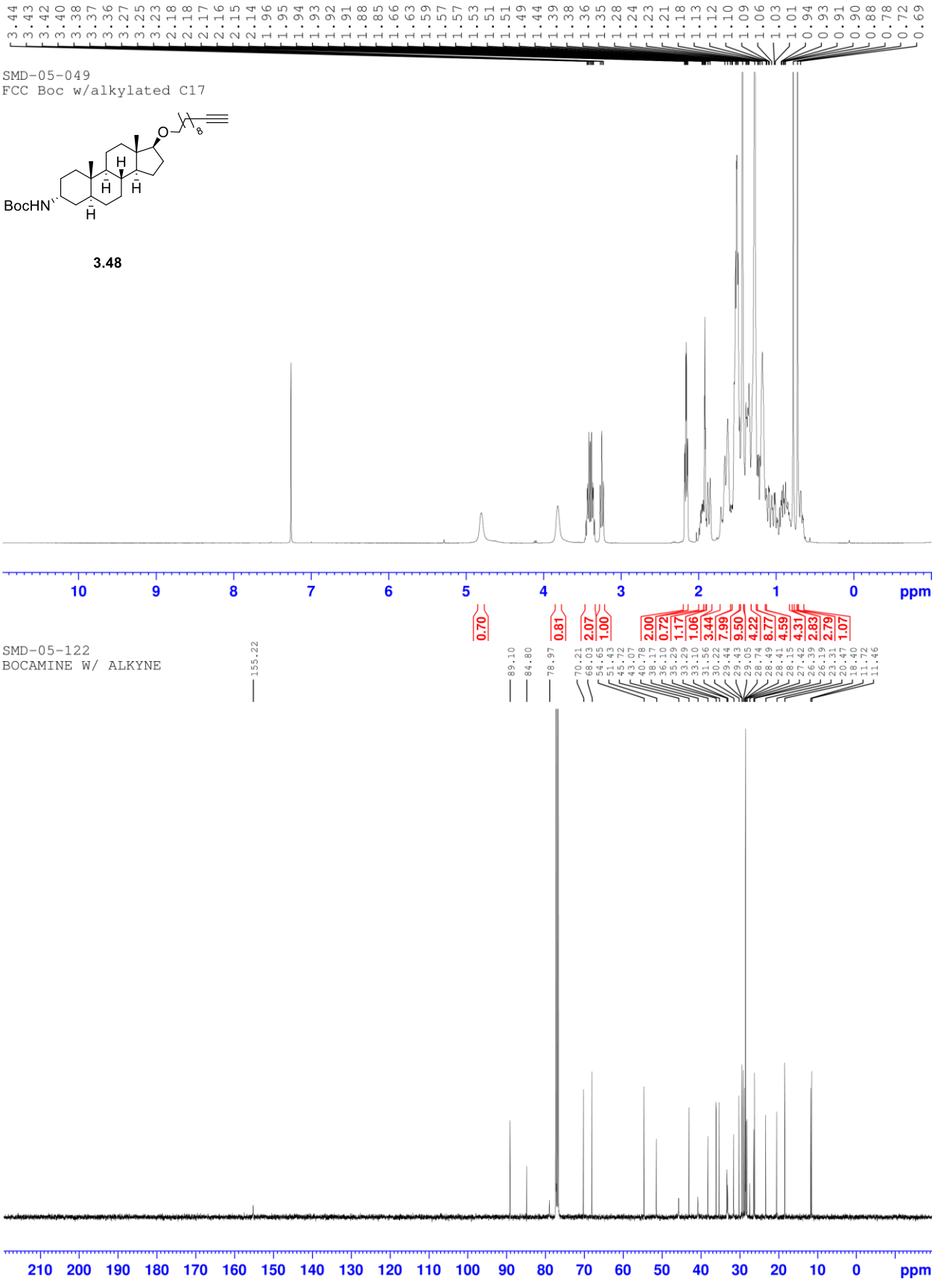
SMD-05-049
FCC Boc w/alkylated C17
BocHN
3.48
SMD-05-122
BOCAMINE W/ ALKYNE
ppm

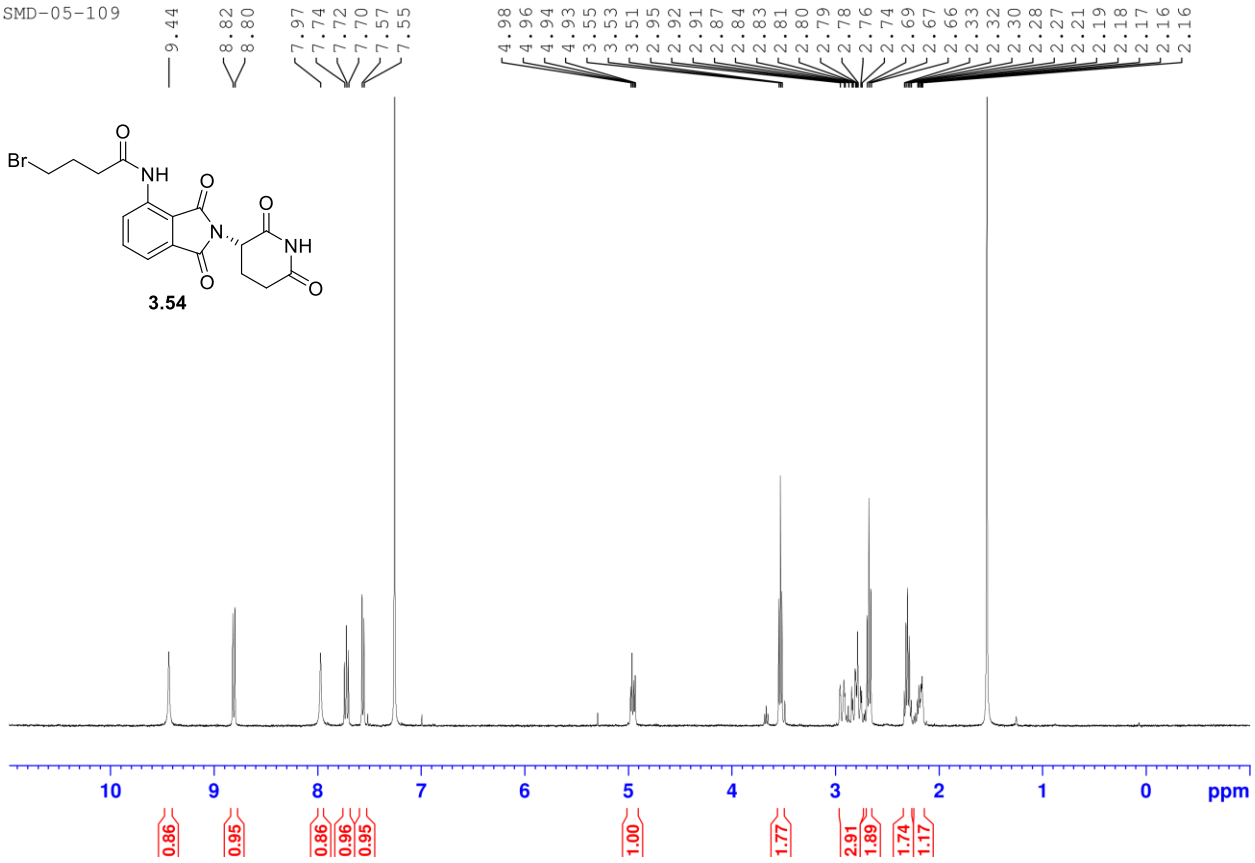
SMD-05-109
9.44
8.82
8.80
7.97
7.74
7.72
7.70
7.57
7.55
4.98
4.96
4.94
4.93
3.55
3.53
3.51
2.95
2.92
2.91
2.87
2.84
2.83
2.81
2.80
2.79
2.78
2.76
2.74
2.69
2.67
2.66
2.33
2.32
2.30
2.28
2.27
2.21
2.19
2.18
2.17
2.16
2.16
Br
NH
O
N
NH
3.54
10
9
8
7
6
5
4
3
2
1
0
ppm
0.86
0.95
0.86
0.96
0.95
1.00
1.77
2.91
1.89
1.74
1.17

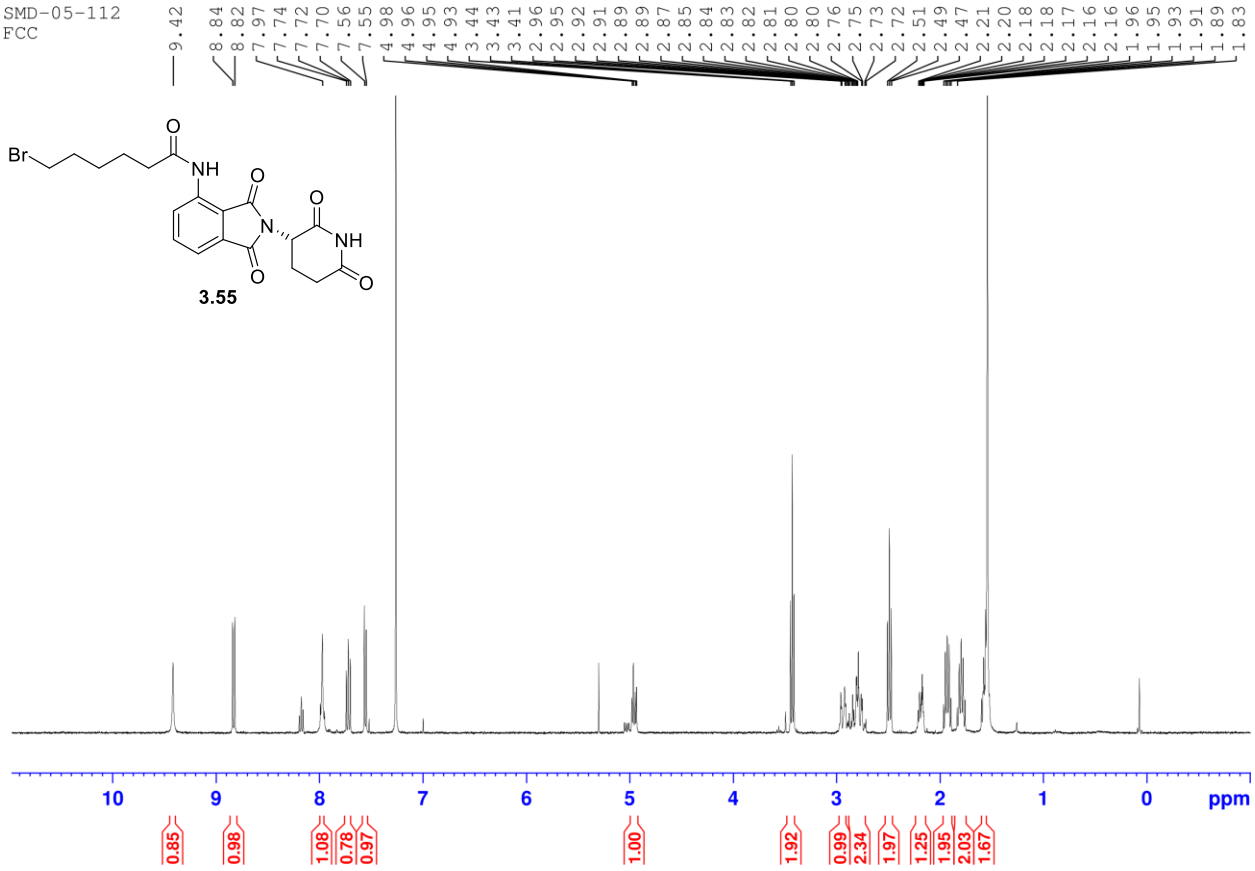
SMD-05-112
FCC
9.42
8.84
8.82
7.97
7.74
7.72
7.70
7.56
7.55
4.98
4.96
4.95
4.93
3.44
3.43
3.41
2.96
2.95
2.92
2.91
2.89
2.89
2.87
2.85
2.84
2.83
2.82
2.81
2.80
2.80
2.76
2.75
2.73
2.72
2.51
2.49
2.47
2.21
2.20
2.18
2.18
2.17
2.16
2.16
1.96
1.95
1.93
1.91
1.89
1.83
Br
O
NH
O
N
O
O
NH
O
3.55
10
9
8
7
6
5
4
3
2
1
0
ppm
0.85
0.98
1.08
0.78
0.97
1.00
1.92
0.99
2.34
1.97
1.25
1.95
2.03
1.67

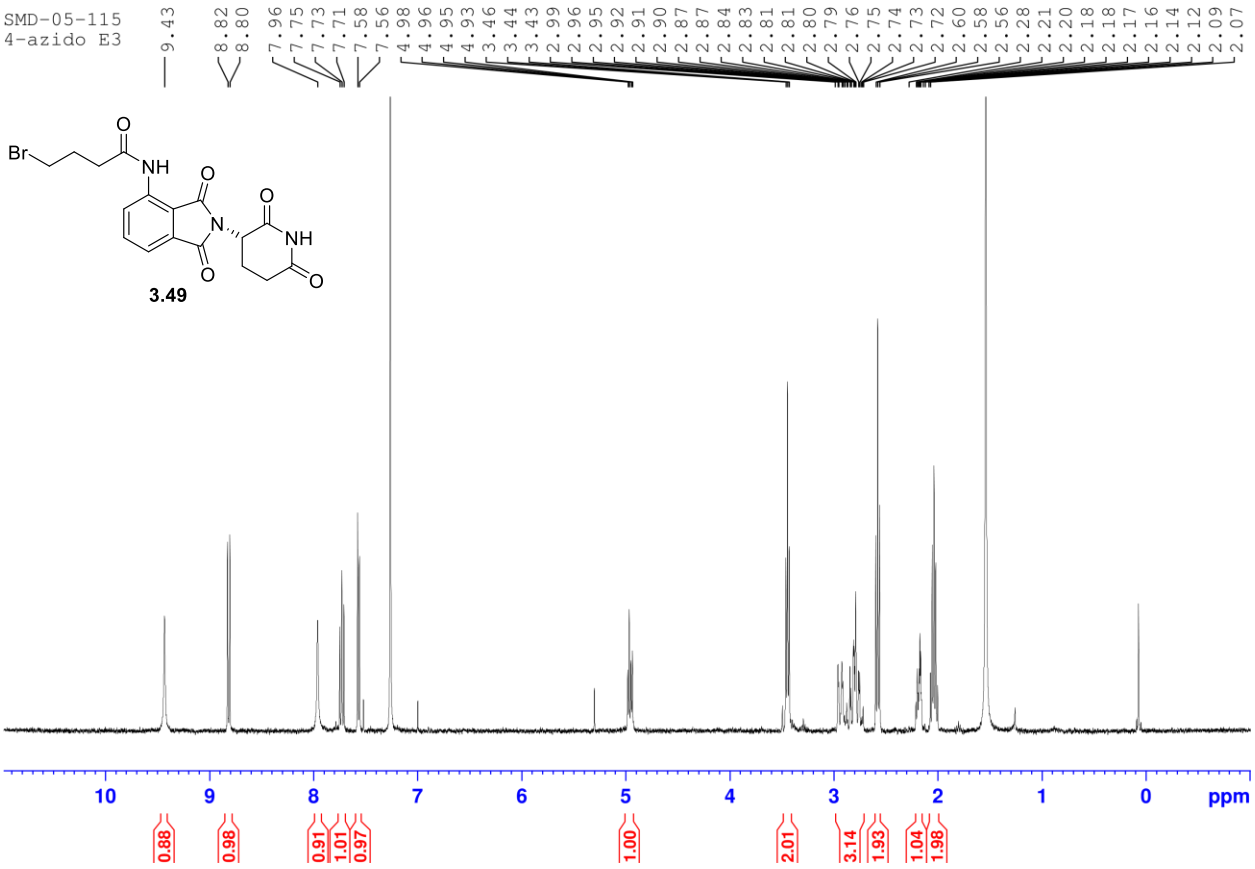
SMD-05-115
4-azido E3
9.43
8.82
8.80
7.96
7.75
7.73
7.71
7.58
7.56
4.98
4.96
4.95
4.93
3.46
3.44
3.43
2.99
2.96
2.95
2.92
2.91
2.90
2.87
2.87
2.84
2.83
2.81
2.81
2.80
2.79
2.76
2.75
2.74
2.73
2.72
2.60
2.58
2.56
2.28
2.21
2.20
2.18
2.18
2.17
2.16
2.14
2.12
2.09
2.07
Br
NH
O
O
N
O
O
NH
O
3.49
10
9
8
7
6
5
4
3
2
1
0
ppm
0.88
0.98
0.91
1.01
0.97
1.00
2.01
3.14
1.93
1.04
1.98

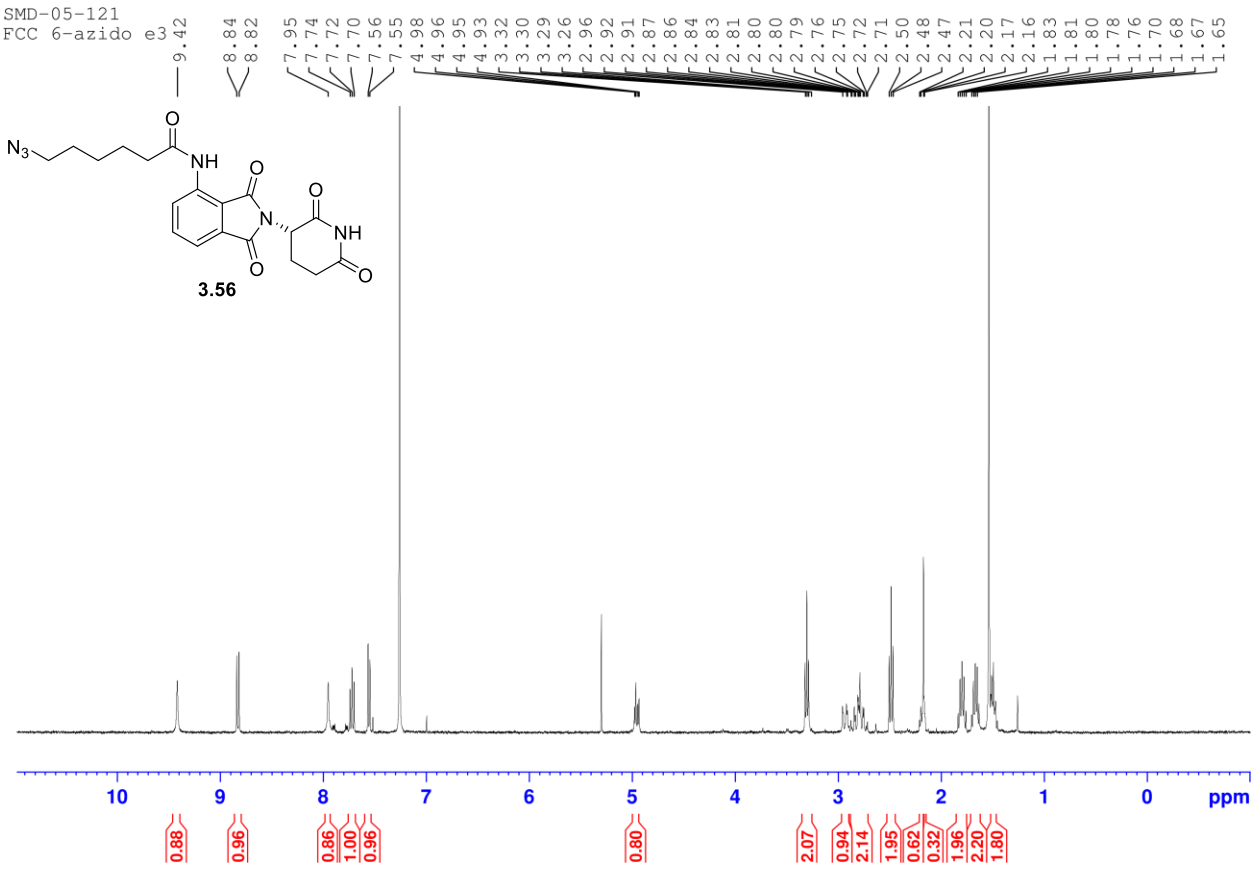
SMD-05-121
FCC 6-azido e3
9.42
8.84
8.82
7.95
7.74
7.72
7.70
7.56
7.55
4.98
4.96
4.95
4.93
3.32
3.30
3.29
3.26
2.96
2.92
2.91
2.87
2.86
2.84
2.83
2.81
2.80
2.80
2.79
2.76
2.75
2.72
2.71
2.50
2.48
2.47
2.21
2.20
2.17
2.16
1.83
1.81
1.80
1.78
1.76
1.70
1.68
1.67
1.65
N3
NH
O
N
NH
3.56
10
9
8
7
6
5
4
3
2
1
0
ppm
0.88
0.96
0.86
1.00
0.96
0.80
2.07
0.94
2.14
1.95
0.62
0.32
1.96
2.20
1.80

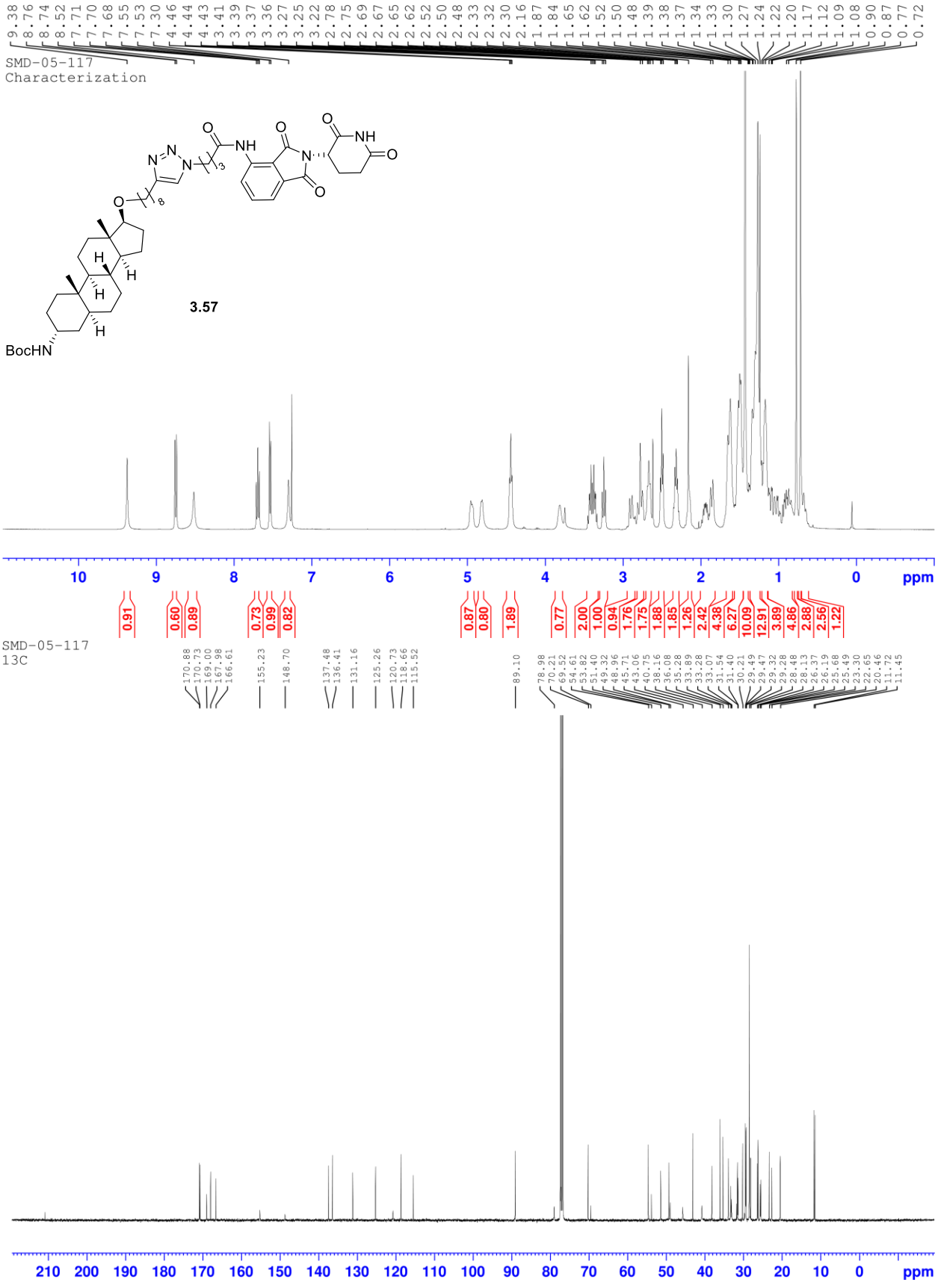
SMD-05-117
Characterization
3.57
BocHN
SMD-05-117
13C
ppm
ppm

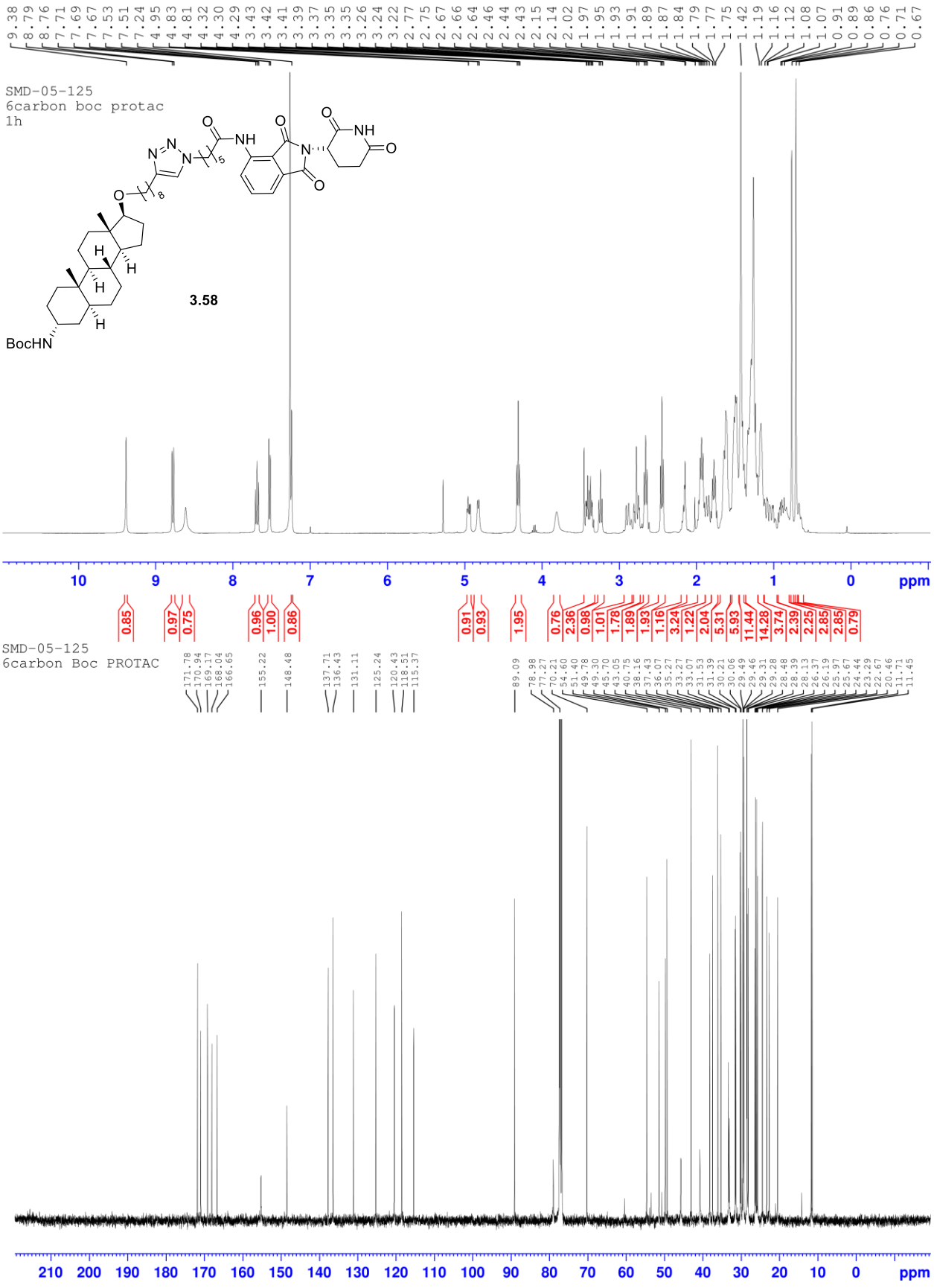
SMD-05-125
6carbon boc protac
1h
3.58
BocHN
SMD-05-125
6carbon Boc PROTAC
ppm

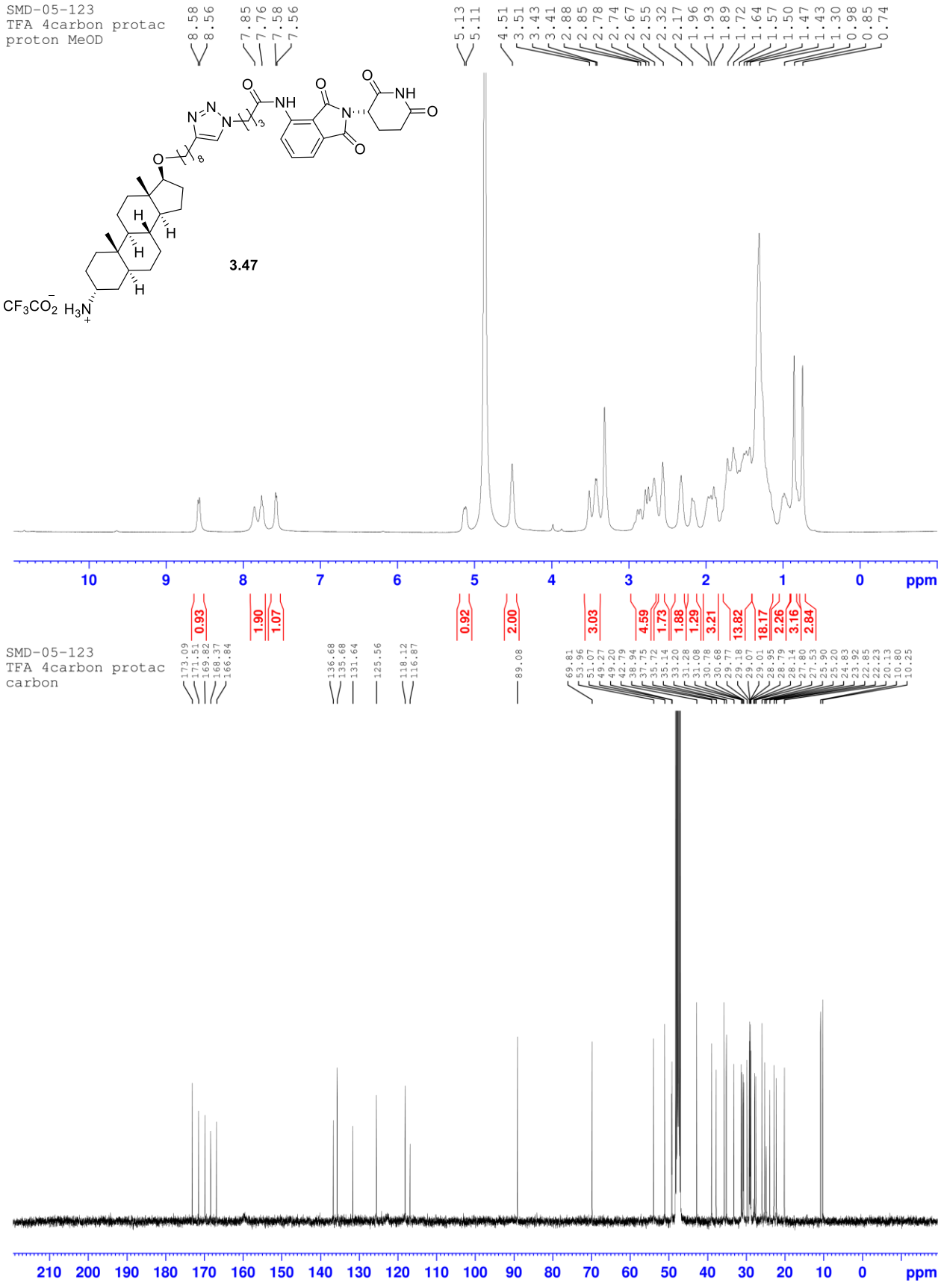
SMD-05-123
TFA 4carbon protac
proton MeOD
8.58
8.56
7.85
7.76
7.58
7.56
5.13
5.11
4.51
3.51
3.43
3.41
2.88
2.85
2.78
2.74
2.67
2.55
2.32
2.17
1.96
1.93
1.89
1.72
1.64
1.57
1.50
1.47
1.43
1.30
0.98
0.85
0.74
3.47
CF3CO2 H3N
10 9 8 7 6 5 4 3 2 1 0 ppm
0.93
1.90
1.07
0.92
2.00
3.03
4.59
1.73
1.88
1.29
3.21
13.82
18.17
2.26
3.16
2.84
SMD-05-123
TFA 4carbon protac
carbon
173.09
171.51
169.82
168.37
166.84
136.68
135.68
131.64
125.56
118.12
116.87
89.08
69.81
53.96
51.07
49.27
49.20
42.79
38.94
37.75
35.72
35.14
33.20
31.28
31.08
30.78
30.68
29.77
29.18
29.07
29.01
28.95
28.79
28.14
27.80
27.53
25.90
25.20
24.83
23.92
22.85
22.23
20.13
10.80
10.25
210 200 190 180 170 160 150 140 130 120 110 100 90 80 70 60 50 40 30 20 10 0 ppm

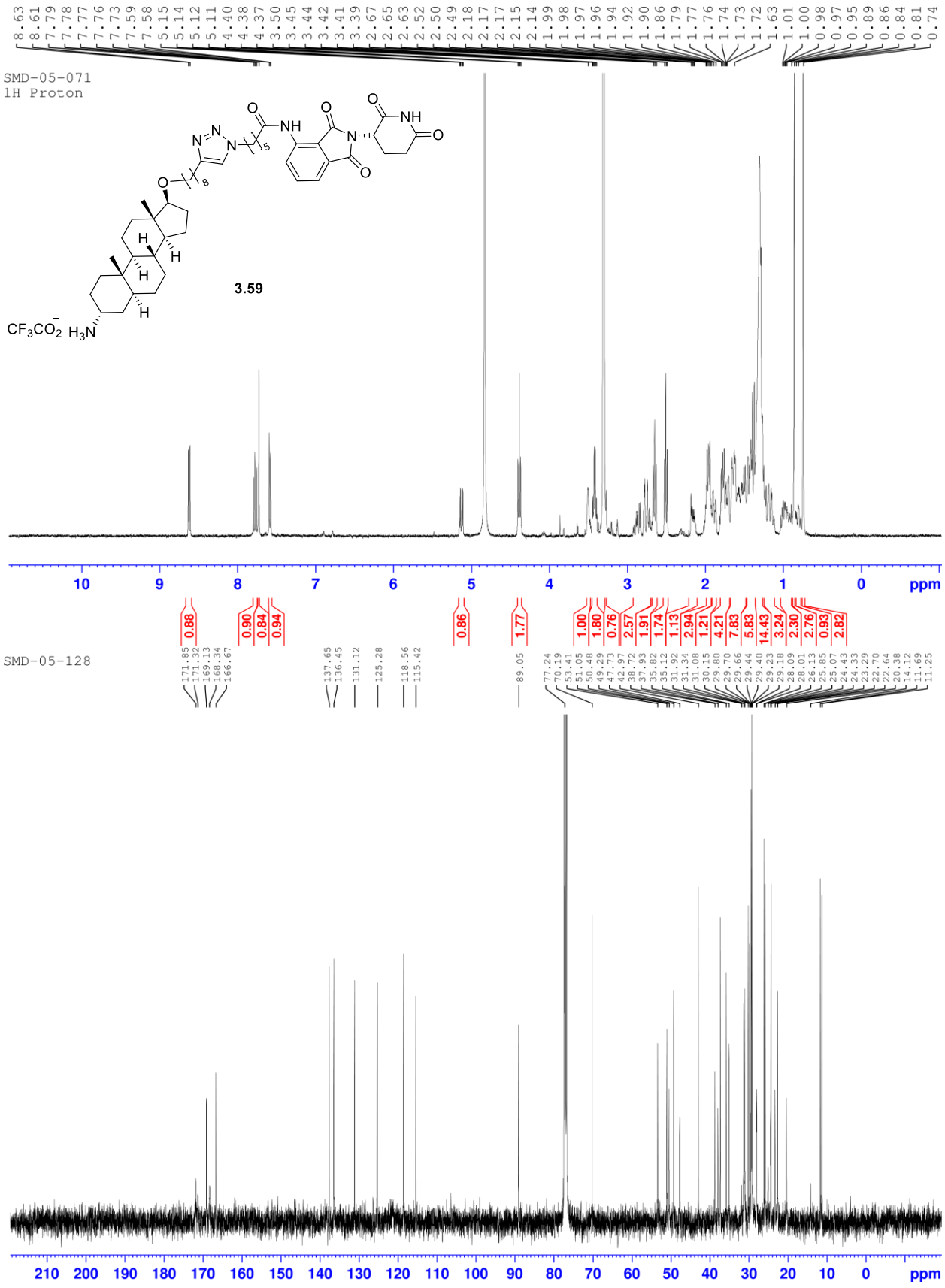
SMD-05-071
1H Proton
3.59
SMD-05-128
ppm

Shawn Dormann
sdormann@syr.edu 716-517-7862

EDUCATION

Syracuse University (Fall 2017-Spring 2023)
- Doctoral Candidate in Chemistry Ph.D program.
- Completed coursework required for Master of Philosophy
- Anticipated Graduation Date: December 2022.

University at Buffalo (2012-2016)
- B.S. in Medicinal Chemistry (May 2016).

AWARDS

- Sol J. Lederman Fellowship (University at Buffalo, 2015)
- Undergraduate Research Award, Center for Undergraduate Research and Creative Activities (CURCA, University at Buffalo, 2016)
- William D. Johnson Award for Outstanding Graduate Teaching Assistant (Syracuse University, 2021)

RESEARCH EXPERIENCE

Graduate Research at Syracuse University (August 2017-present)
- Design and synthesis of aminosteroid SHIP inhibitors
- Development of a catalyst free method for the formation of trimethylsilylethyl esters
- Design and synthesis of a PROTAC aimed at targeting the inositol phosphatase SHIP

Starks Associates, Buffalo, NY - Chemist (April 2016-July 2017)
- Synthesis of small molecules for the treatment of infectious diseases.
- Worked on synthesis of eFDA(4′-ethynyl-2-fluoro-2′-deoxyadenosine) for the NIAID (NIH).

Undergraduate Researcher at the University at Buffalo (May 2014 - May 2016)
- Using chiral copper catalysts to enantioselectively access nitrogen heterocycles (isoindolines).

PUBLICATIONS

Dungan, O. M.; Dormann, S.; Fernandes, S.; Duffy, B. C.; Effiong, D. G.; Kerr, W. G.; Chisholm, J. D. Synthetic studies on the indane SHIP1 agonist AQX-1125. *Organic & Biomolecular Chemistry* **2022**, *20*, 4016-4020. DOI: https://doi.org/10.1039/D2OB00555G

Lin, W.; Meyer, S. T.; Dormann, S.; Chisholm, J. D. “Esterifications with 2-(Trimethylsilyl)ethyl 2,2,2-Trichloroacetimidate.” *Organics* **2021***, 2*, 17-25. DOI:10.3390/org2010002; *ChemRxiv* DOI:10.26434/chemrxiv.13331036.v1 (*Selected*

as the cover article for the March 2021 issue (see https://www.mdpi.com/2673-401X/2/1)

Kerr, W. G.; Pedicone, C.; Dormann, S. D.; Pacherille, A.; Chisholm, J. D. “Small Molecule Targeting of SHIP1 and SHIP2.” *Biochem. Soc. Trans.* **2020***, 48*, 291-300*.* DOI:10.1042/BST20190775.

Pedicone, C., Fernandes, S., Dungan, O. M., Dormann, S. M., Viernes, D. R., Adhikari, A. A., Choi, L. B., De Jong, E., Chisholm, J.D. and Kerr, W.G. "Pan-SHIP1/2 inhibitors promote microglia effector functions essential for CNS homeostasis." *J. Cell Sci.* **2020**, *133*, jcs238030*.* DOI:10.1242/jcs.238030.

Fernandes, S.; Srivastava, N.; Pedicone, C.; Sudan, R.; Luke, E. A.; Dungan, O. M.; Pacherille, A.; Meyer, S. T.; Dormann, S.; Chisholm, J. D.; Kerr, W. G. Obesity control by SHIP inhibition requires pan-paralog inhibition and an intact eosinophil compartment. *iScience* **2023** *”accepted in principle”*

PATENTS

Kerr, W.; Pedicone, C.; Chisholm, J. D.; Dormann, S. (The Research Foundation of the State University of New York and Syracuse University, USA). Preparation of steroidal and indole derivatives as SHIP inhibitors for activating microglial cells. WO2020028552A1, 2020.

TEACHING EXPERIENCE

General Chemistry Recitation
- Fall 2017

General Chemistry Laboratory
- Spring 2018, Fall 2019, Fall 2020, Spring 2021, Spring 2022

Organic Chemistry Recitation
- Fall 2021, Fall 2022

References:

Dr. John Chisholm – Research Advisor – Contact: jdchisho@syr.edu

Gary Bonomo – Course Lead Instructor – Contact: gbonomo@syr.edu

Dr.Deborah Kerwood – Course Lead Instructor - Contact: djkerwoo@syr.edu